The design and performance of non-linear vibration isolating materials.

COLLIER, Paul.

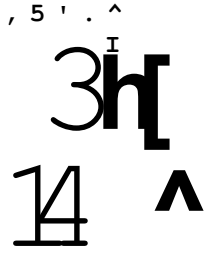

THE DESIGN AND PERFORMANCE OF NON-LINEAR VIBRATION ISOLATING MATERIALS

by

PAUL COLLIER BSc

A thesis submitted to the Council for National Academic Awards in partial fulfilment of the requirements for the degree of Doctor of Philosophy

Sponsoring Establishment : Department of Applied Physics, Sheffield City Polytechnic

Collaborating Establishments : Bruel and Kjaer (UK) Ltd.

JCB reaearch Ltd.

September 1985

THE DESIGN AND PERFORMANCE OF NON-LINEAR VIBRATION ISOLATING MATERIALS

by

P COLLIER

ABSTRACT

The mechanical properties of resilient cellular materials, such as dynamic stiffness and damping, depend on several physical parameters characteristic of the material and the conditions of use, eg permeability, elastic modulus, cellular structure, static pre-strain. In many end use situations the pre-compressions and dynamic amplitudes are large and the material operates in a non-linear regime. The effects of non-linear material behaviour on the performance of systems employing cushion foams has not previously been reported on.

In this work the influence of non-linear material behaviour on the vibration isolation characteristics of the material is examined. Previous theoretical and experimental studies have been confined to small strain conditions where the material behaves in a linear fashion and the properties are independent of deformation. This work extends the theoretical analysis to allow the study of the variation of the mechanical properties and vibration isolation performance with pre-strain. The fluid flow model proposed by Gent and Rusch is shown to be inadequate and an alternative proposed which conforms closely to experiment. This is extended to non-Newtonian fluids and incorporated in a model for fluid flow damping in the non-linear regime.

The response of cushion foams in transportation situations is studied for small and large amplitude dynamic excitations. A multi-degree of freedom model of the person-seat system is presented and used to reproduce the responses of real vehicle seats measured in the field. The model is capable of being used to predict the optimum cushion behaviour, such as stiffness, viscoelastic damping and fluidic damping, required to enhance the ride comfort provided by a particular seat system. At higher vibration amplitudes experimental determinations show that the cushion foam behaves in a non-linear manner with strain dependent properties and several degrees of freedom. Above a certain critical excitation amplitude the classical theories of vibration isolation are shown to break down with the appearence of subharmonic frequencies in the power spectrum of the motion of the isolated mass. The resulting period doubling bifurcation cascade is similar to that found by workers in other fields. The motion of the isolated mass is complex and has not been reported previously. The behaviour is interpreted as a manifestation of chaos.

THE DESIGN AND PERFORMANCE OF NON-LINEAR VIBRATION ISOLATING MATERIALS

ACKNOWLEDGEMENTS

The author wishes to express his appreciation to Dr N C Hilyard, Dr C M Care and Dr H M Kohler for suggesting this research topic and for their guidance throughout the investigation. The author would also like to thank the collaborating establishments; Bruel and Kjaer (UK) Ltd for the loan of equipment and the transfer of ideas, and JCB Research Ltd for the loan of their vehicle seat systems and suggesting the programme of work on the comfort of vehicle operators. Appreciation is also extended to all the staff of the Applied Physics department at Sheffield City Polytechnic. Particular thanks must go to; Dr J S Brooks and Mr M Furness for helpful advice, Mr J Beadman for assistance with the measurement of the air-flow properties, Mrs G Sidda and Mr K Blake for help and advice with the SEM Microscope facilities, and Mr G France, Mr T Hudson and Mr K Jaffrey for help with the construction of the dynamic mechanical spectrometer. Thanks is also due to Mr P Slingsby and Mrs R Thomas of the Metallurgy Department for assistance with the static testing of foam samples.

The author would also like to thank British Vita Ltd, Dunlop Ltd and BP Chemicals Ltd for providing suitable foams for testing.

The Author is indeb ted to Sheffield Local Education Authority for financing the research assistantship.

PUBLICATIONS AND PRESENTATIONS

1 Hilyard N.C., Collier P., McNulty G.J. & Douglas D., 'Influence of seat cushions on vibrations in earth moving vehicles', Proceedings, Internoise '83, Edinburgh, Vol I, 527, July 1983.

2 McNulty G.J., Douglas D., Hilyard N.C. & Collier P., 'Vibration in earth moving vehicles', Proceedings, Internoise '83, Edinburgh, Vol II, 913, July 1983.

3 Hilyard N.C., Collier P. & Care C.M., 'Dynamic Mechanical behaviour of flexible foam cushion materials and its influence on ride comfort', Proceedings, UK Informal Group on Human Response to Vibration, N.I.A.E., Silsoe, Bedfordshire, September 1983.

4 Hilyard N.C., Collier P. & Care C.M., 'Influence of the mechanical properties of cellular plastic cuhion materials on ride comfort', Proceedings, 'Dynamics in Automotive Engineering', Cranfield Institute of Technology, Bedford, p A.1, April 1984

5 Hilyard N.C. & Collier P., 'Effect of vehicle seat cushion material on ride comfort', Proceedings, 'Plastics on the road', London, p 6/1, December 1984.

6 Hilyard N.C. & Collier P., ' Response of a vibration isolator with distributed non-linear stiffness at large excitations', accepted for publication, J. Sound & Vibration letters.

7 Collier P., Norcliffe A. & Hilyard N.C., ' An undergraduate Case study to illustrate the role of computer aided modelling techniques in the control of vibration', Proceedings Fifth British Conference on the Teaching of Vibration and Noise, Sheffield City Polytechnic, p23-32, July 1985.

8 Care C., Collier P., Hilyard N.C., Norcliffe A., Rodgers G.G. & Thomlinson M.M., 'Improving driver comfort in motor vehicles - a case study for Applied Science students', Proceedings, 2nd International Conference on the Teaching of Mathematical Modelling, Exeter, July 1985.

9 Collier P., Care C.M. & Hilyard N.C., 'A microprocessor controlled dynamic mechanical spectrometer', Accepted for publication, Journal of Physics E - Scientific Instruments.

LIST OF SYMBOLS

A	Boolean quantity, defined in table 2.2
A	dc Component of input signals
A	Area
$\underline{A}$	(3x3) Matrix defined in equation 5.6
A_c	Surface area of cell
A_e	Effective cross-sectional area of sample
a	Radius of pipe in section 3.5
a	Curve fitting constant, defined in equation 4.8
a_x, a_y, a_z	Distances shown on figure 5.27
B	Boolean quantity, defined in table 2.2
$\underline{B}$	(3x1) matrix defined in equation 5.6
B_i i=1,∞	Amplitudes of the harmonic content in the input signals
B,B(e)	Flow resistance coefficient
b	Curve fitting constant in equation 4.8
b_i i=1,∞	Amplitudes of fourier series components
$\underline{b}$	Base point used in appendix V
C	Boolean quantity, defined in table 2.2
C	Curve fitting constant in equation 4.65
C	Damping of a viscous element
C_1, C_2, C_3	Damping of human body subcomponents in figure 5.10
C_c	Critical damping of a lumped parameter spring-damper system
C_f	Skin friction coefficient
C_m, C_n	Amplitudes of input signals at 50 Hz and 100 Hz
C_o	Numerical constant in equation 3.5
C(n)	Constant defined by equation 3.34
c	Numerical constant in equation 3.2
c	Constant in equations 5.25 and 5.27

c_i $i=1,\infty$	Amplitudes of fourier series components
D	Radius of pipe diameter to orifice diameter in equation 3.3
D	Curve fitting constant in equation 4.65
d	Average cell diameter
d	Diameter of orifice in equation 3.25
d_1, d_2	Loss tangents of the elements in the person-seat model of figure 5.11
$d_3, d_3(\omega)$	Loss tangent of seat cushion in figure 5.11
d_m	Loss tangent of matrix
$d(\omega)$	Dynamic loss tangent
du/dr	Shear rate
E_f	Zero strain modulus of foam
E_g	Bulk modulus of gas
E_p	Modulus of solid polymer
E'_m, $E'_m(e)$	Storage modulus of matrix
E_t, $E_t(e)$	Transverse modulus of matrix
$E(\omega), E^*(\omega)$	Dynamic modulus, scalar and complex form
$E'(\omega)$	Dynamic storage modulus
$E''(\omega)$	Dynamic loss modulus
e	Fractional static pre-strain
e_b	Critical buckling strain, when $\Psi(e)=0.95$
e_1	Strain when $\Xi(e)$ is minimum
e_{min}	Strain when $\Psi(e)$ is minimum
e_y	Yield strain, when $\Xi(e)=0.95$
$\underline{e}_i$	Unit vectors in appendix V
F	Force due to fluid flow
F	Forcing function in equations 5.25-5.27
$\underline{F}_m$	Inertial force vector
$\underline{F}_s$	Force vector generated by deformation of the test piece

$\underline{F}_t$	Total force vector measured by the dynamic mechanical spectrometer
f_1, f_2, f_3	Resonance frequencies of human body components in figure 5.10
$f(\omega t)$	Fourier series, defined in equation 4.34
G	Gradient of line in figure 3.6
$G(\underline{p})$	Mean square variation used in appendix V
$g(Z)$	Restoring function used in equation 5.27
H	Height of test piece
h_i	Step lengths used in appendix V
I	Intercept of line in figure 3.6
I_0-I_3	Integrals
I_D, I_N	Coefficients defined in equation 5.11
I_x, I_y, I_z	Moments of inertia about the three axes
i	Integer
j	$\sqrt{-1}$
K	Integer defined in equation 2.9
K, K(e)	Permeability of matrix
K(n), K(n,e)	Non-Newtonian permeability
$K(n,\omega)$, $K(n,\omega,e)$	Effective non-Newtonian permeability, defined by equation 4.38
$K(\omega)$, $K(\omega,e)$	Effective permeability, defined by equation 4.16
k	Numerical constant
k_1, k_2, k_3	Stiffnesses shown on figure 5.34b
k_x, k_y, k_z	Stiffnesses shown on figure 5.27
L	Integer defined in equation 2.9
L	Length of test piece
l_e	Effective path length in matrix
M	Integer defined in equation 2.9
M	Mass

M_1, M_2, M_3	Masses of the elements in the person-seat model of figure 5.11
m	Integer, chapter 2
m	Hydraulic radius of voids in chapter 3
N	Number of points sampled in one deformation cycle
n	Fluid index
P	Pressure
P_1-P_N	Sample data point
$P(\omega)$	Power spectrum, defined in equation 5.19
p	Curve fitting constant, equation 4.8
$\underline{p}$	Independent variables in appendix V
Q	Volume flow rate of fluid
q	Integer, chapter 2
q	Curve fitting constant, equation 4.8
R	Growth parameter used in equation 5.18
R_1-R_6	Resistances
R_D, R_N	Coefficients defined by equation 5.11
r	Curve fitting constant, equation 4.10
r	Radius
r	Fluid flow fitting parameter defined in equation 4.61
S	Area of orifice in equation 3.25
S, S(e)	Wetted surface area of matrix/ unit volume
S_1-S_4	Summations defined by equation 2.8
S_1^*, S_2^*, S_3^*	Stiffness of the viscoelastic elements of the person-seat model of figure 5.11
S'_1, S'_2	Storage stiffnesses in the person-seat model
$S'_3, S_3(\omega)$	Storage stiffness of the seat in the person-seat model of figure 5.11
S_t	Transverse stiffness of the seat cushion.
s	Curve fitting constant, equation 4.10

T	Time period of input signals
$T(\omega)$	Transmissibility
t	Time
t_s	Sampling time interval
u	Linear flow velocity
u_e	Effective linear flow velocity
u_m	Mean approach velocity
v	Linear flow velocity, equation 3.1
v	Curve fitting constant, equation 4.10
W	Width of test piece
w	Curve fitting constant, equation 4.10
$\underline{X}_o$	Vector displacement of sample
x	Distance
x	Co-ordinate axis in chapter 5, figure 5.22
x_i	Iterated population value in equation 5.18
x_s	Steady population value in equation 5.20
$Y(\underline{p})$	Function defined in appendix V
y	Co-ordinate axis in chapter 5, figure 5.22
$y(t)$	Input signal to mechanical spectrometer
Z	Amount of sample deformation. Displacement
$\dot{Z}$	Velocity in z direction
$\ddot{Z}$	Acceleration in z direction
$\underline{Z}$	(3x1) matrix defined in equation 5.6
Z_o, Z_{io}	Amplitudes of the displacements of the component masses in the 3-DOF person-seat model
Z, Z_1	Vertical displacements in chapter 5
Z^*, Z^*_{1-3}	Displacements of the component masses in the 3-DOF person-seat model of figure 5.11
z	Co-ordinate axis in chapter 5, figure 5.22
α	Numerical constant in chapter 3

α	Fluid flow parameter, compressible fluids
α	Co-ordinate axis in chapter 5, figure 5.22
α	Feigenbaum universal constant = 2.5029, given in equation 5.22
β	Ratio of cell strut width to length, chapter 3
β	Co-ordinate axis in chapter 5, figure 5.22
$\beta, \beta(e)$	Fluid flow parameter, incompressible fluids
Γ_1, Γ_2	Coefficients, defined by equation 4.50
γ	Co-ordinate axis in chapter 5, figure 5.22
$\gamma, \gamma(e)$	Fluid flow parameter, defined in equations 4.14 and 4.44
γ_{max}	Value of γ at the maximum damping frequency
ΔP	Pressure difference
Δx	Thickness
Δ_i	Quantity defined on figure 5.25
$\Delta(\omega)$	Coefficient defined in equation 4.36
δ	Phase angle, equation 4.1
δ	Feigenbaum universal constant = 4.6692, given in equation 5.21
δ_i $i=1,\infty$	Phase angle of input signal harmonics
δ_m, δ_n	Phase angles of input signals at 50 Hz and 100 Hz
$\varepsilon, \varepsilon(\omega)$	Dynamic strain
$\dot{\varepsilon}$	Rate of change of dynamic strain = $d\varepsilon/dt$
ε_i	Quantity defined on figure 5.25
ε_o	Dynamic strain amplitude
$\zeta(\omega)$	Coefficient defined in equation 4.36
η	Newtonian viscosity
η_a	Apparent viscosity, defined in equation 4.57
θ	Phase angle in figure 2.12
θ	Fluid flow fitting parameter, equation 4.61
κ	Parameter defined in equation 5.24

λ	Dimensionless constant in chapter 3
μ	Zero shear rate viscosity for a power-law fluid
μ	Feigenbaum universal constant = 4.648, given by equation 5.23
ν_x, ν_y	Parameters defined in equation 5.24
$\Xi(e)$	Dynamic storage modulus shape function, defined in equation 4.6
$\Xi(e)_1$	Minimum value of $\Xi(e)$
ξ	Volume fraction of open cells
ρ	Density
σ	Standard deviation
σ_f	Stress due to fluid flow
σ_m	Stress due to deformation of matrix
σ_t	Total stress from deformation of the matrix and fluid flow
$\sigma(\omega), \sigma^*(\omega)$	Dynamic stress, scalar and complex form
τ	Tortuosity
τ	Stress due to fluid flow in a pipe, equation 3.28
τ_o	Stress at walls of pipe, equation 3.18
$\phi_o, \phi(e)$	Volume fraction of polymer
ψ_1, ψ_2	Integral sums defined in equation 2.4
ψ_1, ψ_2	Coefficients defined by equations 4.21 and 4.22
$\Psi(e)$	Rusch shape function, defined by equation 4.6
$\psi(e)_{min}$	Minimum value of $\Psi(e)$
ω	Angular frequency
ω_n	Resonance Frequency of a 1-DOF isolator in equation 5.1
ω_z	Natural frequency of the 1-DOF isolator in the vertical direction
$\omega_{x\beta}$	Frequency ofcoupled oscillation in the x and β directions, given by equation 5.24
ω_{max}	Maximum damping frequency

1. INTRODUCTION

Resilient cellular plastics have widespread practical applications, such as comfort cushioning, shock mitigation, vibration isolation and energy management systems. Under the conditions prevailing in many applications, such as vehicle seating and packaging, the cellular matrix is often subject to large amplitude deformations and large static (or quiescent) compressive deformation. Under these conditions the mechanical properties of the material are highly non-linear. The influence of these non-linearities on the vibration isolating performance of cushion foams has not previously been studied.

Earlier work on material behaviour by investigators such as Gent, Rusch and Hilyard, has led to a reasonable understanding of the mechanisms governing the dynamic mechanical properties of resilient cellular plastics. However the early experimental and theoretical studies were confined, for the most part, to small strain conditions where the response of the cellular material is approximately linear and to deformations about the zero-strain condition. Small strain conditions restricted the compressive deformation of the matrix (both static and dynamic) to a few per-cent of the undeformed height of the test piece. Throughout this investigation the variation of the material properties with imposed static compressive deformation is considered, since this conforms more closely to the conditions found in

practical applications.

During cyclic deformation of a flexible open-cell polymer foam two separate processes occur, one is associated with the polymer matrix and the other associated with fluid enclosed by the matrix. Both of these processes have been studied previously [eg 50,28], but both theoretical and practical work was restricted to small levels of imposed static strain and Newtonian fluid flow.

Energy dissipation is an important feature of resilient cellular plastics in many applications. Three energy dissipation mechanisms operate. These are:

i) Viscoelastic damping processes due to normal deformations in the polymer forming the cellular structure. This process operates at both low and high levels of static compressive strain.

ii) Hysteresis associated with the catastrophic collapse of cell elements, which becomes important at high levels of compressive strain.

iii) Fluid flow processes caused by the motion of the enclosed fluid through the cellular matrix. This mechanism will operate at both low and high levels of compressive strain and at frequencies determined by the foam and fluid in use and test piece geometry.

The relationship between, and relative importance of these three processes in particular applications has received little attention in the literature.

The permeability of the foam is an important factor when considering damping due to fluid flow. The flow of Newtonian fluids through cellular structures has been investigated previously [28]. However the simplified model treatments used have proved incapable of correctly predicting the strain dependence of the fluid flow behaviour. A theoretical analysis is presented in Chapter 3 which uses a model of the cellular structure based on flow through a packed bed. The predicted zero-strain and strain dependent air-flow properties are compared with experimental data and show a better correspondence than earlier treatments. Recent developments in foam manufacture technology have resulted in additives to control the fluid flow energy dissipation process and hence the vibration isolating characteristics of the material via changes in cellular structure [38]. A series of foams containing different amounts of the vibration control additive have been tested in this work. The results have proved interesting and are summarised in chapter 3. An extension to the theoretical model is presented here which includes the flow of a non-Newtonian fluid through the cellular structure. The results of this study are used in Chapter 4 for the prediction of the fluid flow damping process with Newtonian and non-Newtonian fluid flow.

The dynamic mechanical properties of flexible cellular polyurethane foams have been studied in the absence of fluid flow processes. In this case only the first two

energy dissipation systems operate. The modulus and damping of the material are shown to be functions of the imposed level of pre-compression. A study is presented, in Chapter 4, into the relationship between the dynamic mechanical properties, and those measured using quasi-static loading techniques. It is shown that the effective dynamic stiffness at a particular pre-compression is very different to the gradient of the F-D curve at the same compressive strain.

For the case of the mechanical behaviour of cellular materials incorporating fluid flow processes, theoretical equations are developed which relate the observed dynamic response to the physical properties of the material and the fluid. This treatment follows closely that put forward by Gent and Rusch [39,74]. However in this case the work extends the treatment by considering the flow of incompressible non-Newtonian fluids and high levels of static deformation.

A major application of flexible cellular plastics is as vibration isolators. This type of material is commonly used in the construction of full-depth vehicle seat cushions. In Chapter 5, a study is presented into the vibration isolation characteristics of non-linear cellular plastic materials. The study is split into two sections, the first dealing with small dynamic excitations and the second with large dynamic excitations.

In the first section the application of vehicle seating is considered. This is important since since it is not possible to specify a cushion foam providing enhanced ride comfort unless the influence of cushion properties, eg stiffness and damping, on the vibration transmissibility of the person-cushion system is known. A multi degree-of-freedom model of the person-seat system is presented and behaviour predicted by the model compared with responses of vehicle seats measured in the field. This model is much more complex than those used by previous workers and good agreement between predicted behaviour and that measured by other workers is obtained. The model studies are extended to show how fluid flow damping in the cushion material influences dynamic ride comfort. Another group of workers in this field have used the vibration control additive described above to influence the fluid flow process in the cushion material and hence the vibration isolation characteristics. The results of their experimental investigations do not fit a simple 1-DOF model incorporating fluid flow processes.

In the second section the response of a distributed non-linear viscoelastic vibration isolator to large amplitude dynamic excitations considered. Experimental data is presented which indicates that the classical theories of vibration isolation break down at high excitations. For a simple mechanical arrangement the motion of the isolated mass is found to be very complex with coupled modes of vibration and oscillations in six directions. At high

excitations the behaviour of the isolator system appears to exhibit the characteristics of chaotic motion [121].

In order to measure the dynamic mechanical properties of the cellular materials over the frequency range of interest, it has been necessary to design and construct an automated dynamic mechanical spectrometer suitable for the testing of low-stiffness materials. The design of this equipment is outlined in Chapter 2. The system is based around a commercially available electromagnetic exciter and a Nascom III microcomputer. The spectrometer operates over a frequency range of 0.07Hz to 100Hz and uses a novel measurement algorithm to determine the amplitude and phase of the force and deformation signals. The system also allows automatic mass compensation for the elements of the spectrometer between the force transducer and the test piece. A Mass compensation system which will operate at low frequencies is not available commercially and is needed because of the low stiffness of the test pieces used in this work. Operator control over all of the spectrometer's functions is achieved through an interactive microprocessor control system.

2. THE MICROPROCESSOR CONTROLLED DYNAMIC MECHANICAL SPECTROMETER

2.1 General Considerations

Several systems are available commercially for the measurement of the dynamic mechanical properties of resilient materials. The commercial systems investigated included the widely used Rheovibron, manufactured by Toyo Baldwin Ltd, and the DMTA system, availabe from Polymer Laboratories Ltd. Both of these systems suffer from a major (and from a materials scientists standpoint a fundamental) drawback. They can only provide data at a few fixed frequencies with small samples, in the small strain shear deformation mode. The DMTA is convertable to microprocessor control, but is very expensive. The Rheovibron on the other hand has resisted attempts to automate it so far. A better system, from this projects standpoint, is the Dynosat, manufactured by Imass Inc which is capable of continuous operation from 0-200 Hz. This instrument however is only capable of testing small samples under small strain conditions. In addition, the problems associated with using liquid filled samples would be prohibitive.

The lack of available systems prompted the development of the dynamic mechanical spectrometer described here. This system is capable of measuring the mechanical properties of large samples (maximum loaded area > 500 cm^2) under small or large strain conditions. The spectrometer is

capable of operation throughout the frequency range 0.06-100 Hz. Air-filled or liquid-filled test pieces may be used and the system is fully automatic. In addition an automated mass compensation system is included. This facility is not available commercially.

In this chapter the main features of the mechanical spectrometer are described, including the electrical hardware, the sample mounting system and the computer software used to control the instrument. Use is made of a novel measurement algorithm to increase accuracy. This is described, together with an analysis of the effect of random and non-randon noise on the accuracy of the measurements. Finally a section is included detailing the methods used for the testing and calibration of the instrument. Many details of the spectrome ter have had to be omitted from the discussion but more information may by found in the user manual written for the instrument [2]. A description of the dynamic mechanical spectrometer has been published [1].

2.2 The Complete Spectrometer

Figure 2.1 shows in schematic form the layout of the spectrometer. The system is based on commercially available vibration equipment, including an electromagnetic exciter (Bruel and Kjaer type 4801, with general purpose head) and associated power amplifier (B & K type 2707) and exciter control (B & K type 1047). This equipment is designed for operation above 2 Hz, although

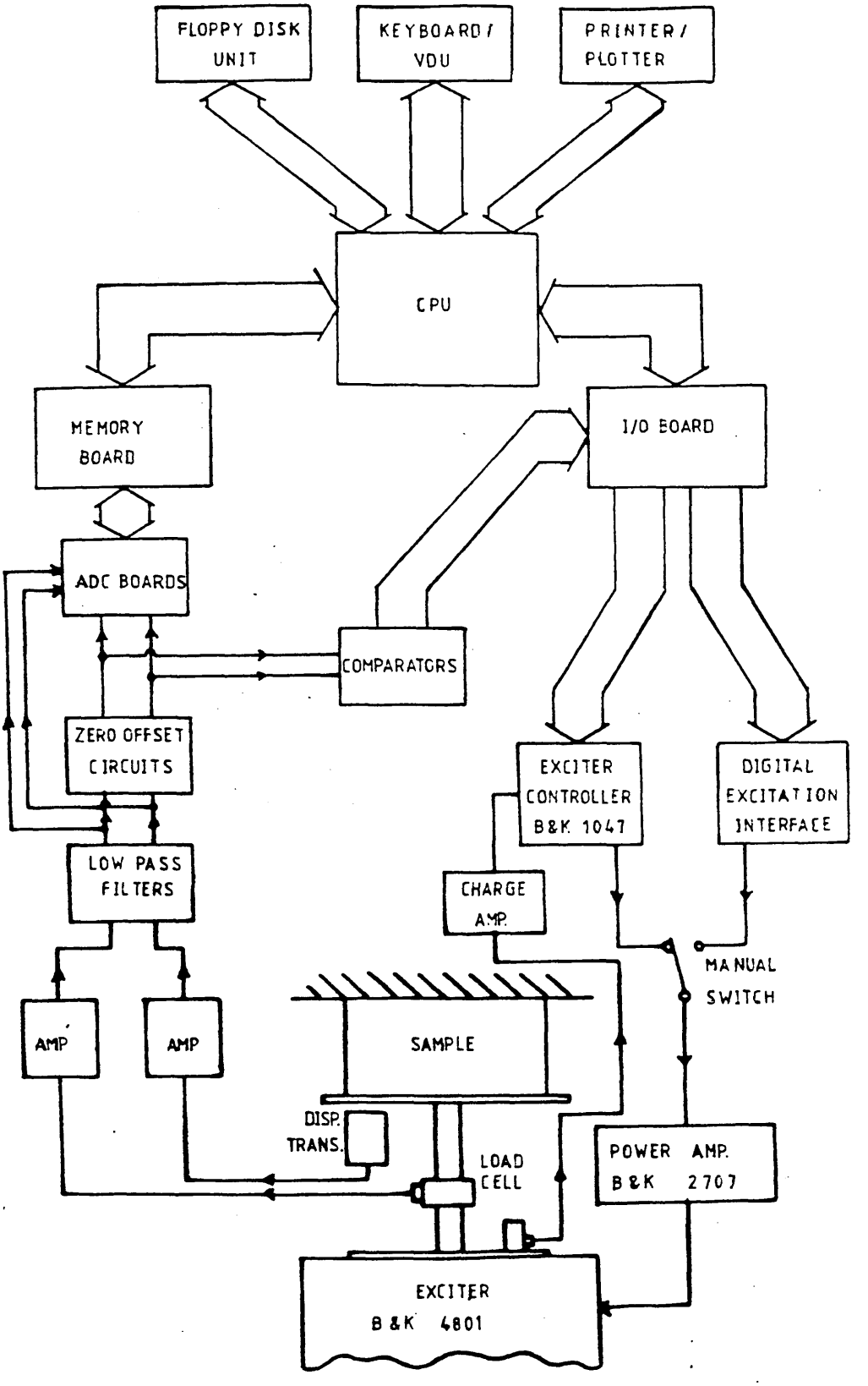

FIGURE 2.1

Schematic layout of the Dynamic Mechanical Spectrometer.

both the exciter and power amplifier will work at reduced specifications down to dc [3,4,5]. For operation at very low frequencies a digital sine wave is produced by the microprocessor control system and output to the exciter via the digital excitation interface. This interface operates in the frequency range 0.06-18 Hz. For frequencies in the range 5-100 Hz the exciter control may be used to generate the exciting signal to the exciter coils.

The computer control system is based on a Nascom III dedicated microcomputer, manufactured by Lucas Logic. The computer has disc storage facilities and is interfaced to an 80 column dot matrix printer (Epsom RX 80) and a Watanabe personal plotter (WX4636). The Nascom III contains several operating systems including a Pascal language compiler and a comprehensive editor/assembler, both of which are disc loaded. The Nascom III uses the versatile Z80A Central processing unit and a total of 48K bytes of dynamic random access memory (RAM) are available. The system clock is 4 MHz.

In order to specify the dynamic mechanical properties of the test piece, two input signals are required. These are the dynamic deformation of the test piece, and the force required to produce this deformation. The control system measures the frequency of operation, the amplitudes of the force and deformation signals and their phase relationship. Because most cellular materials are

highly non-linear the mechanical properties will only be meaningful if they are measured at a constant deformation amplitude throughout the frequency range. The spectrometer provides facilities for compressing the signals to constant displacement amplitude. The amplitude of the dynamic oscillation may be set anywhere in the range 0.01-8 mm, subject to the limitations of the electromagnetic exciter.

The software control system allows the automatic measurement of the dynamic storage modulus and loss tangent throughout the frequency range. Data acquisition and analysis are fully automatic. The results can be stored on floppy disc for future analysis or printout. A special feature of the spectrometer is the availability of automatic mass compensation. For low stiffness test pieces the inertial force generated by the moving elements of the spectrome ter between the sample and the force transducer may mask the behaviour of the test piece at higher frequencies. The mass compensation system allows this contribution to be removed from the data. More details of the algorithm used to achieve this are given in section 2.4.

Appendix I contains a summary of the specifications of the dynamic mechanical spectrometer. Many of the components shown are commercially available and the relevant instruction manuals should be consulted for the microprocessor control system [6,7,8], the Bruel and

Kjaer equipment [3,4,5] and the transducers [9,10,11]. With the exception of the transducers, only the equipment which has been specially constructed or modified for the present application will be discussed.

2.3 The Electrical Hardware

2.3.1 Digital Excitation Output Interface

This interface enables the microcomputer to produce a digital sine wave, with variable frequency and amplitude, to drive the exciter at low frequencies. The sine wave is maintained in memory as a series of 1000 discrete data points which are output to the interface at regular intervals using a counter timer circuit, which produces a CPU interrupt after a programmed time interval. The rate at which the individual points are sent determines the frequency of the resulting signal. The data is delivered to a 12-bit digital to analogue converter (DAC) via two parallel input/output (PIO) ports and results in a sine wave of fixed amplitude. A further DAC (8-bit) is required to specify the amplitude.

Figure 2.2 shows the circuitry used for the digital excitation interface. A single data byte is output to the 8-bit DAC (IC 1) to form a voltage proportional to the required amplitude. This is amplified by IC 2 to produce a dc voltage in the range 0-10 Volts. This voltage forms the reference to the 12-bit DAC (IC 3). Figure 2.3 shows the variation of this reference voltage

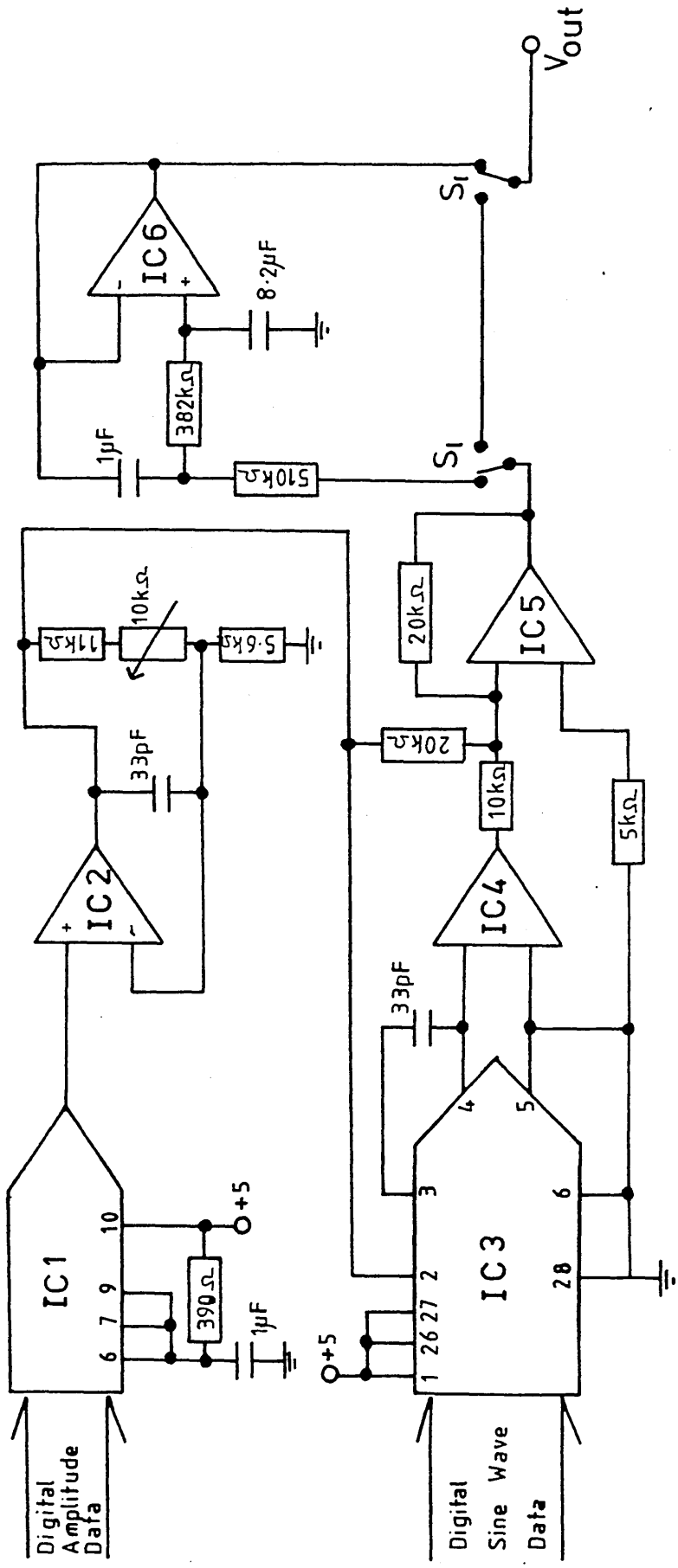

FIGURE 2.2 : Digital Excitation Output Interface.

with the amplitude byte sent from the computer. Linearity is maintained down to very low levels (~100 mV) but distortion of the sine wave was found to occur if reference voltages lower than 150 mV are selected.

The sine wave data is fed into the 12-bit DAC and is converted into a voltage which is determined by the byte sent and the reference voltage selected. IC 4 and IC 5 produce a bipolar output with a maximum amplitude of 10V.

In addition to the circuitry shown in figure 2.2 each operational amplifier has its own recommended offset circuits [13]. The digital to analog converters in use are described more fully in the manufacturers data sheets [14,15].

The resulting signal is not a true sine wave. In fact it is made up of a series of small but discrete steps. A fourier transform of the output signal shows a secondary peak at a frequency determined by the number of data points output per cycle. In the present system this secondary peak occurs at 1 kHz and is 50dB below the main signal. To reduce this further an optional low pass filter is included in the output stage of the interface. With a -3dB point at about 40Hz and an ultimate slope of 6dB per octave, this filter reduces the peak at 1 kHz by a further 27dB. Figure 2.4 illustrates the frequency response of this filter circuit.

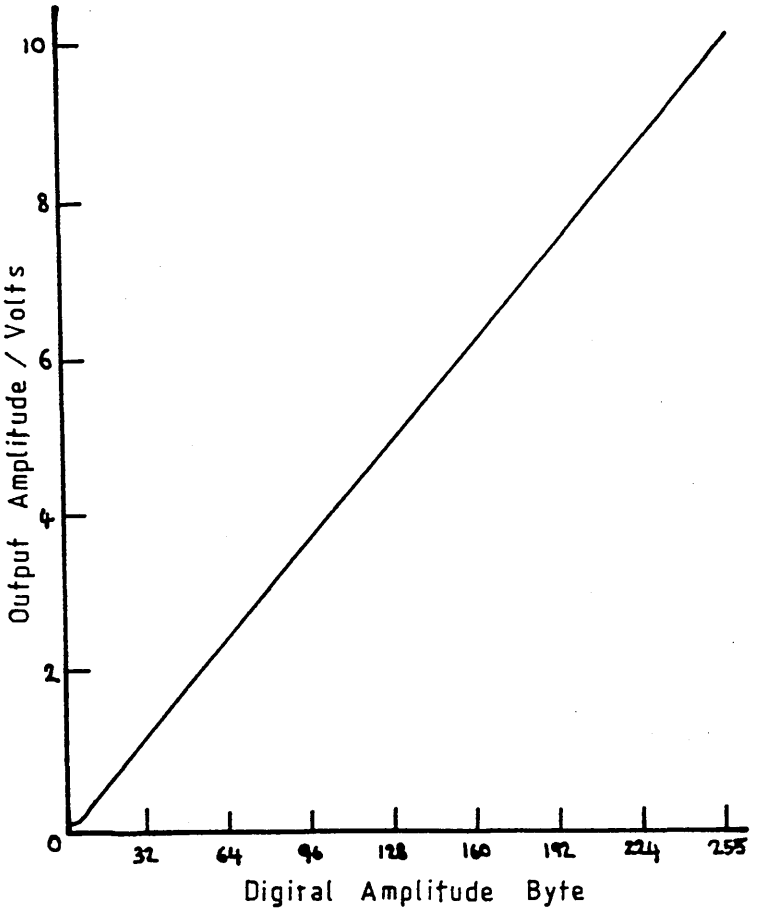

FIGURE 2.3

Output Amplitude vs. Byte Sent to the Excitation Interface.

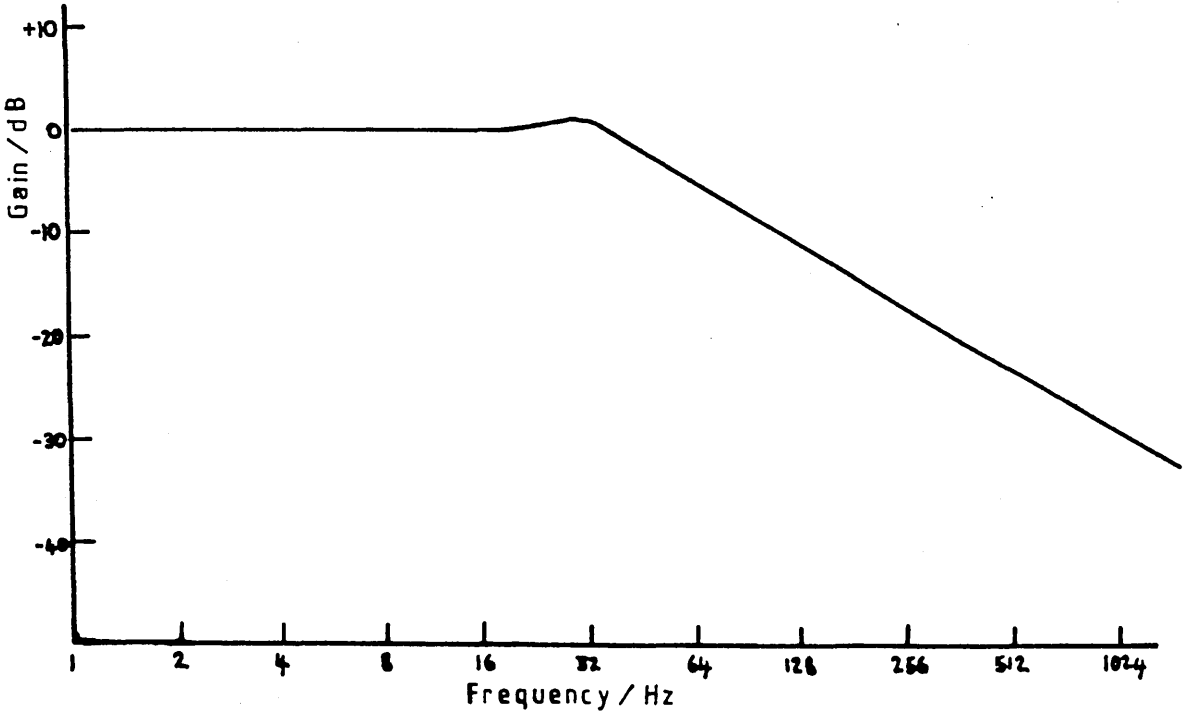

FIGURE 2.4

Frequency Response of the Optional Low Pass Filter.

TABLE 2.1 : PIO Pin assignment

PIO	PORT ADDRESS	BIT	CONNECTION
1A	control: $04 data : $06	7	DISPLACEMENT COMPARATOR
1B	control: $05 data : $07	2 1 0	1047 START DOWNSWEEP PIN START UPSWEEP PIN STOP SWEEP PIN
2A	control: $14 data : $16	7 6 5 4 3 2 1 0	BIT 7 OF SINE WAVE DATA BIT 6 OF SINE WAVE DATA BIT 5 OF SINE WAVE DATA BIT 4 OF SINE WAVE DATA BIT 3 OF SINE WAVE DATA BIT 2 OF SINE WAVE DATA BIT 1 OF SINE WAVE DATA BIT 0 (LSB) OF SINE WAVE
2B	control: $15 data : $17	7 6 3 2 1 0	RL/WR HANDSHAKE LINE RST HANDSHAKE LINE BIT 11 (MSB) OF SINE WAVE BIT 10 OF SINE WAVE DATA BIT 9 OF SINE WAVE DATA BIT 8 OF SINE WAVE DATA
3A	control: $18 data : $1A	7 6 5 4 3 2 1 0	BIT 7 OF AMPLITUDE DATA BIT 6 OF AMPLITUDE DATA BIT 5 OF AMPLITUDE DATA BIT 4 OF AMPLITUDE DATA BIT 3 OF AMPLITUDE DATA BIT 2 OF AMPLITUDE DATA BIT 1 OF AMPLITUDE DATA BIT 0 OF AMPLITUDE DATA

Table 2.1 shows the PIO pin assignment in use. In addition to the 12 sine wave data lines and 8 amplitude data lines, several other lines are used. The two handshake lines attached to bits 6 and 7 of PIO 2 port B are used to pass the sine wave data from the computer to the digital excitation interface.

For analogue signal generation using the exciter control unit, computer control is achieved using the three lines attached to PIO 1 port B. These are connected via transistor interfaces to the rear panel of the exciter control unit [5]. The three lines allow the frequency to be altered by the computer when the exciter control is used to provide the signal to the exciter coils.

2.3.2 Memory Mapped Input ADC Interface

This interface provides a means of taking data into the microprocessor. It is based around two type II04 12-bit analogue to digital (ADC) boards, manufactured by Digital Design and Development Ltd. Each board has a total of eight channels and software programmable gains. Two boards are used so that the displacement and force signals can be sampled at the same time. Six of the eight channels on each board are unused.

The boards have been memory mapped into the Nascom III. Memory mapping is a technique by which the board appears, to the central processing unit (CPU), to act as a block of memory. The CPU can write to and read from the boards using normal memory interrogation instructions. This results in the time required to enter data into the computer being reduced, and simplifies the software.

Details of the type II04 boards are available in the manufacturers instruction manual [16]. In addition to the 8 data lines required by each board (the converted

data is sent to the CPU in the form of two bytes), there are several other lines to provide a link between the board and the CPU. The data lines may be connected directly to the Nascom bus, the other lines require some logic circuits. The input lines required by the II04 boards are:

$\overline{\text{I/O SELECT}}$ - when LOW the board is selected.

$R/\overline{W}$ - when HIGH the CPU may read data from the board. When LOW the board will accept data written to it.

A_0/A_1 - these two lines determine the address on the board being written to or read from. 4 locations are required by each board.

The two boards are inserted into the computer bus in place of one block of RAM. The CPU generates three bus lines which are of interest. These are $\overline{CS}$, $\overline{RD}$ and $\overline{WR}$. In addition 16 address lines are present. Table 2.2 shows the truth table for generating the lines $R/\overline{W}$ and a single $\overline{\text{I/O SELECT}}$ from the CPU lines. The $R/\overline{W}$ line may be connected directly to the $\overline{WR}$ line from the CPU. The boolean algebra to determine $\overline{\text{I/O SELECT}}$ is given by

$$\overline{\text{I/O SELECT}} = A + B.C = \overline{\overline{A}.\overline{B.C}} \qquad 2.1$$

where A, B and C are the three bus lines as shown in table 2.2. Two $\overline{\text{I/O SELECT}}$ lines are required, one for each board. This is achieved by combining the $\overline{\text{I/O SELECT}}$ from equation 2.1 with the address line A_2, from the CPU. Table 2.3 shows the truth table for this. The two boards

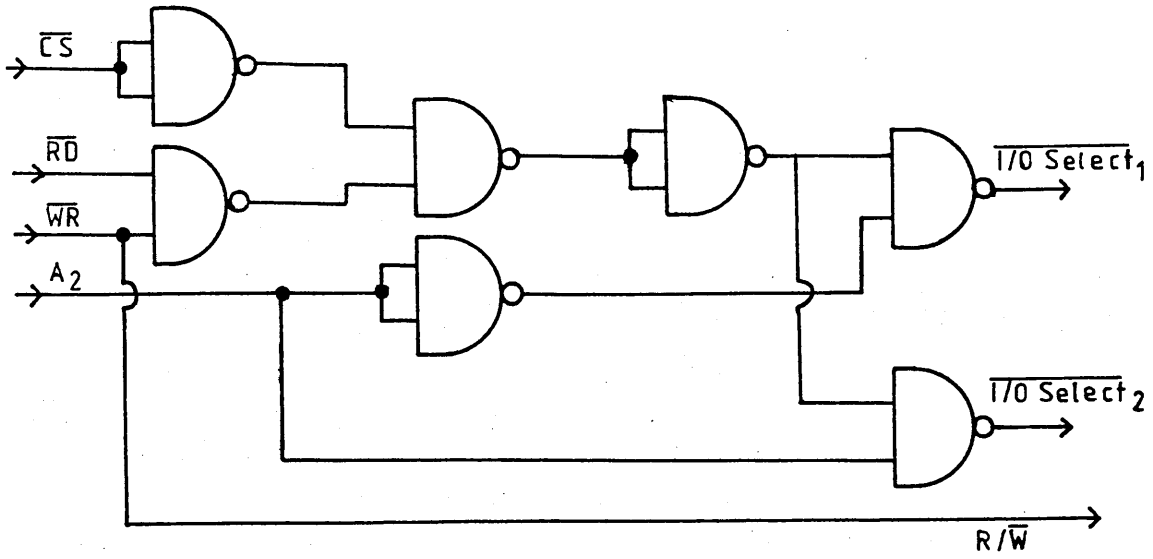

FIGURE 2.5 : Memory Mapping Logic Circuitry.

can never be selected at the same time and the use of the address line A_2 means that they lie in adjacent memory locations.

The logic circuitry required to achieve this is shown in figure 2.5. The signals and data lines are taken from a memory IC socket situated in memory at $B000 to $B3FF (the "$" sign indicates a hexadecimal number). With the logic circuit of figure 2.5 one board will occupy memory locations $B000-$B003 and the other $B004-$B007.

To initiate a conversion a byte is output to the lowest address (base address) of the board. This byte is used to select the channel in use together with the gain to be used. When the conversion is complete the data occupies two nearby memory locations. The displacement signal is

TABLE 2.2 : Truth Table for the Handshake Logic

CPU SIGNALS			BOARD REQUIRED SIGNALS		BOOLEAN ARITHMETIC FOR $\overline{\text{I/O SELECT}}$
A	B	C			
$\overline{CS}$	$\overline{RD}$	$\overline{WR}$	$\overline{\text{I/O SELECT}}$	R/$\overline{W}$	
0	0	0	0	0	A
0	0	1	0	1	A
0	1	0	0	0	A
0	1	1	1	1	B AND C
1	0	0	1	0	A
1	0	1	1	1	A
1	1	0	1	0	A
1	1	1	1	1	A

TABLE 2.3 :Truth Table to produce 2 $\overline{\text{I/O Select}}$ Signals

FROM TABLE 2.2	FROM THE CPU	SIGNALS TO THE II04 BOARDS	
$\overline{\text{I/O SELECT}}$	A_2	$\overline{\text{I/O SELECT}}$ 1	$\overline{\text{I/O SELECT}}$ 2
0	0	1	0
0	1	0	1
1	0	1	1
1	1	1	1

connected to the lower board and the force signal enters the upper board.

2.3.3 Signal Conditioning Circuits

Three circuits assist in passing each signal from the transducer amplifiers to the computer. The circuits employed for each of the input signals are identical in all respects. The low-pass filters and zero-offset circuits provide a means of increasing the signal to noise ratio and removing the unwanted dc component of the force and displacement signals. The comparator circuits, on the other hand, are used to provide a trigger for the microprocessor control system. This trigger informs the control system when to initiate measurements and enables the frequency to be measured. The frequency measurement is insensitive to dc drift of the signals provided that the dc level changes slowly with respect to the oscillatory signal.

Low-Pass Filters

These circuits provide a means of attenuating r.f. noise generated by nearby equipment. They have a cut-off frequency of 500Hz. Figure 2.6 shows the circuits involved. Because an exceptionally flat response is required below the cut-off frequency a multi-stage active filter circuit is used. Figure 2.7 shows the frequency characteristics of the filter. The ultimate slope of the filters is > 30dB/octave. The cut-off frequency is determined by the values of the resistors R_1-R_6 [17].

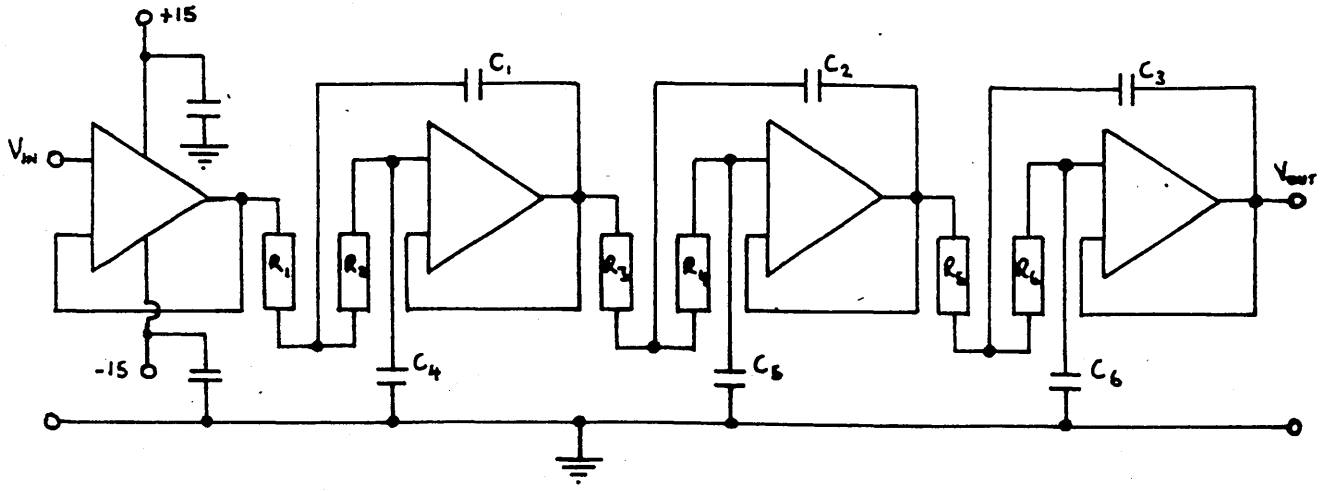

FIGURE 2.6 : Low Pass Filter Circuit.

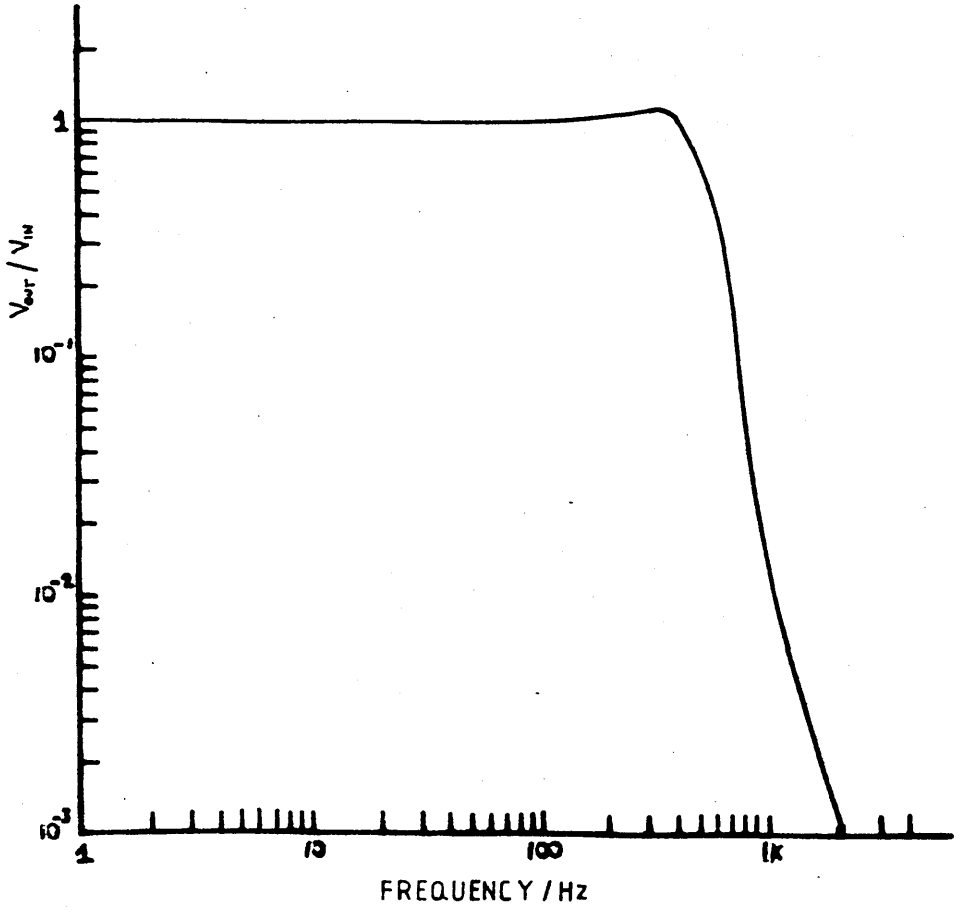

FIGURE 2.7 : Low Pass Filter Characteristics.

Zero-Offset Circuits

The control system incorporates an autoranging system to optimise the conversion accuracy of the II04 boards. This system measures the amplitude of the oscillatory signal and increases the gain as necessary. Any dc level on the signals is not taken into account by the autoranging system and must be removed. Figure 2.8 shows the circuit employed. A negative dc component is added to the signal to offset the dc level from the transducers. The offset voltage may be altered using the cermet trimmer. Facilities for assisting with zeroing the signals are provided in the control system. A residual dc component is permissable, providing it does not exceed 20% of the dynamic signal amplitude.

Comparators

A connection is taken from each input signal to PIO 1 of the computer via a comparator. Table 2.1 gives the PIO pin assignment. The force signal comparator is present only for completeness. It is not used in the present system. The circuit for each comparator is shown in figure 2.9. An operational amplifier is used in the open loop mode. The output of this IC is either +15 or -15 Volts depending on the polarity of the input circuit with respect to the bias level, determined by the potential divider. The transistor on the output reduces the signal to TTL levels. A light emiting diode on the output serves as an indicator to show that the system is triggering correctly. By adjusting the bias voltage, the trigger level may be adjusted.

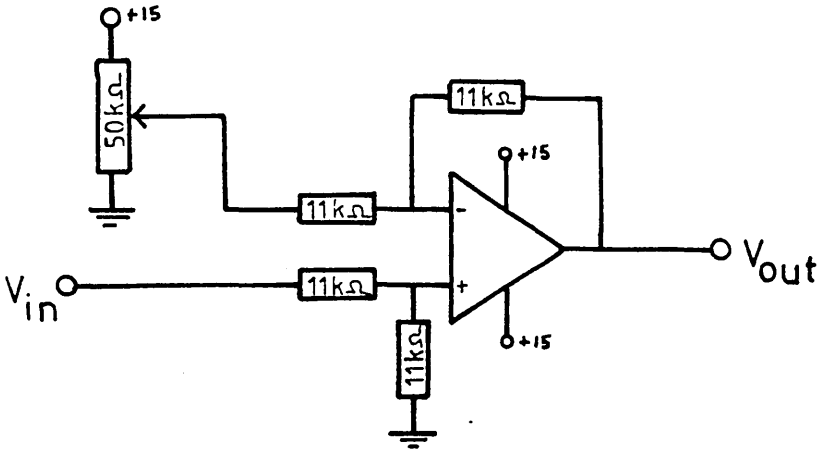

FIGURE 2.8 : The Zero-Offset Circuit.

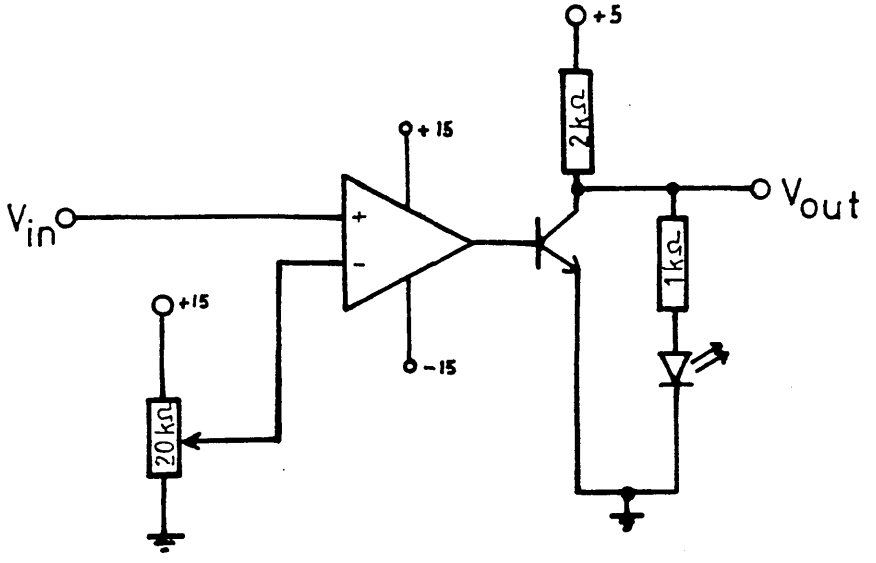

FIGURE 2.9 : The Comparator Circuit.

2.3.4 Transducers

Two transducers are required to specify the mechanical properties of the test piece. These are a sensor measuring the deformation of the sample, and an in-line force transducer. A third transducer shown in figure 2.1 is an accelerometer which is used as part of the exciter control unit's compression loop [5].

Force Transducer

The load cell chosen for this application is a type U2, strain gauge bridge cell manufactured by Hottinger Baldwin Messtechnik GmBH. The conditioning amplifier is a MG 20, also manufactured by HBM. Full details of the transducer and amplifier are given in the manufacturers instruction manuals [9,10].

Strain gauge transducers proved best for this application because of their ability to measure large loads at low frequencies, tolerate high side loads and are insensitive to dc drift. The transducer has a large mass (600g), but the provision of mass compensation facilities reduced the importance of this consideration. The chosen transducer has a full scale measuring range of 2000 N in either tension or compression.

Displacement Transducer

Several transducers were investigated to measure the deformation of the sample. These included accelerometers, linear variable differential transformers (LVDT's) and inductive proximity detectors (IDMS). The

accelerometers proved unsuitable because the level of acceleration at low frequencies is too low. The LVDT is the commonest form of displacement measuring transducer. They have the advantage of frictionless measurement and an essentially infinite resolution. They have several major disadvantages however for the present application. This includes difficulties in mounting on the sample, a low frequency range and residual noise on the output.

A recent advance in the manufacture of IDMS sensors for the Nuclear power industry has resulted in proximity detectors with larger measuring ranges [12]. These transducers work by inducing high frequency eddy currents in a ferromagnetic target. This changes the impedence of the oscillator circuit by an amount which is directly related to the target-sensor gap. The transducer chosen for this application is the I-W-S 20 mm system, manufactured by Dornier GmBH. This type of transducer has the advantage that it is non-contacting, is capable of operation up to high frequencies and is inherantly noise free. In addition any non-conducting material may be placed between target and sensor with no effect on the measurements. The system requires the presence of a ferromagnetic target, although it will work over a smaller measuring range with targets such as aluminium or copper. More details of the I-W-S system may be found in the operating manual [11].

2.4 The Measurement Algorithm

2.4.1 Theoretical Treatment

The system is required to measure the amplitude of the force and displacement signals and the phase difference between them. These signals are essentialy sinusoidal with frequencies in the range 0.07-100 Hz. It was necessary to devise a technique for determining the phase relationship and the amplitudes of each signal, which would function at very low frequencies and which minimised the error due to noise. In this section the basic mathematical method, its realisation as a numerical algorithm and an analysis of the effects of random and harmonic noise are given. The signals of interest are of the form:

$$y(t) = A + B_1 \sin\left[\frac{2\pi t}{T} + \delta_1 \right] \qquad 2.2$$

where A, B_1 and δ_1 are time independent constants and T is the period of the waveform. The following half period integrals may be defined:

$$I_i = \int_{iT/4}^{(i+2)T/4} y(t)\,dt \qquad i = 0,1,2,3 \qquad 2.3$$

and it may be shown that

$$\psi_1 = I_0 - I_2 = \left(\frac{2TB_1}{\pi}\right)\cos(\delta_1)$$

$$\psi_2 = I_3 - I_1 = \left(\frac{2TB_1}{\pi}\right)\sin(\delta_1) \qquad 2.4$$

The amplitude and phase may be written in terms of ψ_1 and ψ_2 as

$$B_1 = \frac{\pi}{2T}(\psi_1^2 + \psi_2^2)^{1/2} \qquad 2.5$$

$$\delta_1 = \tan^{-1}(\psi_2 / \psi_1) \qquad 2.6$$

Hence evaluating the four integrals in 2.3 allows the direct determination of B_1 and δ_1 and the result is independent of the dc component in the signal. The method has the advantage that it considerably reduces the effect of any random noise which has a characteristic time much less than T. However the method does depend upon the signal being mainly sinusoidal and of known frequency. The errors introduced by failure of these assumptions are analysed in section 2.4.3.

2.4.2 Numerical Methods

The input signals under consideration are taken into the computer in the form of N+1 points sampled at fixed time intervals, t_s, and covering one complete period. Figure 2.10 illustrates one input signal and defines many of the parameters to be used. The time period, T, of the signal has been measured previously and is given by

$$T = Nt_s + \Delta T_1 \qquad 2.7$$

where $-\frac{t_s}{2} \leq \Delta T_1 \leq \frac{t_s}{2}$

The four integrals are evaluated for the force and displacement signals by sampling the two waveforms

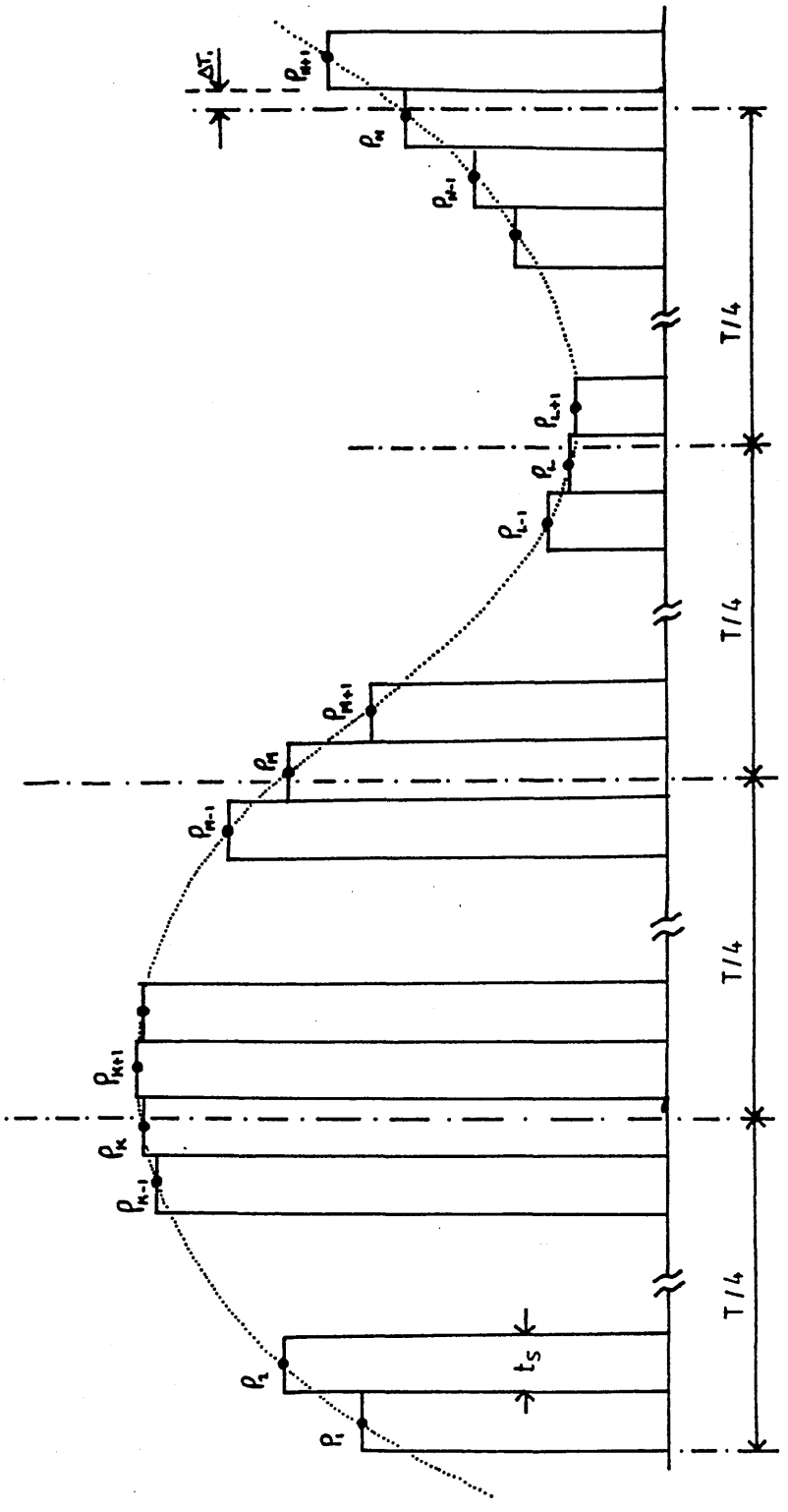

FIGURE 2.10 : Numerical Sampling of the Input Signals.

simultaneously at regular intervals throughout a cycle. The number of samples taken per cycle was fixed at 500 below 13Hz and decreased to approximately 64 at 100Hz. The amplitudes of the two waves and their phase difference is independent of the starting time of the sampling

The integrals I_i are estimated from appropriate sums of the sampled data with interpolated corrections to allow for the discrete nature of the sums. Four summations are made, each covering one quarter of one complete period

$$S_1 = t_s \sum_{q=1}^{K} P_q$$

$$S_2 = t_s \sum_{q=K+1}^{M} P_q$$

$$S_3 = t_s \sum_{q=M+1}^{L} P_q$$

$$S_4 = t_s \sum_{q=L+1}^{N} P_q \qquad 2.8$$

where P_q is the q'th sampled data point. K,L and M are as shown on figure 2.10 and are given by

$$K = \text{int}[\ (T/4 + t_s/2)/t_s\ ]$$
$$M = \text{int}[\ (T/2 + t_s/2)/t_s\ ]$$
$$L = \text{int}[\ (3T/2 + t_s/2)/t_s\ ] \qquad 2.9$$

For simplicity a fifth integral, I_t, is defined as the integral over one complete cycle. In addition to the summations, corrections are made to each integral to account for the discrete nature of the signals. It can be shown that the integrals, I_t, I_0 and I_2, will take the

form

$$I_t = S_1 + S_2 + S_3 + S_4 + \tfrac{1}{2}(T - t_sN).[P_N + P_{N+1}]$$

$$I_1 = S_1 + S_2 + \tfrac{1}{2}(T/2 - t_sM).[P_M + P_{M+1}]$$

$$I_3 = S_2 + S_3 + \tfrac{1}{2}(T/2 - t_sK).[P_K + P_{K+1}]$$

$$\ldots + \tfrac{1}{2}(3T/2 - t_sL).[P_L + P_{L+1}] \qquad 2.10$$

The integral sums ψ_1 and ψ_2 can now be defined as

$$\psi_1 = 2I_1 - I_t \qquad 2.11$$

$$\psi_2 = 2I_3 - I_t \qquad 2.12$$

From equations 2.5 and 2.6 the amplitude, B_1, and phase, δ_1, of each signal can be calculated. By subtracting the phases calculated for the two signals, their phase relationship may be found.

2.4.3 Errors arising in the Algorithm

The principal sources of error in this method arise from (i) harmonic distortion in the measured waveforms (ii) mains noise and (iii) errors in the period over which samples are taken. The size of the error due to harmonic distortion may be estimated by considering the waveform to be periodic in T and of the form:

$$y(t) = A + \sum_{m=1}^{\infty} B_m \sin\left[\frac{2\pi mt}{T} + \delta_m\right]$$

It can be shown that

$$\psi_1 = \sum_{m \text{ odd}} \frac{2TB_m}{\pi m}\cos(\delta_m) \qquad 2.13$$

$$\psi_2 = \sum_{m \text{ odd}} \frac{2TB_m}{\pi m}\sin(\delta_m).(-1)^{(m-1)/2} \qquad 2.14$$

It can be seen from equations 2.13 and 2.14 that even harmonics do not contribute to ψ_1 and ψ_2. A Fast Fourier Transform of typical measured waveforms shows that the third harmonic was always more than 44dB below the driving frequency and the fifth and higher harmonics were insignificant. Using equations 2.13 and 2.14 this can be shown to lead to a maximum error of approximately 0.2%.

The exciter used in the system generates mains related noise at freqencies of 50 and 100 Hz. These signals were 40dB and 35dB below the driving signal respectively. In this case the above analysis can be repeated by assuming a signal of the form

$$y(t) = Cm\sin[100\pi t + \delta m] + Cn\sin[200\pi t + \delta n]$$

where Cm and Cn are the amplitudes of the 50 Hz and 100 Hz contributions respectively. It can be shown that

$$\psi_1 = \frac{C_m}{50\pi}\left\{\cos\delta_m - \cos[50\pi T + \delta_m]\right\} + \frac{C_n}{100\pi}\left\{\cos\delta_n - \cos[100\pi T + \delta_n]\right\} \qquad 2.15$$

$$\psi_2 = \frac{C_m}{50\pi}\left\{\cos[25\pi T + \delta_m] + \cos[75\pi T + \delta_m]\right\} + \frac{C_n}{100\pi}\left\{\cos[50\pi T + \delta_n] - \cos[150\pi T + \delta_n]\right\} \qquad 2.16$$

From equations 2.15 and 2.16 it can be seen that the contribution from 50 Hz and 100 Hz signals will be frequency dependent. The maximum contribution to the integral sums from mains noise sources is given by

$$\pm \frac{2C_m}{50\pi} \cos \delta_m \pm \frac{2C_n}{100\pi} \cos \delta_n \qquad 2.17$$

This can be shown to contribute at most a 2% error to the results. This contribution depends upon the driving frequency and in general the error will be much less than 2%.

The algorithm also depends upon the period of oscillation being known. Errors in the measurement of the period will be reflected in errors in the measured values for the amplitude and phase. These errors can be evaluated using signals of known amplitude and phase and forcing the system to sample at the wrong rate. Figure 2.11 shows the results of such experiments. The maximum error in the period of oscillation is 1% and hence this will contribute at worst 1% to the measurement of amplitude and phase.

2.4.4 Mass Compensation System

Figure 2.12 shows the relationship between the applied deformation, $\underline{X}_o$ and the total force measured by the spectrometer, $\underline{F}_t$. The total force is made up of the force generated by deformation of the test piece, $\underline{F}_s$ and an inertial force $\underline{F}_m = -\omega^2 M \underline{X}_o$ produced by the moving mass elements of the equipment between the force transducer

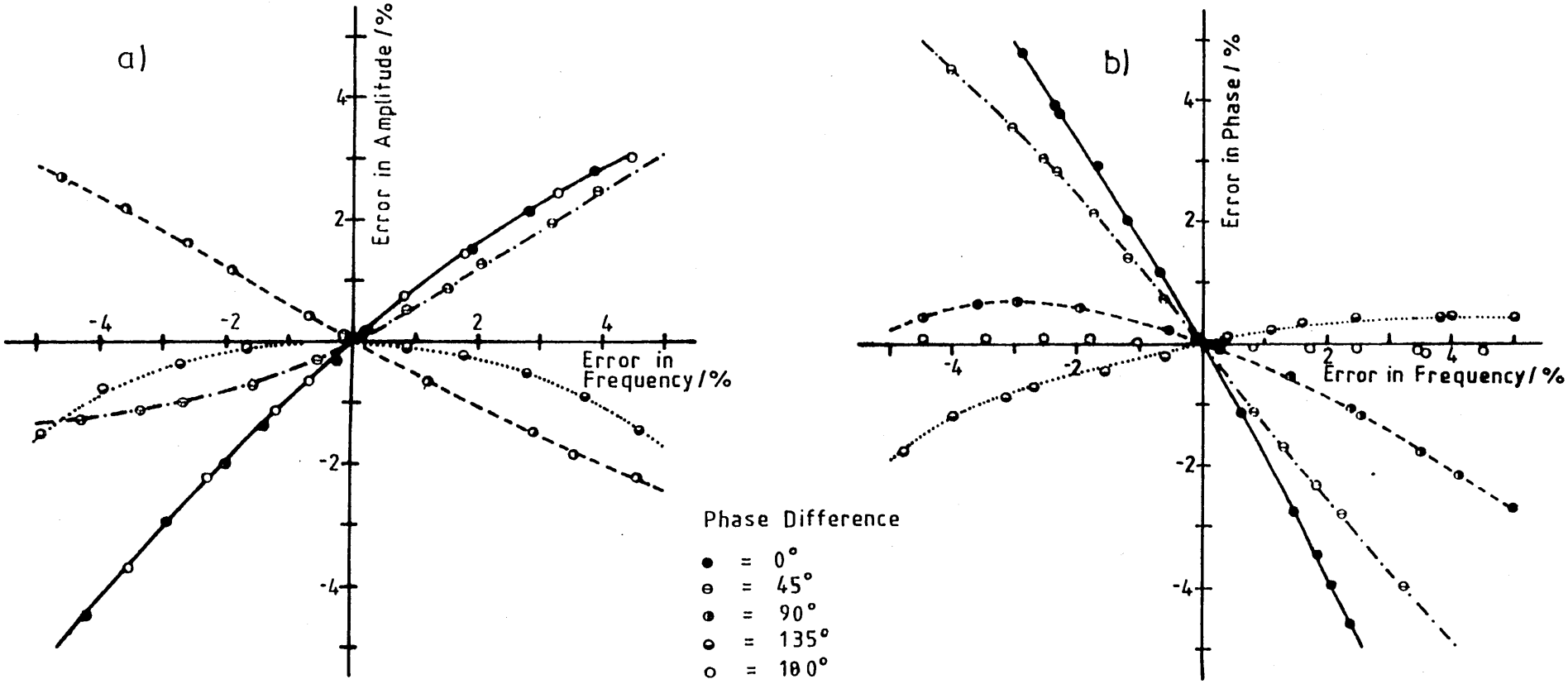

FIGURE 2.11

The Error in a) the Measured Amplitude of the Force Signal and b) the Measured Phase Difference Plotted Against the Error in the Frequency.

and the sample. At high frequencies the size of the inertial force may be similar to or greater than the force generated by deformation of the test piece so that mass compensation is needed when testing low stiffness specimens ($E'(\omega) \sim 10^5$ Pa). The total force measured by the spectrometer, $\underline{F}_t = \underline{F}_s + \underline{F}_m$, must be corrected for mass effects in order to extract the $\underline{F}_s$ signal. This is illustrated in figure 2.13 which shows a set of results for an air-filled sample of a conventional type polyurethane foam before mass compensation.

For the spectrometer several digital procedures have been devised to extract the storage modulus, $E'(\omega) = k|\underline{F}_s|/|\underline{X}_o| \cos\Theta$ and damping, $d(\omega) = \tan\Theta$, where k is a constant related to the sample dimensions. The most successful of these uses data measured without a sample in place to determine $\underline{F}_m$ due to the mass of the moving components alone. A typical example of a measurement of this type is shown in figure 2.14. The inertial force vector, $\underline{F}_m$ generated by such a mass is then subtracted numerically from the results taken with a sample in place. Mass compensation is performed at all frequencies although it only becomes significant with the test pieces in use at present, at frequencies above about 5Hz. Figure 2.15 shows the same results as figure 2.13 after mass compensation has been acheived.

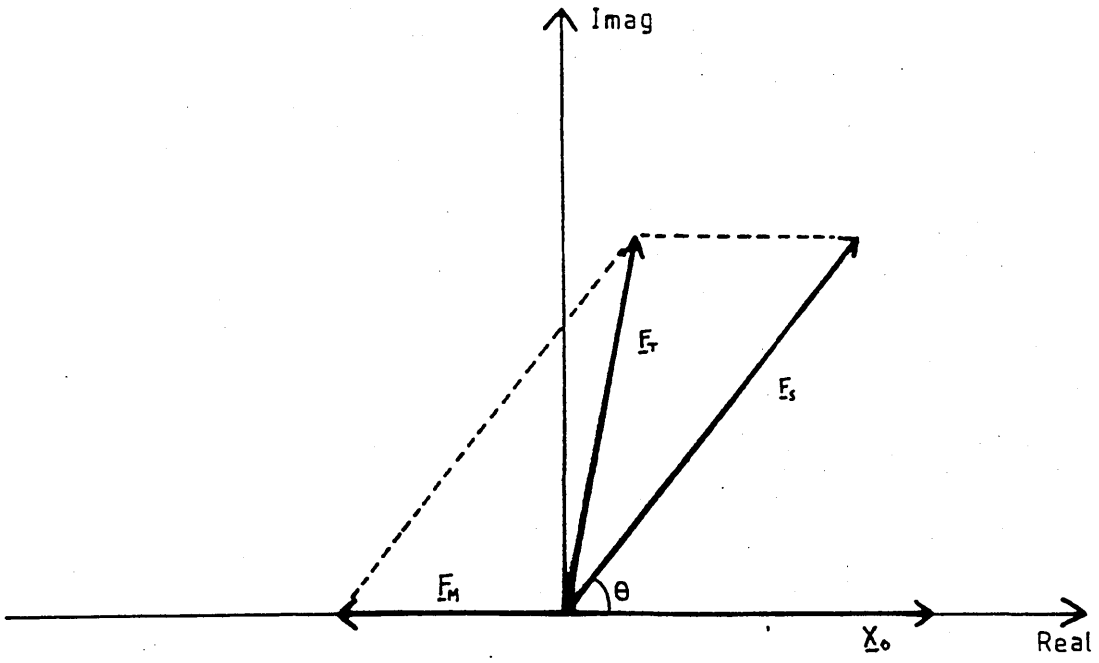

FIGURE 2.12

Vector Diagram of the Forces Involved During Dynamic Deformation of a Low Stiffness Flexible Material.

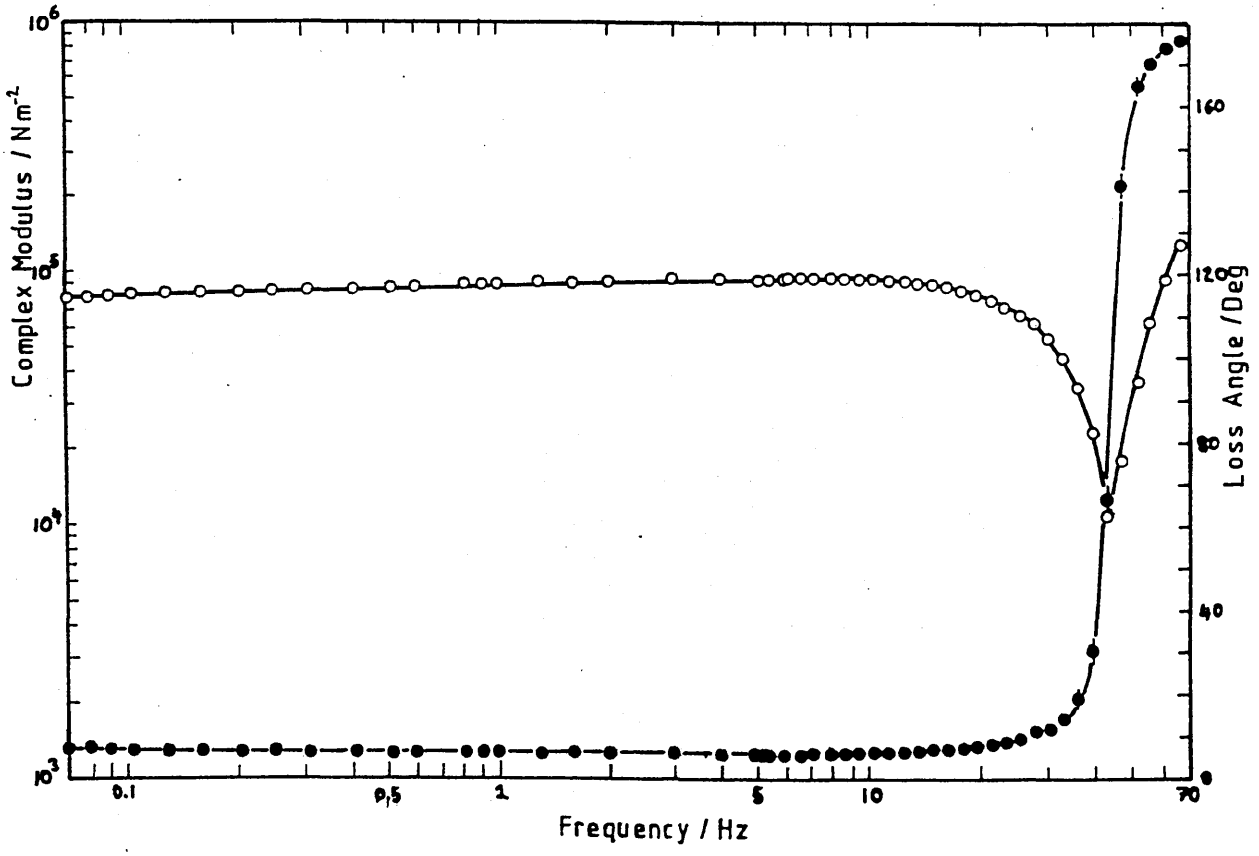

FIGURE 2.13

Variation of $E^*(\omega)$,(○) and θ,(●) with ω for a Flexible PU Foam Before Mass Compensation.

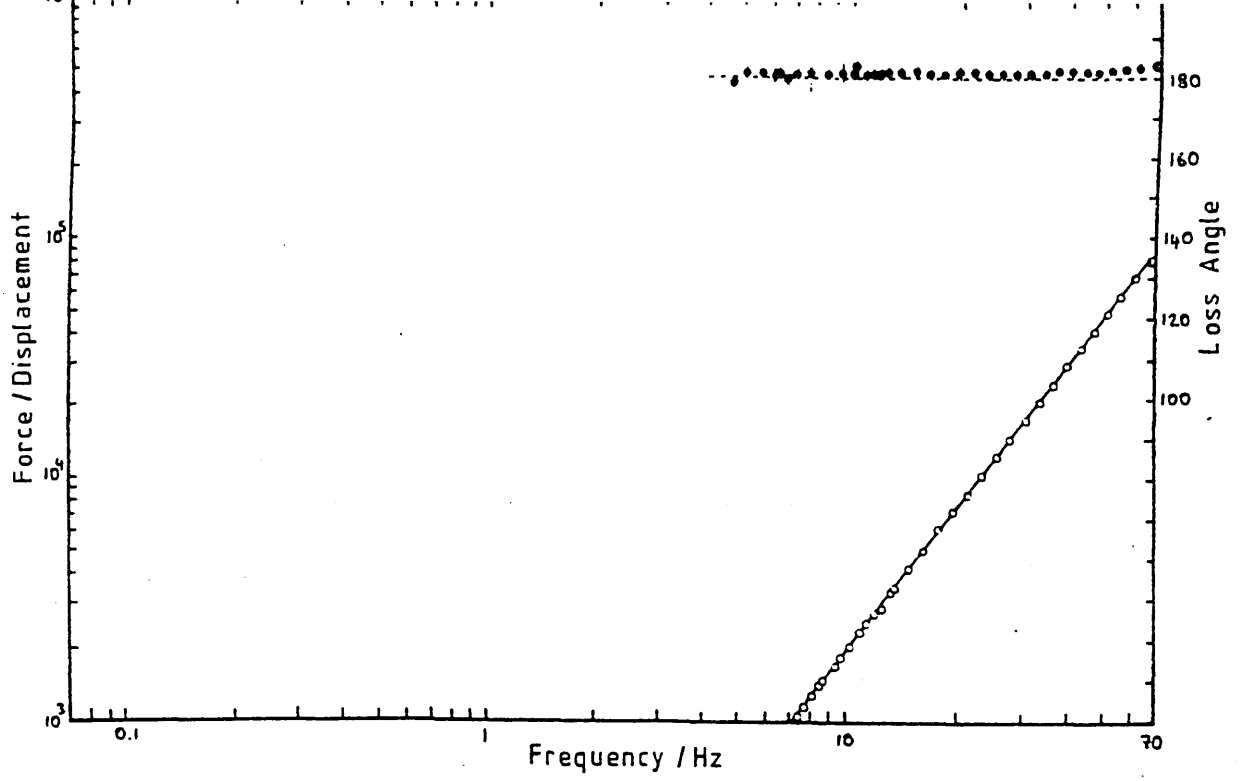

FIGURE 2.14

Typical Measurement Series with No Sample in Place.

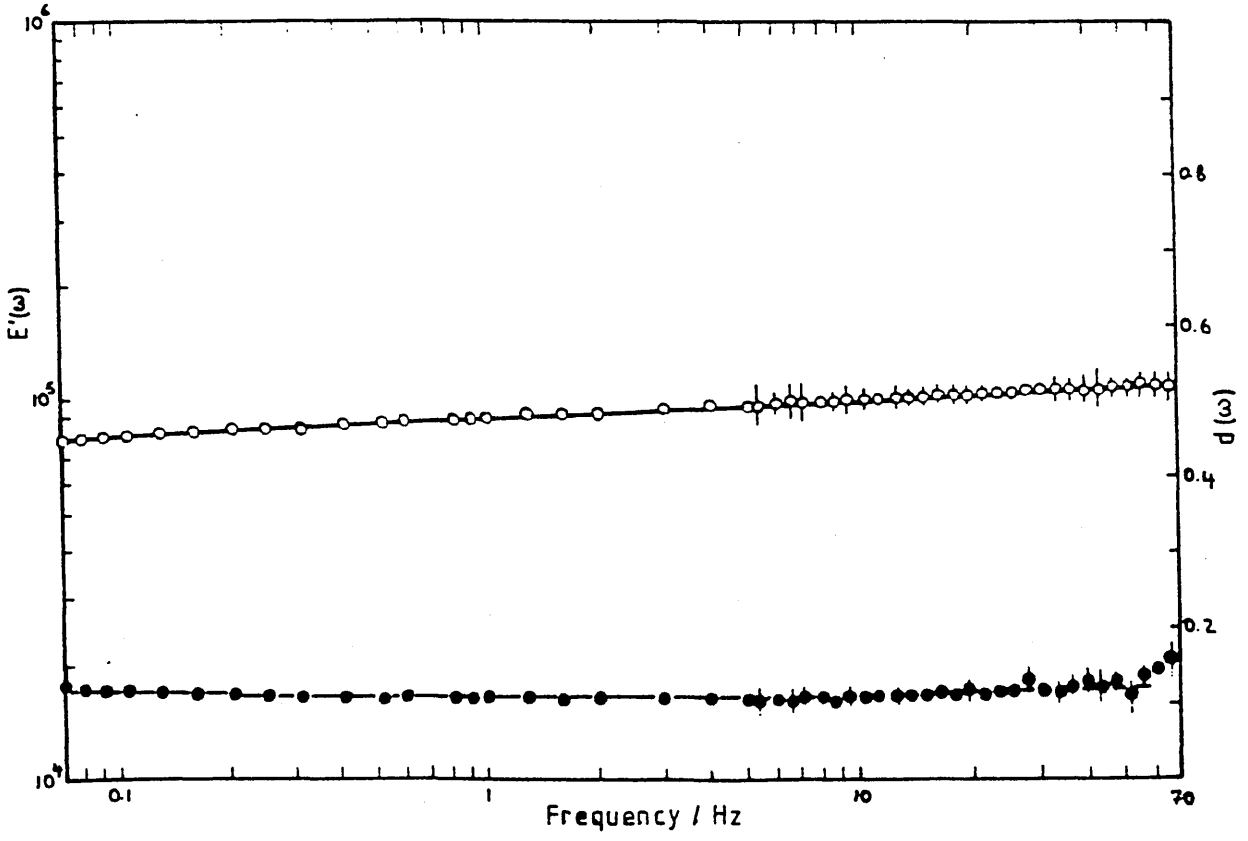

FIGURE 2.15

Variation of E'(ω), (open circles) and d(ω), (closed circles) with frequency for the Data of Figure 2.13 After Mass Compensation.

2.5 The Control Software

2.5.1 Program Structure

The spectrometer interacts with the user via a series of menus. Each menu provides commands relating to a particular aspect of the operation of the system. These menus allow easy access to all of the major system functions and make the spectrometer both interactive and easy to use. The relationship between the menus is shown in figure 2.16 together with the character commands used to move from one to another. Those lines shown broken in figure 2.16 require intermediate disc storage for the results.

The control software is written in two languages to optimise speed and memory requirements. All data acquisition and interface control routines are written in assembled Z80 machine code, wheras data analysis, storage, manipulation and display routines are written in compiled Pascal. In addition, user interaction via the menu system is incorporated into the high level programs.

Because of space constraints within the memory of the Nascom III, the control system is formed from three high level programs. 'CONTROL' is responsible for all data collection and immediate analysis. The zero and calibration program 'CALIBRAT' is used for setting up the system for a measurement series, while 'ANALYSIS' is responsible for off-line analysis and display of the

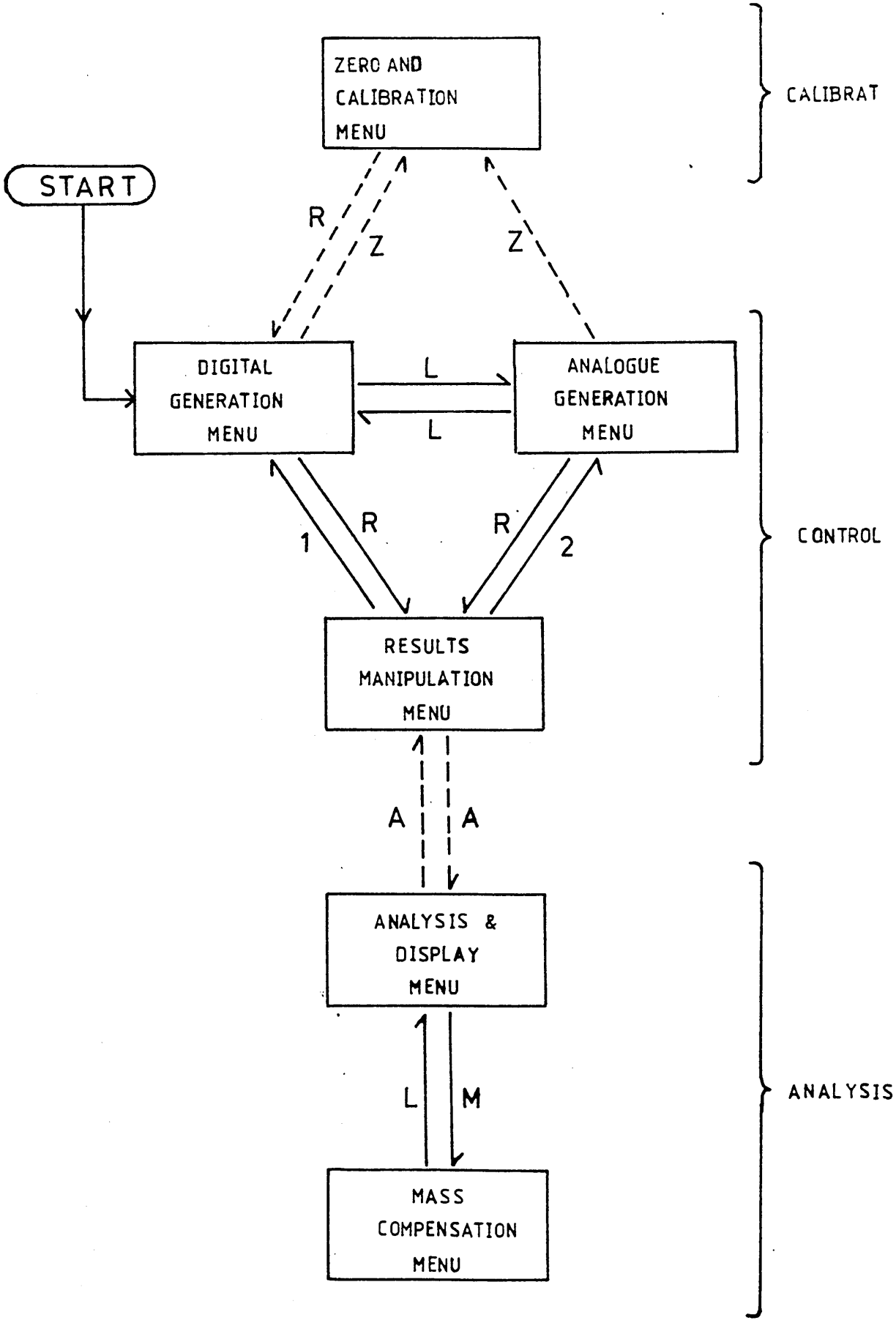

FIGURE 2.16
Relationship Between the Menus and the High Level Programs.

results. The relationship between each of these programs and the menu system is shown in figure 2.16. The computer will automatically load and execute the relevant program when required. Several other programs have been written to perform specialised analysis and display functions [2]. This library of support programs will not be discussed here.

The software system relies heavily on the facilities provided by the operating systems in the Nascom III. For more details the literature available with the equipment should be consulted [6,7,18,19,20,21]. A basic understanding of Pascal and assembly language programming has been assumed. Many textbooks on these languages have been published [22,23,24].

Listings of the spectrometer software are given in the appendices. Appendix II contains the Pascal source text for the three programs; CONTROL, CALIBRAT and ANALYSIS. Appendix III holds the flow charts, and appendix IV an assembler listing of the machine code routines.

2.5.2 High Level Data Analysis

In this section the main data analysis fuctions performed by the high level program CONTROL are described. These include amplitude and phase difference calculation, autoranging and the compression system. Each function takes up the major part of a procedure in the complete program (see appendix II). The relevant procedures are:

AMPLITUDES : amplitude and phase calculation.

AUTORANGE : autoranging system.

ANALYSIS B : autoranging, compression and averaging.

In the complete software system the first two procedures are nested in the third. On initiation of a measurement the ANALYSIS B procedure is called, which then calls AMPLITUDES and AUTORANGE as required. Several minor procedures are called by these main ones during execution. For simplicity these will not be discussed here. Figures 2.17-2.19 show flow charts of the three main data analysis procedures.

The Amplitudes Procedure

This procedure initiates a measurement via the machine code routines described in the next section. From the tables of data generated the amplitude of each signal is computed (in volts), together with the phase difference (in radians) and the signal period (in seconds). The gain of the input boards is automatically taken into account when the calculations are made. The software follows closely the algorithm outlined in section 2.5. By testing the sign of the integral sums ψ_1 and ψ_2 defined in equation 2.4, phase differences in the range $0-2\pi$ can be detected. Figure 2.17 shows the flow chart for this procedure.

The Autorange Procedure

After the first execution of AMPLITUDES control is passed to this procedure. At the start of each measurement the programmable gains of the input boards is set at an

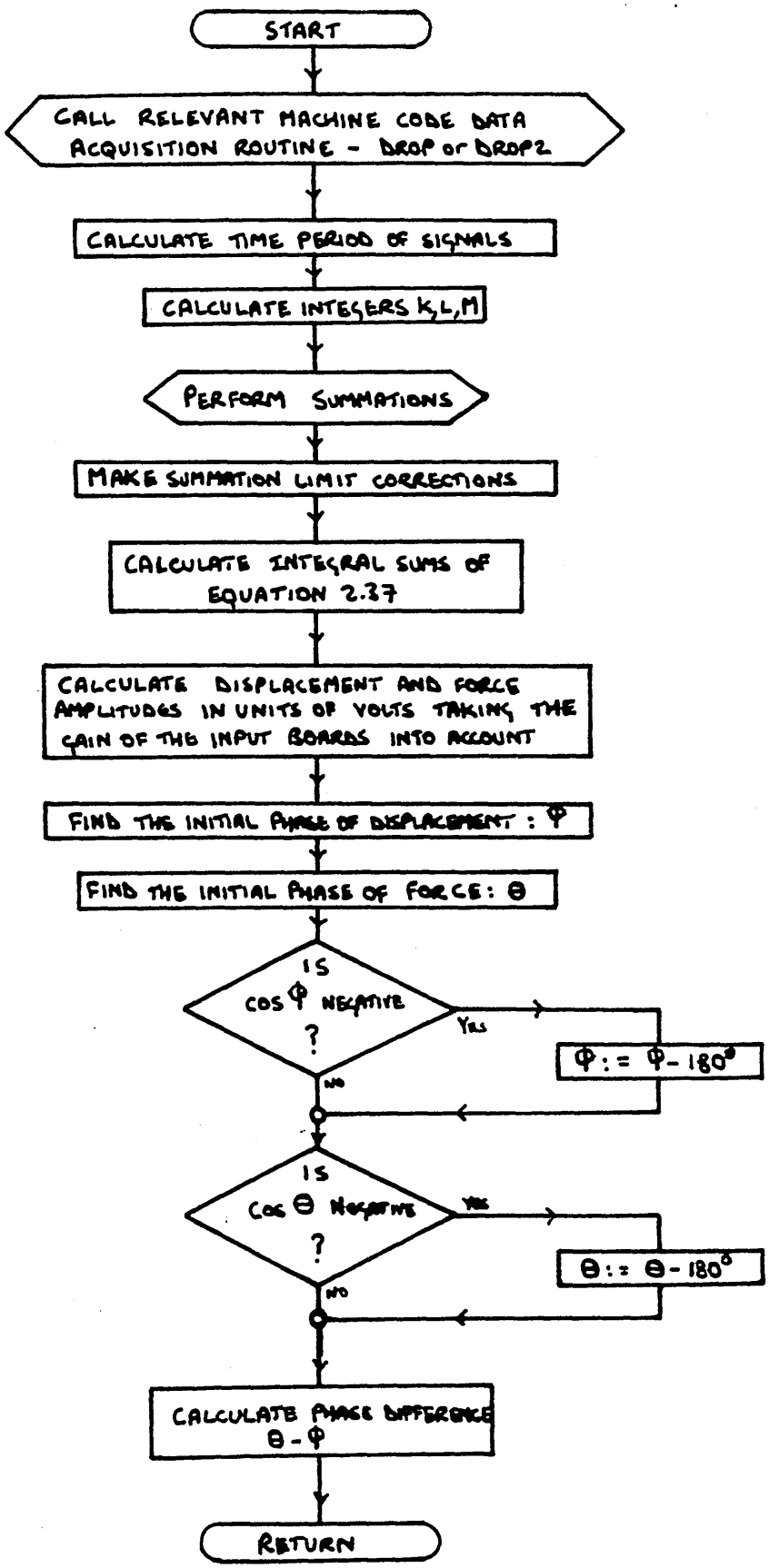

FIGURE 2.17

Simplified Flow Chart for the Amplitudes Procedure.

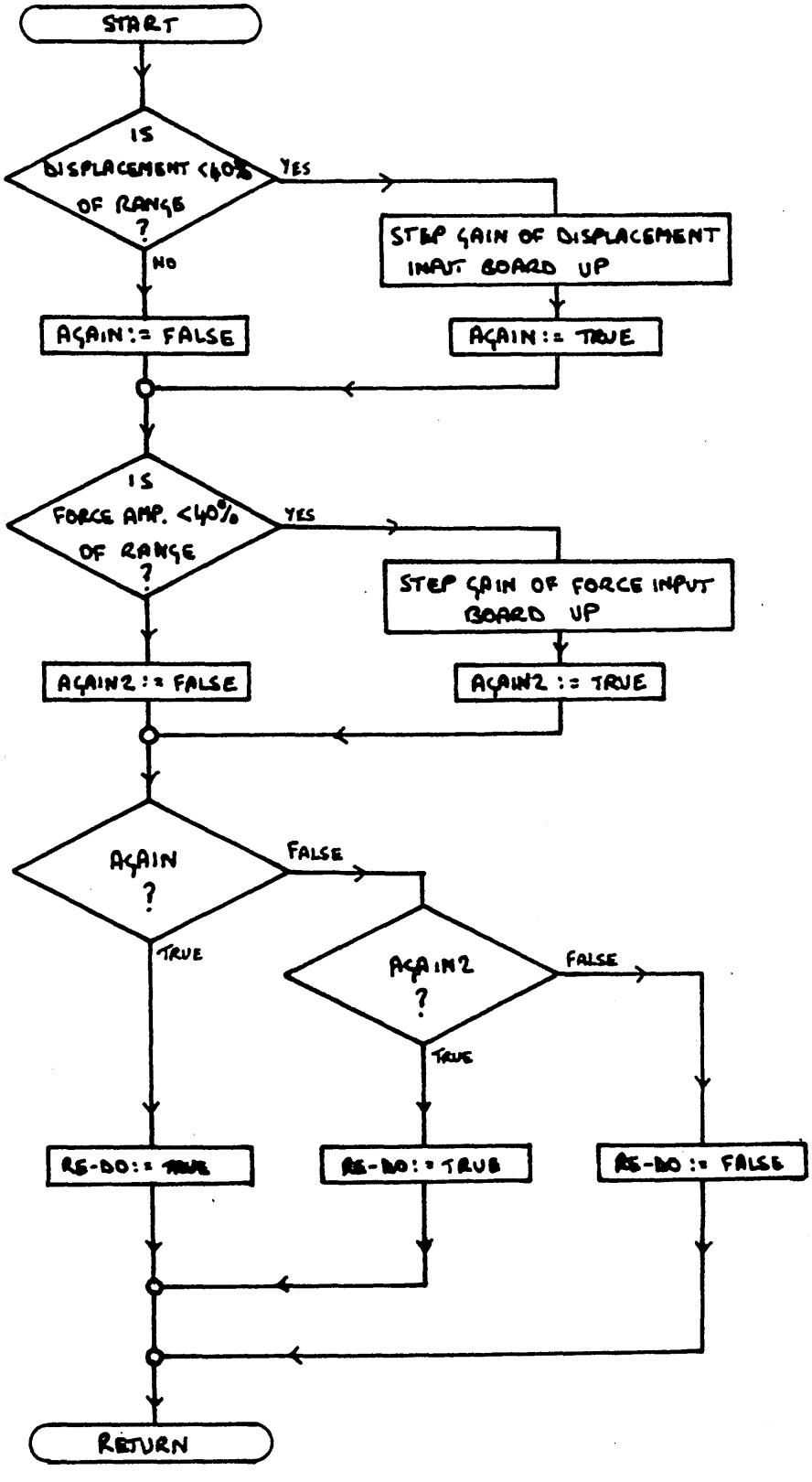

FIGURE 2.18
Simplified Flow Chart for the Autorange Procedure.

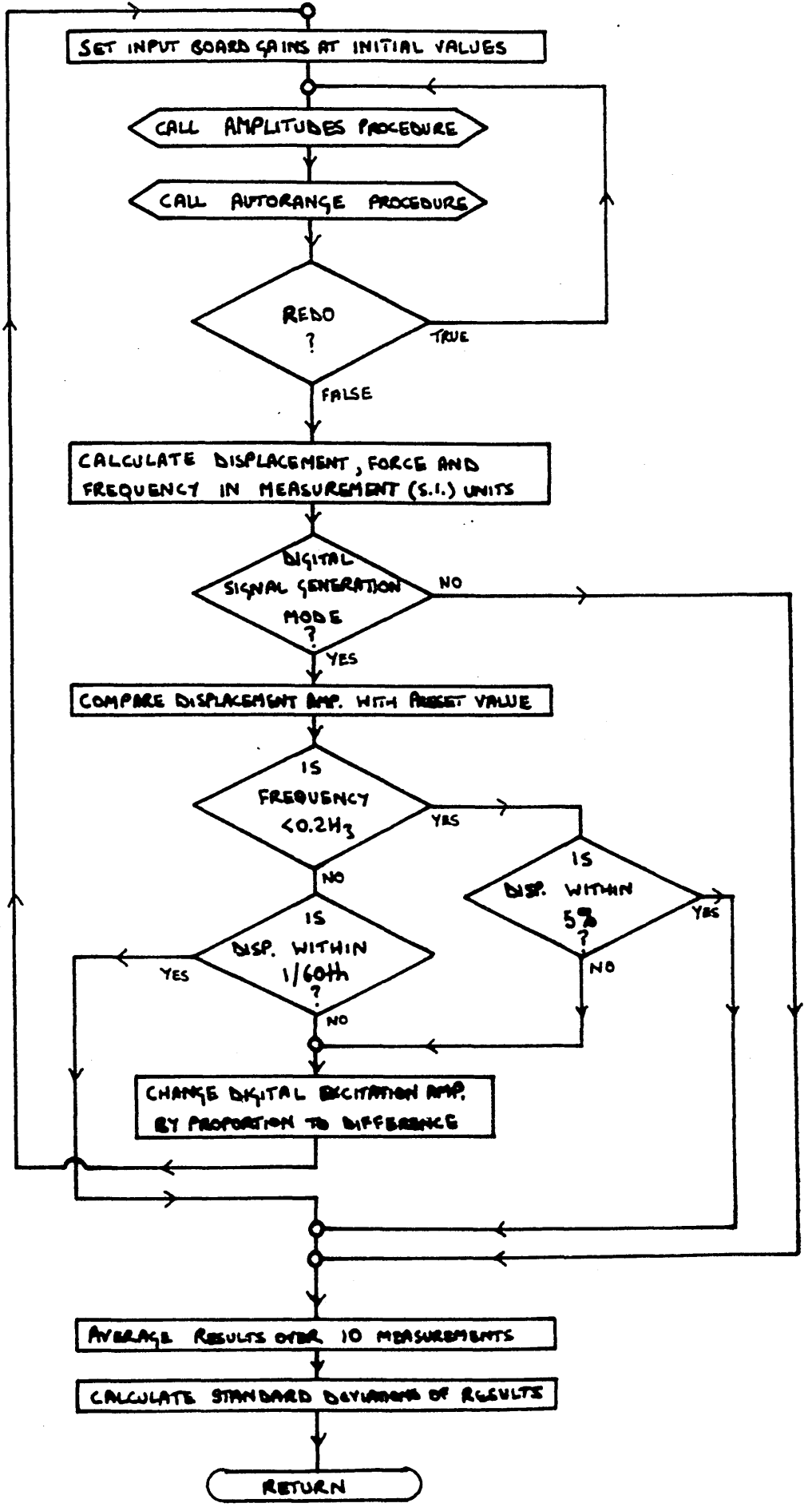

FIGURE 2.19
Simplified Flow Chart for the Analysis B Procedure.

initial value (fixed from the menus). This procedure increases the gain of each board individually in order to optimise the 12-bit accuracy of the analogue to digital conversion. The gain of a board is doubled if the dynamic component of the signal covers less than 40% of the available converter range, to a maximum gain of x128. Figure 2.18 shows the flow chart for this procedure. Autoranging is achieved by repeatedly executing the AMPLITUDES and AUTORANGE procedures until either the signal covers more than 40% of the conversion range, or the maximum gain is set.

The Analysis B Procedure

Figure 2.19 shows the flow chart for this procedure. The execution falls into three parts. Firstly the signals are autoranged by execution of the two procedures described above. The amplitude of the displacement signal is then altered to match the preset level selected by the operator. When the excitation signal is provided by the exciter control unit, this facility is provided by the exciter control's compression system. If the excitation signal is produced digitally then the amplitude of the resulting deformation is compared with the required value. The amplitude of the excitation signal is altered accordingly. After adjustment the program loops back to the begining of the procedure and re-executes the autoranging section. By repeated execution the deformation amplitude approaches the preset level. At frequencies below 0.2 Hz the tolerance is set at 5% of the preset level. For frequencies above this

the amplitude will be set to within 0.01mm of the target value.

Once the compression has been completed the program averages the results over ten measurements. The standard deviation of each parameter about the mean value is recorded to provide a measure of the accuracy of the measurement. Standard deviations of about 1-2% are normal. Finally control is passed back to the main program for display and storage of the results.

2.5.3 Machine Code Routines

The machine code routines split into three types. These are i) initialisation ii) data acquisition and iii) interface control. The third section includes digital signal generation. A listing of the machine code routines is given in appendix IV. The flow charts for each routine are also included, in appendix III. The data is transferred between the machine code routines and the high level programs by two tables; the results table at $A010-$AFFF, which contains the measured data points, and the data table at $96D0-$9700 which holds several single byte values. The various locations in the data table are defined in table 2.4 while table 2.5 outlines the memory map of the Nascom III when loaded with the relevant control software.

Initialisation is performed by the routine INIT which configures the PIO ports and initialises the data table.

TABLE 2.4 : Definition of the data table locations

LOCATION (HEX)	NAME	NO OF BITS	CONTENTS
96D0	$AMPLOC	8	SINE WAVE AMPLITUDE
96D2	$BOGAN	8	DISP. INPUT BOARD GAIN
96D4	$B4GAN	8	FORCE INPUT BOARD GAIN
96D6	$SINPON	16	SINE WAVE POINTER
96D8	$TDELAY	8	SWEEP PERIOD
96E0	$SINTIM	8	SINE WAVE CTC TIME CONST
96E2	$TIMLOC	8	DATA ACQUISITION CTC TIME CONSTANT
96E4	$SINCON	8	SINE WAVE CTC CONTROL WORD
96E5	$TIMCON	8	DATA ACQUISITION CONTROL WORD
96E6	$TOTREM	16	TOTAL CTC REMAINDER
96E8	$TOTSAM	16	TOTAL NUMBER OF CTC ZERO COUNTS
96EA	$SAMLOC	16	NO OF ZERO COUNTS/CYCLE
96EC	$REMLOC	8	CTC REMAINDER/CYCLE
96ED	$CORLOC	16	INTERMEDIATE STORAGE LOC
96F0	$PIOBIV	16	PIO INTERRUPT JUMP ADDRESS
96F8	$CTC0IV	16	CTC Ch 0 INTERRUPT ADDRESS
96FA	$CTC1IV	16	CTC Ch 1 INTERRUPT ADDRESS
96FC	$CTC2IV	16	CTC Ch 2 INTERRUPT ADDRESS

* Several locations in the above table are undefined.

TABLE 2.5 : Simplified Nascom Memory Map

MEMORY LOCATIONS	CONTENTS
0000-07FF	NAS-SYS NASCOM MONITOR
0800-0BFF	VIDEO RAM
0C00-0FFF	NAS-SYS WORKSPACE
1000-9000	PASCAL SOURCE CODE (CONTROL)
96D0-9700	DATA TABLE (SEE TABLE 2.4)
982F-A002	SINE WAVE DATA
A010-AFFF	RESULTS STORAGE TABLE
B000-B3FF	MEMORY MAPPED ADC BOARDS
B400-B44F	ROUTINE JUMP TABLE
B450-B6FF	MACHINE CODE ROUTINES
B700-B900	INTERRUPT SERVICE ROUTINES
B901-BFFF	UNUSED MEMORY SPACE
C000-CFFF	PASCLDOS DISC OPERATING SYSTEM
D000-DFFF	NAS-DOS DISC OPERATING SYSTEM
E000-FFFF	NASCOM BASIC

The data acquisition routines (called DROP and DROP2) take data into the computer in the form of a series of discrete points sampled at regular intervals over one signal period. The data is stored in the results table. The DROP routine is used when the excitation signal is generated by the exciter control while DROP2 operates with digitally generated excitation signals. The only difference between the two routines is that in DROP2 the digital sine wave must continue to be generated during the measurements.

Both routines use interrupts generated by the displacement comparator to start and stop the measurement. The system is triggered on the rising edge of the comparator signal. A counter timer circuit (CTC) within the Nascom III is programmed to time the period between sucessive rising edges. This is the period of the measurement signals. This period is then subdivided into a convenient number of sub-periods and the CTC programmed to time over this period. At the end of each sub-period an interrupt is generated which is used to enter a single data point. Once the required number of points have been entered control is passed back to the high level program for analysis. For frequencies below 13 Hz the number of data points per cycle is set at 500 (due to memory space limitations). Above this frequency the number drops steadily (due to time limitations) to about 64 at 100 Hz.

Generation of the excitation sine wave is controlled by the routine SINGEN which initialises a CTC channel to the time period required to produce a sine wave of the required frequency. The CTC produces an interrupt after this period and prompts the output of the next sine wave data point. Once initiated by SINGEN the CTC will continue to interrupt and output of the sine wave will continue, even when control is passed back to the high level program. Sine wave generation is halted by execution of the routine STOSIN. The sine wave is stored in the computer in the form of a table in memory (see table 2.5). On execution of SINGEN a pointer is set to the start of this table. Each time a data point is output by the CTC interrupt routine SINOUT the pointer is incremented through the table. When the final point in the table has been sent, the pointer is reset to the start of the table.

The above routines comprise the bulk of the real time processing required for the spectrometer. Several other routines have been written. The flow charts for these appear with the others in appendix III.

2.6 The Mechanical Mounting System

The mechanical hardware provides a means of mounting the transducers and test pieces on the electromagnetic exciter in such a way as to allow simple operation and accurate measurements with a variety of sample sizes, filled with either air or a liquid. Figure 2.20 shows

FIGURE ■2.20 : The Mechanical Mounting System

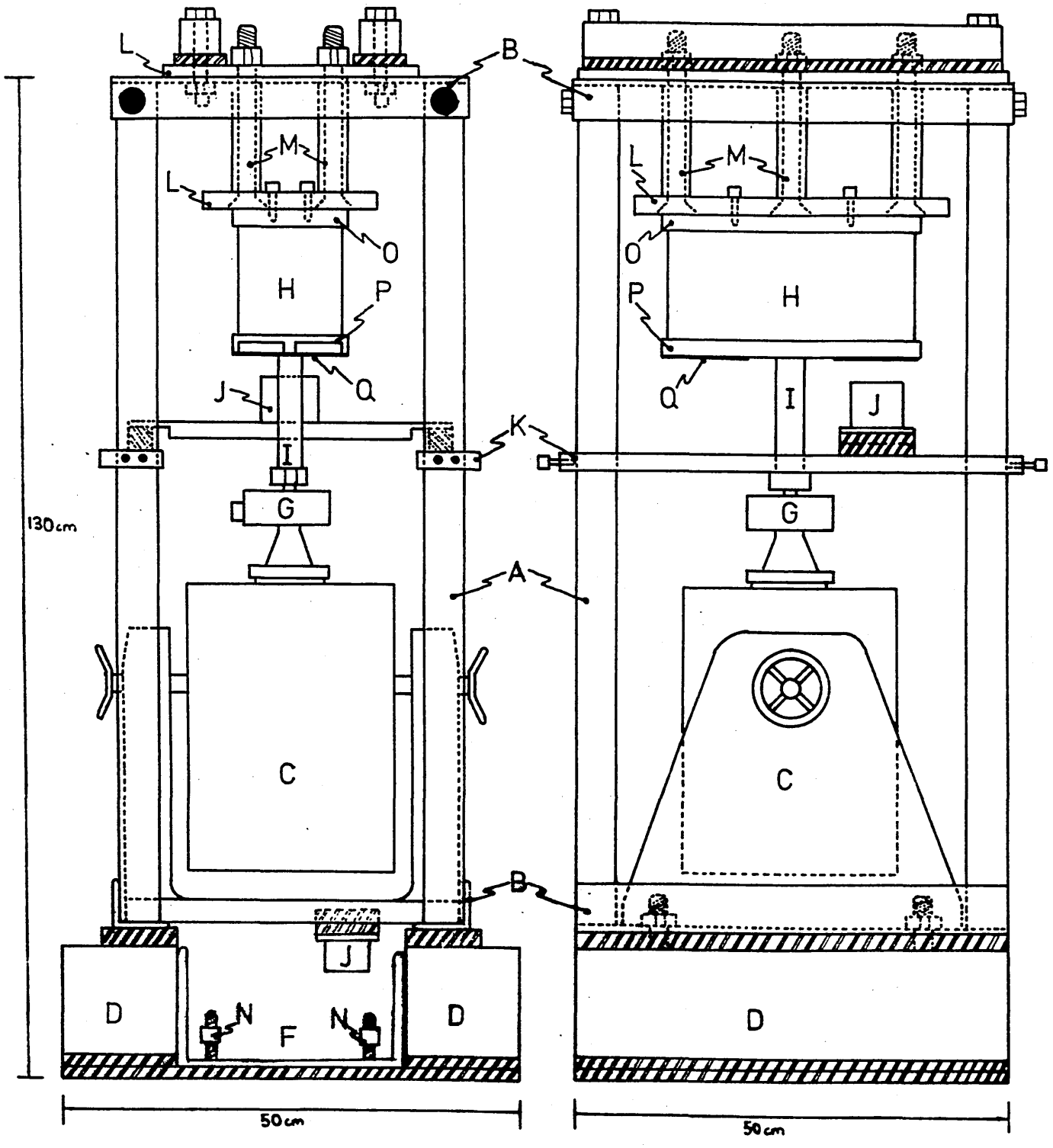

FIGURE 2.21

Front and Side Sectional Views of the Mechanical Mounting System.

the mounting structure set up for testing an air-filled sample while figure 2.21 provides front and side sectional views. The design of the equipment has been influenced by the need to avoid any major structural resonances in the test range and reduce the vibrations transmitted throughout the structure to a minimum.

The main framework of the mounting system is made up of four vertical, square-section pillars, filled with sand (A). The sand gives the pillars a high level of vibration damping. The pillars are connected together, top and bottom, by horizontal 'L' section bars (B). The exciter (C) on its trunion fastens above the bottom bars and its weight is used to give the structure more stability. The whole assembly is mounted on two concrete seismic blocks (D). Resilient pads between exciter and framework, framework and seismic block, and seismic block and floor assist in isolating each section from vibrations generated elsewhere.

The mounting system for air-filled samples bolts to the top of the framework. Beneath the exciter a large tank (F) is provided to contain the liquid and provides fixtures for the attachment of liquid-filled samples.

Between the table of the exciter and the test piece (H) is a drive shaft to transmit the vibration (I). Fitted into this drive shaft is the force transducer (G). Two mountings are provided for the displacement sensor (J).

For air-filled samples the sensor is fastened between two brackets (K) which attach to the main structural pillars. For liquid-filled test pieces the sensor is attached to the underside of the exciter. In both cases resilient pads are used to isolate the sensor from vibrations.

Air-filled samples are fastened to the mounting structure by two rigid plates (L) which are kept apart by tubular spacers (M) around the connecting bolts. The spacers allow ajustment for differing sample geometries and enable a static pre-compression to be imposed. For liquid-filled systems the exciter must be rotated through 180^{o} on its trunion from the position shown in figure 2.21. The table of the exciter now faces vertically downwards and the sample is placed between the exciter and the tank floor. Thin rods (N) are used to fasten the bottom face of the test piece to the floor of the tank. Adjustment for differing sample heights, or to impose a static pre-strain, is achieved by placing spacer plates between the bottom of the sample and the tank floor.

The test pieces themselves are bonded to a force plate (O) and a drive plate (P) by means of a suitable adhesive. The force plate provides attachment points for fastening to the sample mounting system in use. The drive plate allows even loading of the test piece. Attached to the underside of each drive plate are ferromagnetic discs (Q) which act as targets for the displacement sensor.

2.7 Testing and Calibration

The only parts of the spectrometer requiring calibration are the transducers and the input boards. In addition it was necessary to check the validity of the control software algorithm used to calculate the frequency, amplitudes and phase difference of the two input signals.

2.7.1 System Calibration

The calibration of the two transducers was set in the factory. In order to check that the readings given by the transducers matched the manufacturers specifications, calibration experiments were set up.

For the displacement sensor a calibration device was constructed. This consisted of a mount for the transducer with a steel target plate whose distance from the front surface could be accurately set. The target plate was adjusted to be accurately parallel to the front face of the sensor and could be moved towards or away from the sensor by means of a micrometer thread. All other surfaces were constructed from plastic to avoid interference with the target-sensor field. Figure 2.22 shows the calibration curve drawn from measurements made with the calibration device. Over the whole measurement range the transducer was within the specifications quoted by the manufacturers [11] and no re-calibration was necessary.

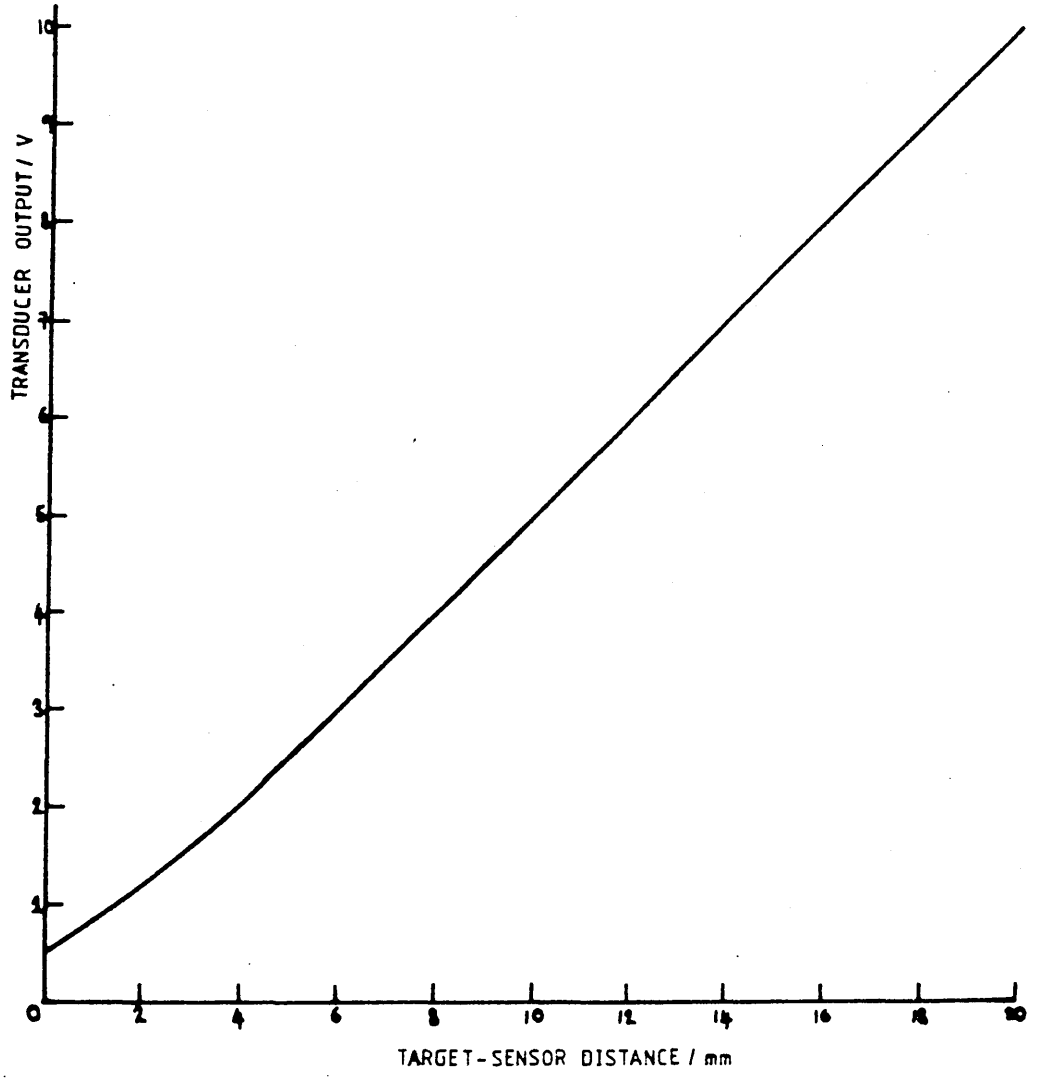

FIGURE 2.22
Calibration Curve for the Displacement Sensor.

In the case of the force transducer a check on the calibration was made by loading with known weights. For compressive forces in the range 0-200 N the output of the transducer was within 0.1% of the quoted specifications.

The above tests were repeated for both systems with the low-pass filter and zero-offset circuits in place. In both cases the deviation from the calibration curves was less than 0.1%. As a further check on the transducer performance the long term drift of the signals was monitored. With the displacement transducer a sensor-target distance of 10mm was maintained for 10 days with regular measurements over this period. The force transducer was similaly monitored whilst loaded with a compressive force of 50 N. In both cases the drift of the signals was undetectable with the available measuring equipment.

The signal input boards were the only interface requiring calibration. Using the calibration procedure oulined in the service manual [16] and unity gain, the output codes from the boards were set to the following specifications:

+5 V = 4090

0 V = 2045

-5 V = 0

Careful calibration allowed this specification to be met to within ± 1 LSB. Both boards were periodically checked for long term drift. Though small, the drift was significant and required re-calibration every 6 months.

2.7.2 System Performance Checks

Before placing any reliance on the spectrometer measurements, the behaviour of the system under various conditions was determined. This included checking the validity of the measurement algorithm and measuring the response of simple mechanical systems (such as helical springs) using the spectrometer.

Measurement Algorithm Validity

This was proved using artificial sinusiodal signals of known amplitude, frequency and phase, produced by a dual channel variable phase oscillator. Amplitudes from 5 mV to 5 V were set independantly for each channel. The phase difference between the two was adjusted across the range 0-359°. The whole measurement series was repeated for selected frequencies in the range 1-100 Hz. For frequencies below 1 Hz the digital signal generation system of the spectrometer formed the signal source. In this case it was not possible to investigate the phase difference as only one signal source was available. In all cases the errors in the measurements were less than 0.5%.

2.7.3 Repeatability

Figure 2.23 shows a set of results taken on a helical spring. A mass element is present due to the drive plate mounting used. This dominates the response at high frequencies. Figure 2.24 shows the same set of results after mass compensation. As expected the stiffness of

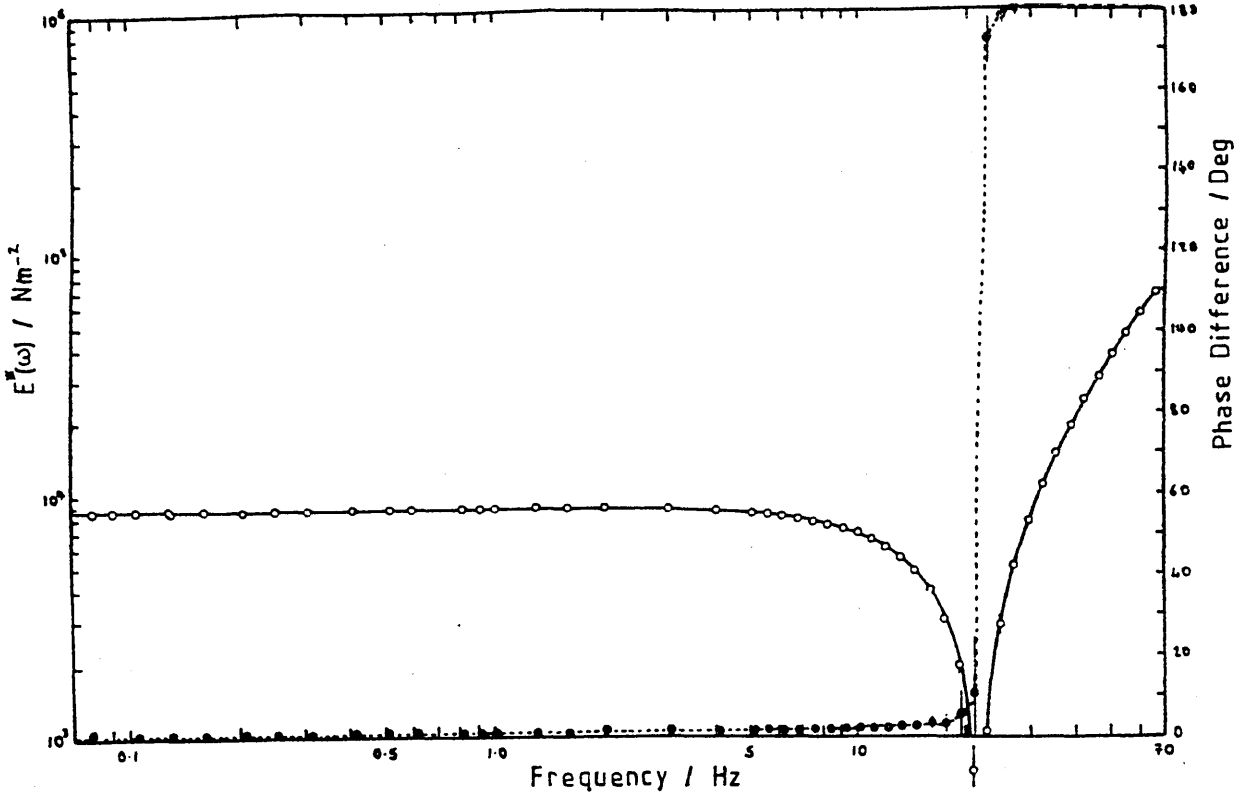

FIGURE 2.23

Dynamic Stiffness (open circles) and Loss Angle (closed circles) for a Helical Spring Before Mass Compensation.

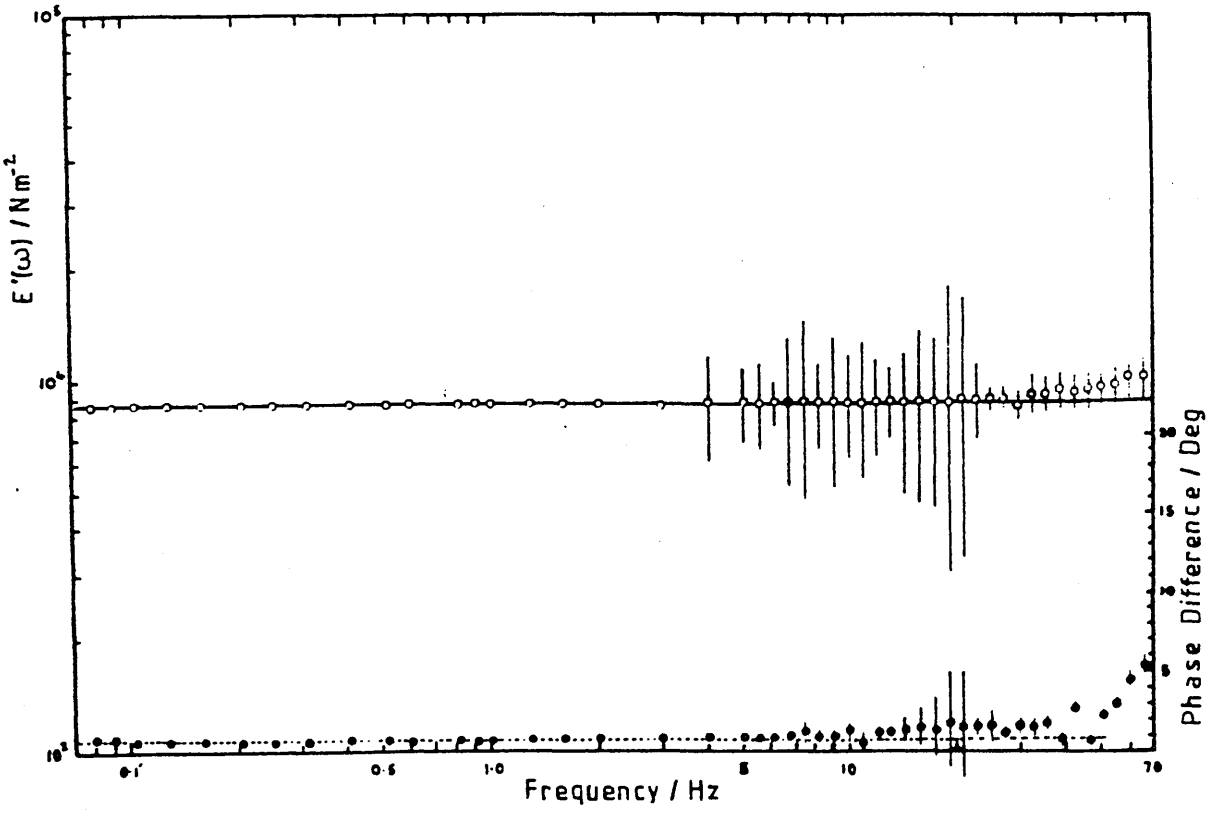

FIGURE 2.24

Data of Figure 2.23 After Mass Compensation.

the spring is independent of frequency over the frequency range of interest, and the phase difference is zero. The slight rise of the phase difference at high frequencies was found to be caused by a transverse resonance of the drive plate when not constrained by a large sample.

In order to judge the repeatability of measurements made with the mechanical spectrometer it is necessary to allow for differing experimental conditions. In order to exclude environmental and sample condition considerations from the repeatability tests, measurements were made on the helical spring and a simple mass system. An example of the response of a simple mass is given in figure 2.14. For each mechanical system a number of measurement series were taken over a period of weeks. The sets of results were found to be self consistant, the variations being within the error fields shown on figures 2.14 and 2.24.

The dynamic mechanical spectrometer described above has been used extensively in the present project. Measurements of the dynamic mechanical properties of a range of flexible polyurethane foam samples have been made for both air-filled and liquid-filled test pieces under various levels of static pre-strain. The results of these measurements are discussed in Chapter 4.

3. THE AIR-FLOW PROPERTIES OF CELLULAR MATERIALS

3.1 Introduction

The pressure gradient, dP/dx required to maintain the flow of a Newtonian fluid through a porous medium is given by a two term relationship

$$\frac{dP}{dx} = \frac{\eta}{K} v + \frac{\rho}{B} v^2 \qquad 3.1$$

where v is the average flow velocity, η and ρ are the viscosity and density of the fluid and K and B are coefficients characteristic of the structure of the medium. The relation of equation 3.1 was first proposed by Forchheimer [25] for permeation through sand and has been shown to be valid over a wide range of flow rates for materials such as porous metal, rock, fibrous filters and cellular plastics [26,27,28]. The permeability, K and the flow resistance coefficient, B have been found to be independent of the fluid.

The first term on the right hand side of equation 3.1 reflects viscous flow processes and dominates at low flow rates. The second term, which becomes increasingly important as the flow rate increases, represents inertial flow losses resulting from irregular flow through the porous medium.

A number of models have been advanced to relate K and B to material structure. All these have assumed that the

permeating fluid is Newtonian. Gent and Rusch [28,29] considered the problem of cellular materials. For the laminar flow region their approach followed that of Kozeny [30] which assumes that the material may be represented by an array of tubes of equal length and cross-section. The permeability, K for this model is

$$K = \frac{c}{\tau}\left(\frac{\xi}{S}\right)^2 \qquad 3.2$$

where c is a constant depending upon the shape of the tube section and τ is the tortuosity of the material, defined as the actual flow path length per unit length of material. ξ is the volume fraction of interconnecting cells and S is the surface area of interconnecting cells per unit volume. In the simplest case where the tubes have circular cross-section and τ is taken to be unity equation 3.2 reduces to

$$K = \alpha d^2/32$$

Here d is the average cell diameter for the foamed material and α is a dimensionless constant taking a value of about 1/3 for the experimental foam samples of Gent and Rusch.

The second term in equation 3.1 was interpreted by Gent and Rusch in terms of expansion and contraction losses as the fluid passes through the irregular flow channel. This approach follows the treatment of Chiltern and Colburn [31] and involved modifying the above model for

laminar flow to include a series of regularly spaced orifices within each tube. Choosing an orifice spacing of 1/d per unit length, Gent and Rusch found that the flow resistance coefficient, B, could be expressed in the form

$$\frac{1}{B} = \frac{1}{2d} (D^2 - 1)^2 \qquad 3.3$$

where D is the ratio of the pipe diameter to that of the orifice. Their origi nal work included a treatment of the effects of pre-strain on the fluid-flow properties of cellular materials. Using the above model they deduced that the permeability and flow resistance coefficient perpendicular to the direction of strain could be expressed as

$$K(e)/K(o) = (1 - e)$$

$$B(e)/B(o) = (1 - e)^{1/2} \qquad 3.4$$

where e is the fractional strain (positive compressive) and K(o) and B(o) are the coefficient values at zero strain.

The experimental work performed by Gent and Rusch found reasonable qualitative agreement with their model predictions for K and B. They did however only test a small range of conventional polyurethane and rubber latex foams. On measuring the variation of the permeability and flow resistance coefficient with imposed pre-strain, the experimental results were found to change more

rapidly with strain than suggested by equations 3.4. Furthermore the experimental work was based on two foam samples at relatively small strains (<20%).

The previous theoretical treatments for fluid-flow in cellular materials, although producing qualitative agreement to measured data for K and B fail to properly predict the strain dependence of these coefficients. The experimental work itself was restricted in both scope and content. It is likely that the failure of the Gent-Rusch theory to correctly predict the strain dependence of the fluid-flow properties is due to the simplified nature of the model in use. In fact the structure of a cellular material is more closely related to that of a packed bed of particles than an array of tubes. In a packed bed the fluid flows around the surface of solid particles whereas in a cellular material the "particles" are in fact the voids, surrounded by solid polymer. The two systems, although having diametrically opposite structure, may be described in a similar manner.

3.2 Theoretical Treatment

Consider a block of cellular material of dimensions H,W,L as shown in figure 3.1. A Newtonian fluid flows through the cellular matrix structure in a direction perpendicular to the W-H face of the block and at a mean velocity, u_m. A differential pressure ΔP is set up across the length of the block due to the passage of fluid. It is assumed that this pressure difference is not high

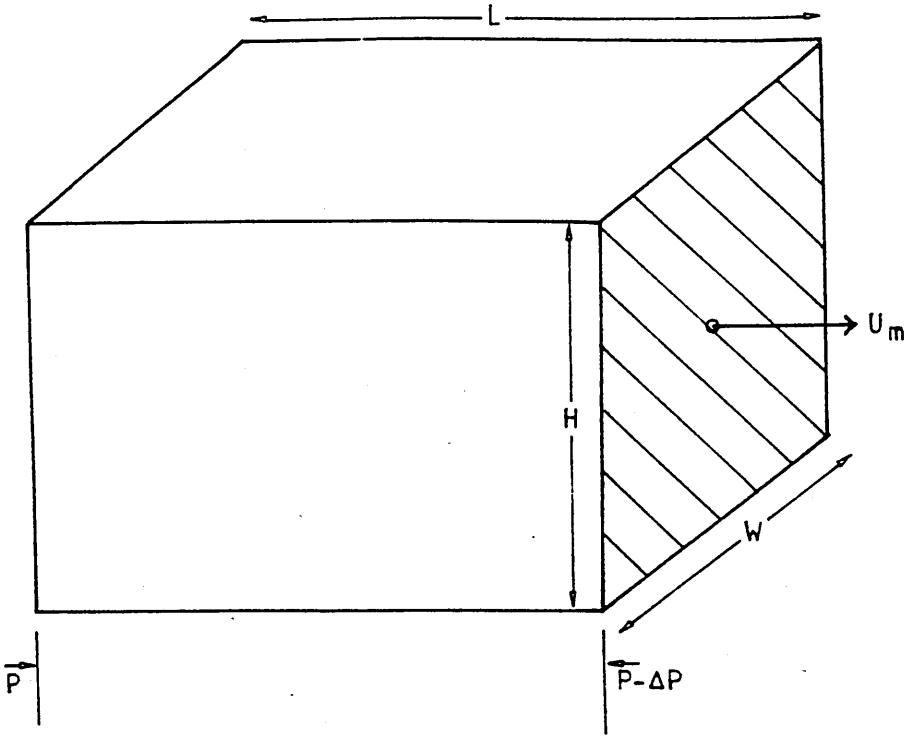

FIGURE 3.1
Air Flow Through a Block of Cellular Material

enough to compress the material. The two term relation of equation 3.1 will hold

$$\frac{\Delta P}{L} = \frac{\eta}{K} u_m + \frac{\rho}{B} u^2_m$$

3.2.1 Viscous Laminar Flow

The first term in equation 3.1 is generated by laminar flow of the fluid through the matrix. For this type of flow the Hagen-Poiseuille law holds for packed beds [32]

$$\Delta P = C_o \eta \frac{\ell_e u_e}{m^2} \qquad 3.5$$

where ue is the effective flow velocity and le the

effective path length over which the pressure drop occurs. m is known as the hydraulic radius of the void passages and C_o is a dimensionless constant depending upon the cross-sectional shape of the passages.

For a cellular material the volume fraction of voids = $A_e/(WxH) = 1 - \phi_0$ where WxH is the total cross-sectional area of the block and A_e is the effective cross-sectional area of the voids. ϕ_0 is the volume fraction of polymer. The linear flow velocity u of the fluid flowing through the block may be determined from the volume flow rate Q by

$$u = \frac{Q}{A_e} = \frac{Q}{WH(1 - \phi_0)} = \frac{u_m}{(1 - \phi_0)} \qquad 3.6$$

where u_m is the mean approach velocity. However due to the tortuous nature of the void passages through which the fluid flows, the effective velocity, u_e, will be lower than given in equation 3.6. Furthermore if ξ is the volume fraction of open cells, u_e may be written

$$u_e = \frac{\tau}{\xi(1 - \phi_0)} u_m \qquad 3.7$$

For a packed bed the hydraulic radius of the voids is given by the ratio of the volume of fluid in the bed to the "wetted surface" of the voids:

$$m = \frac{(1 - \phi_0)}{S} \qquad 3.8$$

where S is the wetted surface per unit volume of material. Thus equation 3.5 may be written as

$$\frac{\Delta P}{L} = C_o \eta \frac{\tau^2 S^2}{\xi(1 - \phi_0)^3} u_m \qquad 3.9$$

By comparison with the first term on the right hand side of equation 3.1, the permeability of the material is

$$K = \frac{\xi(1 - \phi_0)^3}{C_o \tau^2 S^2} \qquad 3.10$$

S, the wetted surface area per unit volume = surface area of each cell x number of cells per unit volume. If the cells are assumed to be spheroids with diameter d then

$$S = \frac{6A_c}{\pi d^3} (1 - \phi_0) \qquad 3.11$$

where A_c is the surface area of each cell. For spherical cells $A_c = \pi d^2$ and Kay [32] states that experimentally the constant $C_o \tau^2$ takes a value of about 5. Hence the permeability of a cellular material reduces to the form

$$K = \xi(1 - \phi_0) d^2/180 \qquad 3.12$$

where for the foams under consideration $\xi \cong 1$. Comparison with equation 3.2 shows that the permeability derived from the consideration of packed beds is very similar to that derived by Gent and Rusch for an array of tubes. The difference being in the numerical constant and the inclusion of the volume fraction of polymer. The numerical constant in equation 3.12 is likely to be in error as the surface area of the cells will be somewhat smaller, but it is thought that the general form is correct.

The strain dependence of the permeability perpendicular to the direction of strain may be investigated by considering the block of cellular material compressed to a height H-Z. From equation 3.10 the permeability is given by

$$K(e) = \frac{\xi\{1 - \phi(e)\}^3}{C_o \tau^2 S(e)^2}$$

If the polymer phase of the material is assumed to be incompressible (an assumption which is valid for strains up to about 60%) then the volume fraction of polymer in the compressed material will be given by

$$\phi(e) = \frac{\phi_0 H}{(H - z)} = \frac{\phi_0}{(1 - e)} \qquad 3.13$$

where ϕ_0 is the volume fraction of polymer at zero strain and $e = Z/H$ is the fractional compressive strain imposed. The wetted surface area per unit volume is again given by $S = A_c \times N_o$, where N_o is the number of voids per unit volume. As cells may not be created or destroyed the number of voids in the block will remain the same. However the block occupies a smaller volume and N_o will increase

$$N_o = \frac{6(1 - \phi_0)}{\pi d^3} \frac{A_c}{(1 - e)} \qquad 3.14$$

and the wetted surface per unit volume becomes

$$S(e) = \frac{6(1 - \phi_0)A_c}{\pi d^3 (1 - e)} \qquad 3.15$$

It is assumed that the cell walls buckle rather than compress. This assumption will be valid for strains up to about 60% where interaction between the buckled cells starts to occur [33]. This point is expanded in section 4.1 where the properties of cellular materials under a pre-compression are discussed. With this assumption it is reasonable to assume that the cells change shape, but the surface area remains essentially the same. Thus the strain dependent permeability for a cellular matrix will be given by

$$K(e) = \left\{1 - \frac{\phi_0}{(1 - e)}\right\}^3 \cdot \frac{\xi(1 - e)^2 d^2}{180(1 - \phi_0)} \qquad 3.16$$

It may be seen from equation 3.16 that the permeability is predicted to be a function of $(1-e)^2$, as ϕ_0 is generally small. Equation 3.16 may also be written in terms of the zero strain permeability, K(o)

$$\frac{K(e)}{K(o)} = \left\{\frac{(1 - e) - \phi_0}{(1 - e)(1 - \phi_0)}\right\}^3 (1 - e)^2 \qquad 3.17$$

The above expression should hold for strains below about 60%, where the assumptions that the polymer is incompressible and the cell surface area remains constant will break down. It is interesting to note that at small strains equation 3.17 will reduce to

$$K(e)/K(o) \cong \lambda(1 - 2e)$$

where $\lambda \cong 1$. This relation is in qualitative agreement with the work of Gent and Rusch and explains why their

results were found to fit a (1-e) variation fairly well at low strains.

3.2.2 Inertial Flow

The second term in equation 3.1 reflects inertial flow losses due to the irregular nature of the void passages. For steady flow of fluid in a pipe of radius r the stress, τ_0 at the walls may be written as

$$\tau_0 = \frac{1}{2} C_f \rho u^2 m \qquad 3.18$$

where C_f is known as the skin friction coefficient and will reflect the irregular nature of the passage. For a pipe of length L and radius r with a pressure drop of ΔP across it then

$$\Delta P \pi r^2 = \tau_0 2\pi r L$$

ie

$$\Delta P = C_f \frac{L}{r} \rho u^2 m \qquad 3.19$$

Following the procedure of Kay [32] equation 3.19 may be generalised for flow through a packed bed

$$\Delta P = \frac{C_f}{2} \frac{\ell_e}{m} \rho u^2 e \qquad 3.20$$

where as previously m is the hydraulic radius of the void passages. Inserting values for u_e and m from equations 3.7, 3.8 and 3.11 will give

$$\Delta P = \frac{3 C_f \tau^3 L \dot{u}^2 m}{\xi(1 - \phi_0) d} \qquad 3.21$$

By comparison with equation 3.1 the flow resistance coefficient, B can be defined to be

$$B = \frac{\xi(1 - \phi_0)^2 d}{3C_f \tau^3} \qquad 3.22$$

where for many practical applications $\tau^2 \cong 2$ [32]. Comparison with the equation 3.3 derived by Gent and Rusch shows a similar dependence on d, the cell diameter, with the addition of a term dependent on the volume fraction of polymer and C_f taking the place of $(D^2-1)^2$.

The strain dependence of the flow resistance coefficient may be found by substituting the strain dependent expressions for the volume fraction of polymer (3.13) and the wetted surface (3.15) into equation 3.20

$$B(e) = \left\{1 - \frac{\phi_0}{(1 - e)}\right\}^3 \cdot \frac{\xi(1 - e)d}{3C_f \tau^3 (1 - \phi_0)} \qquad 3.23$$

The flow resistance coefficient is predicted to be approximately proportional to (1-e). This is in contrast to the work of Gent and Rusch which predicted a $(1-e)^{\frac{1}{2}}$ variation. Equation 3.23 may be written in terms of the zero strain value, B(o) as

$$\frac{B(e)}{B(o)} = \left\{\frac{(1 - e) - \phi_0}{(1 - e)(1 - \phi_0)}\right\}^3 (1 - e) \qquad 3.24$$

3.3 Experimental Considerations

The air flow properties of a total of 22 foam samples have been measured. Manufactured by three different companies; British Vita, Dunlop and B P Chemicals, the

samples were of two types; conventional polyurethane and high-resiliency polyurethane. These have been labelled type I and type II for convenience. Generally the conventional foams have structures composed of ribs outlining the individual cells and very thin membranes between them. In many cases the membranes were damaged or ruptured so that the structure could be considered to be almost completely open cell. The influence of the thin membranes on the air-flow properties of the matrix, however, could be significant. High-resiliency PU foam on the other hand has a structure composed of essentially spherical shells of polymer making up the individual cells. Ajoining cells are connected via pores in the cell wall. Fewer membranes can be seen with the structures of type II foams and once again the matrix can be assumed to be open cell.

For all types of foam a significant amount of anisotropy may be seen. Generally the cell dimensions in the direction of rise were larger than those in the other two directions. For this reason care was taken to ensure that all air-flow measurements were made in the same direction with respect to the rise direction of the foam. Electron-micrographs of typical examples of each of these foam types are shown in figure 3.2.

For all of the cells measured the proportion of completely closed cells was found to be negligible. The volume fraction of polymer, ϕ_o, determined from the bulk density of the foam was found to vary from 0.012-0.036

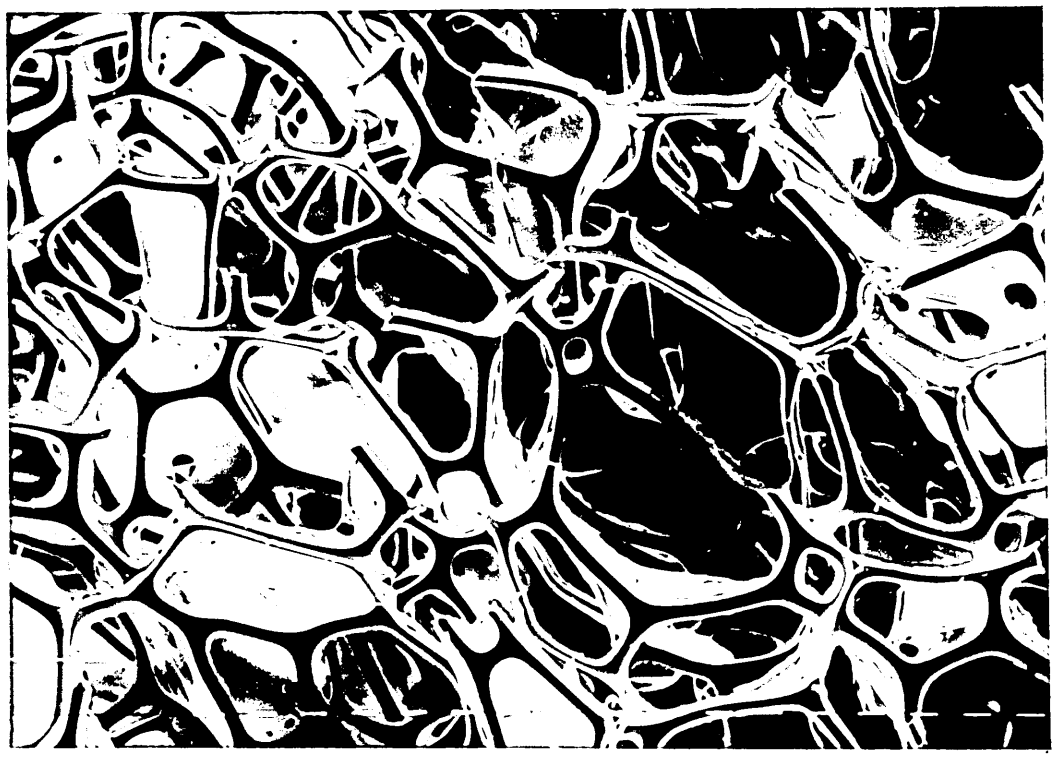

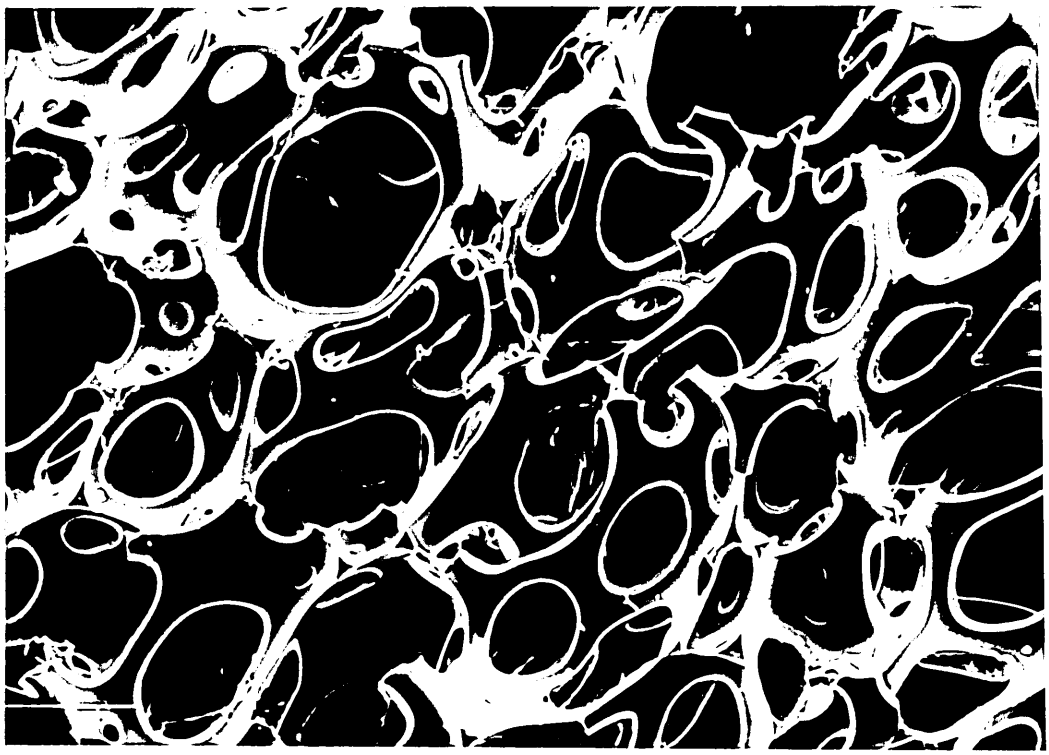

FIGURE 3.2

SEM Micrographs of Typical Examples of a) Conventional and b) High-Resiliency PU Foam.

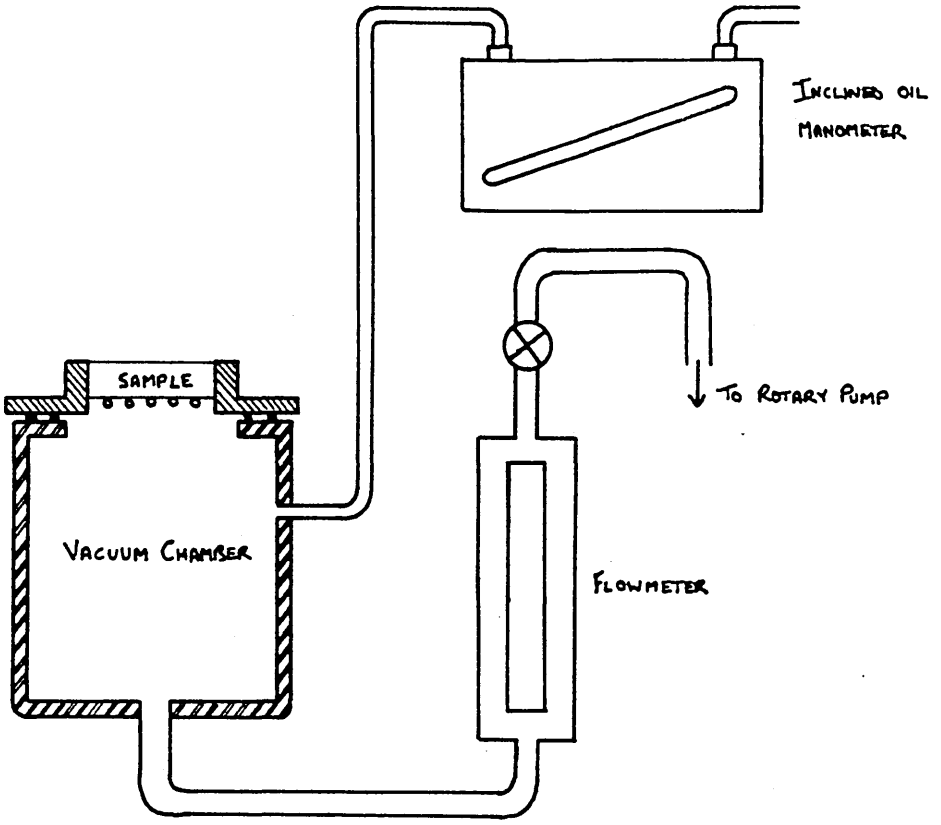

FIGURE 3.3
The Air Flow Apparatus to Comply with BS 4443 [34].

for conventional foams and 0.026-0.06 for high-resiliency samples. The average cell diameter for each sample was determined from measurements made on photomicrographs of the dimensions of twelve randomly chosen cells. Because of anisotropy in the matrix the largest and smallest diameters were averaged for each cell. The measured values of the average cell diameter, d, and the standard deviation, σ, of the cell size distribution are given in table 3.1 along with calculated values for the volume fraction of polymer.

TABLE 3.1 Foam Cell Diameters & Volume Fraction of Polymer

FOAM TYPE	FOAM	ϕ_0	d /10^{-3}m	σ/10^{-3}m
I	VP10	0.017	1.36	0.19
I	VP12	0.012	1.30	0.18
I	VP30	0.018	1.05	0.14
I	VP45	0.021	0.89	0.13
I	VRT300	0.029	0.91	0.23
I	VRT400	0.036	0.67	0.15
I	D2	0.015	1.35	0.14
I	D5	0.015	1.37	0.21
I	D7	0.022	1.08	0.10
I	D10	0.028	0.80	0.10
II	FHR26	0.026	1.36	0.17
II	FHR30	0.030	1.75	0.32
II	FHR50	0.050	1.13	0.17
II	FHR60	0.060	0.90	0.18
II	DHR263	0.030	1.35	0.10
II	DHR268	0.061	0.92	0.23
II	DW0007 00	0.051	1.13	0.22
II	DW0007 06	0.051	1.18	0.23
II	DW0007 07	0.051	1.08	0.18
II	DW0007 08	0.051	1.10	0.21
II	DW0007 09	0.051	1.04	0.22

Air-Flow Apparatus

The air-flow apparatus used for this series of tests was constructed to comply with the British Standard method 16 of BS4443:part 1 [34] for the determination of the air-flow value of cellular materials. This apparatus is shown in figure 3.3. The vacuum chamber, volume 10 litres incorporates a test piece mounting for samples of standard size 50x50x25mm, where the smaller dimension refers to the length through which the air flows.

Supporting the sample was a wire mesh with an open proportion in excess of 85%. Flow rates in the range 5-90 litres/min were used. This corresponds to linear flow velocities through the sample matrix of between 3.3 and 60 cm/sec.

The apparatus was checked for calibration using an orifice plate. This was fastened over the sample mount and a pressure drop of 100Pa imposed across it. The flow rate required to maintain this pressure difference was noted as 40.1 litre/min. The problem of flow through an orifice is well documented [35,36] and generally given by an equation of the form

$$Q = C_d S \left[\frac{2\Delta P}{\rho\{1 - (d/D)^4\}} \right]^{\frac{1}{2}} \qquad 3.25$$

where Q is the volume flow rate and ρ the fluid density. S and d are the area and diameter of the orifice respectively and D the diameter of the vacuum vessel. C_d is a dimensionless constant characteristic of the shape of the orifice and for a circular cross-section takes a value between 0.6 and 0.7. From equation 3.25, for the orifice in use, the volume flow rate required to maintain a pressure of 100Pa is 39.8$\pm$8% litre/min. The measured value of 40.1 is in excellent agreement with the theoretical value from equation 3.25.

Test-Pieces

For the first series of tests, to determine the air-flow properties at very low strains, samples were cut from

each foam with a thickness of 25mm and transverse dimensions slightly larger than the sample mount. This resulted in the measurements being taken under a small ($<1\%$) strain. The reason for this was to provide a good seal between the sample and the surface of the mount. With the relatively high permeabilities of the samples under test this procedure proved adequate to ensure that no air passed between sample and mount. In each case the orientation of the test-piece was such that the air flow properties were measured in the direction of foam rise.

With the second series of measurements where the variation of the air-flow properties with strain was investigated, a compressive deformation was imposed by cutting a test-piece larger than the sample mount in one transverse direction. The same test-piece was used for the measurements at all strains. The test-pieces were cut to an origional length of 125x50mm corresponding to a deformation of 60% when placed in the sample mount. As measurements at a particular strain were completed the test-piece was cut shorter to accomodate the next value of strain required.

Compression of a cellular material to such a great extent is likely to cause permanent damage to the matrix, specifically the membranes present in many of the samples could be ruptured or removed. In order to ensure that any damage occured before the measurements were taken, the test-pieces were first compressed to a strain of 70%.

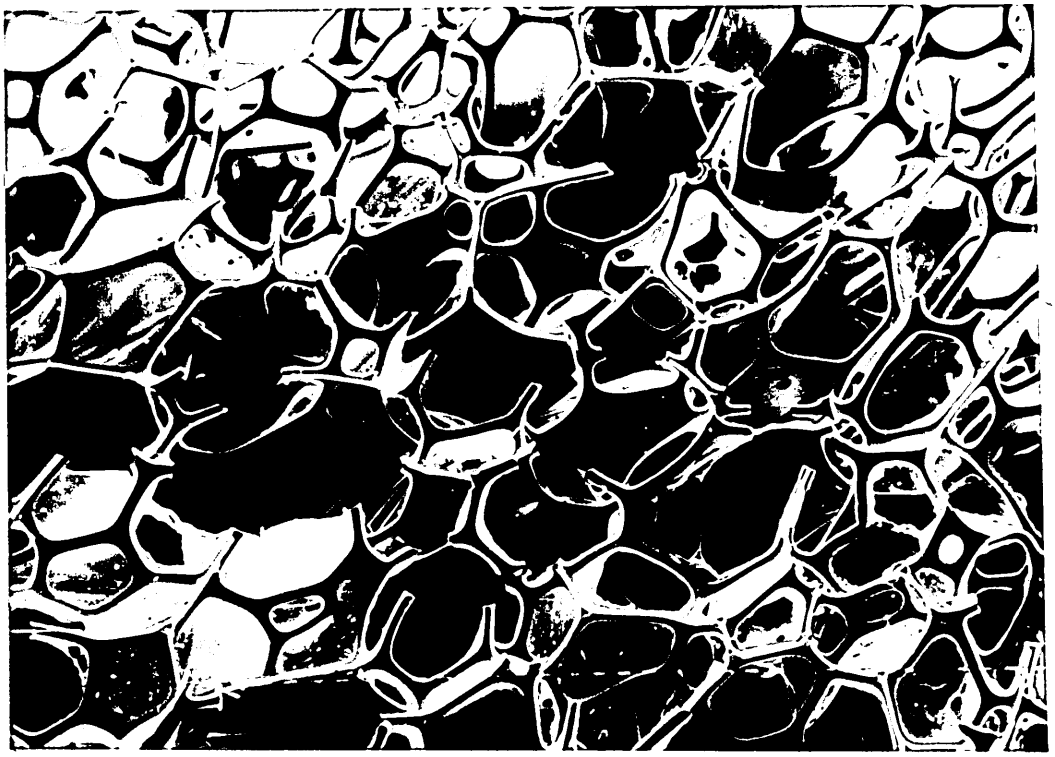

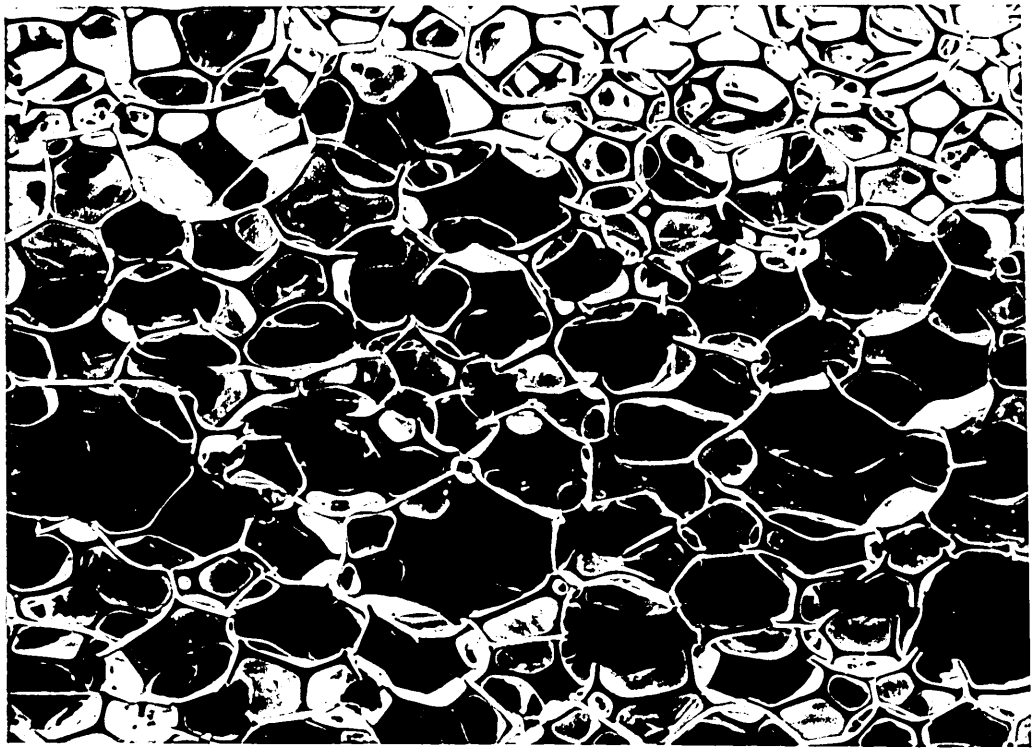

FIGURE 3.4

SEM Micrographs of a Flexible Conventional PU Foam a) Before and b) After Undergoing Compression to 70%.

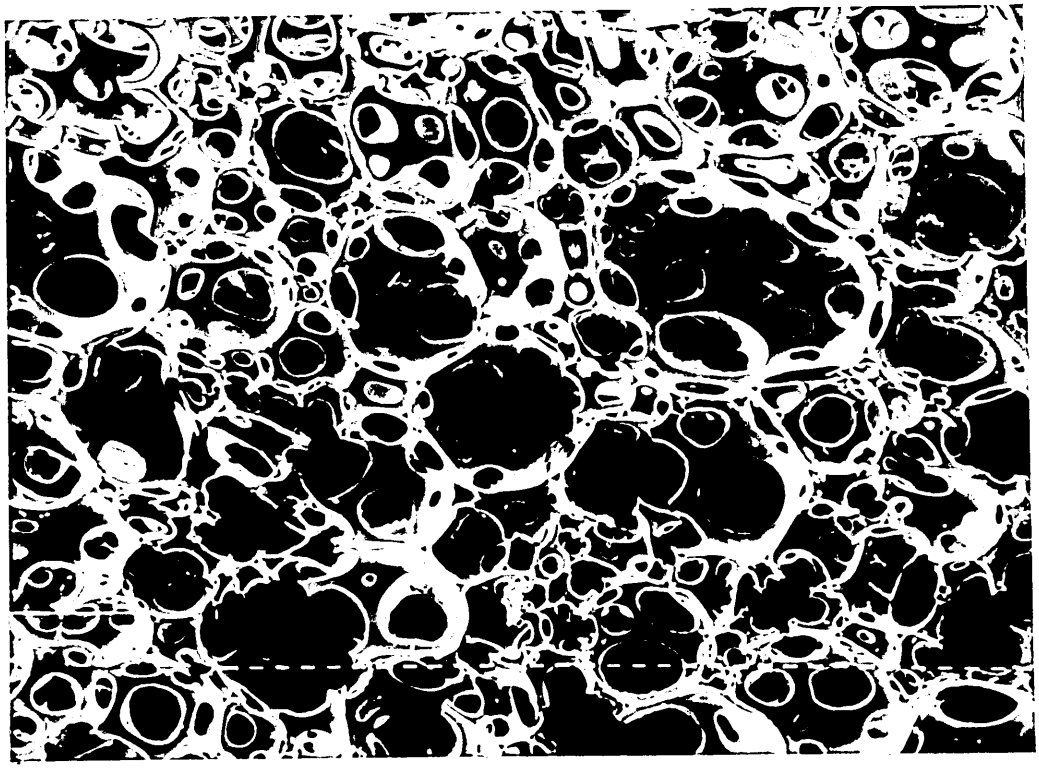

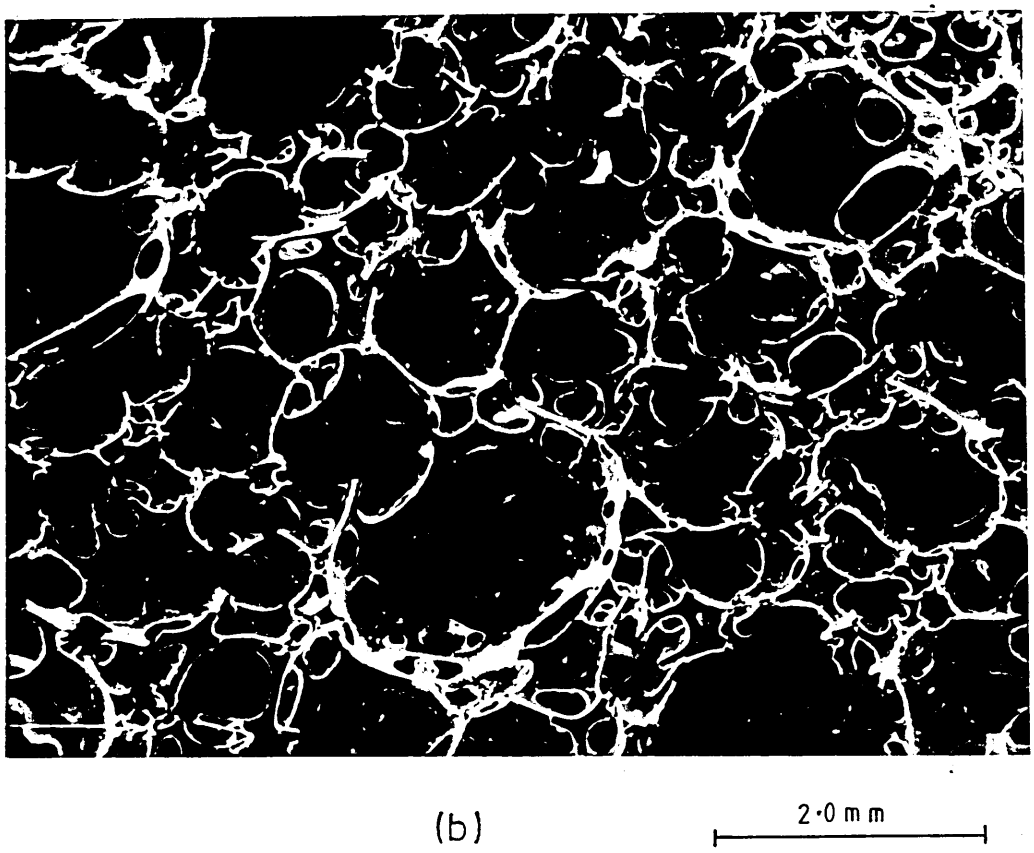

FIGURE 3.5

SEM Micrographs of a Flexible High-Resiliency PU Foam a) Before and b) After Undergoing Compression to 70%.

After being held there for 10 minutes the strain was removed and the test-piece allowed to relax for a further 10 minutes. This procedure was repeated a further two times before the first measurements were taken at 60% compression. Figures 3.4 and 3.5 show electron micrographs of typical example of conventional and high resiliency foams before and after this treatment.

In some cases, especially the less dense foam types, the maximum attainable deformation was 40%. This was because at higher strains the test-piece tended to wrinkle as it was placed in the sample mount. In a few cases this became so bad that air could leak around the edges of the test-piece. This phenomenon was not observed for any foams at or below a strain of 40%.

3.4 Results

3.4.1 Zero-Strain Behaviour

The variation of the pressure drop across the test piece with flow rate has been measured for each foam. The data are plotted as $(1/Q)(dP/dx)$ vs Q, where Q is the volume flow rate of air through the sample. All of the flow data obtained have been found to give a linear relationship when plotted in this way, confirming the validity of the two term relation of equation 3.1. The results for a selection of the foam test pieces are shown in figure 3.6.

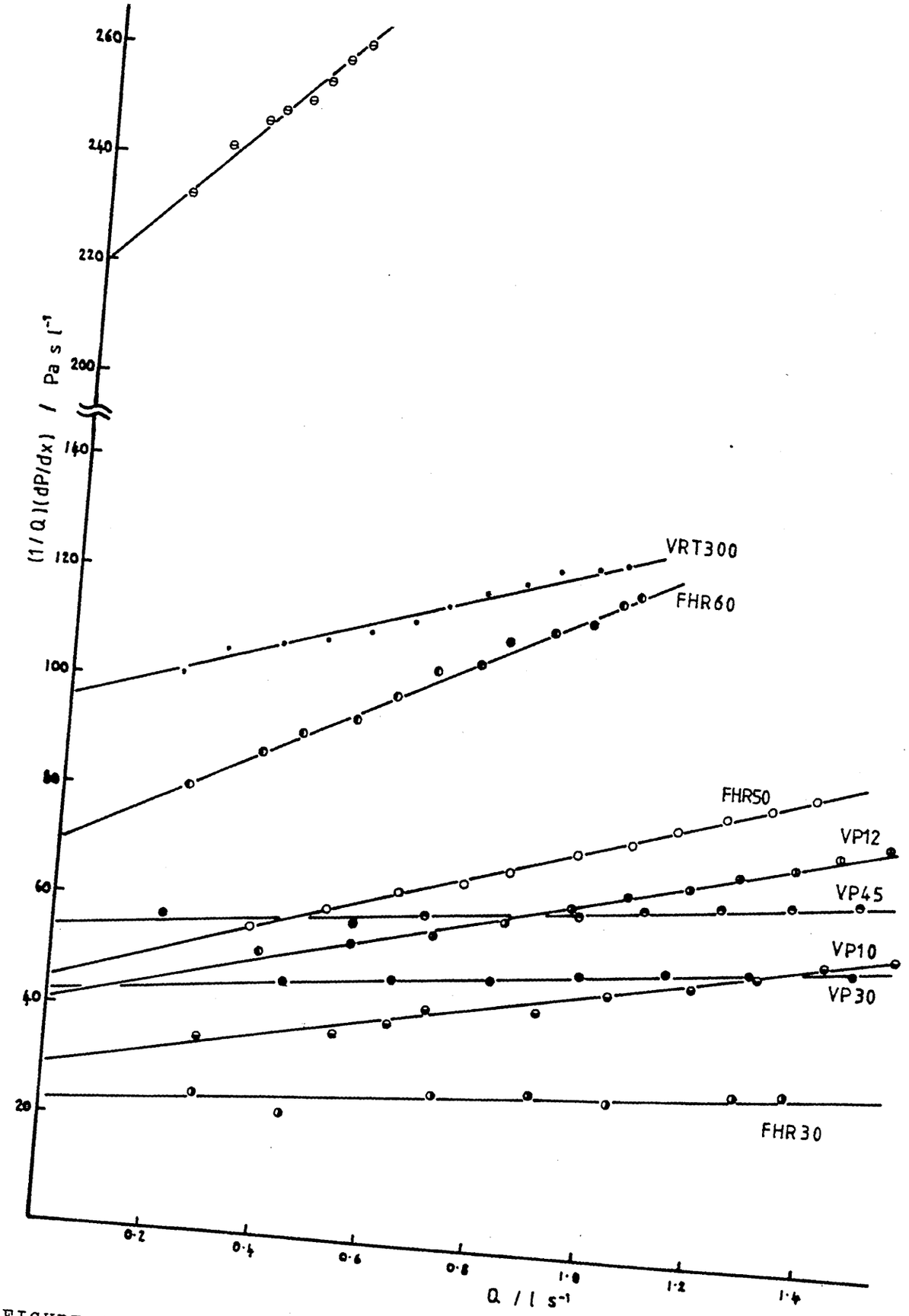

FIGURE 3.6

(1/Q)(dP/dx) vs Q for a Range of Conventional and High-Resiliency PU Foams.

From the intercept and gradient of the plots of figure 3.6 the values for the permeability and flow resistance coefficient may be calculated for each sample. If I is the intercept and G the gradient of a line then

$$K = (\eta \Delta x/6AI) \times 10^{-4} \ m^2$$

$$B = (\rho \Delta x/6A^2G) \times 10^{-7} \ m \qquad 3.26$$

where η and ρ are the viscosity and density of air, A is the cross section area for flow and Δx isthe sample thickness. A was fixed at $25 cm^2$ for all samples while Δx was measured using a micrometer gauge. In all cases the thickness of the sample was in the range 25 ± 1 mm. Values of K and B measured for each test piece are given in table 3.2.

The Permeability Coefficient

In figure 3.7 the permeability is plotted against the average cell diameter, d. On logarithmic scales the data can be seen to lie on a straight line of gradient 2.08. The full line corresponding to the data of figure 3.7 is given by the relation

$$K = d^{2.08}/215$$

This is in good agreement with the relation for the model structure based upon a packed bed given in equation 3.12. Also given in table 3.2 are ratios of the permeability calculated using equation 3.12 to those determined by measurement. In all cases the difference is small. It is interesting to note that the theoretical treatment derived in section 3.1.1 assumes that the cell size is

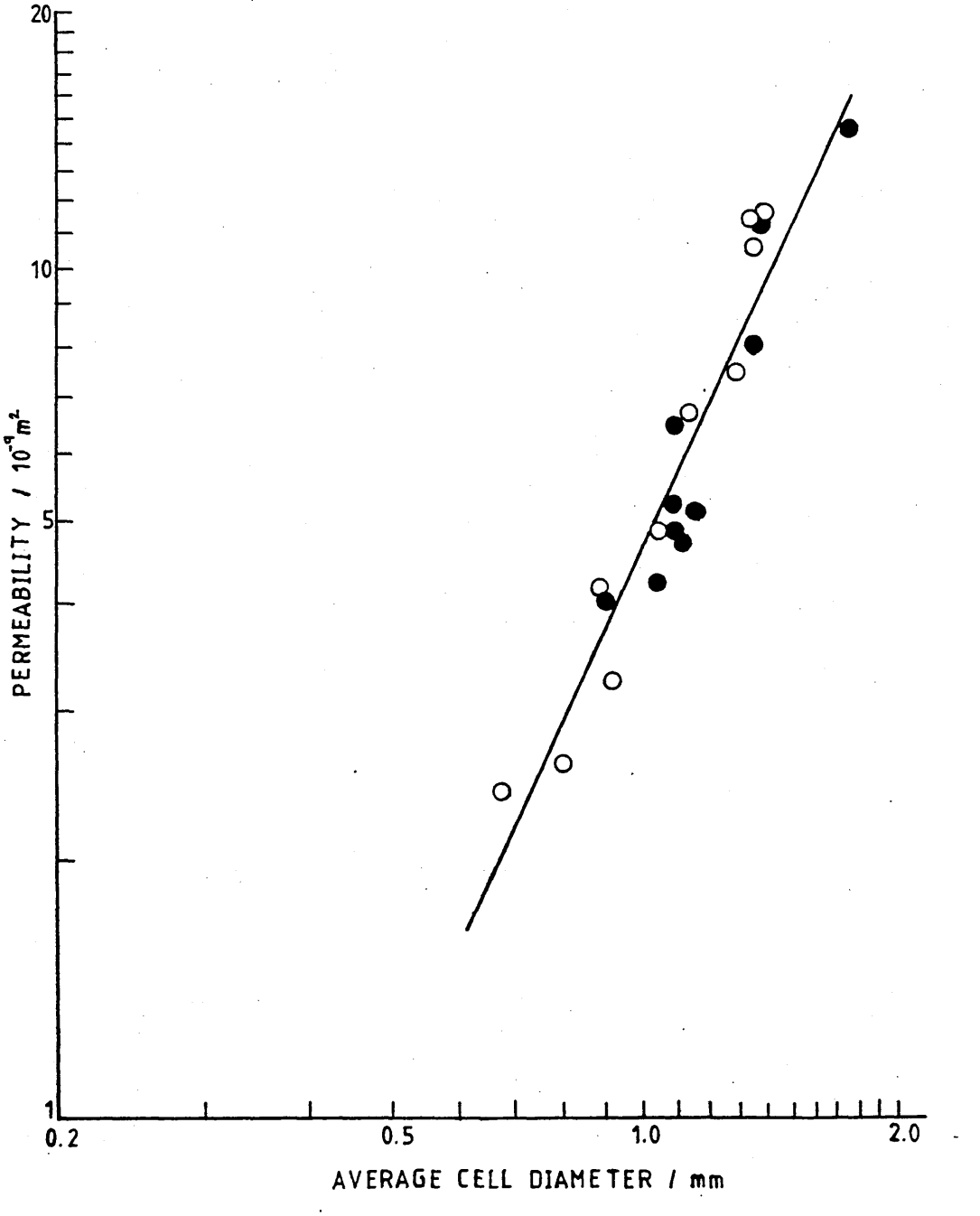

FIGURE 3.7

Variation of the Measured Permeability with Average Cell Diameter. Open Circles; Conventional PU, Closed Circles; High-Resiliency PU Foams.

TABLE 3.2 Permeability and Flow Resistance Coefficients

FOAM TYPE	FOAM	K /$10^{-9}m^2$	$\frac{K_{calc}}{K_{meas}}$	B /$10^{-4}m$	C_f
I	VP10	11.32	0.89	3.94	0.398
I	VP12	7.42	1.25	2.82	0.537
I	VP30	4.81	1.25	2.49	0.487
I	VP45	4.15	1.04	2.82	0.365
I	VRT300	2.21	2.08	1.21	0.860
I	VRT400	2.39	1.01	1.36	0.560
I	D2	7.97	1.24	2.64	0.585
I	D5	11.41	0.90	5.03	0.311
I	D7	6.58	0.96	5.09	0.240
I	D10	2.59	1.33	1.23	0.724
II	FHR26	11.25	0.89	6.56	0.238
II	FHR30	14.41	1.15	5.57	0.359
II	FHR50	6.66	1.01	2.93	0.433
II	FHR60	4.05	1.04	2.32	0.430
II	DHR263	10.62	0.93	4.83	0.311
II	DHR268	3.22	1.38	1.84	0.218
II	DW0007 00	4.74	1.41	2.65	0.451
II	DW0007 06	5.10	1.44	2.65	0.473
II	DW0007 07	5.14	1.20	2.67	0.429
II	DW0007 08	4.88	1.31	1.87	0.624
II	DW0007 09	4.25	1.34	1.10	1.003

the dominant factor controlling the permeability of the matrix. This is borne out by the results for conventional and high-resiliency samples which follow the same relation, although the shape and structure of the cells in each type is very different.

The high-resiliency foams manufactured by B.P. Chemicals exhibit only small changes in the permeability in moving through the foam series. The samples contain different

amounts of a vibration-control (VC) additive which, the manufacturers claim, can control the cell size and hence the air-flow properties [37]. This is desirable because control would be achieved over the dynamic fluid-flow damping process, as described in section 4.2. Although the cell dimensions do vary slightly with varying amounts of the VC additive, this is not sufficient to change the air-flow properties to the extent found by the manufacturers [38]. Figure 3.8 shows electron-micrographs of two samples of foam from this series. The foam shown in figure 3.8a has no VC additive, while that shown in figure 3.8b has the maximum. It is not known precisely how much VC additive is present. It can be seen that the major difference between the two foam samples is in the number of membranes present. The experimental method used for the above measurements involved the removal or rupture of many of the membranes present by compression of the test-piece and explains why so little difference is noted in their air-flow properties.

The rupture of the cell membranes by compression was considered to be advantageous because when used in practical applications such as seating or cushioning, these membranes would quickly be damaged in this way by the loads imposed. To check the validity of the assertion that the cell membranes are responsible for the differences in the air-flow properties found by the manufacturer, the above series of measurements were

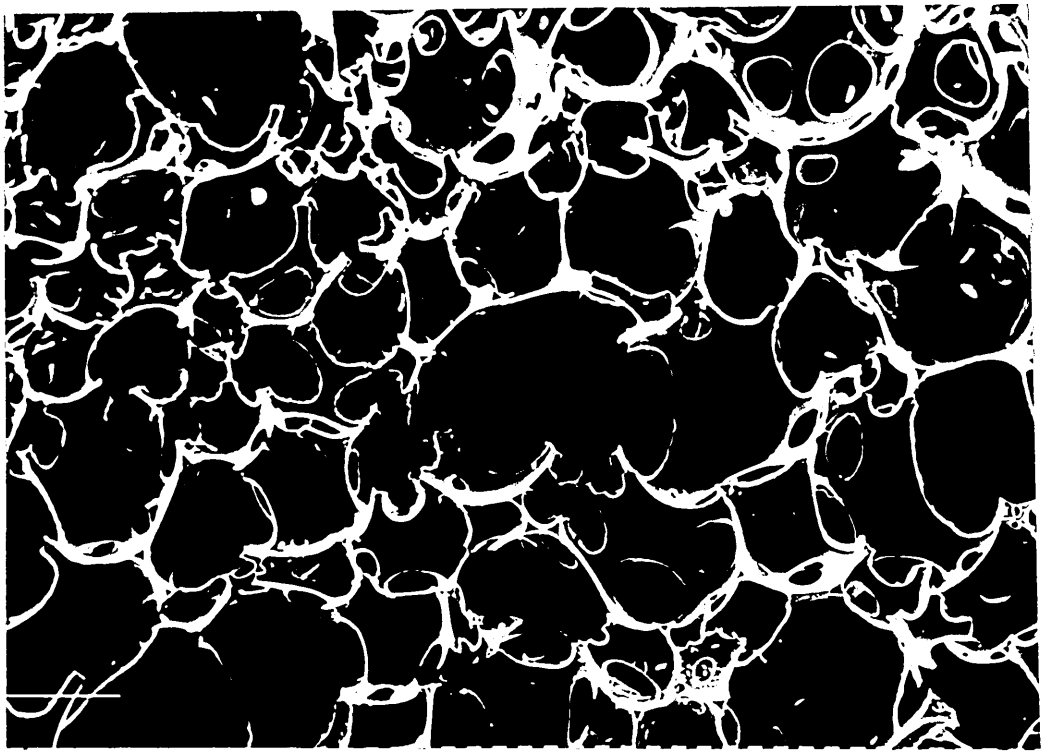

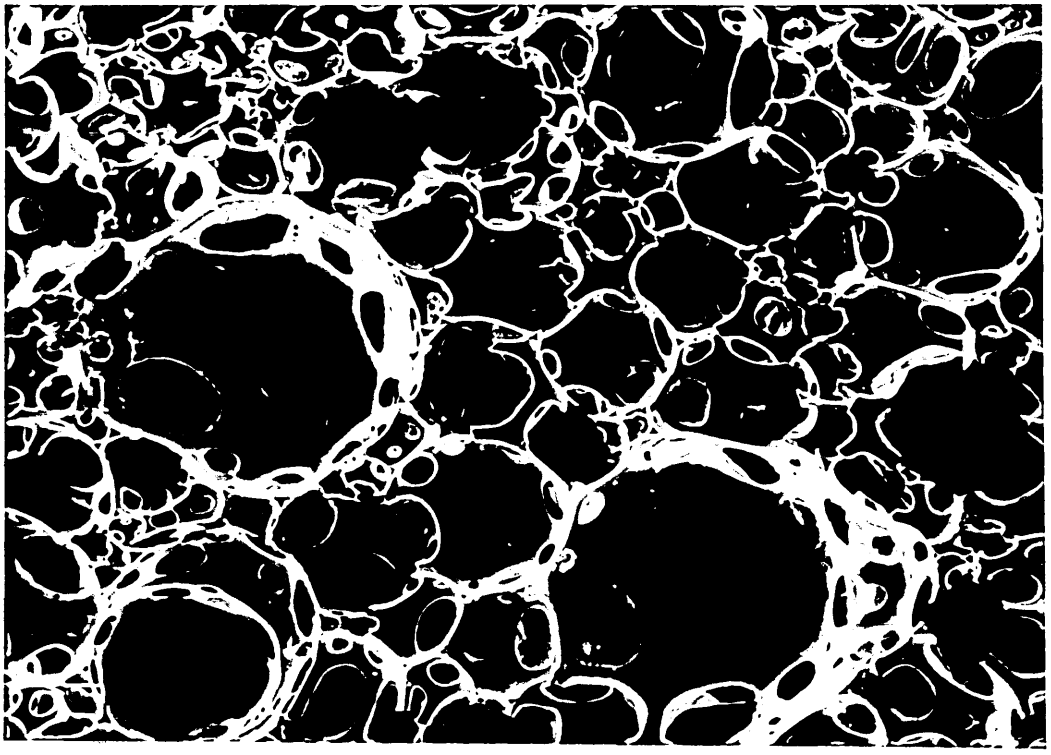

FIGURE 3.8

SEM Micrographs Of the H-R PU Foams a) Containing and b) Not Containing the VC Additive Developed by BP Chemicals [38].

TABLE 3.3 Air Flow Properties of B.P. Chemicals Foam Series DW0007

FOAM	BEFORE COMPRESSION		AFTER COMPRESSION	
	K $/10^{-9}m^2$	B $/10^{-4}m$	K $/10^{-9}m^2$	B $/10^{-4}m$
DW0007 00	2.47	0.320	4.74	2.65
DW0007 06	2.38	0.185	5.10	2.65
DW0007 07	2.15	0.187	5.14	2.67
DW0007 08	2.06	0.175	4.88	1.87
DW0007 09	1.36	0.074	4.25	1.10

repeated for this set of foams with the membranes intact. The results are given in table 3.3 along with the previously measured values of K and B with the membranes damaged by compression.

As may be seen from table 3.3 the coefficients K and B have been dramatically altered by compressing the foam prior to taking the measurements. Typically the permeability has been increased by a factor of 2-3 by rupture of the cell membranes. In the case of the coefficient B the values for the foam with the membranes intact are up to 10 times smaller. Both K and B may be seen to decrease significantly as one moves up the foam series.

The results taken for the B P Chemicals foam series with the membranes intact follow much more closely the trends found by the manufacturers. The data of table 3.3 illustrates that the vibration control additive in use with the foam series changes the air-flow properties by introducing membranes between the cells to restrict fluid flow. This makes the VC additive unsuitable for use with foams in applications such as cushioning, where large deformations are expected. As the membranes ruptured there would be serious degradation of the foams air-flow properties.

The Flow Resistance Coefficient

The flow resistance coefficient,B ,is a measure of the inertial flow losses generated by flow through the irregular structure. It is characterised by the dimensionless coefficient C_f. Table 3.2 gives the values of B for all the foams considered. The value of C_f for each foam type was then calculated from them by means of equation 3.22, using measured values of d from table 3.1 and assuming that $\tau = \sqrt{2}$.

Equation 3.19 which is the starting point for the derivation of the flow resistance coefficient is in fact more properly a definition for C_f. The friction coefficient will be a function of both the roughness of the passage and the Reynolds number. Values of C_f from the test-pieces considered show very little systematic difference between conventional and high-resiliency samples. In figure 3.9 the friction coefficient is

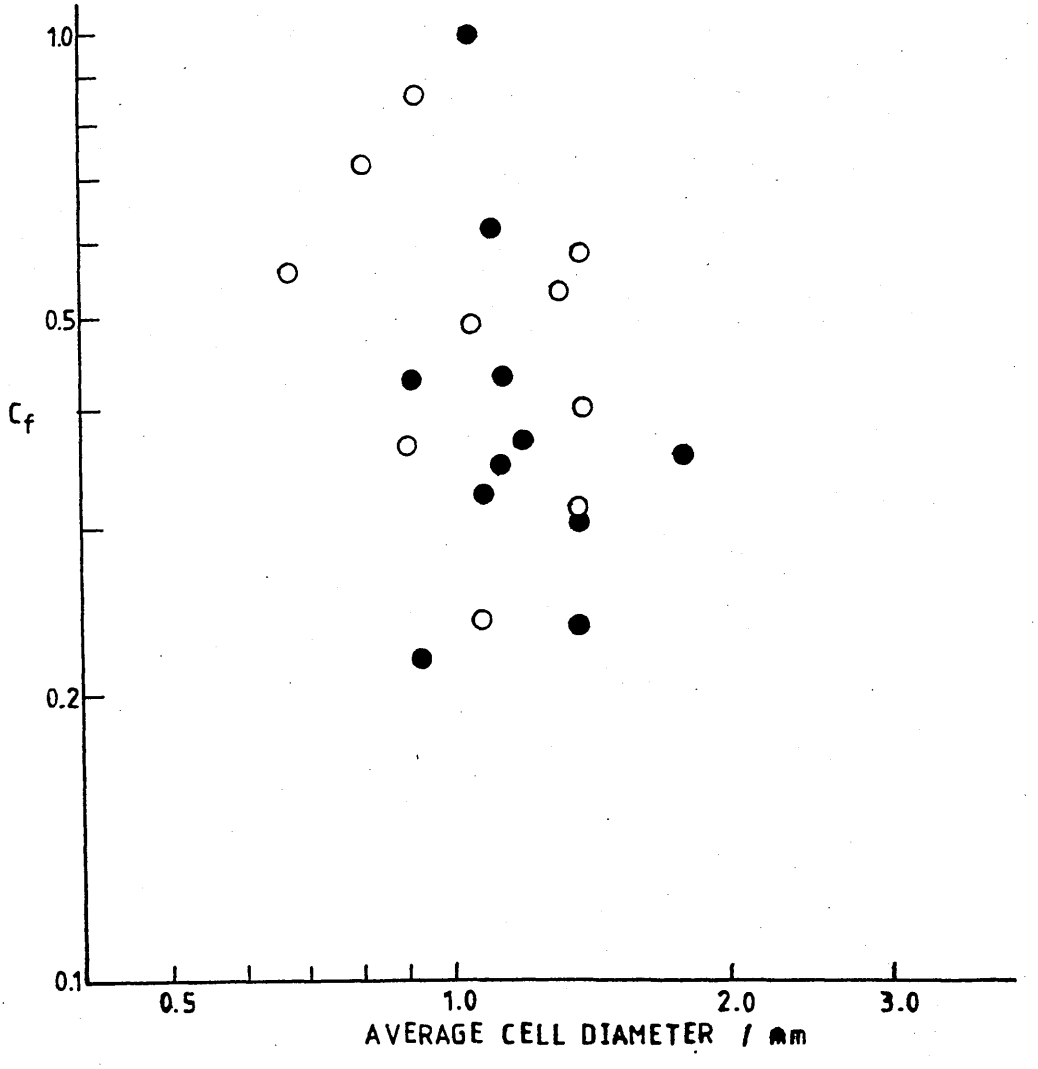

FIGURE 3.9

Variation of the Friction Coefficient, C_f, With Average Cell Diameter. Open Circles; Conventional PU Foams, Closed circles; High Resiliency PU Foam Test Pieces.

plotted against the average cell diameter. It may be seen that there is no correlation between C_f and the size of the cells.

3.4.2 Strain Dependent Behaviour

Values of K and B have been determined for foam samples subjected to varying amounts of transverse, uni-directional, compressive deformation. Fractional strains in the range 0-60% were used. Facilities were not available for the testing of samples subject to tensile deformation.

A typical set of data for a test-piece is plotted in figure 3.10, in the same form as used previously. It can be seen that at each strain level used, the straight line relationship predicted by equation 3.1 holds. Table 3.4 summarises the results of tests of this type. The values are expressed in terms of the zero-strain properties and averaged for all foams of the same type. The standard deviation of the results about the average value is also given.

As expected both K and B decrease as the amount of compression increases. The results in table 3.4 are plotted against (1-e) for conventional foams in figure 3.11 and high-resiliency foams in figure 3.12. In each case the theoretical variations predicted by equations 3.17 and 3.24 for the K and B coefficients respectively are superimposed on the relevant experimental plots.

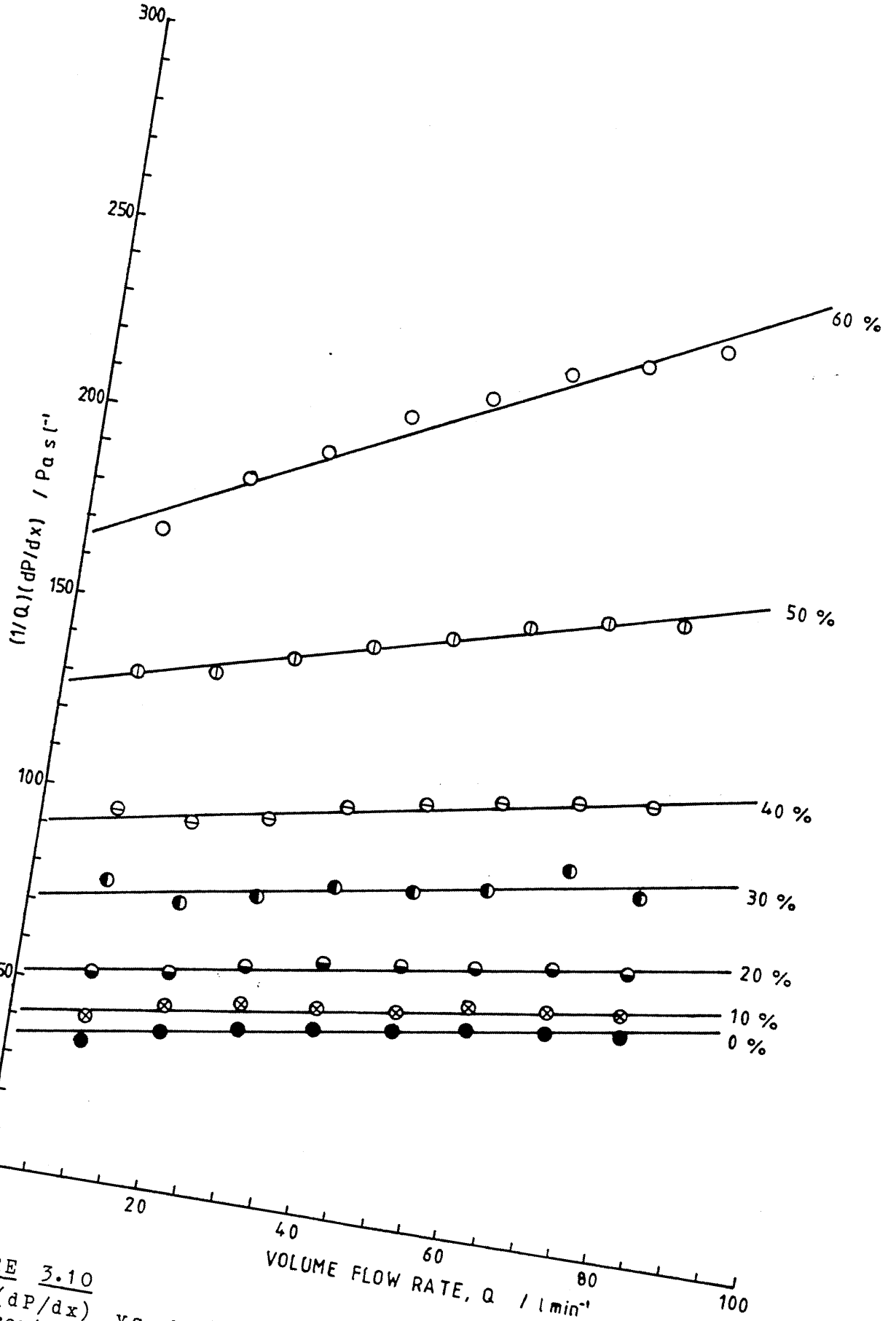

FIGURE 3.10
(1/Q)(dP/dx) vs Q for a Conventional PU foam Under Different Levels of Static Compression.

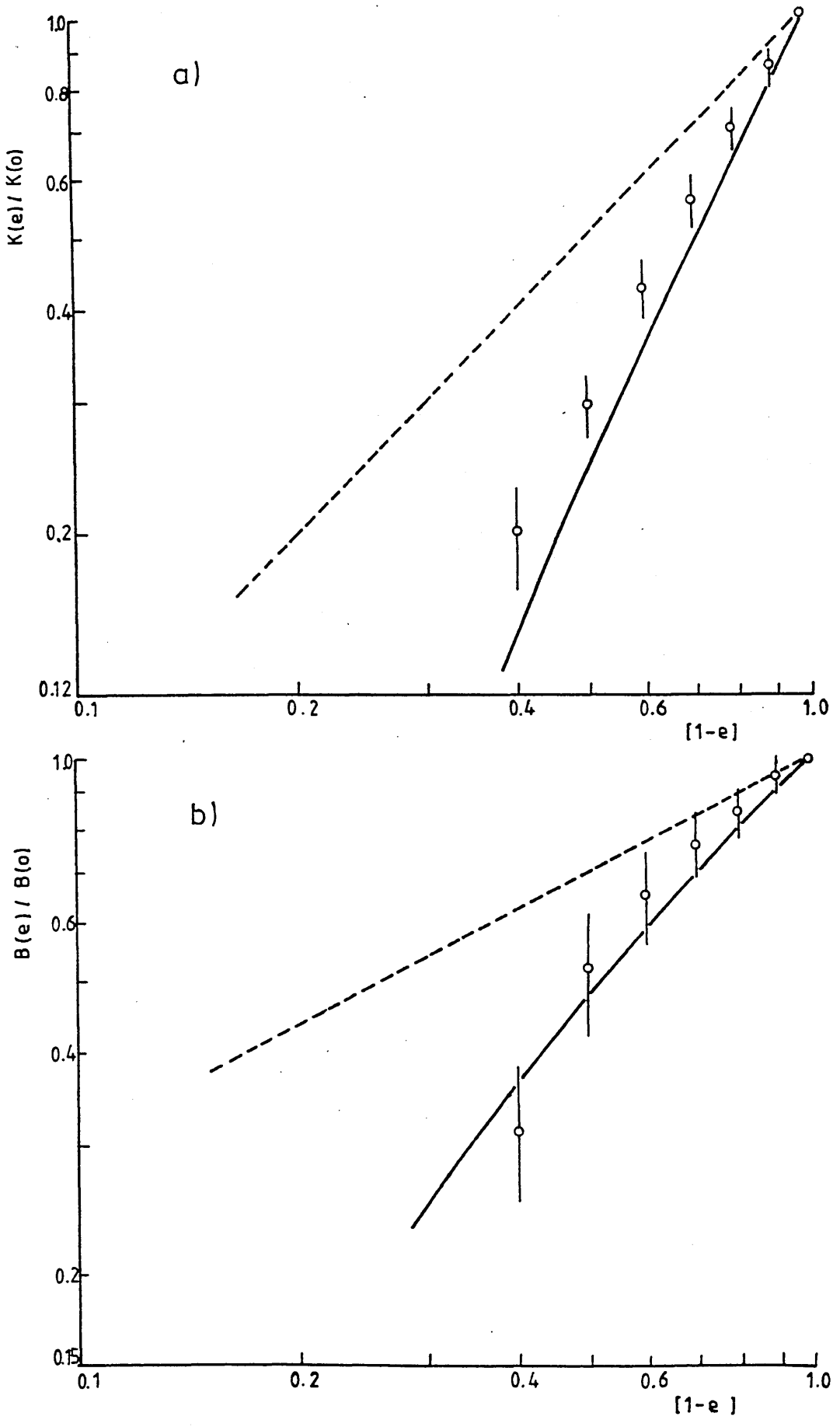

FIGURE 3.11

Variation of a) K and b) B values with (1-e) for Conventional PU Foam Samples. Solid Line; Theoretical Prediction, Broken Line; Variation Predicted by Gent and Rusch [39].

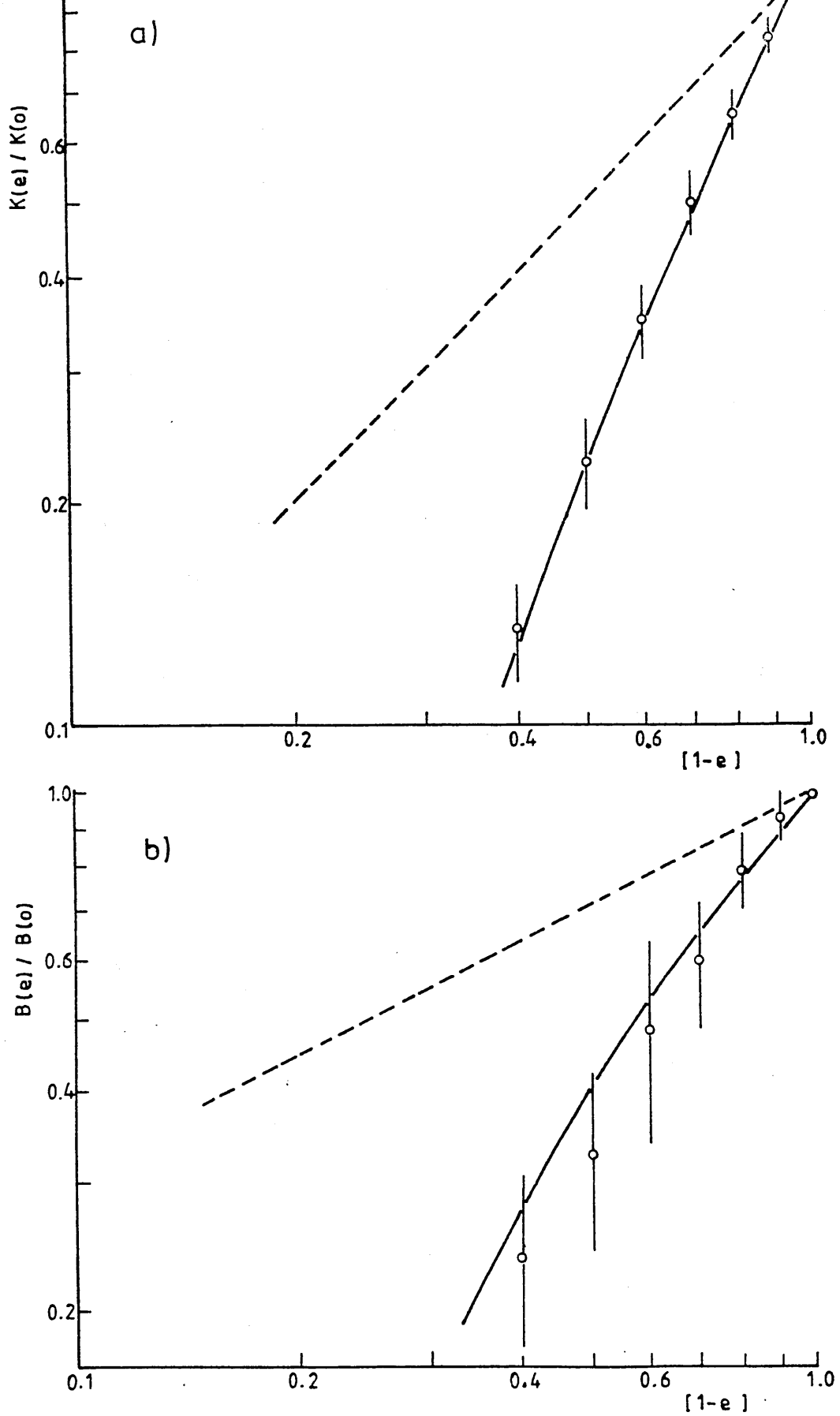

FIGURE 3.12

Variation of a) K and b) B values with (1-e) for High-Resiliency PU Foam Samples. Solid Line; Theoretical Prediction, Broken Line; Variation Predicted by Gent and Rusch [39].

TABLE 3.4 Strain Dependence of the Fluid Flow Coefficients. Data for Type I and Type II Foams Averaged for 12 and 10 Test Pieces Respectively

STRAIN / %	K(e)/K(o)				B(e)/B(o)			
	TYPE I		TYPE II		TYPE I		TYPE II	
0	1.0	0	1.0	0	1.0	0	1.0	0
10	0.85	0.03	0.82	0.04	0.95	0.05	0.94	0.06
20	0.70	0.04	0.65	0.05	0.84	0.05	0.79	0.09
30	0.56	0.04	0.50	0.06	0.76	0.08	0.60	0.11
40	0.43	0.03	0.35	0.04	0.65	0.09	0.48	0.15
50	0.30	0.02	0.23	0.03	0.52	0.09	0.33	0.09
60	0.20	0.03	0.14	0.02	0.31	0.06	0.23	0.05

Also shown on the graphs of figures 3.11 and 3.12 are the theoretical curves predicted using the treatment of Gent and Rusch [28,39]. It may be seen that in all cases the predictions of the model based on flow through a packed bed are superior to those for a model based on arrays of pipes.

The results for the variation of the permeability of high-resiliency foams with compressive strain, in figure 3.12a, show good agreement with the relation predicted by the model. With the conventional foams drawn in figure 3.11a the correspondence is not quite as good. The measured data may be described approximately by a $(1-e)^2$ variation as expected from equation 3.17, but instead of

falling slightly faster than this with imposed strain, as predicted by the model, the opposite is true. It is possible that this small discrepancy is caused by the experimental method used. Several of the lower density foams exhibit a slightly negative Poissons ratio which could lead to air being allowed to pass between test-piece and sample mount. This would result in a slightly higher measured value of K at higher strains. Also the results at the two highest strains for conventional foams are less representative, as they are based on measurements made with fewer foam samples.

For both foam types the variation of the flow resistance coefficient with compressive deformation as predicted by equation 3.24 is well within the error fields of the results for each strain. For a given deformation much more variation in the values of B measured for different foams has been observed than for the permeability. This illustrates that the value of B depends much more critically on the specific structure of the cellular matrix which will vary from foam to foam. This dependence which is contained in the coefficient C_f in the theoretical treatment is also likely to be a function of the imposed strain. This consideration has not been taken into account in the present model treatment.

3.5 Theoretical Extension to Include the Flow of Non-Newtonian Fluids Through Cellular Materials

For Non-Newtonian Fluids the viscous laminar flow term of

equation 3.1 must be modified to take account of the variation of the viscosity with shear rate. The second term in equation 3.1 will not be affected by the use of non-Newtonian fluids as it is generated by inertial flow processes. There are many types of non-Newtonian fluids [40], this derivation is restricted to fluids which can be described in terms of a power-law variation. The empirical power-law relation for non-Newtonian fluids was first proposed by Ostwald [41] and has since been fully described by Reiner [42].

In the following derivation the Hagen-Poiseuille law for the flow of a non-Newtonian fluid through a pipe is discussed and generalised to packed beds. The same approach is then used as in section 3.1.1 to derive the permeability

3.5.1 Zero Strain Behaviour

Consider a power-law fluid flowing steadily through a circular pipe of radius a, as shown in figure 3.13. The relation between the stress, τ, and the shear rate, du/dr, on the surface of a cylinder of the fluid of radius r is [43,44]

$$\tau = \mu \left(\frac{du}{dr}\right)^n \qquad 3.27$$

where μ is the viscosity at zero shear rate and n is the fluid index. If n is greater than unity then the viscosity increases with shear rate and the fluid is

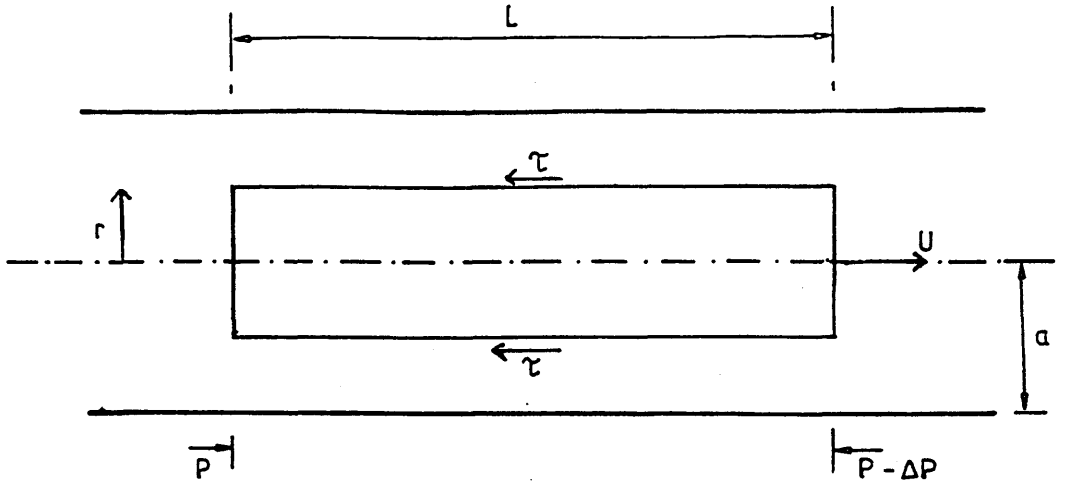

FIGURE 3.13 : Laminar Fluid Flow Through a Pipe

termed dilatant [45]. If on the other hand the fluid index is less than unity the viscosity will decrease as the shear rate increases and the fluid is shear-thinning [46]. n = 1 is the case for a Newtonian fluid.

The total viscous force on the cylindrical element shown in figure 3.13 will be given by

$$2\pi r\, L\, \tau \equiv -2\pi r L\, \mu \left\{\frac{du}{dr}\right\}^{n} \qquad 3.28$$

This force must be balanced by the pressure drop, ΔP, along the pipe if the flow is to remain steady. If u_o is the maximum velocity, which occurs at the centre of the pipe then

$$-\int_{u_0}^{0} u\,du = \left\{\frac{\Delta P}{2L\mu}\right\}^{1/n} \int_{0}^{r} r^{1/n}\,dr \qquad 3.24$$

If it is assumed that there is no slip at the walls of the pipe, then the velocity distribution across the tube will take the form

$$u(r) = \frac{n}{(1+n)} \left\{\frac{\Delta P}{2L\mu}\right\}^{1/n} \cdot \left[a^{(1+n)/n} - r^{(1+n)/n}\right] \qquad 3.30$$

Integrating the velocity distribution over the area of the pipe will give the volume flow rate of fluid through the pipe. As the mean velocity, $u_m = Q/\pi a^2$ this gives

$$u_m = \frac{1}{\pi a^2} \int_0^a 2\pi r U(r) dr = \frac{n}{(1+3n)} \left\{\frac{\Delta P}{2L\mu}\right\}^{1/n} a^{(1+n)/n} \qquad 3.31$$

Equation 3.31 may be rearranged to give the pressure drop as a function of the mean velocity of the fluid. ie

$$\frac{\Delta P}{L} = \left[\frac{(1+3n)}{n}\right]^n \frac{2\mu}{a^{1+n}} u_m^n \qquad 3.32$$

Equation 3.32 is the generalised Hagen-Poiseuille law for the pressure drop along a long pipe due to laminar viscous flow. By putting n=1 equation 3.32 reduces to the standard form of the law [32,47].

Following the treatment used previously for Newtonian fluid flow equation 3.32 is generalised for flow through a packed bed. If u_e and l_e are the effective velocity and length of the porous material, then

$$\Delta P = C(n)\, \mu \frac{l_e u_e^n}{m^{1+n}} \qquad 3.33$$

where m is the hydraulic radius of the void passages and C(n) is a dimensionless constant depending upon the fluid

index. If C_o is the constant used in equation 3.5 then C(n) may be written

$$C(n) = C_o \left\{\frac{1 + 3n}{4n}\right\}^n \qquad 3.34$$

From equation 3.7 the effective velocity of flow through the cellular material is given by

$$u_e = \frac{\tau}{\xi(1 - \phi_0)} u_m$$

The hydraulic radius will be the same as that used in the previous derivation (equations 3.8 and 3.11). For cells of diameter d and surface area $A_c = \pi d^2$ the pressure drop from viscous laminar flow becomes

$$\frac{\Delta P}{L} = C(n)\,\mu \left\{\frac{6\tau}{d}\right\}^{1+n} \cdot \left[\frac{U_m}{\xi(1 - \phi_0)}\right]^n \qquad 3.35$$

Comparison with equation 3.1 shows that for non-Newtonian fluids the two term relation should be generalised to

$$\frac{dP}{dx} = \frac{\mu}{K(n)} u^n_m + \frac{\rho}{B} u^2_m \qquad 3.36$$

where the permeability, K(n) is now a function of the fluid as well as the geometry of the matrix. From equation 3.35 the permeability for a cellular matrix with a non-Newtonian fluid flowing through it may be written

$$K(n) = \frac{\xi^n(1 - \phi_0)^n}{C(n)} \cdot \left\{\frac{d}{6\tau}\right\}^{n+1} \qquad 3.37$$

where n is the fluid index and C(n) is given by equation

3.34. If the fluid index is taken to be unity (Newtonian fluid) then equation 3.37 reduces to that given in equation 3.12. The variation of the permeability with n can also be expressed in terms of the Newtonian permeability, K as

$$\frac{K(n)}{K} = \left[\frac{(1 + 3n)}{n}\right]\left\{\frac{\xi(1 - \phi_0)d}{6\tau}\right\}^{n-1} \qquad 3.38$$

3.5.2 Effect of Pre-Strain on the Non-Newtonian Permeability

For non-Newtonian fluid flow the permeability of the matrix can be expressed as

$$K(n,e) = \frac{[1 - \phi(e)]^{2n+1}}{C(n)\{\tau S(e)\}^{n+1}} \qquad 3.39$$

where S(e) is the previously defined wetted surface per unit volume. The volume fraction of polymer and the wetted surface are both functions of the imposed strain. Their strain dependence is given in equations 3.13 and 3.15. Thus the strain dependence of the material permeability to non-Newtonian fluid flow becomes

$$K(n,e) = \frac{\xi^n}{C(n)}\left\{\frac{d(1 - e)}{6\tau(1 - \phi_0)}\right\}^{n+1}\left[1 - \frac{\phi_0}{(1 - e)}\right]^{2n+1} \qquad 3.40$$

or

$$\frac{K(n,e)}{K(n,o)} = \left\{\frac{(1 - e) - \phi_0}{(1 - e)(1 - \phi_0)}\right\}^{2n+1}(1 - e)^{n+1} \qquad 3.41$$

where K(n,o) is the permeability at zero strain. Both

equations 3.40 and 3.41 reduce to the Newtonian cases (equations 3.16 and 3.17) when n becomes unity.

For shear-thinning fluids the strain dependence of the permeability is less strong than the Newtonian case. For dilatant fluids the opposite is true.

The derivation given above for the flow of a non-Newtonian fluid through a cellular matrix is used as the starting point for the treatment of non-Newtonian fluid-flow damping effects, given in section 4.2.2. The equations generated above for the two term flow equation (3.36), and the zero-strain and strain dependent permeability (equations 3.37 and 3.41) have not been justified by experimentation. However the form of the relations reduces to the Newtonian case when the fluid index becomes unity, and it is assumed that the results are qualitatively correct.

The air flow properties discussed above, together with the theoretical extension to predict the non-Newtonian fluid flow behavior, are used extensively in the discussion of the fluid flow damping process in cellular materials subject to oscillatory deformation. This process is discussed in section 4.2 for both Newtonian and non-Newtonian fluid flow.

4. EFFECT OF COMPRESSIVE PRE-STRAIN ON DYNAMIC PROPERTIES

4.1 The Small Strain Dynamic Mechanical Properties in the Absence of Fluid-Flow Damping

4.1.1 Introduction

For resilient materials exhibiting stiffness and damping the stress $\sigma(\omega)$ generated by an oscillatory deformation $\varepsilon(\omega)=\varepsilon_o \sin(\omega t)$ is given by

$$\sigma(\omega) = E(\omega)\ \varepsilon_0\ \sin(\omega t + \delta) \qquad 4.1$$

where $E(\omega)$ is known as the dynamic modulus and δ is the phase angle the stress lags behind the strain. Equation 4.1 is normally written in complex form [48,49,50]

$$\sigma^*(\omega) = E^*(\omega)\ \ \varepsilon(\omega) \qquad 4.2$$

where $\varepsilon(\omega)$ can be any oscillatory deformation. The complex modulus $E^*(\omega)=E'(\omega)+jE''(\omega)$ is both frequency and temperature dependent, although for materials well above their glass transition temperature the temperature dependence is small [48]. The storage modulus, $E'(\omega)$, is associated with elastic processes which are in phase with the applied strain. The loss modulus, $E''(\omega)$, on the other hand is that part of the stress strain ratio which is 90^o out of phase with the applied strain and is associated with viscous loss processes. $E^*(\omega)$ is more often written in the form

$$E^*(\omega) = E'(\omega)\ \{1 + jd(\omega)\} \qquad 4.3$$

where $d(\omega) = E''(\omega)/E'(\omega)$ is the loss tangent. $d(\omega)$ is related to the phase angle, δ, given in equation 4.1 by

$$d(\omega) = \tan \delta \qquad 4.4$$

In addition to being frequency and temperature dependent the dynamic storage modulus and loss tangent will be functions of the past deformation history of the test piece and the amount of static pre-strain imposed. The former has been reviewed elsewhere [51,52,53] and attention is concentrated on the latter effect. Previous work on the dynamic mechanical properties of cellular plastics has restricted the level of pre-compression to very low values, where the response of the material is essentially linear. The effect of pre-strain on the dynamic properties has not been reported in the literature.

A note should be made of the difference between the terms strain amplitude and pre-strain. Throughout this work the terms pre-strain or pre-compression refer to the static compressive deformation imposed upon the test piece. This is given the symbol e, and is expressed as a fraction of the undeformed height of the sample. The symbol e is also used for the strain in quasi-static force-deformation measurements. The strain amplitude refers to the amplitude of an oscillatory deformation

about the level of pre-strain imposed. This is expressed as a fraction of the height of the sample under the chosen pre-strain and is denoted by the symbol ε. In the following discussions pre-strains in the range 1% to 70% have been used. In all cases studied in this work the dynamic strain amplitude was small, at about 0.5-1%.

Use is made of small strain amplitudes because under these conditions the dynamic mechanical properties may be considered to be piecewise linear with respect to pre-strain. This is equivalent to assuming that the properties vary smoothly with pre-strain and everywhere remain essentially constant over a change in pre-strain equivalent to the dynamic strain amplitude.

The mechanical properties of resilient materials under non-oscillatory loading conditions have been considered by many workers [54,55,56,57]. The mechanical behaviour is usually characterised in terms of force-deformation (F-D) diagrams, such as that shown in figure 4.1. The curve of figure 4.1 splits into 3 distinct regions. In the first region, up to 4-10% strain, the stress increases in proportion to the strain. This almost Hookean region where the cell elements deform under normal forces is dominated by viscoelastic processes within the polymer forming the matrix. Above a critical value of strain the deformation increases with little or no increase in the applied force. The rapid collapse of the matrix is caused by buckling of the cell elements.

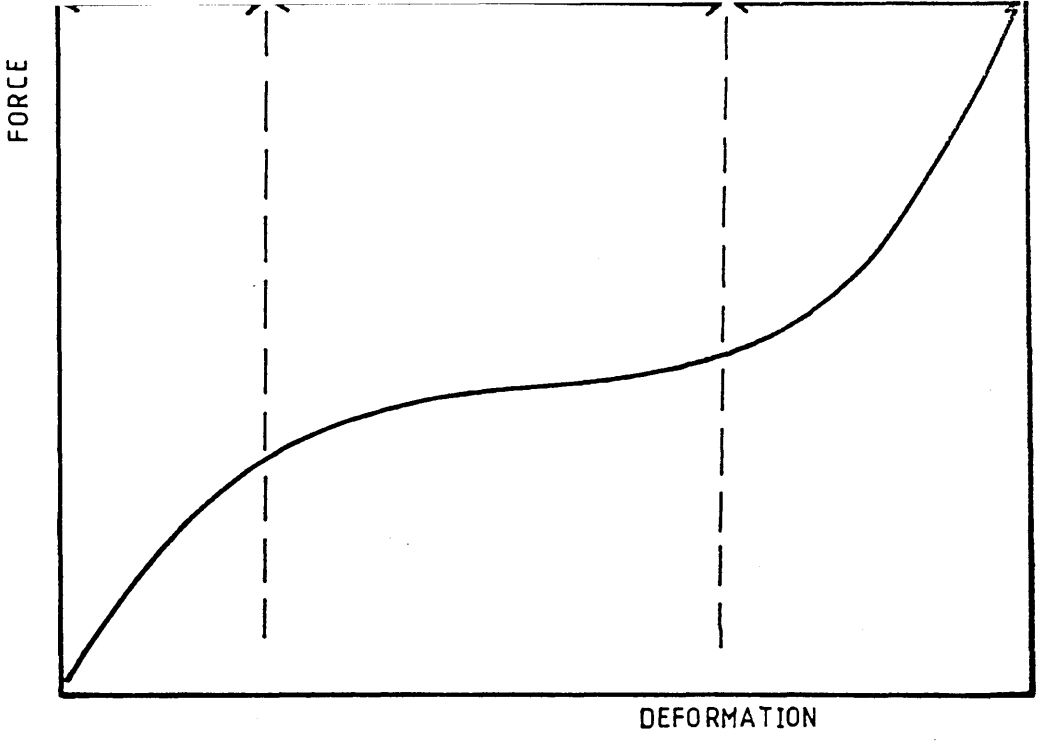

FIGURE 4.1

Typical Compressive Force-Deformation Curve Showing: I- Approximately Hookean Region, II- Plateau Region and III- Strain Hardening Region.

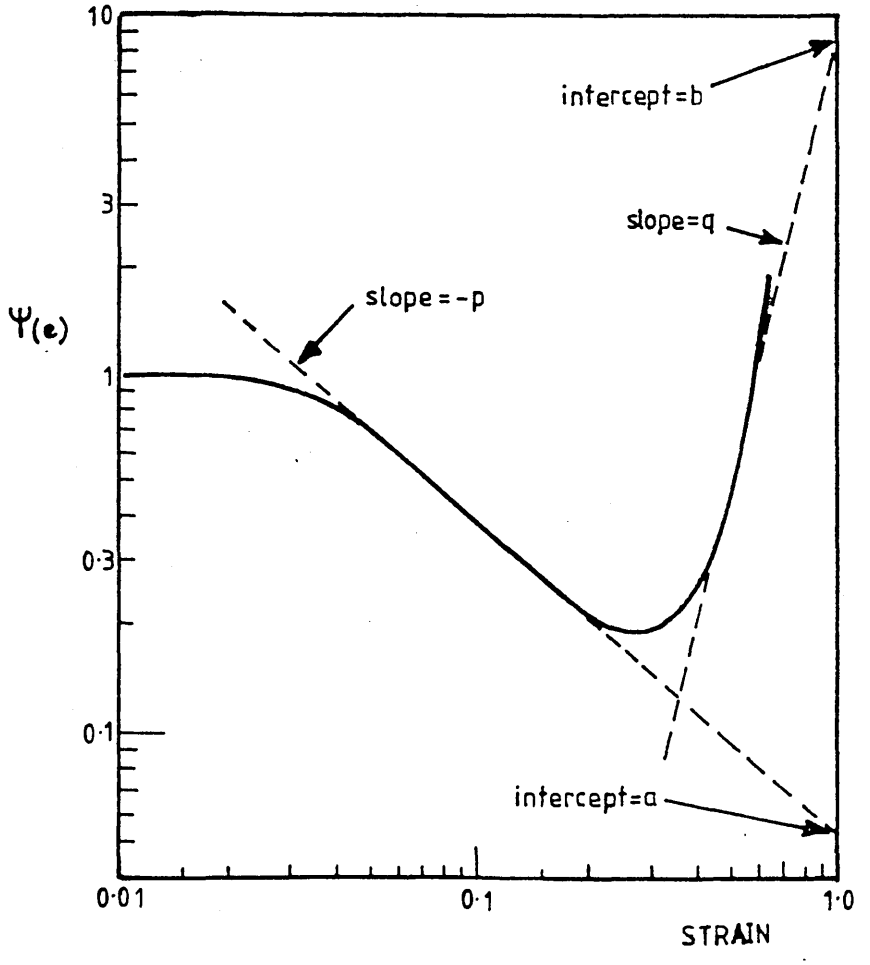

FIGURE 4.2

Idealised Rusch Shape Function Showing the Origin of the Coefficients in Equation 4.8.

Following the plateau region is an area where the material becomes effectively strain hardening. In this final region the buckled cell walls begin to interact, collapse is completed and the structure compacted. At very high strains when $e \cong 1-\phi_o$, (where ϕ_o is the volume fraction of polymer) which typically is about 97%, the free volume is zero and the material should exhibit properties similar to the solid polymer.

Several investigators have attempted an analysis of the shape of the F-D diagram associated with a particular material. Because of the complex nature of the interdependence between cellular structure and the deformation characteristics most of these have been in the form of empirical equations relating the imposed strain to the measured stress. [54,58,59,60,61]. One of the exceptions is the work of Dement'ev and Tarakanov [62,63,64] who have developed equations relating the stress-strain characteristics to the dimensions of the struts forming the cellular structure. They claim that the equations they derive work well with regular structures where the cell walls can be thought of as a series of thin rods. They do not work as well when more irregular structures are discussed, such as those found in high-resiliency foams. Dement'ev and Tarakanov found that the modulus of the foam in the initial Hookean region could be related to the volume fraction of polymer, ϕ_o and the ratio of strut width to length, β by

$$E_f = (E_p/18)\phi_o(2 + \beta) \qquad 4.5$$

where E_p is the modulus of the solid polymer. Of the empirical relations developed the work of Hilyard and Djiauw [60] is notable in that it provides a relation to fit to the F-D curve drawn as the load is reduced. This work has been used sucessfully in the prediction of the impact behaviour of cellular materials. The most widely used empirical relation however, is that due to Rusch [54]. Here the stress at a strain e is factorised into strain dependent and strain independent factors

$$\sigma(e) = E_f \psi(e) e \qquad 4.6$$

where

$$E_f = E_p(\phi_0/12)(2 + 7\phi_0 + 3\phi_0^2) \qquad 4.7$$

The Rusch shape function $\psi(e)$ has been found to follow a relation of the form

$$\psi(e) = ae^{-p} + be^{q} \qquad 4.8$$

where a,b,p and q are empirically determined curve fitting constants. Figure 4.2 shows a typical shape function for a flexible cellular plastic and illustrates the origin of the constants in equation 4.8. According to Rusch, $\psi(e)$ and hence the shape of the compressive stress-strain diagram can be characterised in terms of four measurable quantities; e_b, the critical buckling strain, which is defined as the strain at which $\psi(e)$ has fallen to 0.95, the slope of the $\psi(e)$-e curve post yield (ie the constant p in equation 4.8), the value of

$\psi(e)_{min}$, and the strain e_{min} at the minimum of the curve.

The value of e_b has been found to be independent of cell size, but increases as ϕ_o increases. Generally e_b lies in the range 4-10%. For uniform cell structures the gradient of $\psi(e)$ above e_b should approach 1, this is equivalent to a flat plateau in the F-D diagram. For less uniform structures this gradient will be lower, ie a positive gradient in the F-D curve.

The value of strain at which the minimum value of the shape function occurs, ie e_{min}, has been equated by Ashby [33] to the point at which the buckled cell walls begin to interact. At this strain, Ashby states, the free volume in the foam has fallen to half of its initial value. Because the interaction of adjacent buckled cell walls complicates the behaviour of the material this strain was taken as the upper limit for much of the present work. For practical purposes this strain has been taken to be about 60%.

The mechanical properties measured under non-oscillatory loading conditions are related to the dynamic behaviour of the material. In this investigation the dynamic mechanical properties of a range of conventional and high-resiliency polyurethane (PU) foam samples were measured over a range of values of pre-compression, and the results compared and contrasted with those measured using quasi-static loading techniques.

4.1.2 Experimental Methods

The small strain dynamic mechanical properties of the foam samples were measured over a frequency range of 0.07-70Hz, using the microprocessor controlled dynamic mechanical spectrometer described in Chapter 2. For each test piece the storage modulus and loss tangent were measured over the full frequency range at various levels of pre-compression, in the range 1-60% of the undeformed sample height. The upper level of pre-compression could not be exceeded due to practical limitations to the loading capability of the electromagnetic shaker in use with the spectrometer. In each case the amplitude of the dynamic deformation was set at 0.35mm, or 0.5% of the undeformed height of the sample, and remained at this level throughout the frequency range. A typical example of the variation of the storage modulus and loss tangent with frequency and imposed pre-strain is shown in figure 4.3, in the form of a 3-dimensional graph. Although the test pieces were filled with air and therefore could be subject to fluid flow damping processes, the high permeabilities observed with these foams resulted in the contribution to the mechanical properties from motion of the air in the matrix being negligible in the frequency range of interest

The properties of the test-pieces have been characterised using two other experimental techniques. Force-deformation diagrams such as that shown in figure 4.1 have been generated for each foam sample. The

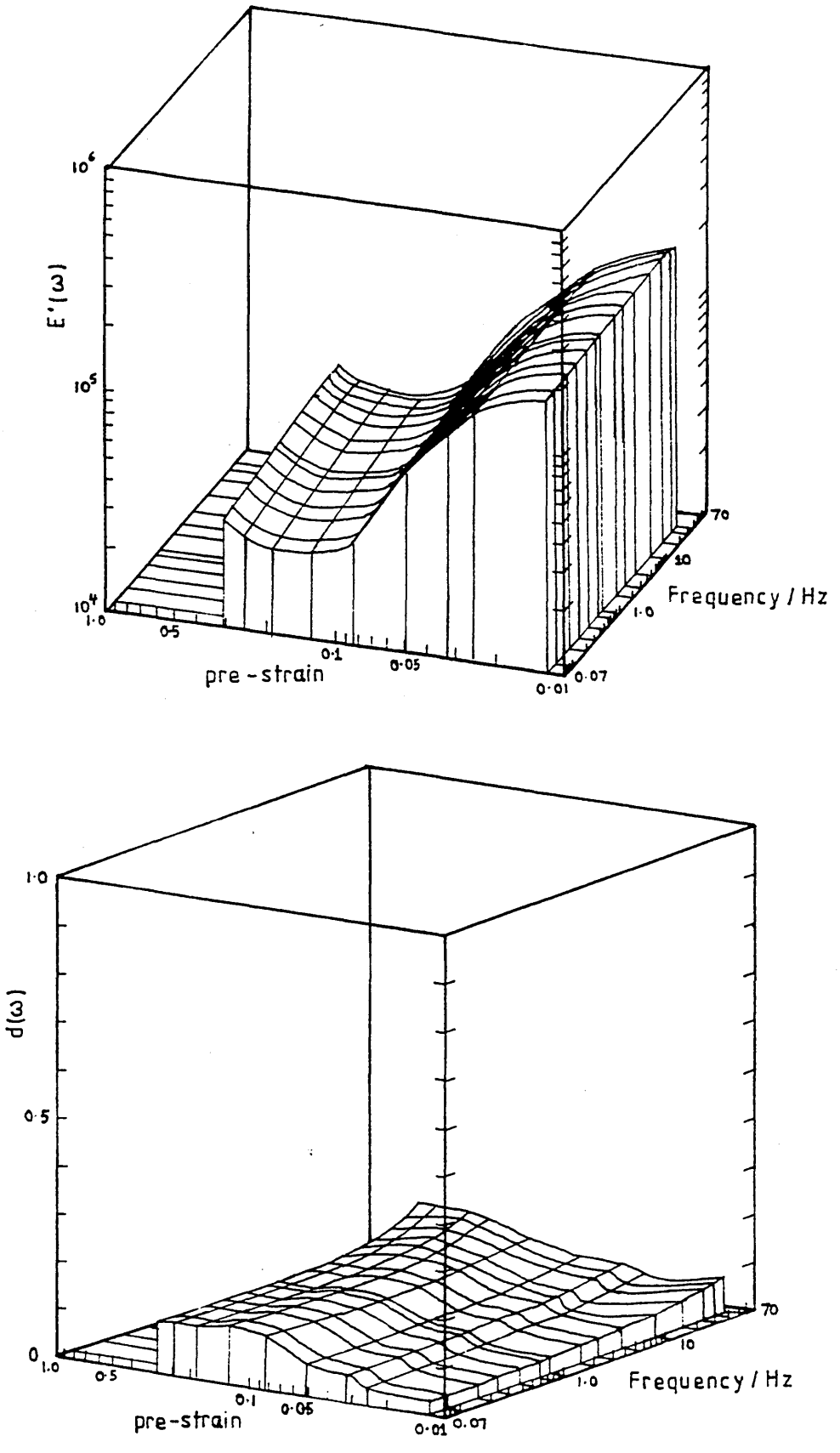

FIGURE 4.3

3-D Graph Showing a) E'(ω) and b) d(ω) as a Function of Frequency and Pre-Strain for a High-Resiliency PU Test Piece.

Table 4.1 Parameters from the Rusch Shape Function

	FOAM	a /10^{-2}	b	p	q	e_b /10^{-2}	$\psi(e)_{min}$	e_{min}
I	VP10	6.4	1.3	0.97	4.5	6.1	0.158	0.50
I	VP12	6.0	2.0	0.96	5.5	4.0	0.152	0.48
I	VP30	6.0	1.0	0.91	3.7	4.0	0.136	0.48
I	VP45	7.6	1.5	0.92	4.1	5.4	0.184	0.47
I	VRT300	5.5	1.2	0.93	4.4	4.0	0.143	0.48
I	VRT400	4.3	0.9	0.97	3.9	3.3	0.123	0.47
II	FHR26	9.3	1.1	0.81	2.5	4.4	0.250	0.41
II	FHR30	3.2	1.0	0.85	3.3	1.2	0.117	0.38
II	FHR50	6.6	1.6	0.80	3.8	2.5	0.182	0.40
II	FHR60	6.8	1.4	0.83	3.5	3.2	0.189	0.40

measurements were made using an Instron Universal Testing Facility, model TT-CM with compression load-cell. Appart from non-standard environmental conditions of temperature relative humidity and sample geometry, all testing was performed to comply with BS4443 [65] and involved loading the sample at a fixed compression rate of 10cm/min, up to a maximum level of 70%. The load was then reduced at the same rate. Tests were performed on samples having a standard size of 240x80x75mm. The test procedure was repeated using the test piece geometry required by BS 4443. Once converted into stress-strain plots, the

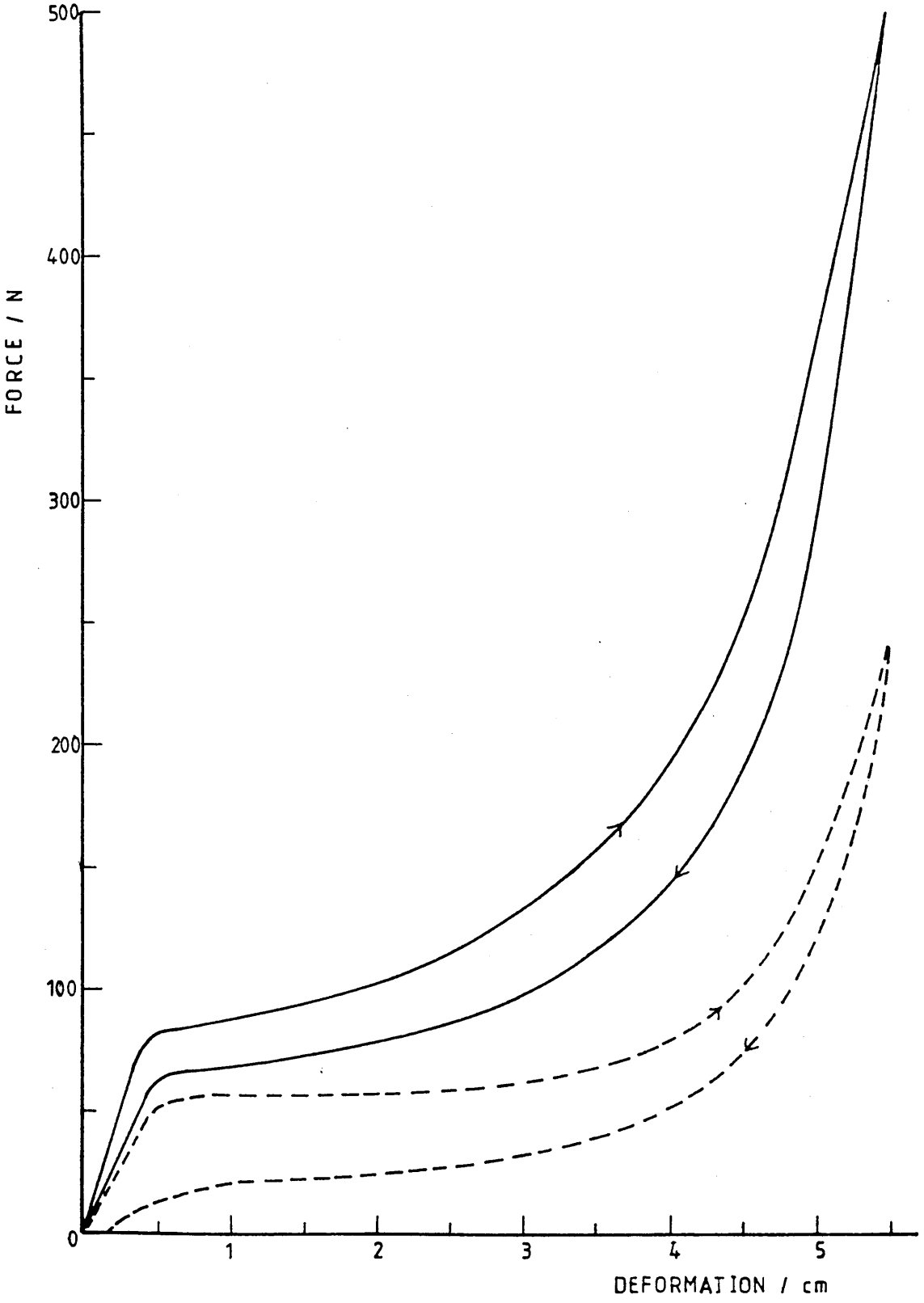

FIGURE 4.4

Compressive F-D Curves for Flexible Test Pieces with the Same Geometry. Solid Line High-Resiliency PU Foam, Broken Line; Conventional PU Foam. Arrows Indicate Direction of Deformation.

difference between the results for the two different geometries was negligible. Figure 4.4 shows typical F-D curves for type I (conventional) and type II (high-resiliency) PU samples having the same test-piece geometry. From curves such as figure 4.4 the Rusch parameters a, b, p, q, e_b, e_{min} and $\psi(e)_{min}$ have been calculated. Table 4.1 sumarises the results for the foam types tested.

The final test method involved the use of an Electro Servo Hydraulic Testing Machine, manufactured by ESH Testing Ltd. This facility has the capability of testing both dynamically and quasi-statically [66]. In these tests the compressive deformation cycle was a half sinusiod at an effective frequency of 0.07 Hz. The preset upper limit was varied in the range 5-70% of the undeformed sample height, and families of curves were drawn. Figure 4.5 shows families of curves for samples of type I and type II. The data is plotted as force against deformation. These are related to the stress and the strain by the sample dimensions.

Test Pieces

The same test-piece geometry was used for all measurements. The samples were a standard shape, forming a rectangular parallelepiped with edge dimensions 240x80x75mm. The smallest dimension in each case applied to the test-piece height and formed the direction of deformation. Uniform loading was achieved by bonding

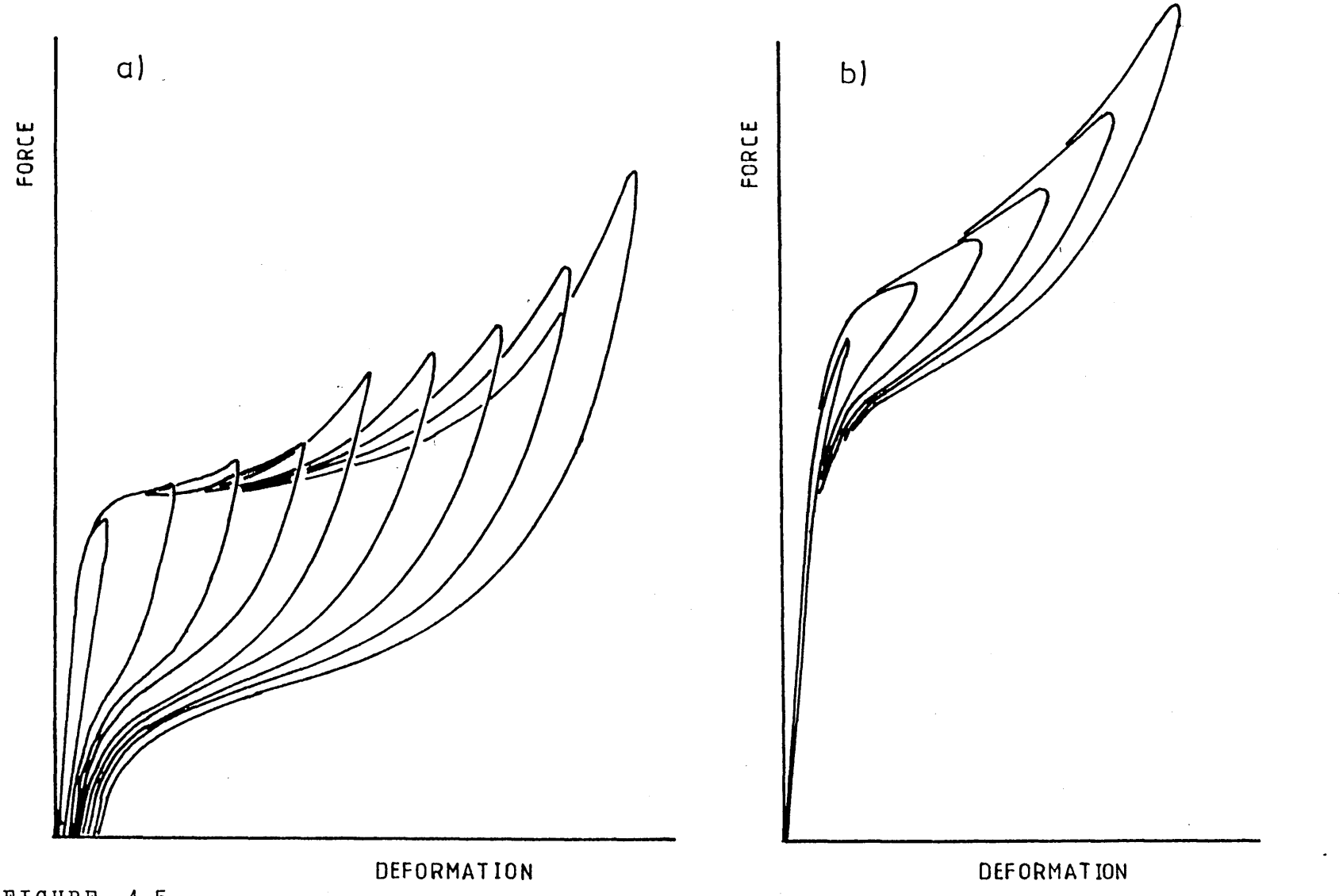

FIGURE 4.5

Force-Deformation Curve Families For a) Conventional and b) High-Resiliency Flexible PU Foam Test Pieces Having the Same Geometry.

flat aluminium plates to the loaded surfaces, by means of a suitable adhesive. The dimensions of each sample could then by measured using a micrometer gauge.

As no environmental control facilities were available, the tests were made at ambient atmospheric temperature and humidity. In all cases the local temperature during the tests lay in the range 22 ± 3 °C. The relative humidity of the environment was checked and found to be in the range 45 ± 10 %. When not in use the test-pieces were stored in a dark place.

4.1.3 Results and Discussion

The small strain dynamic mechanical properties were measured with pre-compression for a range of conventional and high-resiliency foam samples. The storage modulus, $E'(\omega)$, on a logarithmic scale, and the loss tangent, $d(\omega)$, on a linear scale have been plotted against logarithmic pre-strain. Figures 4.6 and 4.7 show typical results for type I and type II samples respectively. In each case the variation is drawn at frequencies of 0.07, 1 and 10 Hz. All test pieces of the same type were found to have properties which vary with pre-strain in a similar manner. Considerable differences may be noted, however, between the results for foam types I and II.

Small Strain Dynamic Storage Modulus

For the type I foam test pieces, $E'(\omega)$ appears to

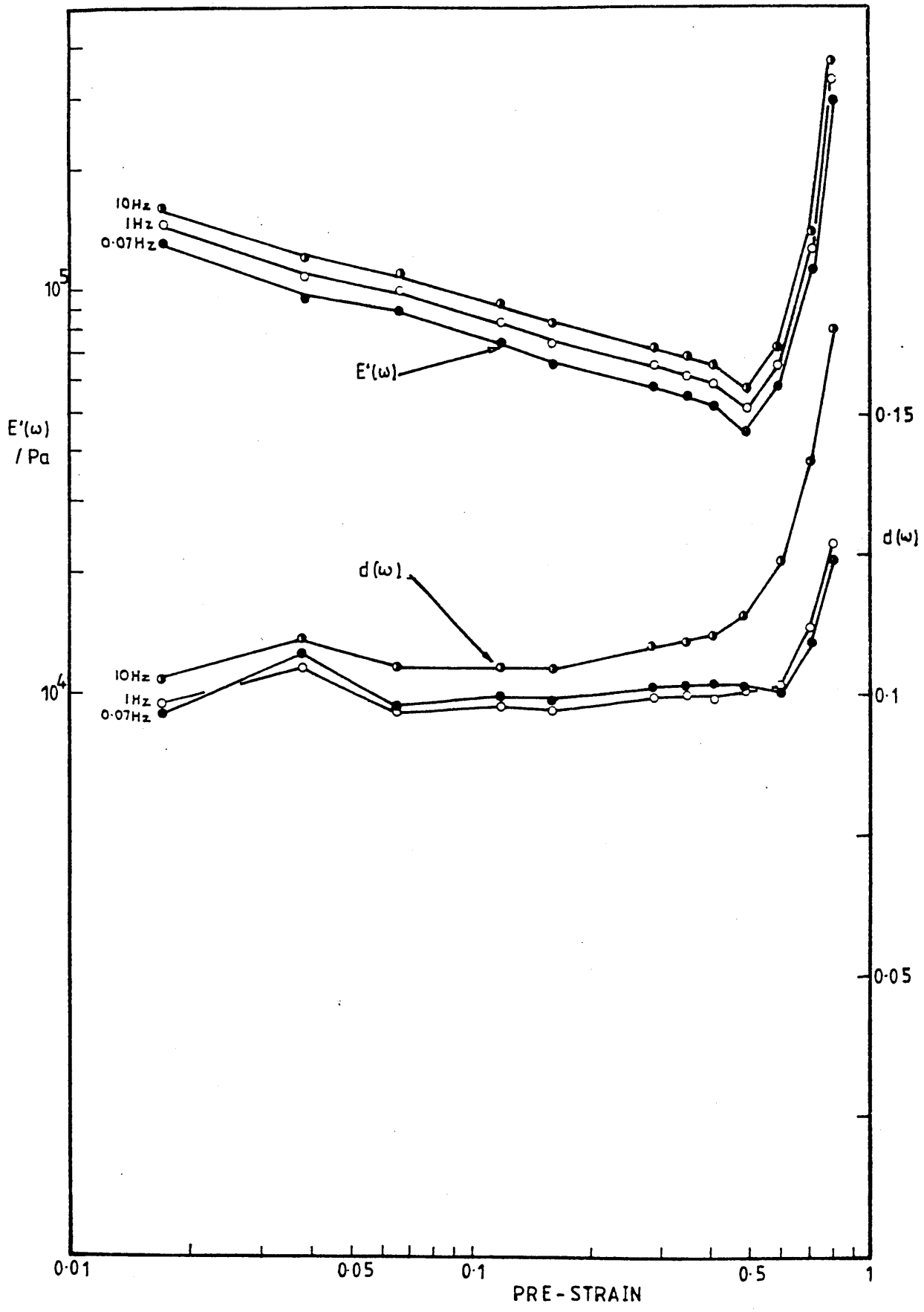

FIGURE 4.6

Variation of E'(ω) and d(ω) with Pre-Strain for a Sample of Conventional PU Foam, at Frequencies of 0.07 Hz, 1 Hz and 10 Hz.

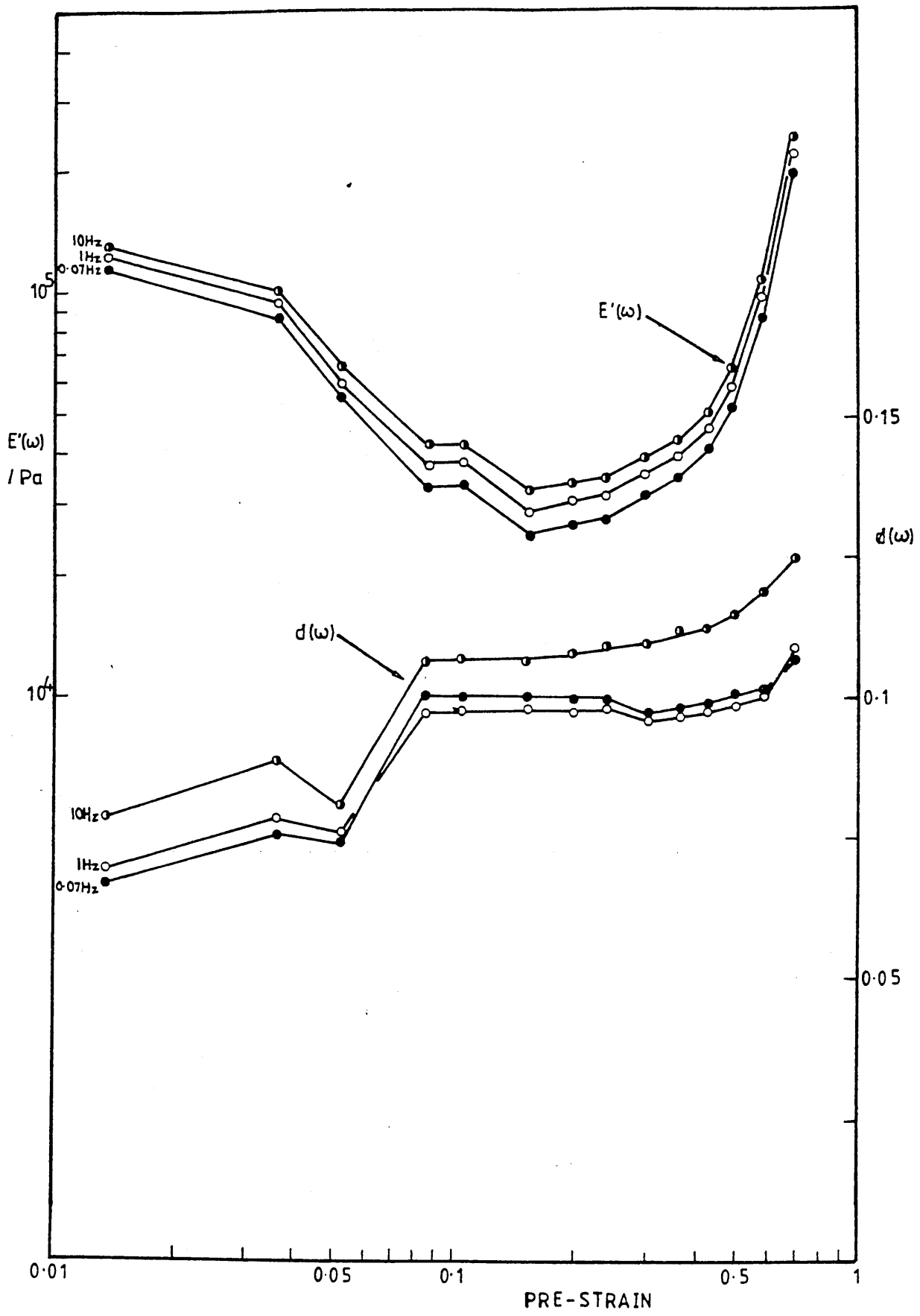

FIGURE 4.7

Variation of E'(ω) and d(ω) with Pre-Strain for a Sample of High-Resiliency PU Foam, at Frequencies of 0.07 Hz, 1 Hz and 10 Hz.

decrease smoothly with increasing pre-compression, to a minimum at about 40-50% strain. In all the samples measured no yield strain was apparent at low frequencies. This is contrary to the accepted view that below the buckling strain, e_b, of the material, the dynamic properties are independent of pre-strain. Above the minimum of the curve, $E'(\omega)$ begins to increase once more. In all cases the variation with pre-strain has been found to be independent of frequency. The systematic increase with frequency of $E'(\omega)$ in figure 4.6 can be attributed to the normal frequency dependence of the viscoelastic properties of resilient materials, and this is consistent with an elastomeric material well above its transition temperature [48].

In the case of type II foam samples a yield strain is noted in the range 1-4%. Below the yield strain $E'(\omega)$ may be considered to be independent of the static deformation imposed. Above the yield value the storage modulus then falls rapidly to a minimum in the strain range 20-30%. $E'(\omega)$ then rises, but less steeply than is the case for type I samples. Once again the curves have the same shape at different frequencies.

The results have been interpreted by defining a shape function in a similar manner to that used by Rusch in the treatment of non-oscillatory deformation. The small strain dynamic storage modulus has been factored into frequency dependent and strain dependent parts

$$E'(\omega) = E_f(\omega) \Xi (e) \qquad 4.9$$

where $\Xi (e)$ takes the form

$$\Xi(e) = re^{-v} + se^{w} \qquad 4.10$$

The coefficients r, s, v and w are empirical curve fitting constants, and are defined in a similar manner to the Rusch coefficients of equation 4.8. In order to fully characterise the curve a further three measurable quantities are defined; the yield strain, e_y, defined as the strain at which $\Xi(e)$ has fallen to 0.95, $\Xi(e)_1$, the minimum value of $\Xi(e)$, and e_1, the strain at the minimum.

Table 4.2 gives the values of these coefficients together with $E_f(\omega)$ measured at 0.07 Hz, for the foams tested in this way. The slope of $\Xi(e)$ post yield has a tendency to be lower for type I foams. Significant differences may also be noted between the constants r and s for the two foam types. The gradient of the shape function above the minimum shows no systematic variation. This was expected as at high levels of pre-strain both types of foam will tend to exhibit properties similar to the solid polymer. As noted previously no yield strain has been observed with conventional foams. In the case of high-resiliency foams no obvious dependence on the foam density or cell size has been found.

The values of strain at the minimum for type II foams

Table 4.2 Parameters from the Dynamic Shape Function $\Xi(e)$

TYPE	$E_f(\omega)$ /10^5 Nm^{-2}	r	s	v	w	e_y /%	e_1 /%	$\Xi(e)_1$
I	1.15	0.068	1.39	0.70	3.58	-	39	0.135
I	1.49	0.138	1.29	0.60	3.03	-	38	0.211
I	1.40	0.150	1.14	0.60	4.45	-	49	0.186
I	1.72	0.055	1.40	0.76	3.89	-	49	0.092
II	0.80	0.010	2.25	1.38	3.01	2	19	0.325
II	1.63	0.006	1.90	1.34	3.51	2.5	18	0.254
II	1.30	0.020	2.04	1.09	3.52	2.7	20	0.185
II	1.51	0.027	1.70	1.23	2.66	3.5	24	0.255
II	1.75	0.056	2.06	0.82	2.99	2.1	26	0.234
II	1.86	0.070	1.78	0.88	2.44	2.2	27	0.188

were consistantly lower than those measured with type I foams. This follows the pattern in table 4.1 for e_{min} defined for the Rusch shape function. In all cases however, e_1 is considerably lower than e_{min}.

The relationship between the Rusch coefficients a, b, p and q, and those defined by equation 4.10 has been investigated. If the small strain dynamic modulus is taken to be the gradient of the stress-strain diagram then by differentiating equations 4.6 and 4.8

$$E(\omega) = \frac{\partial \sigma}{\partial \varepsilon} = E_f\{a(1 - p)e^{-p} + b(1 + q)e^{q}\} \quad 4.11$$

TABLE 4.3 Comparison between $\psi(e)$ and $\Xi(e)$ parameters

FOAM	FROM $\Xi(e)$				CALCULATED FROM $\psi(e)$			
	r	s	v	w	a(1-p)	b(1+q)	p	q
VP10	0.068	1.39	0.70	3.58	0.002	7.3	0.97	4.56
VP12	0.150	1.14	0.60	4.45	0.003	13	0.96	5.50
VP45	0.138	1.29	0.60	3.03	0.006	7.7	0.92	4.14
VRT400	0.055	1.40	0.76	3.90	0.001	4.4	0.97	3.91
FHR26	0.020	2.04	1.09	3.52	0.002	3.8	0.81	2.48
FHR50	0.010	2.25	1.38	3.08	0.001	7.7	0.80	3.78
FHR60	0.006	1.90	1.34	3.51	0.002	6.3	0.83	3.50

The coefficients calculated from equation 4.11 are shown in table 4.3, together with those calculated from $\Xi(e)$. It can be seen that there is little correspondence between the two. The assumption that the effective dynamic modulus of cushion foams can be estimated from the gradient of the F-D curve is obviously false. This has also been recently reported by Crockett [67] for solid rubber vibration mounts.

Dynamic Loss Tangent

The loss tangent, $d(\omega)$ is a measure of the amount of damping exhibited by the test piece. The two foam types exhibit different variations for $d(\omega)$ with the level of

pre-strain imposed, especially at low strains. The variations shown in figures 4.6 and 4.7 for specific samples are typical for each foam type.

Generally at low strains the inherent damping of the matrix for type I foams is higher than type II. However at the level of pre-strain at which the storage modulus is decreasing most rapidly, $d(\omega)$ for type II foams suddenly increases by a factor of up to 2. Type I foams do not exhibit this sudden change in the level of damping. Above this strain the loss tangent for the two types of foam is comparable. $d(\omega)$ remains essentially constant up to a strain of about 50% where it begins to rise for both types of foam.

The value of damping is related to the amount of energy absorbed per deformation cycle. Intuitively it is thought that buckled cellular structures will be more efficient energy absorbers than undeformed matrices. However this does not explain why type I foams exhibit a similar level of small strain dynamic damping before and after the buckling of the cell elements. No published work has been found on the damping characteristics of buckled cellular structures. The increase in $d(\omega)$ at strains above 50% has been interpreted in terms of interaction between the buckled cell walls. The value of strain at which this starts to occur is e_{min} [33]. This is consistent with the observations that e_{min} for the foams under consideration is about 50%.

The variation of $d(\omega)$ with pre-strain is different for different frequencies of deformation. It may be seen from figures 4.6 and 4.7 that in the strain range where $d(\omega)$ changes for type II foams, the damping at 1 Hz becomes lower than that at 0.07 Hz for both foam types. This inversion is reversed at high strain levels. Published work on the variation of the small strain dynamic damping with frequency [50,68,69] does not explain this observation.

Origin of the Small Strain Dynamic Modulus

If a certain level of pre-compression is imposed on a foam sample, then the force required to produce this deformation may be found by inspection of the loading curve of the F-D diagram. A slight reduction of the deformation, however will result in a larger drop in the force than would be expected from the loading F-D plot. Due to hysteresis, the downward loading F-D curve follows a different path to the loading one. If the effect of fatigue is ignored, then on returning the deformation to its origional level the force will return to the previous value determined from the loading F-D diagram. The stiffness, or modulus, of the foam is defined by the rate of change of the force with deformation. As the initial part of the unloading F-D curve has a gradient which is much higher than the loading one, the modulus exhibited by the foam for cyclic deformation will be dominated by the unloading characteristics of the material at the level of pre-strain imposed.

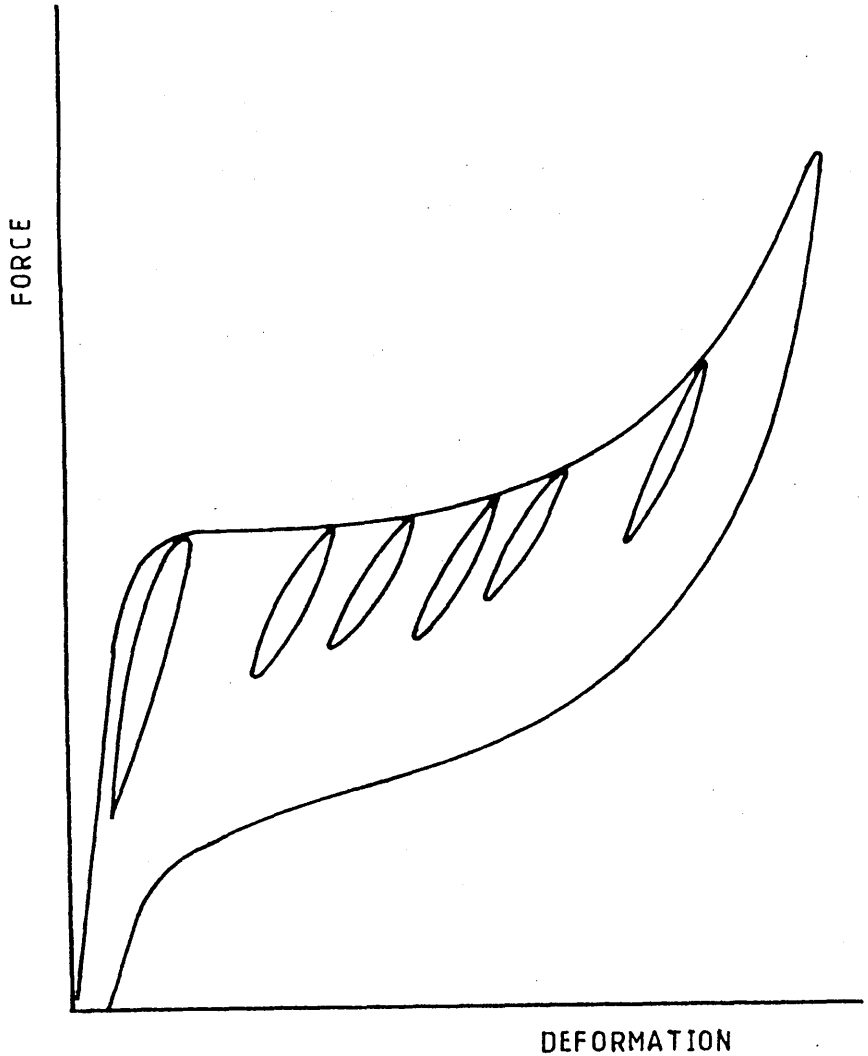

FIGURE 4.8

Dynamic Force-Deformation Cycles with an Amplitude of 2.5 mm Superimposed on a Static F-D Plot. Conventional Flexible PU Foam.

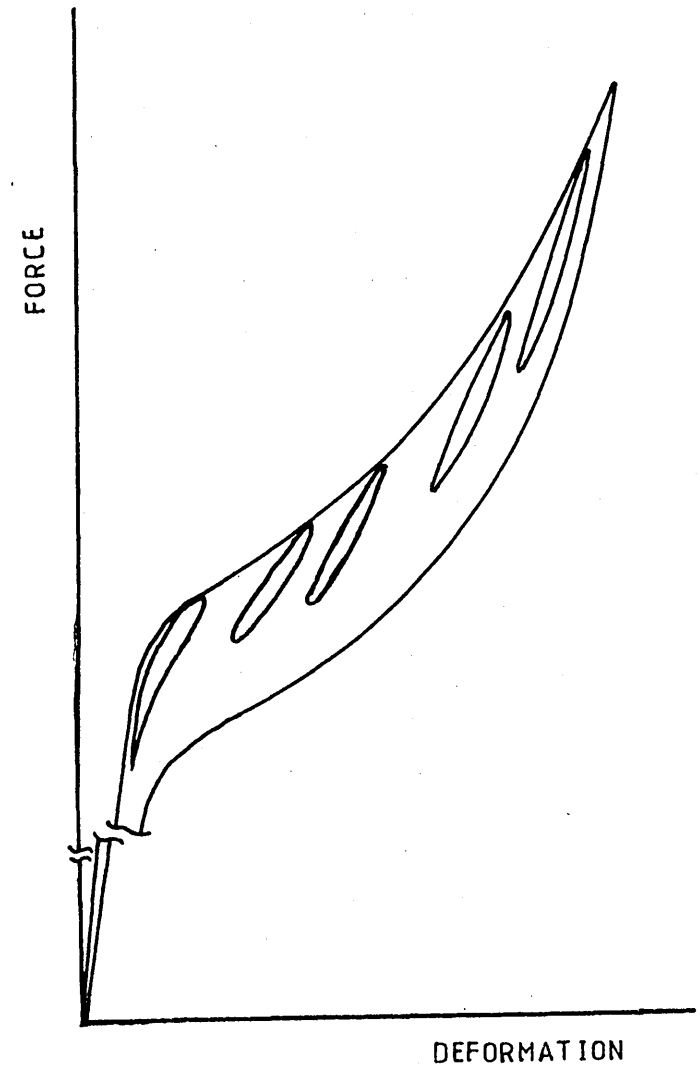

FIGURE 4.9

Dynamic Force-Deformation Cycles with an Amplitude of 2.5 mm Superimposed on a Static F-D Plot. High-Resiliency Flexible PU Foam.

This hypothesis is supported by data taken using the ESH testing machine. For a sample of each foam type the F-D curve was drawn for a maximum deformation of 70%. variable levels of pre-compression were then imposed and measurements of the force-deformation responce to small oscillatory deformations made. The frequency of the oscillatory deformations was fixed at 0.07Hz to be comparable with dynamic measurements. In order to observe the response, amplitudes of 2.5mm were used. The results are shown in figures 4.8 and 4.9 for foam samples of type I and II respectively. It may be seen that the cyclic deformation characteristics do not follow the loading curve of the F-D diagram. The average gradient of the oscillatory curves is much higher than the F-D curve at a strain similar to the level of pre-strain imposed. This is as expected if the dynamic properties are dominated by the initial part of the unloading F-D characteristics at the relevant pre-strain.

The variation of the unloading gradient with strain has been measured from families of curves such as those shown in figure 4.5. Figures 4.10-4.13 show the variations for two samples of each type of foam. Also plotted on these diagrams are the dynamic storage modulus, measured at 0.07 Hz, and the gradient of the loading part of the F-D diagram.

It may be seen from figures 4.10-4.13 that in all cases the correspondence between the initial gradient of the

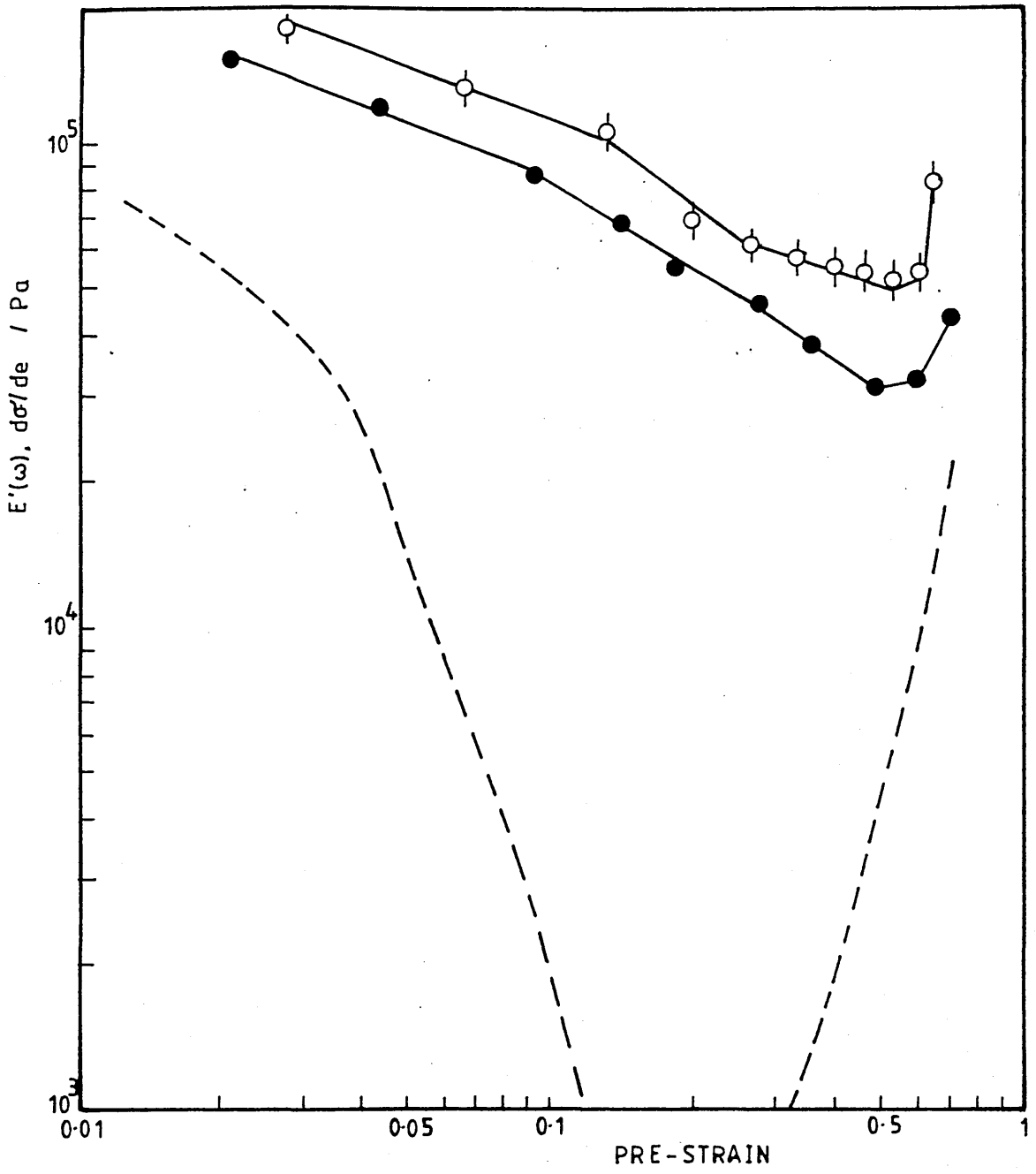

FIGURE 4.10

Comparison Between E'(ω) (Closed Circles) and the Initial Gradient of the Downward Loading F-D Curve (Open Circles) for the Conventional Flexible Foam; VP10. Broken Line; Gradient of the Loading F-D Curve.

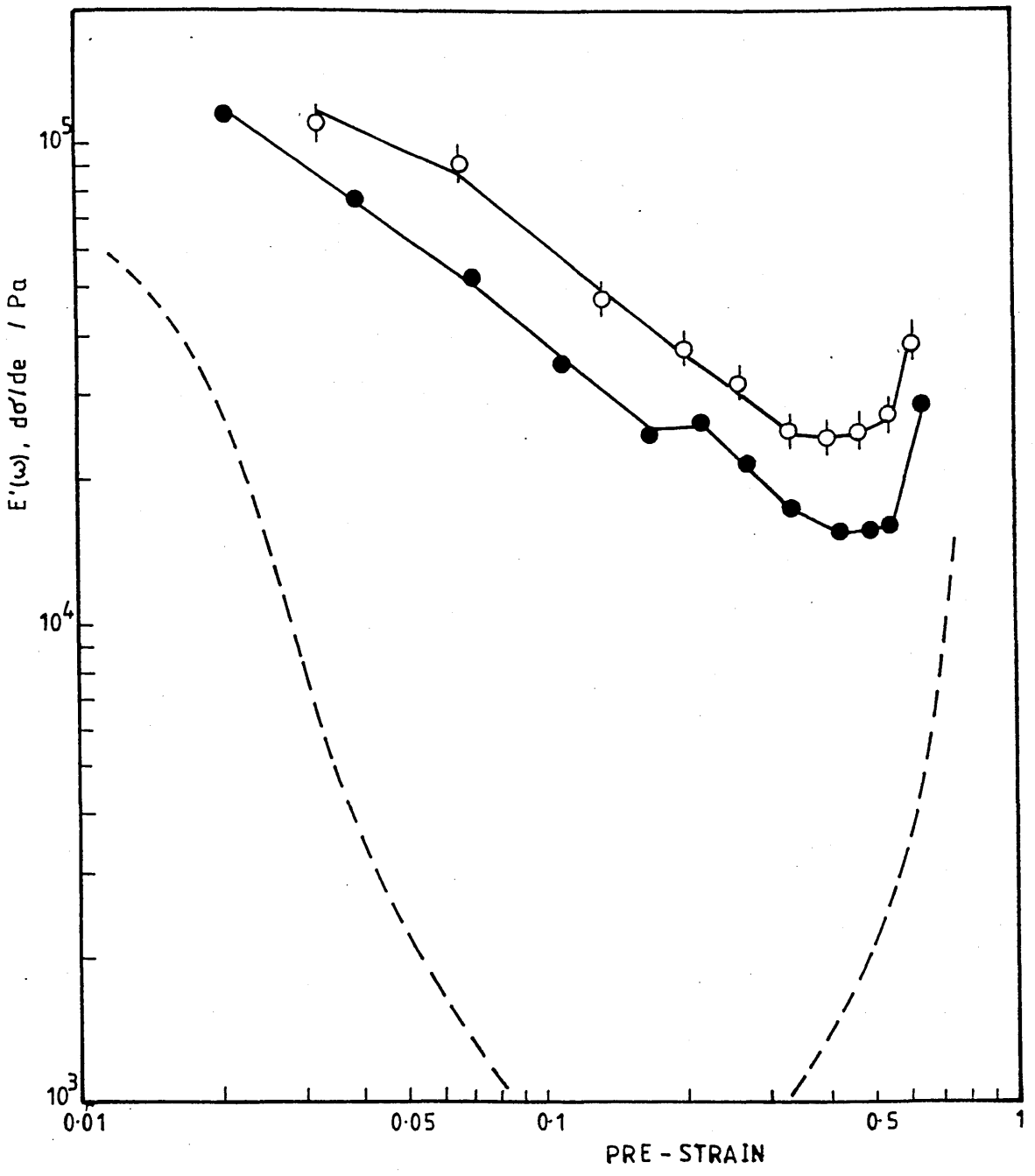

FIGURE 4.11

Comparison Between E'(ω) (Closed Circles) and the Initial Gradient of the Downward Loading F-D Curve (Open Circles) for the Conventional Flexible Foam; VP45. Broken Line; Gradient of the Loading F-D Curve.

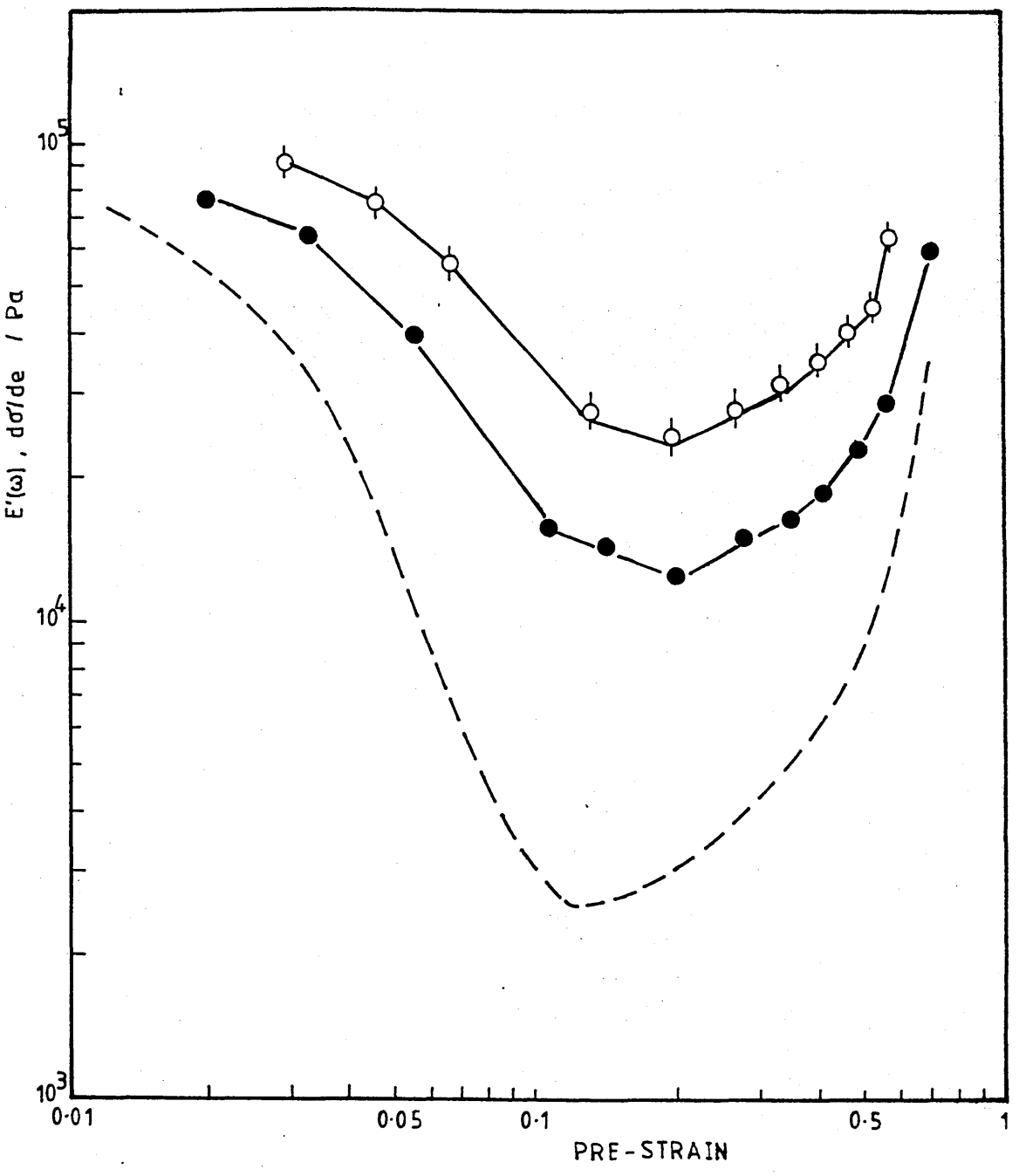

FIGURE 4.12

Comparison Between E'(ω) (Closed Circles) and the Initial Gradient of the Downward Loading F-D Curve (Open Circles) for the High-Resiliency Flexible Foam; FHR 50. Broken Line; Gradient of the Loading F-D Curve.

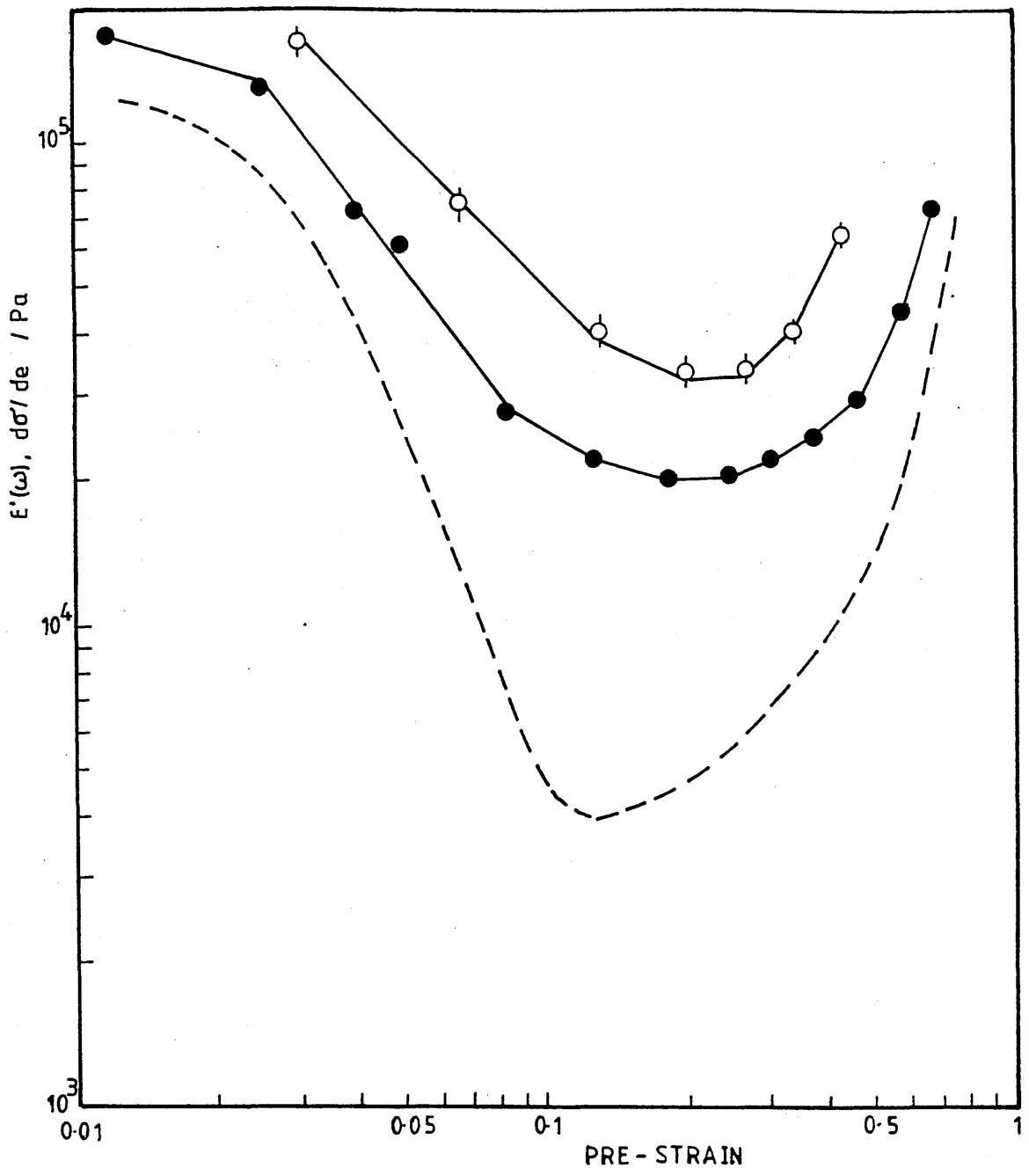

FIGURE 4.13

Comparison Between E'(ω) (Closed Circles) and the Initial Gradient of the Downward Loading F-D Curve (Open Circles) for the High-Resiliency Flexible Foam; FHR 60. Broken Line; Gradient of the Loading F-D Curve.

unloading F-D curve and the small strain dynamic modulus is good. The unloading gradient follows the same variation with strain as the dynamic properties and reproduces the differences between the two types of foam. The dynamic modulus is however consistantly below the unloading gradient, although the difference is less than a factor of 2.

The unloading gradient has been measured at the point at which the deformation changes direction. Inspection of figures 4.8 and 4.9 reveals that the dynamic modulus will be determined by the average gradient over the whole of a deformation cycle. This is always lower than the initial gradient, and may explain the difference between the values measured using the two techniques.

4.2 Dynamic Mechanical Properties of Liquid Filled Systems

4.2.1 Review of Newtonian Fluid Flow Processes

Under dynamic compression, flexible open cell polymer foams sometimes exhibit a higher mechanical damping than can be attributed to the polymer matrix alone [70]. This is caused by the flow of fluid through the matrix and will occur with both compressible and incompressible fluids. Gent and Rusch [28,29,39] found that the fluid flow damping depends on the test-piece geometry, the cell structure, the mechanical properties of the fluid and the frequency of mechanical excitation.

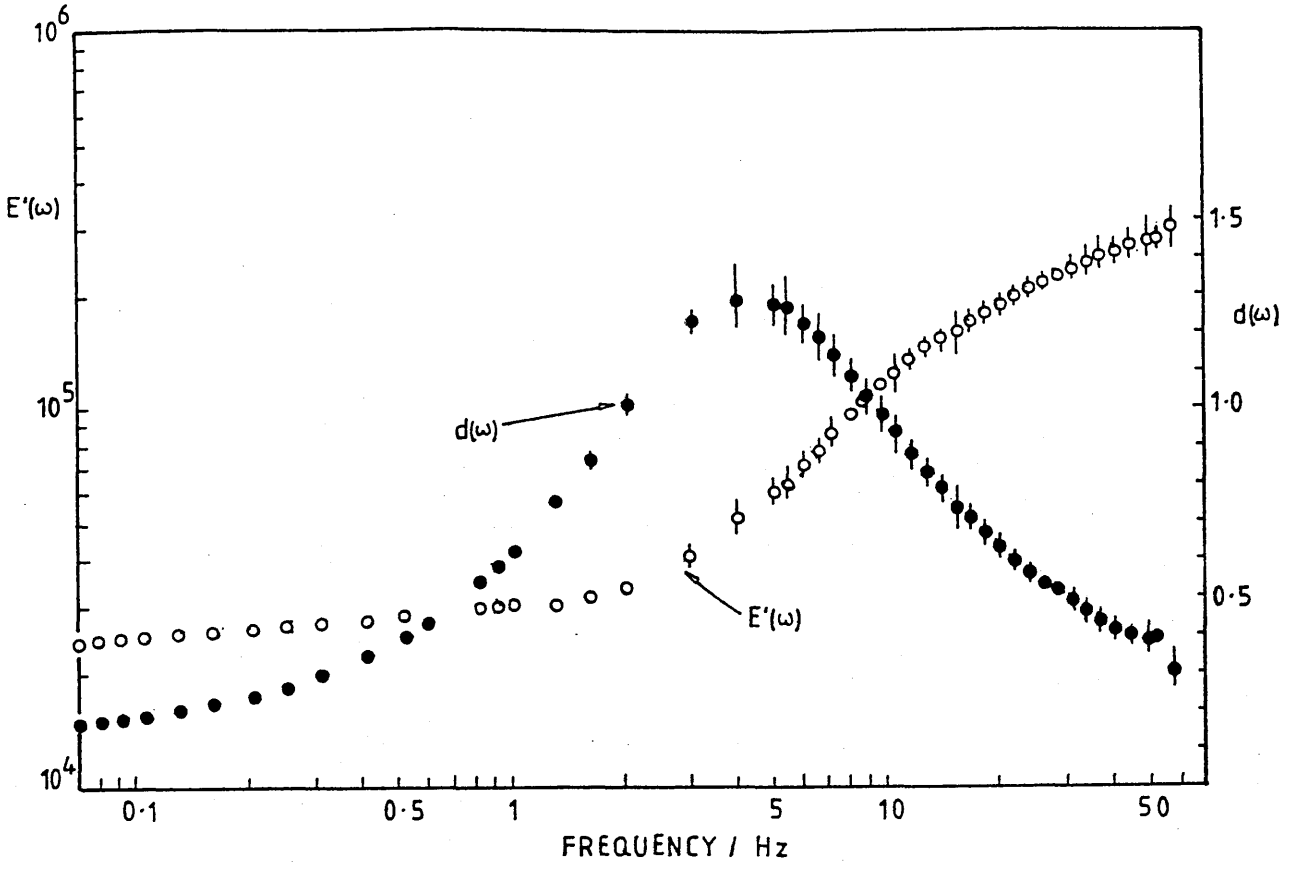

FIGURE 4.14
Variation of E'(ω) and d(ω) with Frequency for a Conventional PU Foam Filled with Water.

The variation of the storage modulus, E'(ω), and loss tangent, d(ω) with frequency for a Newtonian fluid-filled system is shown in figure 4.14. The fluid in this case was water. It may be seen that the damping initially increased with frequency, passed through a maximum value and then decreased. The value of E'(ω) increased with frequency until an equilibrium value was reached. This behaviour is similar to that exhibited by a polymer matrix close to its transition temperature [48,50]. However in this case the transition occurs over a relatively small frequency range.

Energy dissipation resulting from fluid flow has been described qualitatively by several workers [71,72]. The original theoretical approach to fluid flow damping was put forward by Kosten and Zwikker [73]. This was used as the basis for the theoretical treatment of Gent and Rusch [28,39,74] who considered both compressible and incompressible Newtonian fluids. The derivation of the resulting equations has been well summarised by Hilyard [49] and only the conclusions will be discussed here.

For a block of foam of length L, height H, and width W, filled with an incompressible fluid and subject to an oscillatory deformation $\varepsilon = \varepsilon_o \sin\omega t$, the dynamic storage modulus and loss tangent may be written

$$E'(\omega) = \frac{E'_m\{1 + \beta(1 + \beta)\gamma^2\}}{1 + \beta^2\gamma^2} \qquad 4.12$$

$$d(\omega) = \frac{d_m\{1 + \beta^2\gamma^2\} + \gamma}{1 + \beta(1 + \beta)\gamma^2} \qquad 4.13$$

where $$\gamma = (\omega\eta W^2)/(12\xi E'_m K(\omega)) \qquad 4.14$$

$$\beta = 3(E'_m/E_t)(H/W)^2 \qquad 4.15$$

η is the viscosity of the fluid and E'_m the modulus of the matrix in the absence of fluid flow damping.

The height of the damping peak in figure 4.14 is controlled by the parameter β. As β decreases the maximum value of $d(\omega)$ increases. The frequency at which

the damping maximum occurs is determined by the value of γ. Increasing the value of γ increases the maximum damping frequency.

$K(\omega)$ is the effective permeability of the foam and is related to the fluid flow coefficients of the matrix, K and B, discussed in Chapter 3, by the equation

$$\frac{1}{K(\omega)} = \frac{1}{K} + \frac{3W\rho\varepsilon_0\omega}{8\sqrt{2}\xi B\eta} \qquad 4.16$$

where ρ is the density of the fluid. Equation 4.16 represents a simplification to the treatment. This was justified by Gent and Rusch by stating that in the frequency range of interest the inertial flow effects are small in comparison with those generated by viscous flow.

The value of the parameter γ at the maximum fluid flow damping may be found by setting the differential of $d(\omega)$ with respect to γ equal to zero. For small values of d_m this is given approximately from equation 4.13 by

$$\gamma_{max} \cong 1/(\beta + \beta^2)^{\frac{1}{2}} - d_m/(1 + \beta) \qquad 4.17$$

If ω_{max} is the frequency at which the maximum occurs in the damping, then γ may be written

$$\gamma = \omega(\gamma_{max}/\omega_{max}) \qquad 4.18$$

The above equations governing Newtonian fluid flow effects due to incompressible fluids work well for

frequencies up to the damping maximum. At higher frequencies $E'(\omega)$ tends to be higher and $d(\omega)$ lower than predicted. This may be attributed to several factors. Both E'_m and d_m are assumed to be independent of frequency. In fact both will vary with frequency in line with the properties exhibited by viscoelastic materials [48,49,50]. Also the term containing the flow resistance coefficient is not properly accounted for. Additional inertial terms have been proposed by Hilyard and Kanakkanatt [75,76]. These inclusions give better agreement between theory and experiment at high frequencies.

In the case of compressible fluids the mechanical behaviour exhibited is qualitatively very similar to liquid filled foams. The mechanisms governing this behaviour and the derivation of the equations describing compressible fluid flow are described by Hilyard [49]. The variation of the storage modulus and loss tangent have been found to follow relations of the form [28,74]

$$E'(\omega) = E'_m\{1 + 1/\alpha + 8\psi_1/\alpha\} \qquad 4.19$$

$$d(\omega) = \{\alpha d_m + 8\psi_2\}/\{\alpha + 1 - 8\psi_1\} \qquad 4.20$$

where

$$\psi_1 = \sum_{m=1,3,5}^{\infty} \{(m\pi)^2/[(m\pi)^4 + (12\alpha\gamma)^2]\} \qquad 4.21$$

$$\psi_2 = 12\alpha\gamma \sum_{m=1,3,5}^{\infty} \{1/[(m\pi)^4 + (12\alpha\gamma)^2]\} \qquad 4.22$$

The parameter $\alpha = \frac{1}{3}E'_m/E_g$, where E_g is the bulk modulus of the gas, is analogous to the parameter β for incompressible fluids. γ is again given by equation 4.14.

The equations formulated by Gent and Rusch, and discussed above, assume that the level of static compressive deformation imposed on the sample and the dynamic strain amplitude is small. Also the matrix material is assumed to be Hookean. Extensions to the basic treatment to include the effects of pre-strain and the flow of non-Newtonian fluids on fluid flow damping processes, such as described in the following section, have not been reported in the literature.

For incompressible fluid flow the level of pre-strain will influence the mechanical behaviour in several ways. Both β and γ will become strain dependent. β will be altered through the change in the height of the sample, and the variation of the matrix modulus with pre-strain. This latter effect has been discussed in section 4.1. For an imposed compressive pre-strain, e, β will be given by

$$\beta(e) = 3[E'_m(e)/E_t(e)][H(1 - e)/W]^2 \qquad 4.23$$

where from equations 4.9 and 4.10

$$E'_m(e) = E'_m\{re^{-v} + se^{w}\} \qquad 4.24$$

As a first order approximation the frequency dependence

of E'_m has been neglected in equation 4.24. The variation of E_t with strain is not known, E_t is approximately equal to the tensile modulus [39] and a strain dependence similar to that for the tensile modulus may be assumed. It is not known how compressive deformation will affect the tensile modulus in a direction transverse to the direction of deformation, but the tensile modulus in this direction is thought to be relatively insensitive to changes in pre-strain compared to the compressive modulus. The parameter γ will be modified through E'_m and $K(\omega)$. Thus

$$\gamma(e) = [\omega\eta W^2]/[12\xi E'_m(e)K(\omega,e)] \qquad 4.25$$

The strain dependence of the effective permeability, $K(\omega)$ is not known quantitatively. It may be assumed however that it has a similar strain dependence as that of the permeability discussed in chapter 3. This assumption is valid because for the frequencies of interest the first term in equation 4.16 will dominate. From equation 3.17

$$K(\omega,e) \cong K(w,o) \left\{\frac{(1 - e) - \phi_0}{(1 - e)(1 - \phi_0)}\right\}^3 (1 - e)^2 \qquad 4.26$$

where $K(\omega,o)$ is the effective permeability at zero strain. Because so many parameters are affected by the level of pre-strain imposed, the effect of a static deformation on the dynamic mechanical properties is difficult to predict.

Gent and Rusch further restricted their treatment of

fluid flow damping to fluids whose viscosity is independent of the rate of shear. These Newtonian fluids are in fact a special case of a class of non-Newtonian fluids [45]. This class, including dilatant and shear-thinning fluids may be described using the empirical power-law variation proposed by Ostwald [41].

This chapter introduces a theoretical extension to the treatment of fluid flow damping to include foams filled with non-Newtonian fluids, and also discusses the effect of compressive pre-strain on the mechanical properties with both Newtonian and non-Newtonian fluids. Data are presented for foam test pieces filled with a shear-thinning fluid. Reasonable agreement is found between experiment and theory.

4.2.2 Theoretical Treatment of Non-Newtonian Fluid-Flow Damping

The following analysis follows the treatment described by Rusch [39]. However in this case account is taken of static pre-compressions, the non-linear dynamic mechanical force-deflection behaviour of the matrix and non-Newtonian fluid flow processes. For the class of fluids under consideration the stress, τ, on a fluid element a distance r from the centre line of the flow may be related to the shear rate, du/dr, across the element by

$$\tau = \mu \left(\frac{du}{dr}\right)^n \qquad 4.27$$

where n is known as the fluid index and μ is the apparent

viscosity at zero shear rate. For values of n greater than unity the viscosity increases with shear rate. This is the behaviour exhibited by dilatant fluids. Where n is less than one the fluids described are known as shear-thinning. n=1 is the special case for Newtonian fluids. The above equation assumes that at constant temperature and pressure the apparent viscosity is a function of the shear rate alone. This excludes many non-Newtonian fluid types including viscoelastic and Bingham plastic fluids, and those exhibiting a stress memory. The discussion of non-Newtonian fluid types has been undertaken extensively in the literature [40,45,46]. By far the most common theoretical treatment of non-Newtonian fluid flow involves the use of the empirical power-law variation of equation 4.27, and hence is used as the basis of the present work.

Because equation 4.27 is an empirical relation there is a problem with the direction of the stress with respect to the shear rate. It is assumed that a positive shear rate leads to a positive stress. As the viscosity is always positive, equation 4.27 should be written in the form

$$\tau = \mu \left| \left(\frac{du}{dr} \right)^{n-1} \right| \frac{du}{dr} \qquad 4.28$$

This procedure has been used by Jarzebski and Thuille previously for flow through tapered ducts [44]. A derivation of the two term flow equation for power-law type fluids flowing through a cellular matrix has been

undertaken in section 3.1.4. It was found that for a block of material having length L and unit cross-section area, the pressure drop, dP, observed along a length of the foam, dx, is related to the volume flow rate, Q by

$$\frac{dP}{dx} = \frac{\mu}{K(n)} Q^n + \frac{\rho}{B} Q^2 \qquad 4.29$$

where ρ is the density of the fluid and B is a coefficient characteristic of the cellular structure. In a similar manner to equation 4.28 the first term of this flow equation must be modified to correctly predict the sense of the pressure drop with respect to the direction of flow. Thus

$$\frac{dP}{dx} = \frac{\mu}{K(n)} |Q^{n-1}|Q + \frac{\rho}{B}|Q|Q \qquad 4.30$$

The second term has also been modified in a similar manner. If this had not been done then the pressure drop due to inertial flow losses would have been predicted to be in the same direction regardless of the direction of fluid flow. This point was overlooked by Gent and Rusch in their origional derivation for the fluid flow damping arising from Newtonian fluid flow [39]. This does not alter the relevance of their analysis, or the conclusions they reached, as this term was so small that it was effectively ignored.

Consider a block of foam of width W, height H and infinite length subject to a sinusoidal deformation $\varepsilon = \varepsilon_0 \sin \omega t$ as shown in figure 4.15. It is assumed that

C. -£0

— >

W/l

FIGURE 5.15
A Block of Foam Undergoing Dynamic Compressive Deformation, Showing Transverse Deformation Due to the Fluidic Process.

sufficient pre-strain has been imposed in the same direction as the dynamic deformation, such that the foam is in compression throughout the deformation cycle. The volume flow rate, Q, at a plane a distance x from the central plane of the block is given by

$$Q = xe \qquad 4.31$$

The volume fraction of open cells, incorporated into equation 4.51 by Gent and Rusch in their origional treatment, in this case is taken into account in the expression for the permeability. The pressure drop resulting from the flow resistance of the material is

$$\int_{x}^{W/2} (\rho x \cdot W \quad \blacksquare \quad f \quad (\S i \, dx$$

Thus substituting for dP/dx from equation 4.30 and integrating

$$(P_x - P_{W/2}) = \frac{\mu|\dot{\varepsilon}^{n-1}|\dot{\varepsilon}}{(n+1)K(n)}\left\{\left(\frac{W}{2}\right)^{n+1} - x^{n+1}\right\} + \frac{\rho|\dot{\varepsilon}|\dot{\varepsilon}}{3B}\left\{\frac{W^3}{8} - x^3\right\} \qquad 4.32$$

The total compressive force per unit length of material, F, may be calculated from equation 4.32. If pressure differences with respect to the surroundings are considered then

$$F = 2\int_0^{W/2}(P_x - P_{W/2})dx$$

The stress per unit length resulting from the resistance to fluid flow, $\sigma_f = F/W$ will therefore be given by

$$\sigma_f = \frac{\mu|\dot{\varepsilon}^{n-1}|\dot{\varepsilon}}{(n+2)K(n)}\left(\frac{W}{2}\right)^{n+1} + \frac{\rho|\dot{\varepsilon}|\dot{\varepsilon}W^3}{32B} \qquad 4.33$$

For a sinusiodal deformation the stress from fluid flow may be written

$$\frac{\sigma_f}{\varepsilon_0} = \frac{\mu\varepsilon_0{}^{n-1}\omega^n}{(B+2)K(n)}\left(\frac{W}{2}\right)^{n+1} f(\omega t) + \frac{\rho W^3\omega^2\varepsilon_0}{32B}|\cos(\omega t)|\cos\omega t \qquad 4.34$$

where

$$f(\omega t) = |\cos^{n-1}(\omega t)|\cos\omega t$$

It will be assumed that $f(\omega t)$ can be expressed in terms of a fourier series. Thus

$$f(\omega t) = \sum_{p=1}^{\infty} b_p\cos(p\omega t) + c_p\sin(p\omega t) \qquad 4.35$$

In practice the coefficients b_p and cp must be evaluated

numerically for each fluid under consideration. Equation 4.34 may now be written in the form

$$\frac{\sigma_f}{\varepsilon_0} = \Delta(\omega)b_1\cos\omega t + \Delta(\omega)c_1\sin\omega t + \aleph(\omega)|\cos(\omega t)|\cos\omega t + \sum_{p=2}^{\infty} b_p\cos(p\omega t) + c_p\sin(p\omega t) \qquad 4.36$$

where $$\Delta(\omega) = \frac{\mu\varepsilon_0{}^{n-1}\omega^n}{(n+2)K(n)}\left(\frac{W}{2}\right)^{n+1}$$

$$\aleph(\omega) = \frac{\rho\varepsilon_0 W^3\omega^2}{32B}$$

In general the coefficients b_p, for $p > 1$ will be small in comparison to b_1. Also it will be assumed that the coefficients c_p are all small. This is equivalent to assuming that the phase difference introduced between the fluid stress and the applied strain is negligible.

In addition $\Delta(\omega)$ will tend to be much larger than $\aleph(\omega)$ except at high frequencies. The highest frequency under consideration in the present work is 70Hz. At this frequency an order of magnitude calculation using typical values for the foams and fluids in use gives $\Delta(\omega)/\aleph(\omega) \cong 50$. Therefore it is reasonable to assume that the first term in equation 4.36 will dominate. Thus equation 4.36 can be simplified by defining an effective permeability $K(n,\omega)$. If the average value of $\cos(\omega t)$ is taken to be $1/\sqrt{2}$ then

$$\frac{\sigma_f}{\varepsilon_0} = \frac{\mu\varepsilon_0{}^{n-1}\omega^n}{(n+2)K(n,\omega)} \left(\frac{W}{2}\right)^{n+1} \cos\omega t \qquad 4.37$$

where

$$\frac{1}{K(n,\omega)} = \frac{b_1 + c_1}{K(n)} + \frac{\rho(n+2)}{4\sqrt{2}B\mu} \left\{\frac{\omega\varepsilon_0 W}{2}\right\}^{2-n} + \frac{\sqrt{2}}{K(n)} \sum_{p=2}^{\infty} (b_p + c_p) \qquad 4.38$$

Note that $K(n,\omega)$ will be a function of the frequency, the strain amplitude and the sample width in addition to being dependent on the matrix geometry and the fluid in use. The dynamic response of the foam matrix to the sinusoidal deformation in the absence of fluid flow effects can be written

$$\frac{\sigma_m}{\varepsilon_0} = E'_m \sin \omega t + E''_m \cos \omega t \qquad 4.39$$

where σ_m is the stress resulting from deformation of the foam matrix in the absence of fluid flow effects, and E'_m and E''_m are the storage and loss components of the modulus respectively. The total stress, σ_t, may be obtained by adding equations 4.37 and 4.39. The dynamic response of the fluid-filled matrix may be expressed in the form

$$\frac{\sigma_t}{\varepsilon_0} = E(\omega) \sin (\omega t + \delta) \qquad 4.40$$

where
$$E(\omega) = E'_m(1 + \tan^2\delta)^{\frac{1}{2}} \qquad 4.41$$

$$\tan\delta = d_m + \gamma \qquad 4.42$$

$$d_m = E''_m/E'_m \qquad 4.43$$

$$\gamma = \frac{\mu\varepsilon_0{}^{n-1}\omega^n}{(N+2)E'_m K(n,\omega)} \left(\frac{W}{2}\right)^{n+1} \qquad 4.44$$

Equations 4.40 to 4.44 are only valid for relatively low frequencies where the forces generated by the resistance to fluid flow are small relative to the stiffness of the material. As the frequency increases the fluid forces will become sufficiently large to deform the matrix laterally. As the lateral deformation increases the flow resistance losses will decrease as fluid and matrix tend to move together. This will result in a reduction in the fluid flow damping effect.

The contribution to the compressive stress resulting from the lateral deformation of the matrix, σ_l is given, according to Rusch [39] by

$$\frac{\sigma_t}{\varepsilon_0} = \frac{E_t}{3}\left(\frac{W}{H}\right)^2 \sin(\omega t) \qquad 4.45$$

where E_t represents the modulus of the foam for lateral deformation. This is approximately equal to the tensile modulus of the foam. The same stress that causes the fluid to flow will deform the foam laterally. Again following Rusch, from equation 4.37

$$\frac{d\varepsilon}{dt} = \frac{\omega\sigma}{E'_m\gamma} \qquad 4.46$$

and from equation 4.45

$$\frac{d\varepsilon}{dt} = \frac{3}{E_t}\left(\frac{u}{W}\right)^2 \frac{d\sigma}{dt} \qquad 4.47$$

In this case the strains must be added, as the stress will produce motion of the fluid and deformation of the matrix laterally. Thus equations 4.46 and 4.47 may be

combined

$$\frac{d\varepsilon}{dt} = \frac{\omega}{E'_m\gamma} + \frac{3}{E_t}\left(\frac{H}{W}\right)^2 \frac{d\sigma}{dt} \qquad 4.48$$

Putting $\beta = 3(E'_m/E_t)(H/W)^2$ the solution of equation 3.48 will take the form

$$\frac{\sigma}{\varepsilon_0} = \frac{E'_m\beta\gamma^2}{1+\beta^2\gamma^2}\sin\omega t + \frac{E'_m\gamma}{1+\beta^2\gamma^2}\cos\omega t \qquad 4.49$$

The total stress may be obtained by adding the response of the matrix given by equation 4.39 to equation 4.49. The resulting relation will take the form

$$\frac{\sigma_t}{\varepsilon_0} = E'_m\,\Gamma_1\sin\omega t + E'_m\,\Gamma_2\cos\omega t \qquad 4.50$$

where $\Gamma_1 = \dfrac{1 + \beta(1 + \beta)\gamma^2}{1 + \beta^2\gamma^2}$

and $\Gamma_2 \quad \dfrac{d_m\{1 + \beta^2\gamma^2\} + \gamma}{1 + \beta^2\gamma^2}$

Equation 4.50 can also be written in a form similar to that of equation 4.40

$$\frac{\sigma_t}{\varepsilon_0} = E(\omega)\sin(\omega t + \delta) \qquad 4.51$$

where $E(\omega) = E'_m\{\Gamma_1^2 + \Gamma_2^2\}^{\frac{1}{2}}$

$$\tan\delta = \Gamma_2/\Gamma_1$$

It is more usual to express the properties in terms of a storage modulus, $E'(\omega)$, and loss tangent, $d(\omega)$. From a consideration of equations 4.50 and 4.51, we can define

$$\frac{\sigma_t}{\varepsilon_0} = E'(\omega)\{1 + jd(\omega)\}\sin \omega t \qquad 4.52$$

$$E'(\omega) = \frac{E'_m\{1 + \beta(1 + \beta)\gamma^2\}}{1 + \beta^2\gamma^2} \qquad 4.53$$

$$d(\omega) = \frac{d_m\{1 + \beta^2\gamma^2\} + \gamma}{1 + \beta(1 + \beta)\gamma^2} \qquad 4.54$$

For completeness the following definitions are re-stated

$$\beta = 3(E'_m/E_t)(H/W)^2$$

$$\gamma = \frac{\mu\varepsilon_0{}^{n-1}\omega^n}{(n+2)K(n,\omega)E'_m}\left(\frac{W}{2}\right)^{n+1}$$

In the case when the fluid index is unity (Newtonian fluid) equations 4.52 to 4.54 reduce to those given by Gent and Rusch in their origional treatment.

Strain Dependence of the Fluid Flow Damping Effect

If a pre-compression is applied to the test piece prior to the dynamic deformation, the fluid flow damping effect will be modified. Both β and γ will change. In the case of β the modification comes from the change in the height of the sample and changes to the moduli of the foam. For γ both the effective permeability and the modulus of the matrix (in the absence of fluid effects) will become strain dependent. If the amplitude of the deformation is kept constant then the strain amplitude, ε_0 will also change. Thus for an imposed pre-strain, e, β and γ will be given by

$$\beta(e) = 3\{E'_m(e)/E_t(e)\}\{H(1 - e)/W\}^2 \qquad 4.55$$

$$\gamma(e) = \frac{\mu\omega^n\varepsilon_0^{n-1}}{(n+2)E'_m(e)K(n,\omega,e)} \qquad 4.56$$

The variation of the matrix modulus, E'_m, is discussed in section 4.1. Section 3.1.4 includes expressions for the strain dependent coefficients K(e) and B(e). Both of these will contribute to the strain dependent effective permeability $K(n,\omega,e)$ through equation 4.38. The exact variation expected for increasing pre-strain, however, is complex and not known at the present.

4.2.3 Experimental Details

The experimental measurement of the mechanical properties of samples of foam filled with Newtonian and non-Newtonian fluids was made using the dynamic mechanical spectrometer described in chapter 2. Measurements of the storage modulus and loss tangent at many frequencies in the range 0.07-70 Hz were made. These were at a fixed vibration amplitude of 0.7mm pk-pk. The prepared sample was placed in a large tank of the liquid beneath the electromagnetic shaker (see figure 2.21). The bottom face of the sample was fastened to the floor of the tank while the upper face was connected via a drive shaft and force transducer to the shaker table. More details of the mechanical mounting system are given in section 2.6. The test-piece was compressed several times to a high level of strain in order to remove the air from the

cellular matrix and replace it with the test fluid. This procedure was not found to cause any further damage to the cellular structure. Measurements were performed on three different foam samples.

The effect of pre-strain on the dynamic mechanical properties could be investigated by inserting spacer plates between the sample and the tank floor. This produced a static deformation on the height of the test-piece. The dynamic deformation was superimposed on this static level. The actual level of pre-strain was measured using a micrometer and expressed as a fraction of the undeformed height of the sample. Pre-strains in the range 1-60% were used.

Temperature could not be controlled during the experiment. However the use of a large tank of liquid (capacity $\sim$15 litres) resulted in the thermal inertia of the system being large, and the temperature of the sample could be assumed to remain constant throughout the test. The temperature of the liquid in the tank was measured at the end of each test. In all cases the temperature was within the range 18 ± 3 ^{o}C.

The top plate attached to the sample just broke the surface of the liquid. At high frequencies it was found that standing waves were set up on the surface of the liquid. These standing waves only became a serious problem for frequencies above 70 Hz. The use of a large

tank and small amplitude dynamic oscillations (0.35mm) enabled the standing waves generated to be kept small, at the frequencies of interest.

Test-Pieces

The foam samples to be tested were cut to form a rectangular parallelepiped with standard sides 240x80x75 mm, where the smallest dimension applies to the height of the sample. The length to width ratio of 4:1 was chosen because for test-pieces with this geometry, the foam block approximates to an infinitely long block [39]. To prevent the fluid flowing through the top and bottom of the block, these faces were bonded to rigid plates. These plates additionally provided a means of applying the mechanical deformation evenly to the loaded area of the test-piece, and a fixing point for the bottom of the block to the floor of the tank.

Fluid Preparation

For this series of measurements two fluids were used, one Newtonian and one shear thinning. The Newtonian fluid used was water. The shear thinning fluid was freshly prepared by dissolving 0.5% bw Carboxymethylcellulose (CMC) in water. This solution forms a liquid with a relatively high viscosity and a behavior which may be described adequately by the empirical power-law variation of equation 4.27 [41].

The properties of the CMC solution were ascertained using

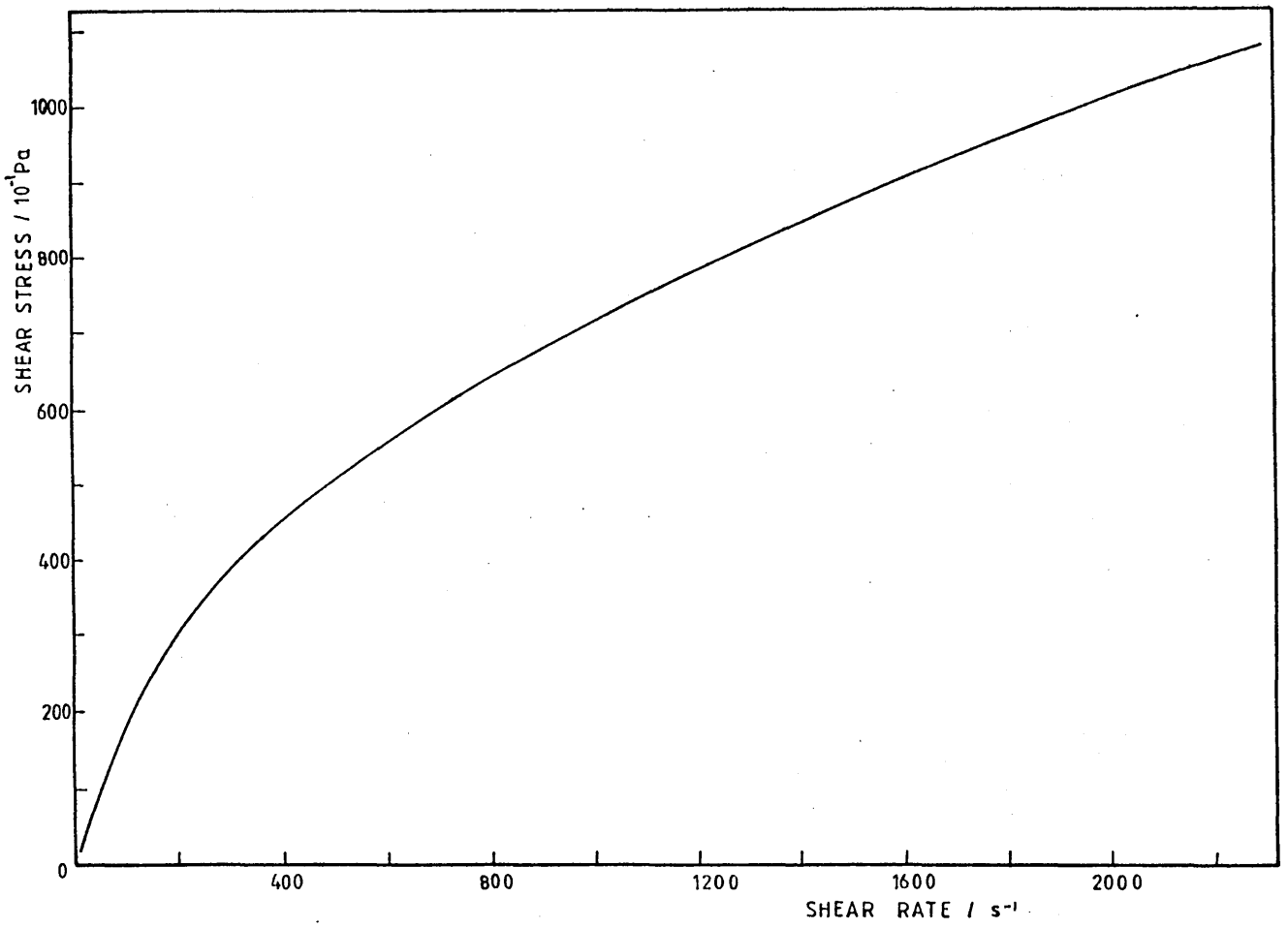

FIGURE 4.16

Variation of Shear Stress with Shear Rate for a Solution of 0.5% Carboxymethylcellulose.

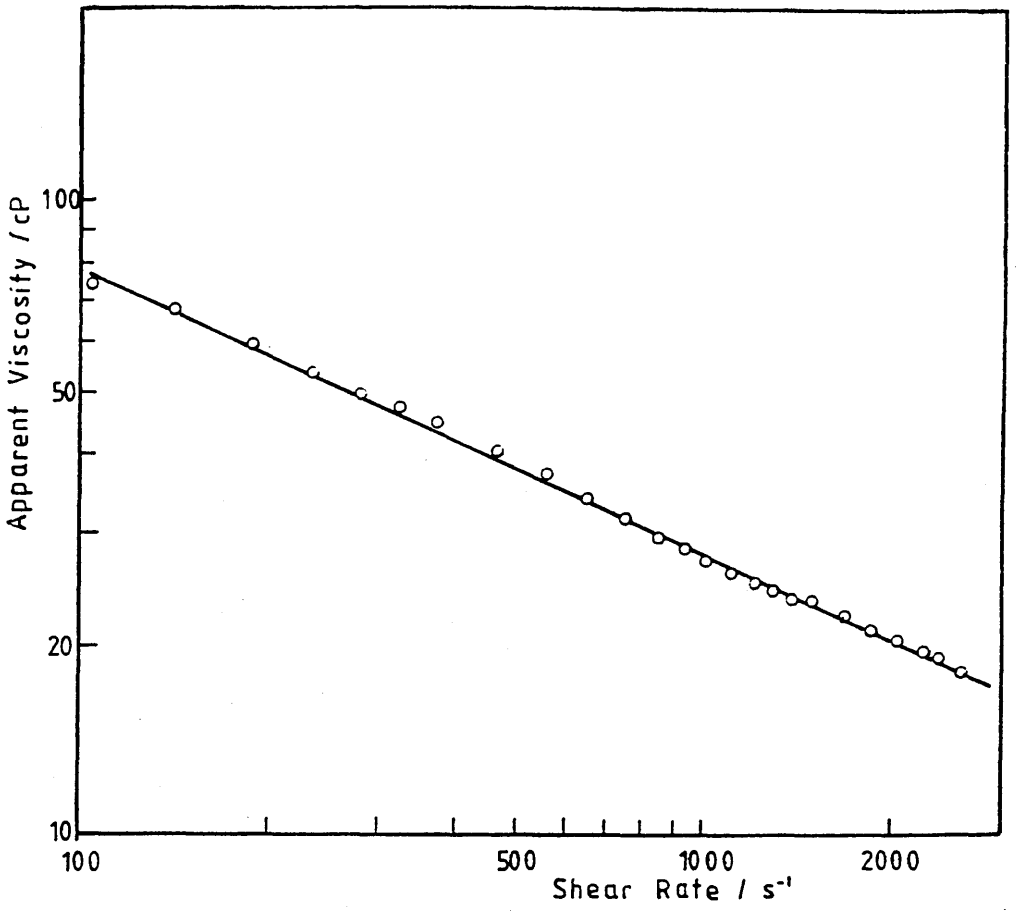

FIGURE 4.17
Apparent Viscosity Against Shear Rate for the 0.5% CMC Solution.

a Haake viscometer, model rotovisco RV3 MK 5000. The Haake viscometer uses concentric cylinders and with the particular cylinders in use gave readings of stress against shear rate, to a maximum shear rate of 2500 s^{-1} [77]. Figure 4.16 shows the variation of stress with shear rate for the solution in use. The form of the curve is typical of a shear thinning fluid. The data of figure 4.16 were taken by increasing the shear rate at a fixed rate from zero to the maximum level. No change in the form of figure 4.16 was noted when the shear rate was reduced from the maximum to zero, or when a different

TABLE 4.4 Mechanical properties of the Fluids Under Test

FLUID	ZERO-SHEAR VISCOSITY / Nsm^{-1}	FLUID INDEX n
WATER	1.0×10^{-3}	1.00
0.5% CMC	7.7×10^{-2}	0.55

rate of change of shear rate was chosen. This indicated that the solution was not viscoelastic and does not exhibit a stress memory.

Figure 4.17 shows the variation of the viscosity with shear rate, both on logarithmic scales. The viscosity is defined as the stress divided by the shear rate. Thus from equation 4.27 the apparent viscosity, η_a is given by

$$\eta_a = \mu \left| \left(\frac{du}{dr} \right)^{n-1} \right| \qquad 4.57$$

where μ is the viscosity at zero shear rate and n is the fluid index. It may be seen that on logarithmic scales equation 4.57 forms a straight line of gradient n-1 and intercept μ. From consideration of the data of figure 4.17 it was found that n=0.55, making the CMC solution strongly non-Newtonian. Table 4.4 gives the zero strain viscosity and the fluid index for the fluids in use.

4.2.4 Results and Discussion

Figure 4.18 shows the variation of $E'(\omega)$ and $d(\omega)$ with frequency for a water filled sample at three different levels of pre-strain. As the level of pre-strain is increased both the height of the damping peak and the frequency of maximum damping are altered. The trend towards higher damping maxima, at lower frequencies, with increasing pre-strain is in qualitative agreement with the expected variations of β and γ in equations 4.55 and 4.56. The variation of $E'(\omega)$ and $d(\omega)$ with frequency and pre-strain can best be illustrated in the form of a 3-D surface plot, such as that shown in figure 4.19 for the results with a water filled test piece. Comparison with the equivalent plot for an air filled test piece (figure 4.3) reveals much more structure in the damping surface generated by test pieces including fluid flow processes.

Figure 4.20 shows a typical measurement series for a non-Newtonian fluid filled system. The results are plotted as logarithmic storage modulus and linear loss tangent against logarithmic frequency. By comparison with figure 4.18 it may be seen that the gross features of the curves are similar for Newtonian and non-Newtonian fluids.

Although the gross shape of the fluid flow curves are similar for the two types of fluid, differences do exist. This is illustrated in figure 4.21 where the damping peaks for water filled and CMC solution filled test pieces are superimposed. For the shear thinning fluid

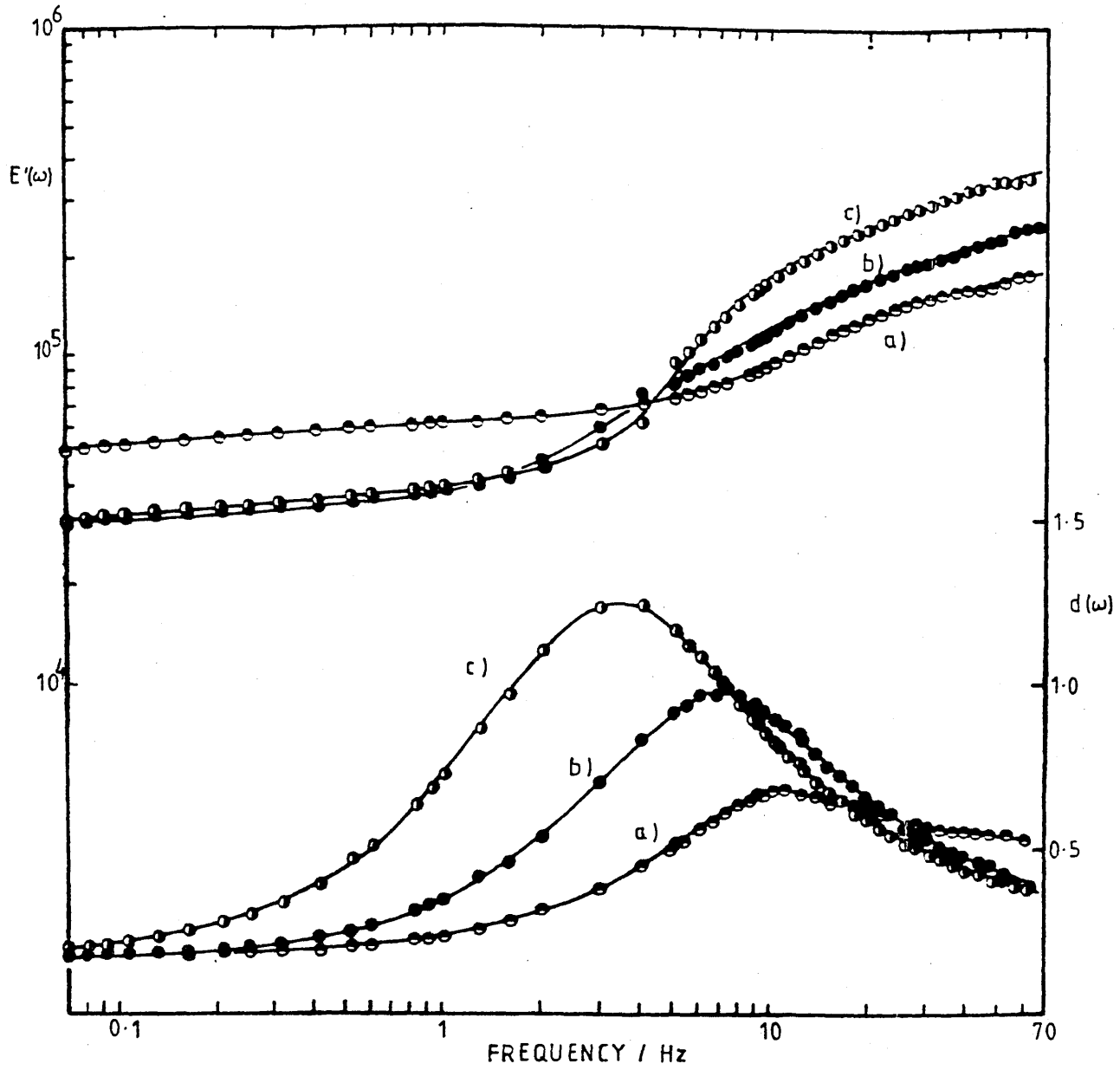

FIGURE 4.18

Variation of E'(ω) and d(ω) with Frequency for a Water Filled Conventional PU Foam Test Piece under a Pre-Strain of a) 8.5%, b) 23% and c) 35%.

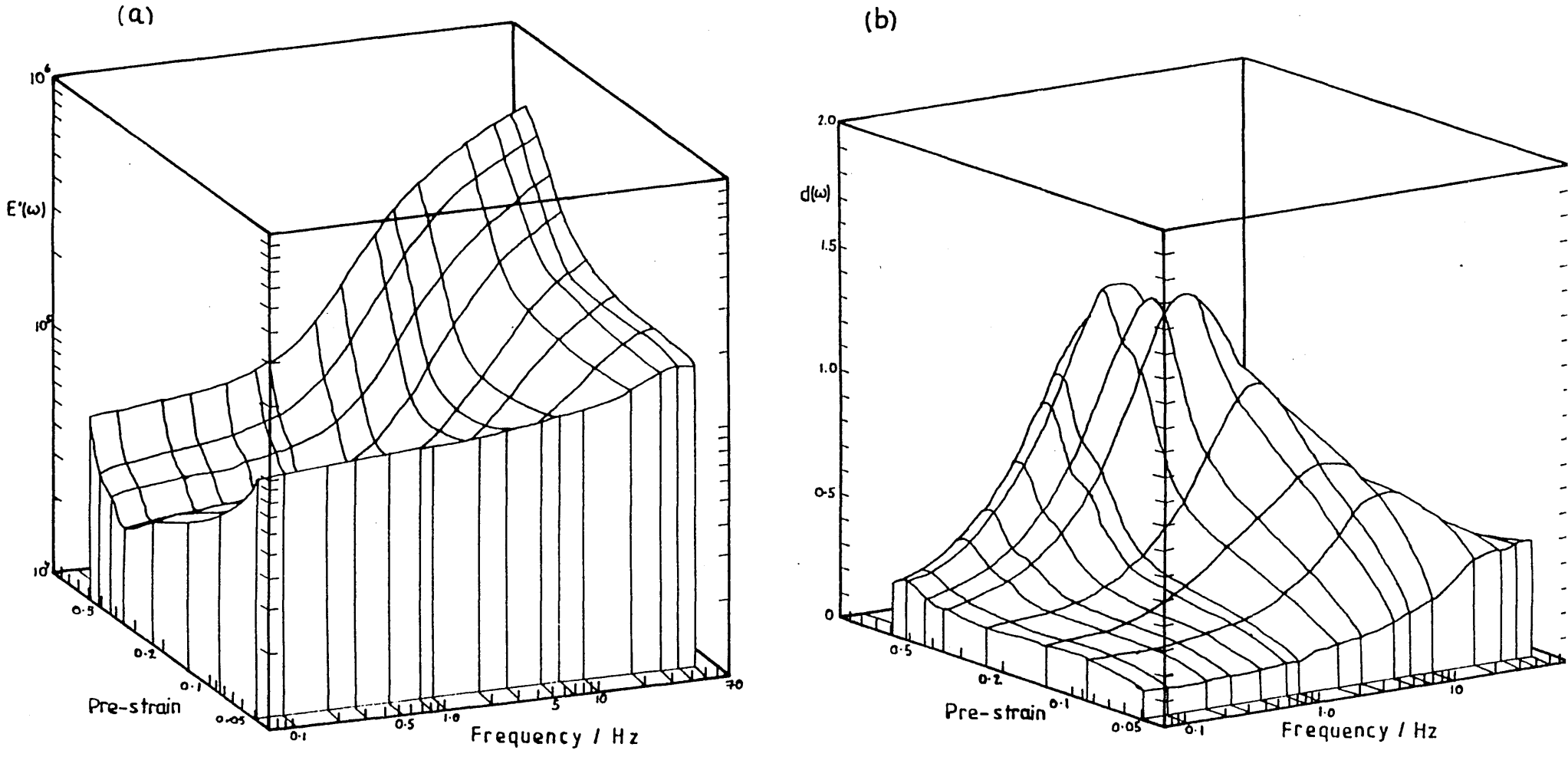

FIGURE 4.19

3-D Graph Showing the Variation of a) E'(ω) and b) d(ω) with frequency and Pre-Strain for a Water Filled Conventional PU Foam Test Piece.

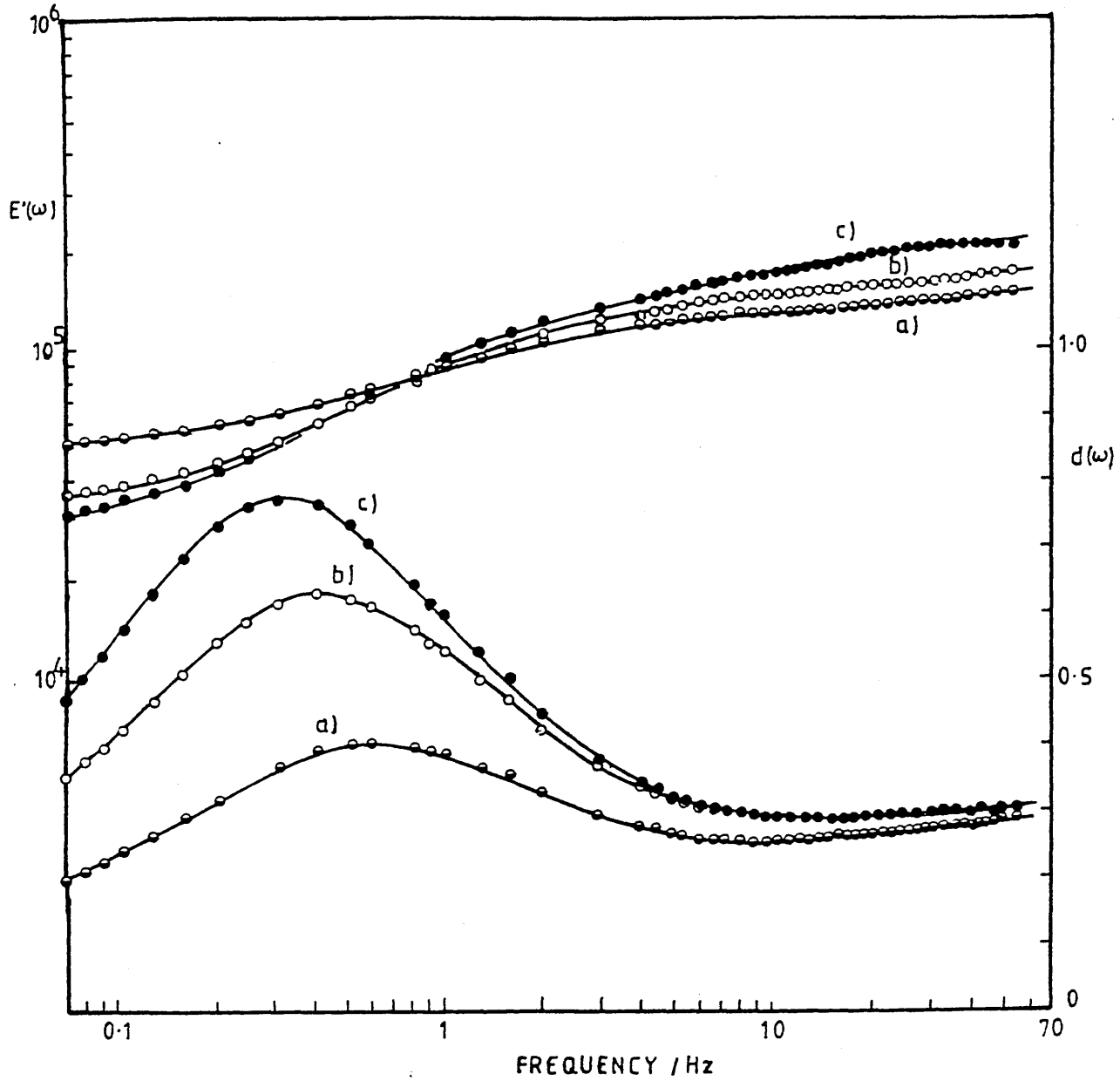

FIGURE 4.20

Variation of E'(ω) and d(ω) with Frequency for a High Resiliency Test Piece Filled with a 0.5% CMC Solution and under a Pre-Strain of a) 6.4%, b) 11.3% and c) 15.6%.

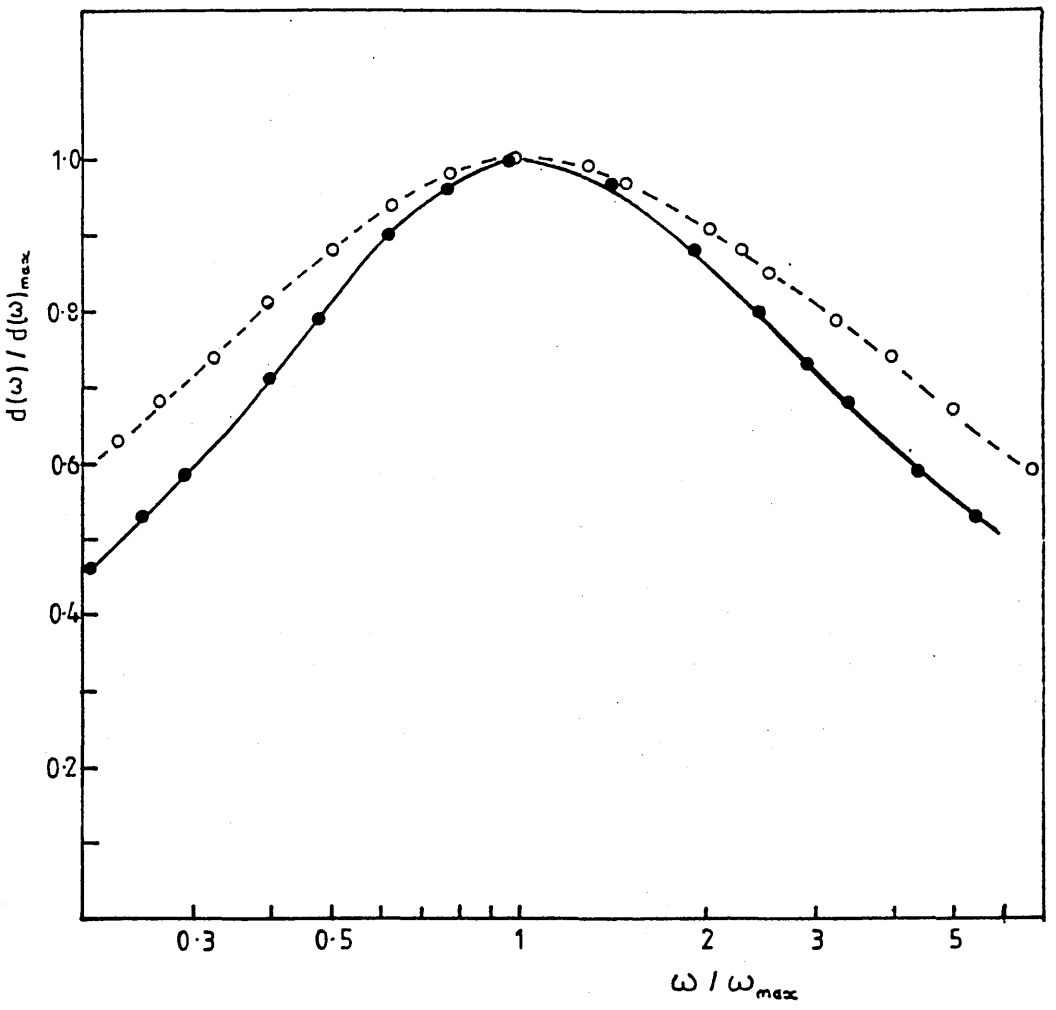

FIGURE 4.21
The Variation of $d(\omega)$ with Frequency Around the Damping Maximum. Closed Circles; Newtonian Fluid Filled System. Open Circles; Foam Filled with 0.5% CMC Solution.

the width of the damping peak is increased. From the curves such as figures 4.18 and 4.20 several parameters can be measured. The value of the damping at the maximum, $d(\omega)_{max}$, the maximum damping frequency, ω_{max} and the width of the peak, in the form of a Q-factor have been measured. These are included in table 4.5, together with the static pre-strain imposed.

The frequency dependence of the fluid flow process is contained in the parameter γ, defined in equation 4.44.

TABLE 4.5 Values Measured From the Damping Peaks

FOAM	FLUID	STRAIN /%	ω_{max} /Hz	$d(\omega)_{max}$	Q-FACTOR
VRT 400	WATER	8.54	11.5	0.66	-
		23.2	7.3	0.97	0.48
		35.4	4.0	1.28	0.44
		42.7	3.3	1.23	0.42
		51.2	2.6	1.29	0.43
		58.5	2.1	1.15	0.41
DW0007 00	WATER	33.3	11.0	1.28	-
		40.6	6.1	1.12	-
		47.6	5.1	0.99	0.40
		58.6	1.6	0.74	0.39
DW0007 00	CMC	7.96	0.6	0.40	0.20
		11.3	0.4	0.63	0.22
		15.6	0.32	0.77	0.23
		22.3	0.28	0.87	0.25
		28.7	0.20	0.97	0.28
DW0007 09	CMC	3.25	1.8	0.45	-
		6.83	1.6	0.61	0.23
		12.2	0.95	0.84	0.25
		18.2	0.66	1.02	0.28
		23.6	0.52	1.12	0.31
		29.3	0.39	1.18	0.31
		37.1	0.40	1.18	0.30
		42.8	0.35	1.19	0.32

Previous workers have ascertained the value of γ and its frequency dependence by examining the experimental results at low frequencies. Under these conditions γ is assumed to be small and equation 4.54 can be approximated by

$$d(\omega) \cong d_m + \gamma \qquad 4.58$$

Furthermore, previously the parameter β has been ascertained from an investigation of the damping maximum. Knowing the value of γ at a particular frequency from equation 4.58, the value of γ_{max} may be calculated. By differentiating equation 4.54 with respect to γ, β may be calculated. ie

$$\gamma_{max} \cong 1/(\beta + \beta^2)^{\frac{1}{2}} - d_m/(1 + \beta) \qquad 4.59$$

The above procedure suffers from the drawback that the parameters γ and β are calculated from consideration of relatively few of the measured data points, and the frequency dependence of γ cannot be ascertained without prior knowledge of the approximate dependence.

For the present work a procedure has been developed whereby the values of β, γ, d_m and E'_m can be calculated, together with the frequency dependence of γ, without making any a priori assumptions. The method has the added advantage that it makes use of all the data points in the frequency range of interest. The method, using a non-linear curve fitting technique, involves factorising the parameter γ into frequency dependent and frequency

independent parts

$$\gamma = \Theta\omega^{r} \qquad 4.60$$

where

$$\Theta = \frac{\mu\varepsilon_0{}^{n-1}}{(n+2)E'_m K(n,\omega)} \left(\frac{W}{2}\right)^{n+1} \qquad 4.61$$

For Newtonian fluids the parameter r should be unity and Θ will reduce to the form

$$\Theta = (\eta W^2)/)12E'_m K(\omega)) \qquad 4.62$$

where η is the Newtonian viscosity and $K(\omega)$ is given by equation 4.16. According to the theoretical treatment of section 4.2.2 in the case of a non-Newtonian fluid the parameter r will equal the fluid index, n and Θ will be given by equation 4.61. Substituting the factorised form of γ into the equations governing the storage modulus and damping of a test piece including fluid flow effects (equations 4.53 and 4.54)

$$E'(\omega) = \frac{E'_m\{1 + \beta(1 + \beta)\Theta^2\omega^{2r}}{1 + \beta^2\Theta^2\omega^{2r}} \qquad 4.63$$

$$d(\omega) = \frac{d_m\{1 + \beta^2\Theta^2\omega^{2r}\} + \Theta\omega^{r}}{1 + \beta(1 + \beta)\Theta^2\omega^{2r}} \qquad 4.64$$

where E'_m, d_m, β, Θ and r are curve fitting parameters to be found using non-linear optimization techniques.

Several non-linear curve fitting techniques have been advanced (see for example [78,79]). These include methods using maxima [80], gradient techniques [81,82]

and linearisation using a first order Taylor expansion [83,84]. One of the most widely used is the direct search method of Hooke and Jeeves [85]. This technique has the advantage of simplicity over other available methods. This method is outlined in appendix V.

In the Hooke-Jeeves method initial estimated values of the fitting parameters are input to provide a base point. The value of the function to be fitted is found and the mean square variation of the experimental data about this curve evaluated. The method then requires the exploration of the area of the function surrounding the base point. If any nearby point produces a mean square variation which is smaller than that at the base point, this point becomes the new base point and the process continues until the minimum is found.

The method works well with complex and ill-defined functions and is relatively easy to perform on a computer. The disadvantage is that it will only find the local minimum to the starting point. This is not necessarily the point at which the mean square variation is the lowest. This problem is overcome by repeating the fitting procedure at several widely spaced starting points. If all these converge to the same point then it may be assumed that the true minimum of the mean square variation of the experimental data about the fitted curve has been found.

The Hooke-Jeeves method outlined in appendix V has been used to fit the data taken with foam samples filled with water and the CMC solution. The fitting program was written in Pascal on a Nascom III microcomputer and drew the data directly from the disc storage library of the mechanical spectrometer. Tables 4.6 and 4.7 give the parameters found by fitting a relation of the type of equation 4.64 to the data for the loss tangent, together with the standard deviation of the measured values of $d(\omega)$ about the fitted line. Also shown are values of E'_m found by fitting equation 4.63 to the measured storage modulus. The data of table 4.6 refers to measurements made on test pieces in water while table 4.7 includes the parameters from samples tested in the CMC solution.

For the foam test pieces in water the fitting parameter, r, representing the frequency dependence of γ is close to unity. With samples tested in the CMC solution the value of r is in the range 0.53-0.69. The results for the two liquids are in qualitative agreement with the theoretical analysis based on the flow of a power-law fluid through a cellular matrix. There is also a reasonable degree of quantitative agreement between theory and experiment. From measurements of the mechanical properties of the CMC solution, the theory predicts that r=0.55. At low levels of pre-strain the correspondence between theory and experiment is good. As the level of pre-strain increases however, the value of r for CMC filled samples increases and the agreement is not as good.

TABLE 4.6 Fitted Fluid Flow Coefficients for Foam Test Pieces in Water

STRAIN /%	E'_m /$10^4 Nm^{-2}$	d_m	β	Θ /10^{-1}	r	std. devn. of $d(\omega)$
Foam VRT400						
8.54	5.20	0.148	0.532	0.135	0.982	0.0230
23.1	3.31	0.144	0.248	0.395	1.052	0.0133
35.4	2.62	0.145	0.151	0.804	1.021	0.0199
42.7	3.24	0.146	0.161	0.998	1.004	0.0142
51.2	3.74	0.152	0.147	1.490	0.952	0.0299
58.5	5.72	0.120	0.180	1.526	0.916	0.0292
Foam DW 0007 00						
6.37	4.45	0.118	1.170	0.073	0.941	0.0194
12.4	2.89	0.135	0.544	0.116	0.929	0.0289
15.1	2.83	0.135	0.518	0.156	0.906	0.0334
26.6	3.22	0.154	0.280	0.301	0.945	0.0447
33.3	3.63	0.138	0.242	0.430	0.894	0.0318
40.6	4.12	0.127	0.223	0.622	0.962	0.0296
47.6	5.57	0.133	0.240	0.821	0.916	0.0147

As the level of static deformation increases the standard deviation of the measured values of $d(\omega)$ about the fitted curve increases considerably for test pieces filled with the CMC solution. This indicates that the relation given in equation 4.62 becomes less suitable for the prediction of the fluid flow damping effect at higher levels of pre-strain. The theoretical model given in section 4.2.2

TABLE 4.7 Fitted Fluid Flow Coefficients for Foam Test Pieces Filled With 0.5% CMC Solution

STRAIN /%	E'_m /$10^4 Nm^{-2}$	d_m	β	Θ /10^{-1}	r	std. devn. of $d(\omega)$
Foam DW 0007 00						
7.96	-	0.035	0.939	3.19	0.568	0.0534
11.3	3.32	0.043	0.493	7.09	0.601	0.0823
15.6	2.97	0.058	0.363	10.99	0.625	0.0906
22.3	3.11	0.141	0.332	13.25	0.668	0.1063
Foam DW 0007 09						
3.25	5.35	0.070	0.859	2.00	0.534	0.0231
6.83	4.60	0.077	0.548	3.33	0.588	0.0356
12.2	2.77	0.059	0.302	6.22	0.610	0.0435
18.2	2.47	0.080	0.223	11.07	0.660	0.0636
23.6	2.80	0.046	0.181	15.06	0.680	0.0714
29.3	2.95	0.076	0.173	18.66	0.690	0.0941
37.1	3.55	0.052	0.168	18.22	0.692	0.0994
42.8	4.32	0.055	0.166	21.69	0.692	0.1215

makes several simplifying assumptions. The frequency dependence of the effective permeability, $K(n,\omega)$, is not taken into account in the fitting method outlined above.

$K(n,\omega)$ varies with frequency through the correction terms incorporated into it (equation 4.38). At low levels of pre-strain these correction terms are very small and the effective permeability may be considered to be

independent of frequency. As the level of pre-strain increases, however, the relative magnitude of the correction terms in equation 4.38 will change in comparison with the dominant first term, resulting in a different frequency dependence for $K(n,\omega)$. The resulting effect on the frequency dependence of γ is complex and at present unknown. However as $K(n,\omega)$ becomes more dependent on the frequency of excitation, the factorisation of γ into frequency dependent and independent parts in equation 4.60 will break down. This may explain the increase in the standard deviation of the measured data about the fitted curve as the level of pre-strain is increased.

Furthermore the theoretical analysis takes no account of the frequency dependence of the compressive matrix modulus, E'_m, the transverse (tensile) modulus, E_t and the matrix damping, d_m. Both E'_m and d_m have been found to vary with frequency. The frequency dependence of E_t is not known. The breakdown of these and other assumptions as the level of pre-strain increases may account for the departure from the behaviour predicted by equation 4.64.

From equation 4.61 the value of the fitting parameter Θ (and hence γ and $d(\omega)$) is predicted to be a function of the amplitude of the dynamic deformation, ε_o. For a shear thinning fluid Θ will decrease as ε_o increases. At frequencies below the damping maximum this will result in

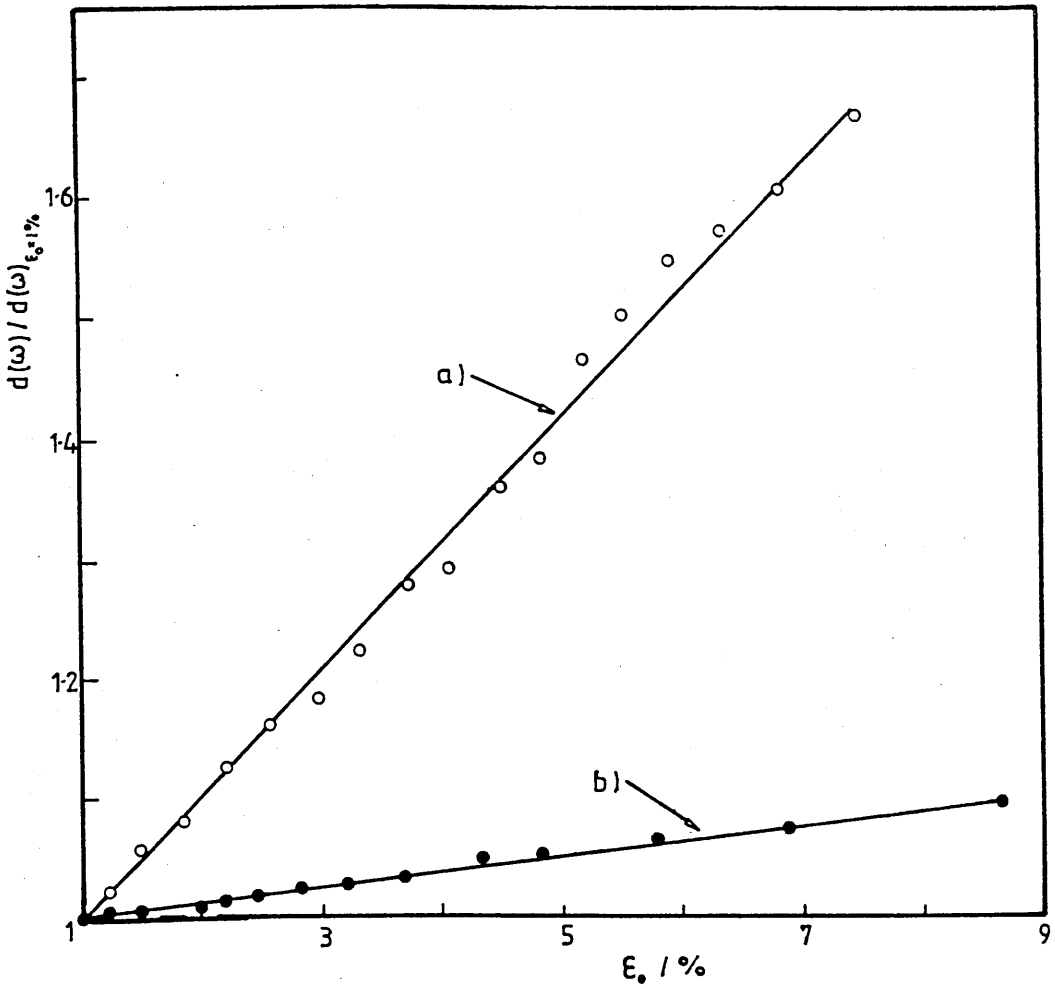

FIGURE 4.22

The Variation of the Loss Tangent with the Amplitude of the Dynamic Deformation for a) Water Filled and b) 0.5% CMC Filled Foams. The Data are Expressed as a Ratio of the Value at an Amplitude of 1%.

a reduction in the level of damping observed.

Figure 4.22 shows the variation of $d(\omega)$ with ε_o for test pieces filled with water and the CMC solution. The data of figure 4.22 is expressed as the ratio of the damping at a strain amplitude of 1% for comparison. Both samples were subject to a static pre-strain of 35% and measurements recorded at a frequency of 0.1 Hz. For the test piece in the CMC solution $d(\omega)$ varies only slightly

with ε_o and the trend is towards higher values, rather than lower values as predicted by the model. However the damping of the matrix in the presence of water shows a strong dependence on the strain amplitude. As the matrix behaviour is likely to be similar for water filled and CMC filled samples, some other mechanism must be present which acts to reduce $d(\omega)$ as ε_o increases. It is thought that this mechanism is characterised by the strain dependence of the fluid flow effect in equation 4.61.

The values of Θ in tables 4.6 and 4.7 have been used to calculate the effective permeability of the foam. For each test piece the effective permeability has been found at the lowest level of pre-strain used. This has been compared to the permeability of the material to the flow of the particular fluid, K(n). In the case of water filled test pieces this is the same as the the K value measured in Chapter 3, and is independent of the fluid.

For test pieces filled with the non-Newtonian fluid it has been shown (in section 3.5.2) that the permeability will depend on the fluid index. Using equation 3.38 the non-Newtonian permeability has been calculated from the air-flow permeability and compared with $K(n,\omega)$. The results are given in table 4.8.

The values of the permeability , K(n), are adjusted using equation 3.41 to account for the level of pre-strain imposed. In each case the effective permeability

TABLE 4.8 Comparison Between $K(n,\omega)$, Calculated from Θ, and $K(n)$, Inferred from the Air-Flow Measurements of Chapter 3

FOAM	FLUID	PRE-STRAIN /%	$K(n,\omega)$ /10^{-9} m^2	$K(n)$ /10^{-9} m^2
VRT 400	WATER	8.54	0.760	2.175
DW0007 00	WATER	6.37	2.497	4.191
DW0007 00	CMC	11.3	242	439
DW0007 00	CMC	3.25	302	485

calculated from Θ is within a factor of 3 of the K or K(n) values from Chapter 3. Considering the simplified treatment, the correspondence, especially in the case of the CMC solution, is considered to be good.

Strain Dependence of the Fitted Parameters

The dynamic matrix modulus , E'_m, varies with pre-strain in a similar manner to the small strain dynamic modulus in the absence of fluid flow damping. For the conventional PU foam sample the minimum value of E'_m occurs at a pre-strain of about 30%, while for the high resiliency samples the minimum is closer to 20%. This is in agreement with the variations found in section 4.1. However for a given level of pre-strain E'_m is consistantly lower than that expected from measurements on the modulus in the absence of fluid flow effects. This difference is attributed to the plasticising action

of the water in the liquids which tends to break the weak hydrogen bonds between adjacent polymer molecules and reduce the stiffness of the foam [51].

The predicted damping of the matrix, d_m, from equation 4.64 appears to be too small for test pieces filled with the CMC solution. As d_m for water-filled samples has similar values to the dynamic loss tangent in the absence of the liquid, it is not thought that the low value of d_m for CMC samples is caused by the presence of the liquid. Rather it indicates that equation 4.62 does not totally explain the fluid flow process in foams filled with non-Newtonian fluids.

The fitting parameters Θ and β both vary considerably with the level of pre-strain imposed. β is related to the static deformation by equation 4.55. From the values of β found using the non-linear curve fitting technique the ratio of the moduli, E'_m/E_t, calculated from equation 4.55 is plotted in figure 4.23 as a function of $(1-e)^2$. The broken line is the behaviour predicted by equation 4.55 assuming that $E'_m(e)=E_t(e)$. It may be seen that the measured data departs considerably from the dashed line. The variation follows a similar form for all the foam-fluid combinations tested. The shape of the curves in figure 4.23 indicates that the transverse modulus, E_t has a different strain dependence to E'_m.

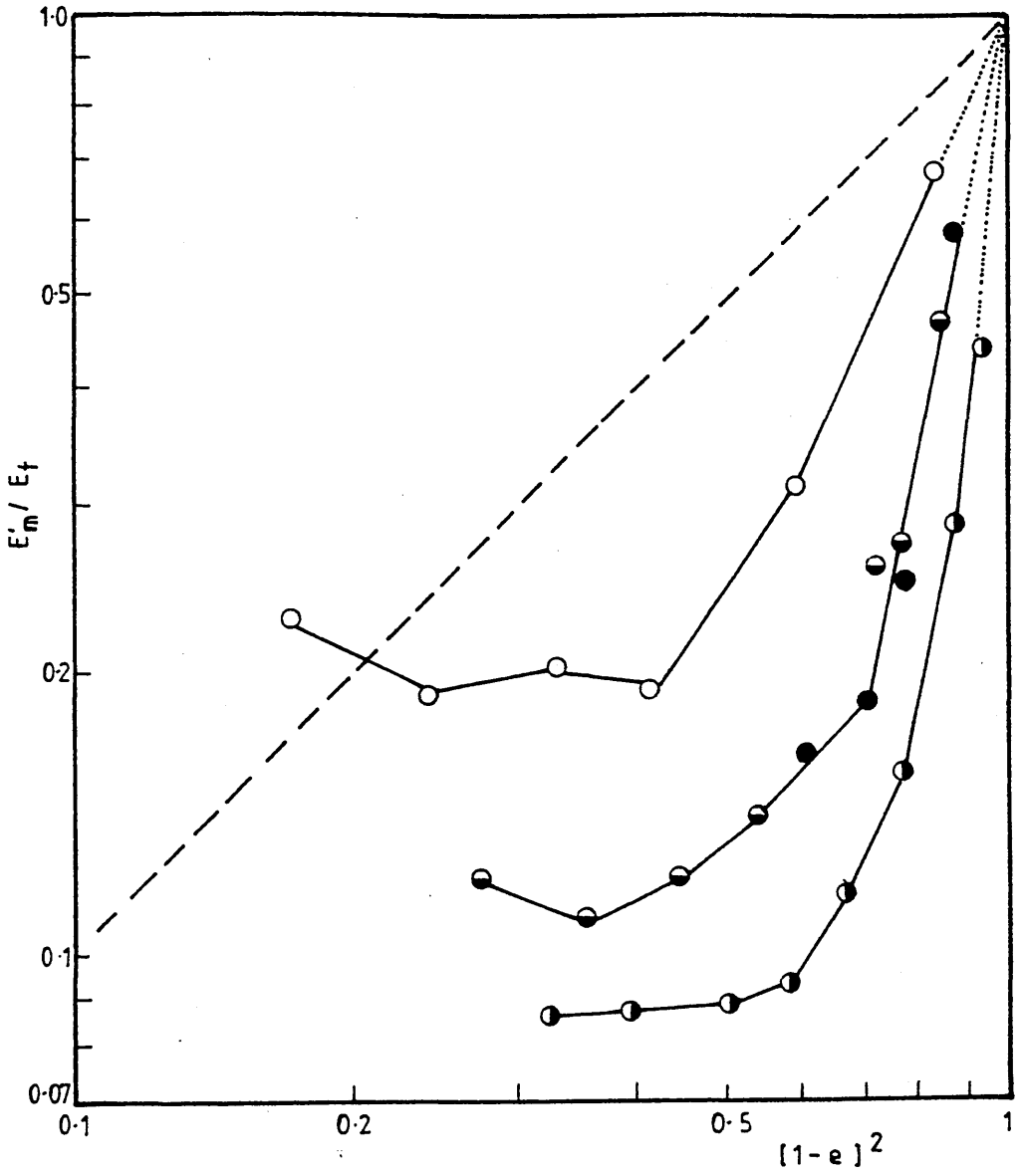

FIGURE 4.23

E'_m/E_t, Calculated From Fitted Values of β vs $(1-e)^2$ for Foam Type; VRT 400 in Water (○), DW0007 00 in Water (●) and CMC (◒), and DW0007 09 in CMC Solution (◑). Broken Line; Prediction assuming that $E'_m=E_t$.

The moduli used in the definition of β are those measured for oscillatory deformation. These are not necessarily the same as those measured from the F-D curves of the test piece. This has been discussed in the case of the dynamic compressive modulus in section 4.1. The variation of the dynamic tensile modulus with strain has not been reported in the literature. However some qualitative analysis is possible if the strain dependence of the tensile modulus, measured from the F-D curves in tension, is considered.

At very low strains the two moduli are approximately equal [54]. This is reflected in the data of figure 4.23 as the curves for the different foams appear to tend towards a value of unity at small deformations. At higher values of pre-strain it has been shown by several workers that the the tensile modulus is a much weaker function of strain than that for compression [54,58,86]. This dependence is assumed to carry over into the dynamic tensile modulus. The result of this is that the ratio E'_m/E_t will fall as the level of strain exceeds the yield value for the foam, e_y (see section 4.1.3). At higher strains the modulus ratio will cease to fall and may rise as the level of pre-strain exceeds the value e_1 for the foam. The data of figure 4.23 is in qualitative agreement with this proposed mechanism. Until specific details of the strain dependence of the dynamic tensile modulus are found, the detail of the variations shown in figure 4.23 remain unexplained.

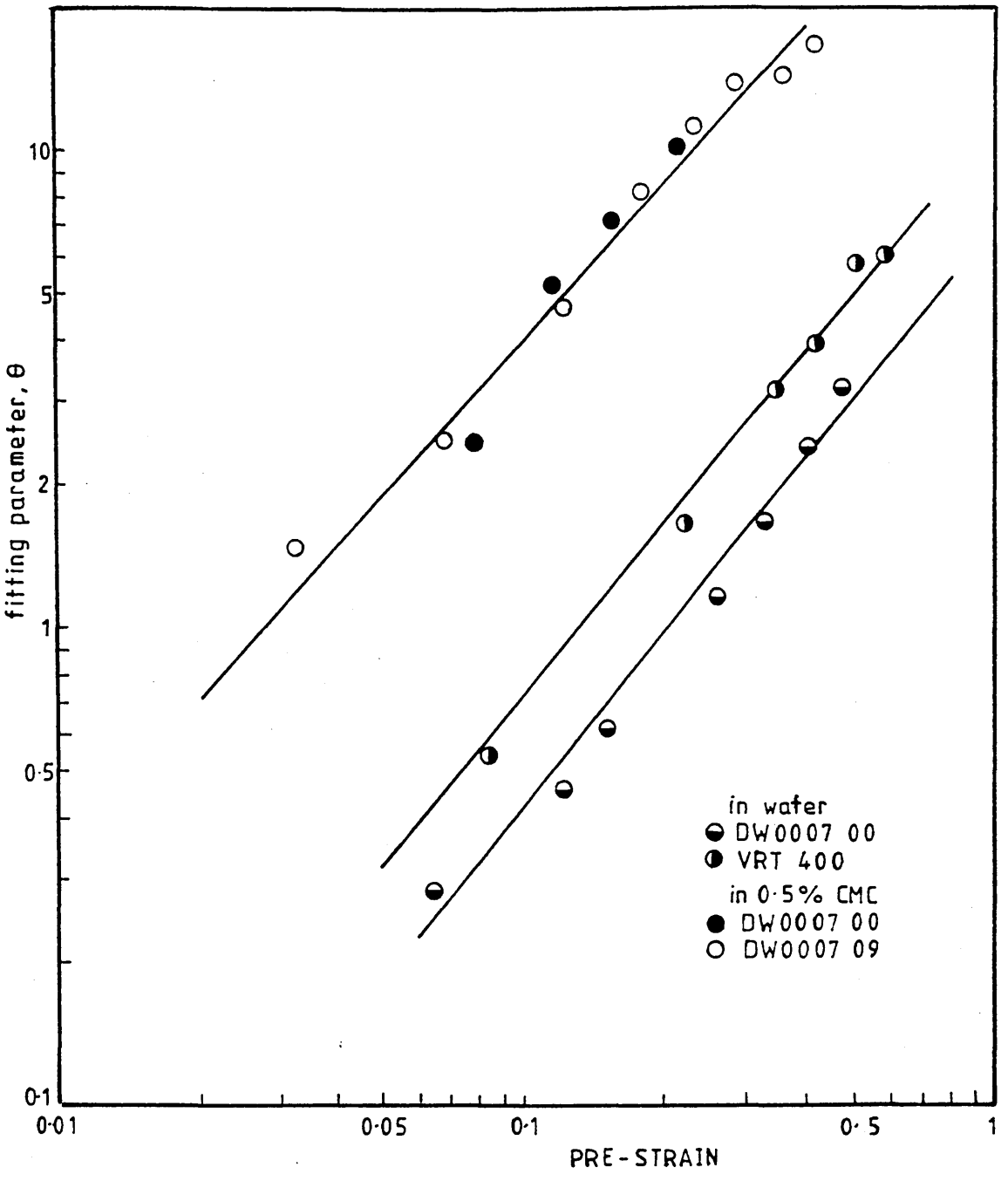

FIGURE 4.24

Variation of the Fitting Parameter, θ, with Pre-Strain for Liquid Filled Test Pieces.

Figure 4.24 shows the strain dependence of the fitting parameter Θ for the foam-fluid combinations tested. On logarithmic scales the data for each combination follow a curve which is approximately a straight line of gradient 1.2. Each curve may therefore be approximated by a relation of the form

$$\Theta = C + De^{1.2} \qquad 4.65$$

where C and D are constants related to the sample geometry, the fluid viscosity and the properties of the test piece at zero strain. It may be noticed that the results for the two foams tested in the CMC solution lie approximately on the same line. This is because the sample geometry was the same for both test pieces. For the water filled results the width of the VRT400 test piece was about half that of the DW0007 00 test piece. This is reflected by the results for the two foams occupying different lines.

The fitting parameter Θ is related to the fluid flow parameter, γ, through equation 4.60, and to the properties of the foam and fluid in use by equation 4.61. Considering the complexity of the strain dependence of $K(n,\omega)$ and E'_m in equation 4.61, it is suprising that the strain dependendence of γ is so simple. This parameter controls the frequency at which the maximum damping level occurs. The significance of the measured strain dependence of γ is that the maximum damping frequency will decrease as the level of static pre-strain

increases, in a way that is a relatively simple function of the imposed pre-strain.

5. THE RESPONSE OF NON-LINEAR VIBRATION ISOLATORS

5.1 Small Strain Amplitude Dynamic Behaviour, Applied to the Problem of Vehicle Seating and Dynamic Ride Comfort

5.1.1 Introduction

Historically, vehicle seating was a composite system of springs and cushions formed from burlap or hair. In the 1930's, rubber latex foam was introduced and became popular in the 1950's. This type of seating became, and still is, the standard for comfortable seating. Later, however, cost and quality considerations led to the introduction of flexible cellular polyurethane (PU) foam for seat cushions, which soon accounted for a large part of the market.

More recently full depth foam cushions have been introduced, mainly for ease of manufacture and cost [87]. In this type of seating, all the cushioning is performed by a moulded foam seat. Unfortunately the conventional PU foams then in production did not completely satisfy the market demands for comfortable seating. This in turn led to the introduction of high-resiliency PU foam cushions [88,89], with a mechanical behaviour intermediate between cellular rubber and conventional PU foam. Other recent technical advances in cushion technology have resulted in seats with variable hardness across their width [90] (to increase comfort and support), and integral skin cushions [91] (to improve adhesion and reduce unit costs).

FIGURE 5.1

Photograph of a Full-Depth Foam-Cushion Seat system Taken from a JOB Earth Moving Vehicle.

Recent trends in automobile design have increased interest in the material requirements of cushions for vehicle applications. This has resulted, in part, from a reduction in the vehicle weight (to achieve fuel economy), enhanced suspension stiffness (to improve road holding) and more widespread use of full depth foam cushions [89], such as the seat system shown in figure 5.1 from a JCB earth moving vehicle. These innovations have meant that it has been necessary to enhance the functional performance of the cushion material so as to provide an acceptable level of ride comfort.

The cushion in a vehicle seat performs three primary functions [92]; it provides comfort under static conditions, an appropriate thermal environment (eg temperature and humidity at the buttocks-cushion interface) and reduces to acceptable levels the mechanical vibration experienced by the seated person. The vehicle, either on-road or off road, creates vibration in the passenger/operator compartment.

The passenger compartment in the vehicle is subject to periodic and stochastic vibrations [93]. Random vibrations are associated with the terrain over which the vehicle is passing wheras periodic vibrations are generated by resonances in the vehicle system. Figure 5.2 shows a simple lumped-parameter representation of the suspension system in a vehicle and illustrates the sprung and unsprung mass components of the vehicle. The

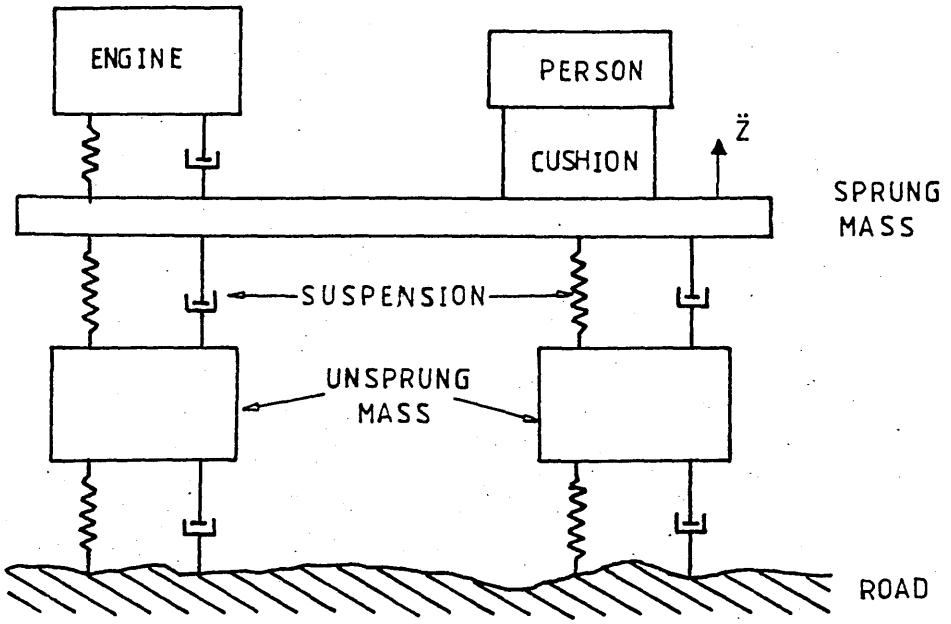

FIGURE 5.2

Representation of the Suspension System in an Automobile, Illustrating the Sprung and Unsprung Masses in the Vehicle.

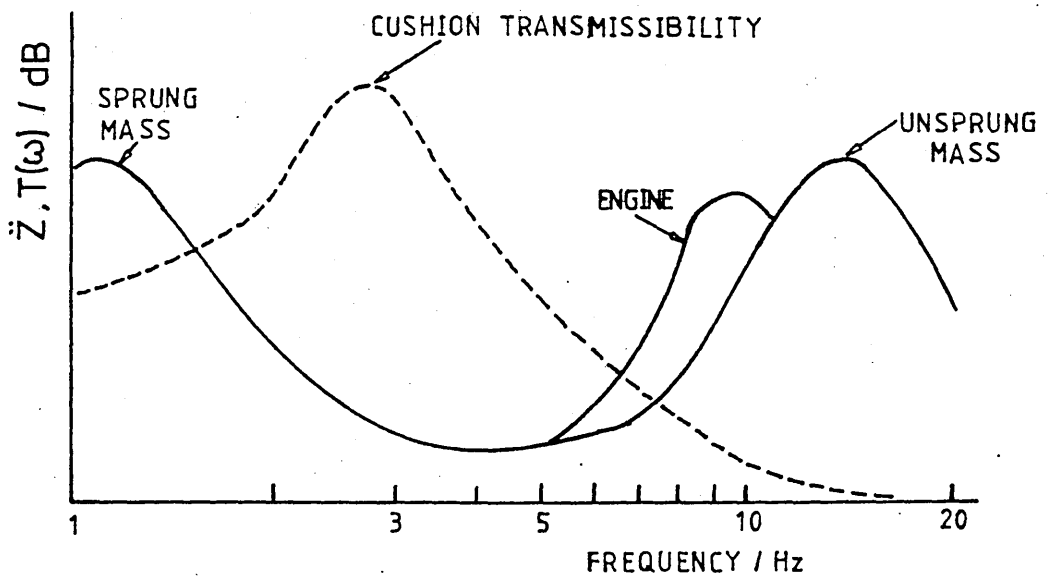

FIGURE 5.3

Solid Line; Frequency Spectrum of the Periodic Vibrations Entering the Vehicle Cab. Broken Line; Typical Seat Cushion Transmissibility Curve. Taken From [93].

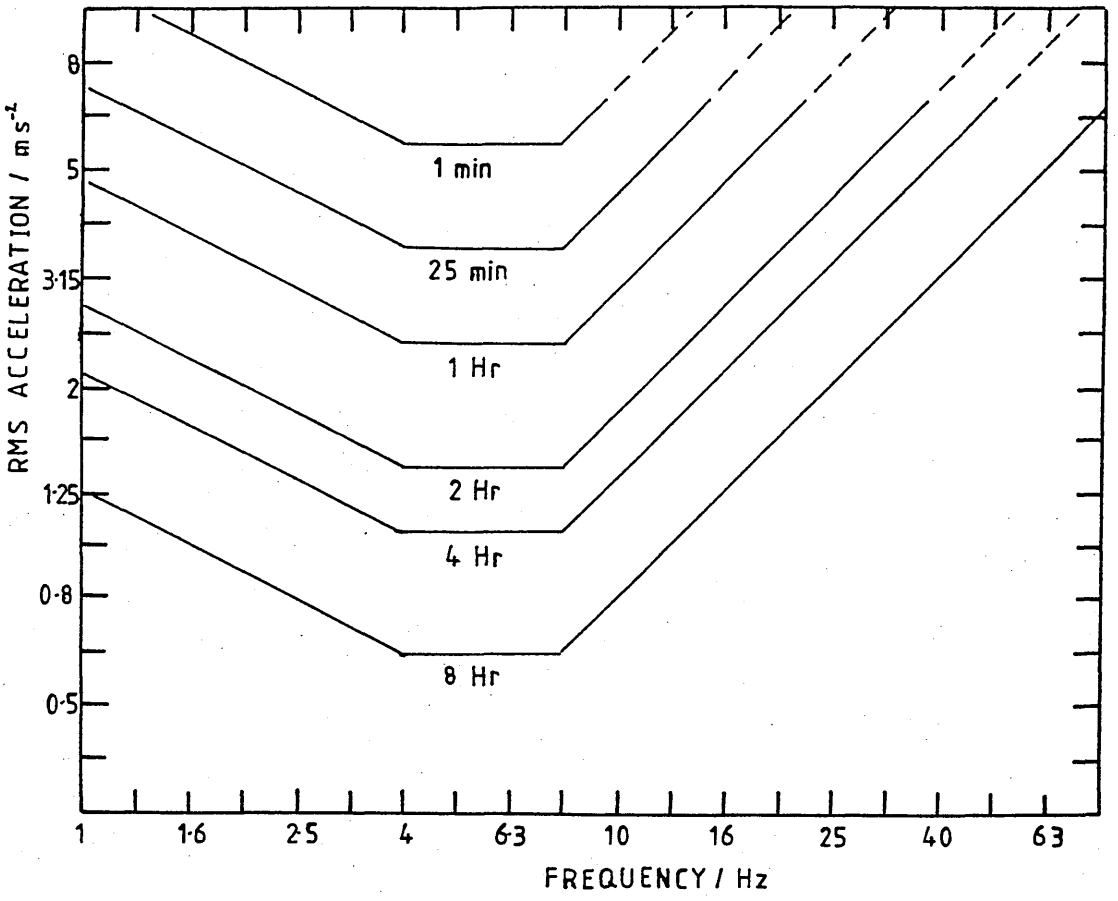

FIGURE 5.4

Reduced Comfort Boundaries For a Seated Person Subject to Vertical Whole Body Vibration. Taken From ISO 2631 [94].

frequency spectrum of the periodic component of the acceleration, Z_1 , entering the passenger compartment for a typical on-road vehicle is shown in figure 5.3 [93], together with a typical person-cushion transmissibility. Magnification of the passenger compartment vibration occurs at frequencies around 3 Hz, which is in the range of maximum human discomfort [94]. The reduced comfort boundaries for different exposure times are shown in figure 5.4. Exceeding these boundaries can lead to fatigue and decreased proficiency.

The factors influencing the ride quality in a particular

vehicle, and the criteria used to specify the level of static comfort provided by a seat cushion have been reviewed by the author and co-workers elsewhere [95,96]. The hardness of a cushion is usually characterised by its indentation-load-deformation (IFD) behaviour, as described in BS 4443 [97]. This is related to, but not the same as, the FD curve for the foam material. The IFD characteristics are measured by deforming the whole cushion using an indentor which is smaller than the area of the cushion and corresponds more closely to the deformation mechanism for a seated person [98,99]. In this case there are deformations outside the loaded area of the cushion as shown by figure 5.5. These peripheral deformations have a significant influence on the mechanical behaviour exhibited by the foam cushion and hence the comfort properties.

The dynamic performance of a seat cushion is normally characterised by the vibration transmissibility, defined as the ratio of the acceleration at the buttocks-cushion interface to that entering the seat pan for vertically directed (Z) vibration. The vibration transmissibility of vehicle seat cushions have been measured by several workers in the field [100,101,102], and in the laboratory [103,104]. A typical example of the transmissibility of the seat cushion in a family car is shown in figure 5.6. It can be seen that the transmissibility is a complex function of the frequency of mechanical excitation. Previous models put forward to explain this behaviour

FIGURE 5.5

A Flexible Cellular Foam Undergoing Indentation Loading Showing the Region Around the Periphery of the Indentor where Parts of the Foam are Subject to Tensile and Shear Stresses.

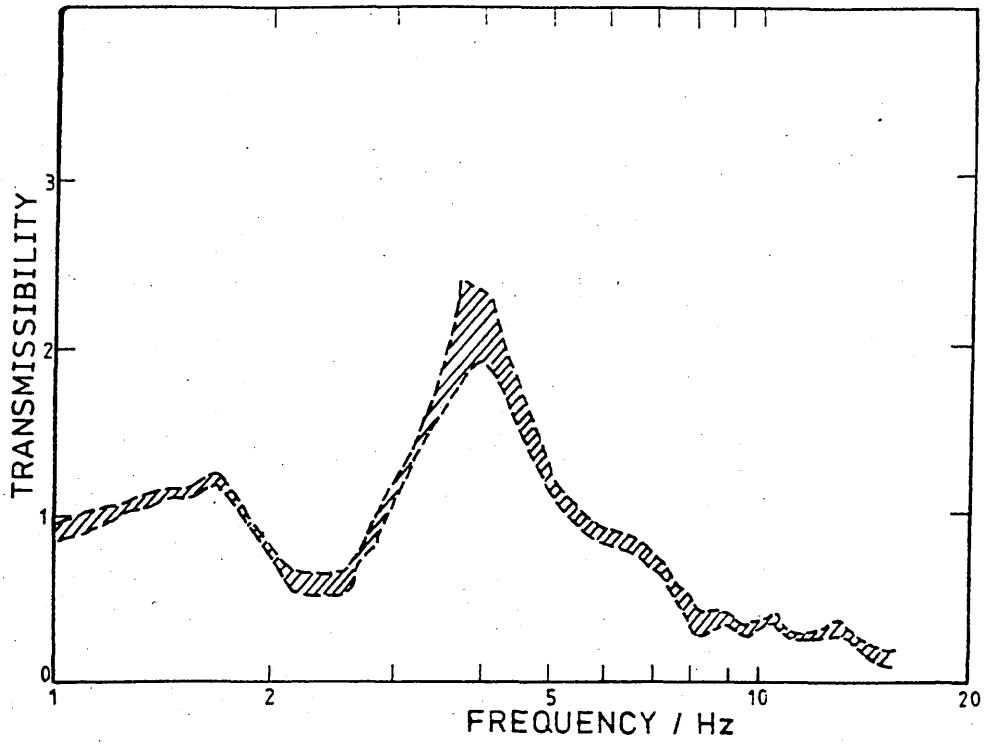

FIGURE 5.6

Typical Transmissibility Curve for an On-Road Vehicle Seat cushion [97].

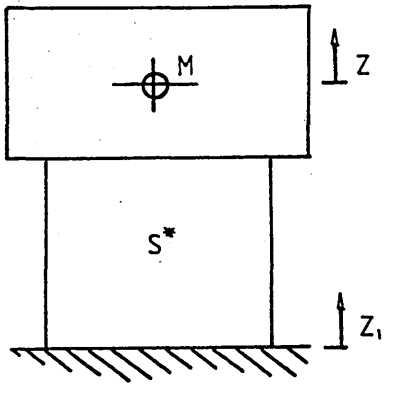

FIGURE 5.7

A Single Degree-Of-Freedom Model of a Person on a Vehicle Seat.

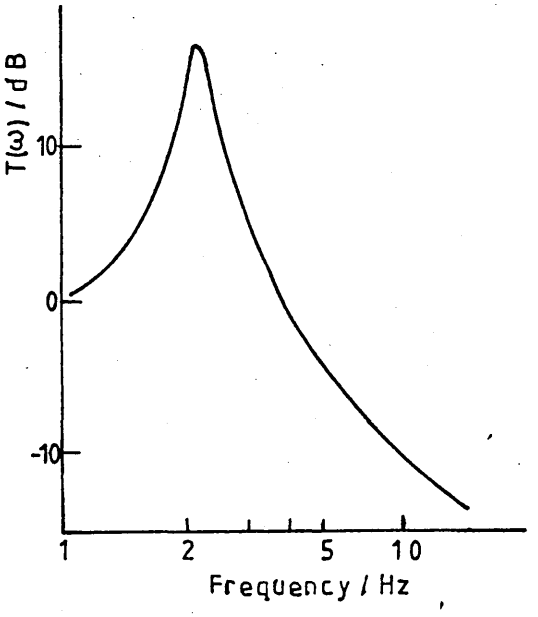

FIGURE 5.8

Typical Frequency Response for the Model of Figure 5.9.

have proved naive in assuming that the person on the seat acts as a passive mass [103,104,105,106]. It has been shown by Fairley and Griffin [107,108] and Hilyard et al [109] that the person in a person-seat system cannot be represented in this way.

The position of the person-cushion resonance frequency is of critical importance when designing seat systems; this is due to other vehicle resonances as explained above. If the seat cushion is designed in such a way that a seat resonance occurs close to one of these vehicle resonances then high vibration levels could be experienced by the operator, leading to reduced ride comfort.

It is therefore important to have a realistic model of the person-seat system in order to understand how cushion parameters, such as stiffness and damping, influence functional performance. This should ultimately allow the specification of a cushion in a particular vehicle which provides enhanced ride comfort. In addition it allows a study of the possible effects of so called vibration control additives [37,38] which have recently become available commercially.

5.1.2 Multi Degree-Of-Freedom Person-Seat Modelling

As mentioned previously attempts to model the person-seat system in the past have assumed that the person acts as a passive mass. This single degree-of-freedom (1-DOF) model, shown in figure 5.7, has a transmissibility, $T(\omega)$,

which is given by the relation [111]

$$T(\omega) = \left\{ \frac{1 + d^2}{1 - (\omega/\omega_n)^2 + d^2} \right\}^{\frac{1}{2}} \qquad 5.1$$

where ω_n is the resonant frequency of the system. The loss tangent, d, of the cushion is assumed to be independent of frequency. The form of equation 5.1 is shown in figure 5.8 as $T(\omega)$ against frequency. It can be seen that the 1-DOF model of figure 5.7 cannot reproduce measured cushion responses, such as that shown in figure 5.6. In order to explain the multiple resonance peaks in figure 5.6 it is necessary to assume that the person on the seat is not a passive mass. For modelling purposes it is necessary to incorporate this assumption by using multi degree-of-freedom representations of the seated person.

The human body is a complex biomechanical system. Figure 5.9 shows a representation of the person-seat system in an automobile. The form of figure 5.9 is complicated, and from a modelling point of view, impractical. Instead it is necessary to use simpler models for the seated person. Several whole body representations have been described in the literature to reproduce the response of the human body to cyclical oscillations [112,113,114]. Most of these were developed to reproduce the driving point impedence of the human body. The present investigation is based on the 3-DOF model of Payne and Band [112].

The Payne-Band model used in this work is shown in figure

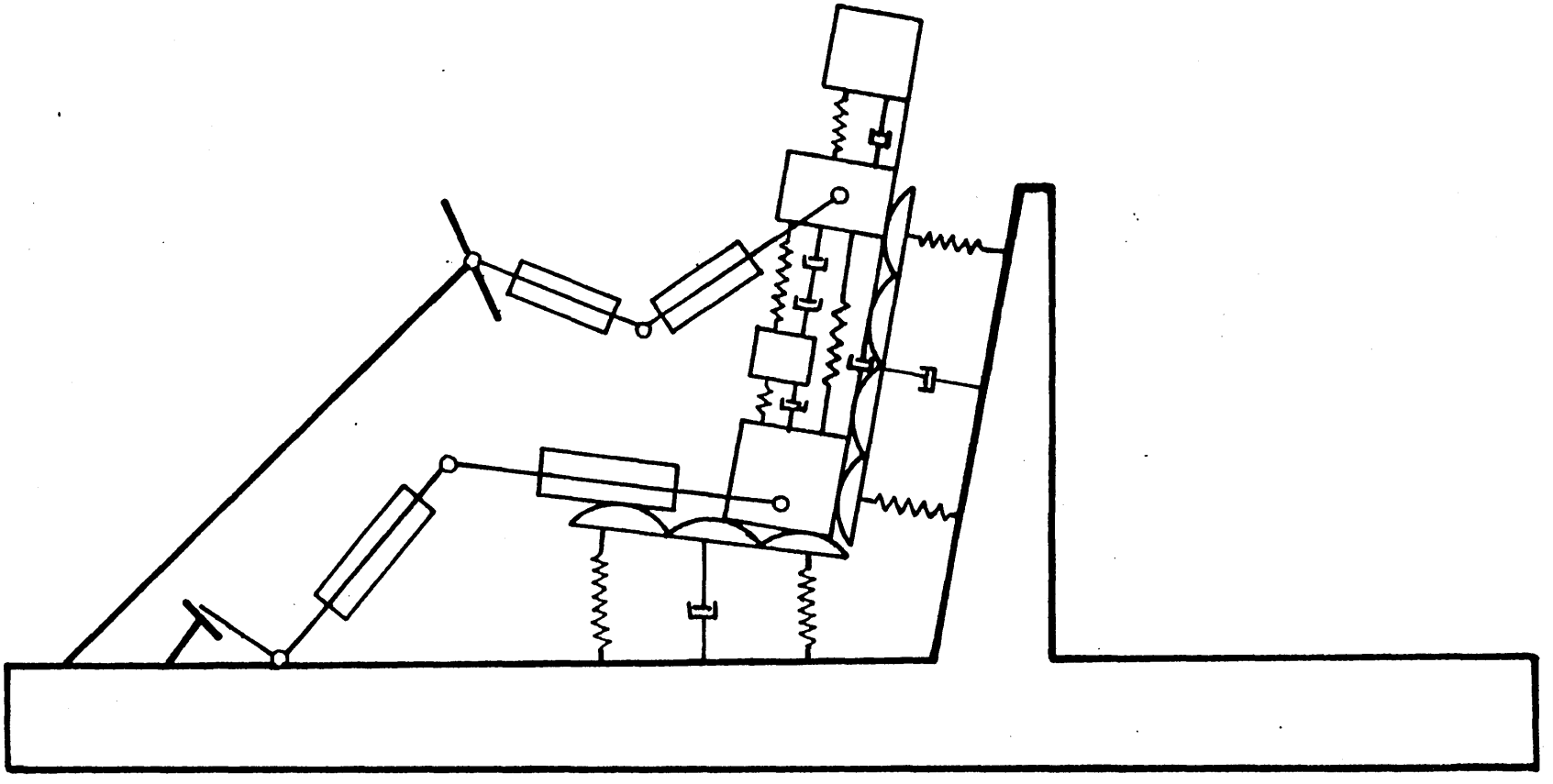

FIGURE 5.9
Lumped Parameter Representation of a Person Sat on a Vehicle Seat.

5.10. The model is formed from lumped mass and linear spring-damper systems. In the origional paper the different components of the model were related to sub-components of the body, as shown in figure 5.10. These comparisons are not strictly valid, they are merely labels attached to each model area by Payne and Band to clarify the model structure [115]. The values assigned to the model parts were ascertained from measurements made on the human body. Due to the effects of muscle tone, age and posture [116,117,118] each component of the human body model devised by Payne and Band has mechanical properties which can vary over a range of values.

The Payne-Band model represents a major simplification to the person-seat system shown in figure 5.9. Notably the influence of the arms and legs is ignored and the effect of the presence of the seat backrest is neglected. The former is reasonable as the mass in the arms and legs is small and will only influence the dynamic behaviour of the person-seat system at frequencies above the range of interest. The backrest will have an effect on the response of the person-seat system. This is ignored in the present analysis and like earlier workers it is assumed that ride comfort is associated with motion in the vertical direction. Motion in the other directions has been noted previously [102,107]. The influence of this on the ride comfort has not been investigated in the present or previous investigations.

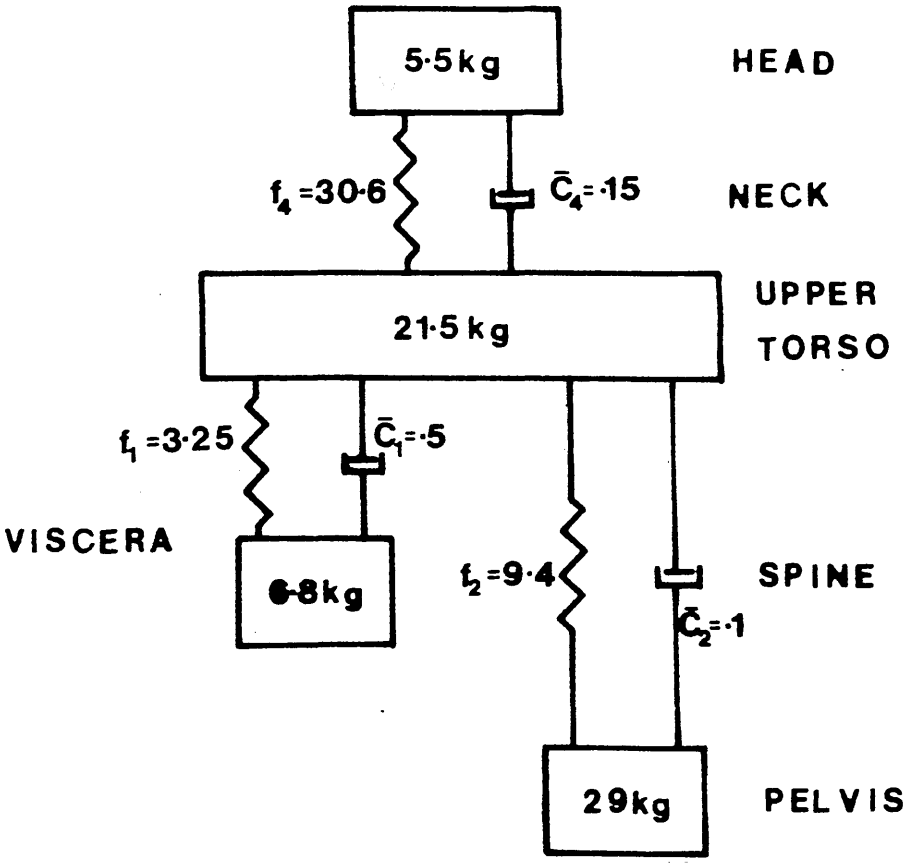

FIGURE 5.10

The Multi Degree-Of-Freedom Model of Payne and Band [112]. The f_i (i=1,2,4) are Resonant Frequencies. The Elements of the Model do not Correspond Directly to the Body Components.

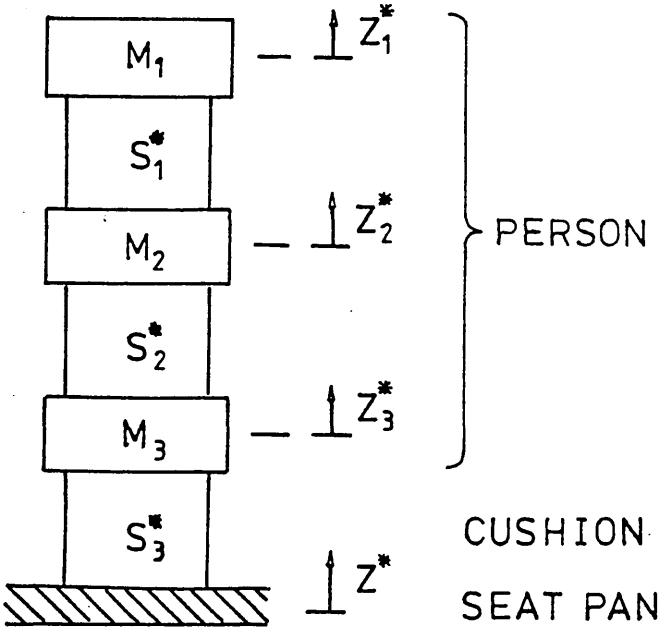

FIGURE 5.11

3-DOF Model Representation of the Person-Seat System with Lumped Masses, Distributed Stiffness and Full Depth Cushion.

The reduced proficiency boundaries of the International Standard [94] show that the frequency range 1-20 Hz, where most major vehicle and seat resonances occur, is also the range where the human body has least tolerance to mechanical vibration. By restricting the investigation to a consideration of this frequency range, the component of the model associated with the head can be rigidly attached to the shoulders, enabling the model of figure 5.11 to be drawn.

The parallel spring-damper system used by the origional workers poorly represents the dynamic mechanical properties of distributed systems [111]. The muscles, bones and internal organs of the human body form distributed systems, and are best described using distributed model components, such as viscoelastic elements. Consequently a materials approach is used and the system described in terms of lumped masses and resilient elements, having a mathematically complex stiffness, S^*.

The 3-DOF Person-Seat Model

The model details described below have been published [119]. As mentioned previously, several assumptions have been made to simplify the analysis of the person-seat model. These include

1) Vertical sinusoidal excitation input to the base of the cushion.
2) No non-linearities in the dynamic mechanical

properties of the cushion and the body components.

3) No frequency dependence of the mechanical properties.

4) No fluid flow damping effects in the cushion material.

5) Mass concentrated in the lumped masses of figure 5.11.

6) Person does not lose contact with the seat cushion.

Assumption 4) is removed later in the treatment, when the effect of fluid flow damping will be considered. Many of the other assumptions may also be removed by a more rigorous analysis of the basic model. These model extensions and improvements are suggested as areas for future study.

For an oscillatory input displacement of the form $Z^{*}=Z_{o}\exp[j\omega t]$, the resulting displacement of each of the masses M_1, M_2 and M_3 will be given by a relation of the form

$$Z_i = Z_{io} \exp [j(\omega t + \phi_i)] \quad i = 1,2,3 \qquad 5.2$$

The equations of motion for the model of figure 5.9 are

$$M_1\ddot{Z}_1* = S_1*(Z_2* - Z_1*) \qquad 5.3$$

$$M_2\ddot{Z}_2* = S_2*(Z_3* - Z_2*) - S_1*(Z_2* - Z_1*) \qquad 5.4$$

$$M_3\ddot{Z}_3* = S_3*(Z* - Z_3*) - S_2*(Z_2* - Z_2*) \qquad 5.5$$

Equations 5.3-5.5 may be more conveniently written in matrix form

$$\underline{A}.\underline{Z} = \underline{B} \qquad 5.6$$

where

$$\underline{Z} = (Z_1* \; Z_2* \; Z_3*)$$

$$\underline{B} = (0 \quad 0 \quad S_3*Z*)$$

$$\underline{A} = \begin{bmatrix} (S_1^* - M_1\omega^2) & -S_1^* & 0 \\ -S_1^* & (S_1^* + S_2^* - M_2\omega^2) & -S_2^* \\ 0 & -S_2^* & (S_2^* + S_3^* - M_3\omega^2) \end{bmatrix}$$

If $\det(\underline{A}) \neq 0$ then $\underline{Z}=\underline{A}^{-1}.\underline{B}$ and the components of $\underline{Z}$ may be written

$$Z_i^* = A_{i_3}^{-1} S_i^* Z^* \quad i = 1,2,3 \qquad 5.7$$

where

$$\underline{A}^{-1} = \frac{\text{adj}(\underline{A})}{\det(\underline{A})}$$

Because the motion is assumed to be sinusoidal, the transmissibility of the cushion, defined as $\ddot{Z}_3^*/\ddot{Z}^*$, can be written in terms of the displacements Z_3^* and Z^*

$$T(\omega) = \left|\frac{Z_3}{Z^*}\right| = \left|A_{3\,3}^{-1} S_3^*\right| \qquad 5.8$$

Expanding equation 5.8, the transmissibility of the cushion can be expressed in terms of the complex quantities S_i^*. The required relation takes the form

$$T(\omega) = \left|\frac{S_3^*[(S_1^*-M_1\omega^2)(S_1^*+S_2^*-M_1\omega^2)-(S_1^*)^2]}{(S_1^*-M_1\omega^2)[(S_1^*+S_2^*-M_1\omega^2)(S_2^*+S_3^*-M_3\omega^2)-(S_2^*)^2]-(S_1^*)^2(S_2^*+S_3^*-M_3\omega^2)}\right| \qquad 5.9$$

In a similar manner to the complex modulus used in Chapter 4, the complex stiffness may be split into real and imaginary parts

$$S_i^* = S'_i(1 + jd_i) \quad i = 1,2,3 \qquad 5.10$$

where S'_i are the storage stiffness's and d_i are loss tangents. Substituting equation 5.10 into equation 5.9,

the transmissibility of the cushion takes the form

$$T(\omega) = \left\{\frac{R_N^2 + I_N^2}{R_D^2 + I_D^2}\right\}^{\frac{1}{2}} \qquad 5.11$$

where

$$R_N = M_1M_2S'_3\omega^4-[M_1S'_2S'_3(1-d_2d_3)+S'_1S'_3(1-d_1d_3)(M_1+M_2)]\omega^2 +$$
$$+ S'_1S'_2S'_3(1 - d_1d_2-d_1d_3-d_2d_3)$$
$$I_N = M_1M_2S'_3d_3\omega^4-[M_1S'_2S'_3(d_2+d_3)+S'_1S'_3(d_1+d_3)(M_1+M_2)]\omega^2 +$$
$$+ S'_1S'_2S'_3(d_1+d_2+d_3-d_1d_2d_3)$$
$$R_D = -M_1M_2M_3\omega^6 + [S'_2(M_1M_2+M_1M_3)+S'_1(M_1M_3+M_2M_3)]\omega^4 +$$
$$- [(M_1+M_2+M_3)S'_1S'_2(1-d_1d_2)]\omega^2 + R_N$$
$$I_N = [S'_2d_2(M_1M_2+M_1M_3)+S'_1d_1(M_1M_3+M_2M_3)]\omega^4 +$$
$$-[(M_1+M_2+M_3)S'_1S'_2(d_1+d_2)]\omega 2 + I_N$$

5.1.3 Comparison of Predicted Response to Field Measurements

The theoretical person-seat responses predicted by the 3-DOF model, based on the work of Payne and Band have been produced using a computer. A Nascom III microcomputer was used, together with a Watanabe personal plotter. The computer language used was Pascal, both for speed and accuracy. All calculations were performed to 12 places of decimal, in order to avoid truncation errors. The results have been plotted in the form of transmissibility on a linear scale versus frequency on a logarithmic scale.

Table 5.1 gives the nominal values for each parameter, together with the range of values used by Payne and Band.

Table 5.1 The Nominal Values and Ranges of Each Parameter Together with the Ranges Required for the Model Studies.

PARAMETER	NOMINAL VALUE	RANGE	MODEL STUDIES
M_1 /kg	6.8	6.8	6.8
S'_1 /kN m^{-1}	2.4	1.5-4.0	2.6-5.0
d_1	0.3	0.2-0.9	0.1-0.5
M2 /kg	27.2	27.2	27.2
S'_2 /kN m^{-1}	50	35-92	45-70
d_2	0.2	0.1-0.5	0.1-0.2
M_3 /kg	29	29	29
S'_3 /kN m^{-1}	15	10-50	20-45
d_3	0.2	0.1-0.3	0.1-0.3

The values assigned to the dampers in the Payne Band model were converted to equivalent loss tangents using the treatment given by Snowdon [111]. In the case of the cushion parameters, the range of values was estimated from measurements of the gradient and hysteresis of IFD curves for full depth foam cushions from a JCB earth moving vehicle, at the point in the IFD curve where the load was equivalent to a 70 kg person. The values of stiffness obtained are numerically similar to the dynamic stiffness of cushion materials measured in section 4.1 for the strain range 0-60%. The hysteresis damping values from the IFD curve are rather larger than the

measurements of the dynamic loss tangent in section 4.1. This difference is attributed to the influence of the peripheral deformations in indentation loading where the cellular material is subject to a system of combined stresses. When in tension, for example, hysteresis is much less than that in compression.

The mass of each component in the body was not varied in the origional work by Payne and Band. This was because the relative sizes of the masses are similar for different persons and are insensitive to effects such as muscle tone and posture. Figures 5.12 and 5.13 illustrate the effect varying the stiffness and mechanical damping of the cushion material has on the vibration transmissibility predicted by the person-seat model. All other parameters were set at their nominal values. Both the height and position of the three resonance peaks in the response curve can by altered by changing the mechanical properties of the cushion. Changes in the parameters assigned to the human body parts can also influence the shape of the $T(\omega)$ curve. Altering these parameters to fit the model response to measured data is justified as the mechanical properties exhibited by the human body will vary from person to person and depend on posture and muscle tone.

Four measured vehicle seat cushion responses were chosen. Three due to Griffin [100] and one from the data collected by Mc Nulty et al from an off-road vehicle

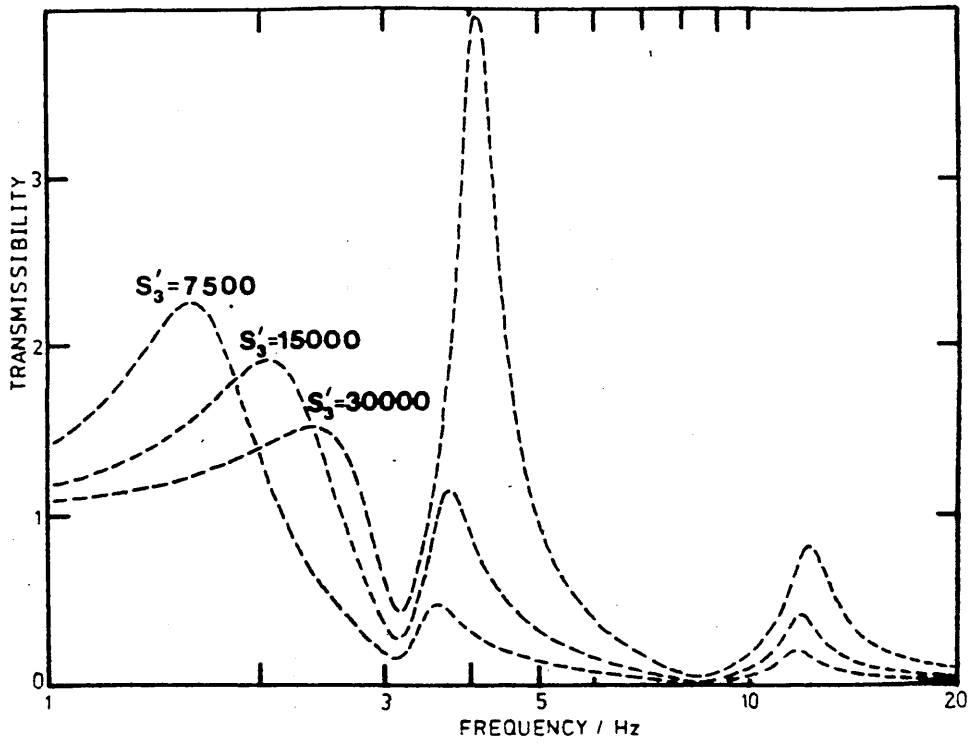

FIGURE 5.12

The Effect of Varying the Stiffness of the Seat Cushion on the Transmissibility Predicted by the Model. All Other Model Parameters were Set at the Nominal Values.

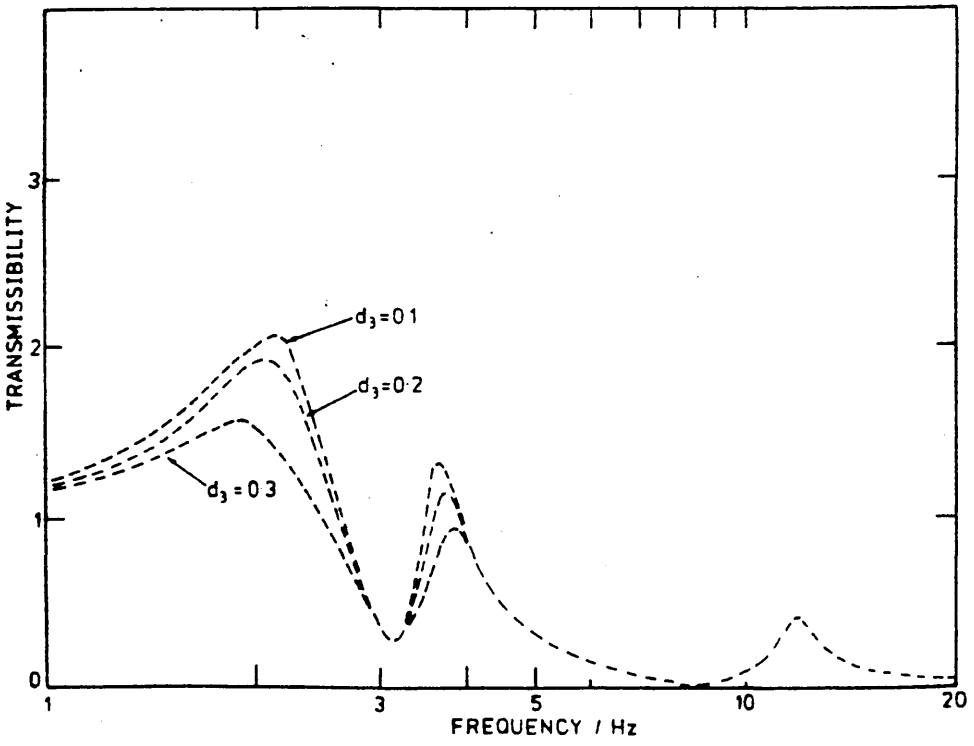

FIGURE 5.13

The effect of Varying the Damping of the Seat Cushion on the Transmissibility Predicted by the Model. All Other Model Parameters were Set at the Nominal Values.

[102]. The fitting process was performed by trial and error. Figures 5.14-5.17 show the measured seat cushion response curves, together with the closest theoretical variation predicted by equation 5.11. The values of each model parameter required to produce the fitted curve are given in table 5.2. Considering the simplicity of the model, the level of agreement between measurement and theory is good. In all cases, the fitting parameters were within, or close to the ranges determined by Payne and Band in their origional treatment.

The worst correspondence between theory and measurement occurs with the data taken from a JCB earth moving vehicle, shown in figure 5.17. With off-road vehicles the vibration amplitudes experienced by the operator are likely to be much greater than those in on-road vehicles. With the JCB vehicle tested, peak accelerations at the buttocks-cushion interface in excess of 1g were recorded [102]. Under these conditions, small strain amplitudes in the cushion cannot be assumed and the cushion material will have highly non-linear mechanical properties.

The differences between the model prediction and the measured response for the on-road vehicles tested by Griffin are attributed to the simplifications made in the desription of the person-seat system. Notably the influence of the seat backrest and non-linearities in the cushion and the person have not been considered. The viscera in particular form a highly non-linear system

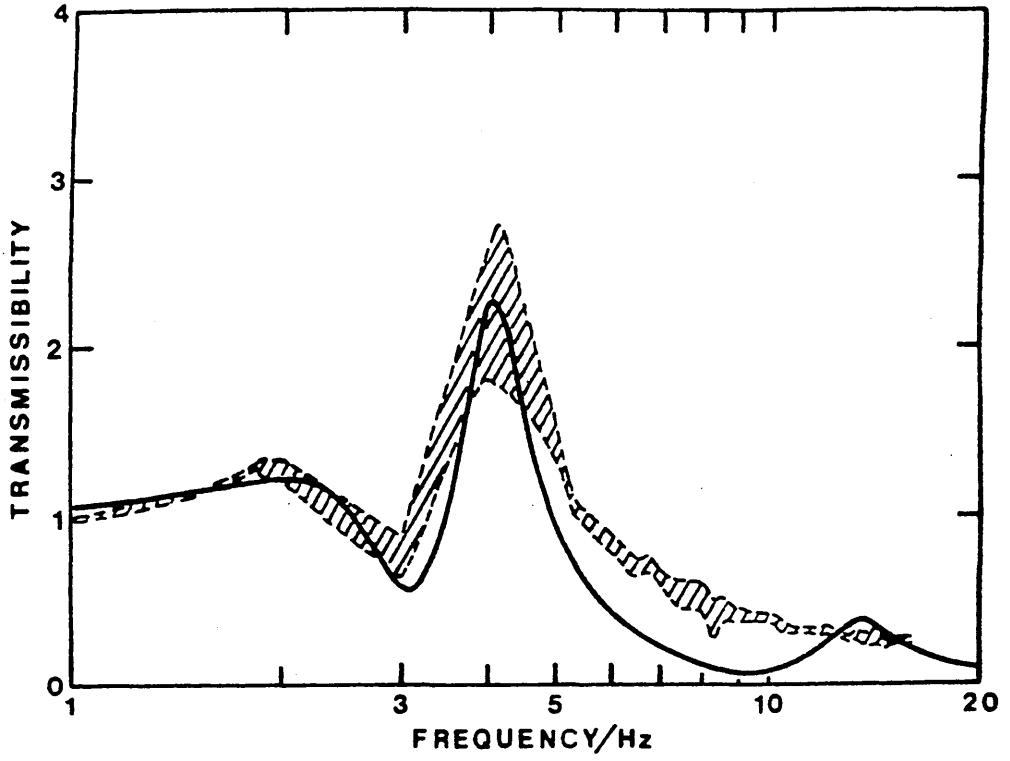

FIGURE 5.14

$T(\omega)$ Against Frequency For a Small, Low-Cost, 5-Door Car [100]. Hatched area; Field Measurements, Solid Line; Model Prediction.

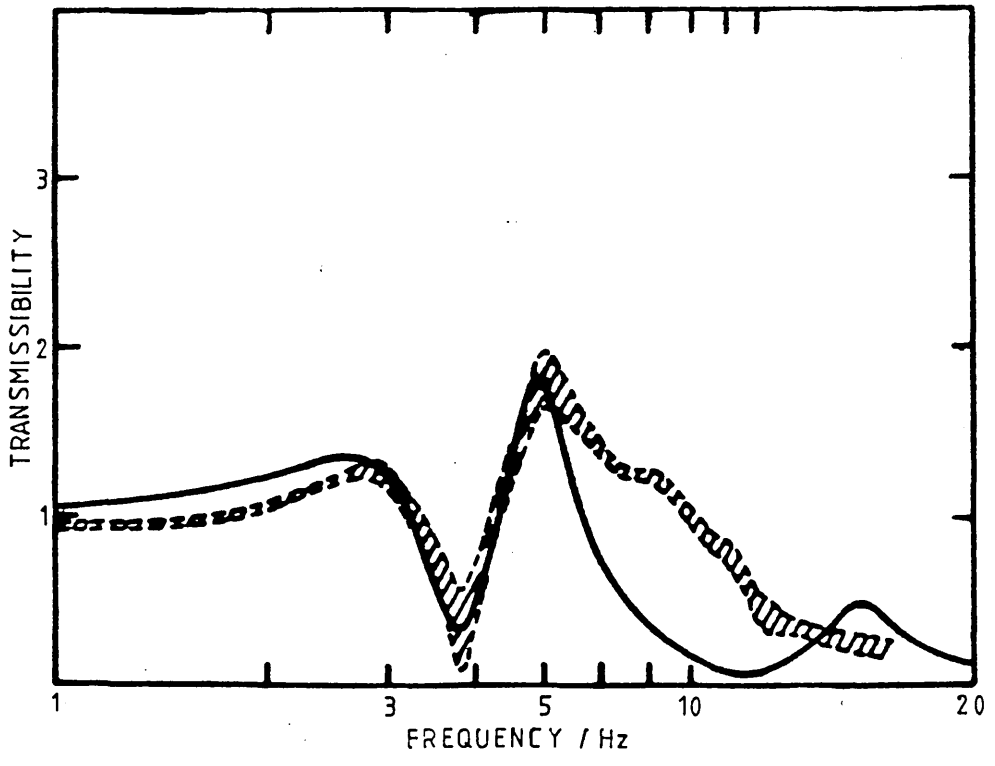

FIGURE 5.15

$T(\omega)$ Against Frequency For a Small Van [100]. Hatched area; Field Measurements, Solid Line; Model Prediction.

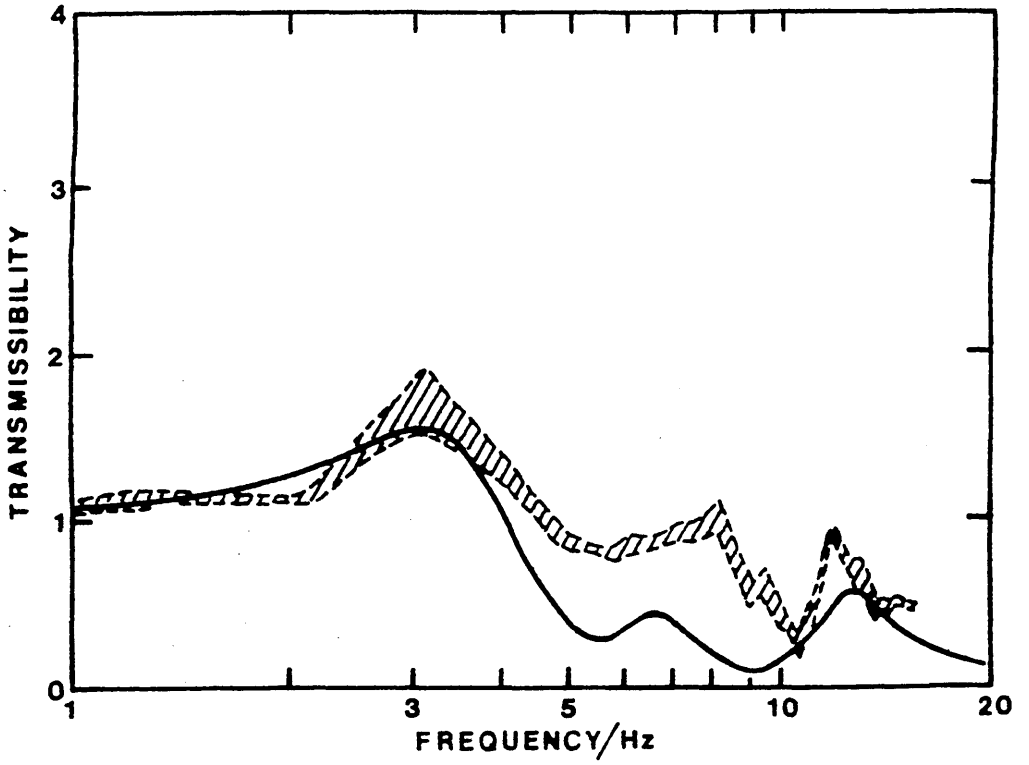

FIGURE 5.16

$T(\omega)$ Against Frequency For a 12-Seat Light Bus [100]. Hatched area; Field Measurements, Solid Line; Model Prediction.

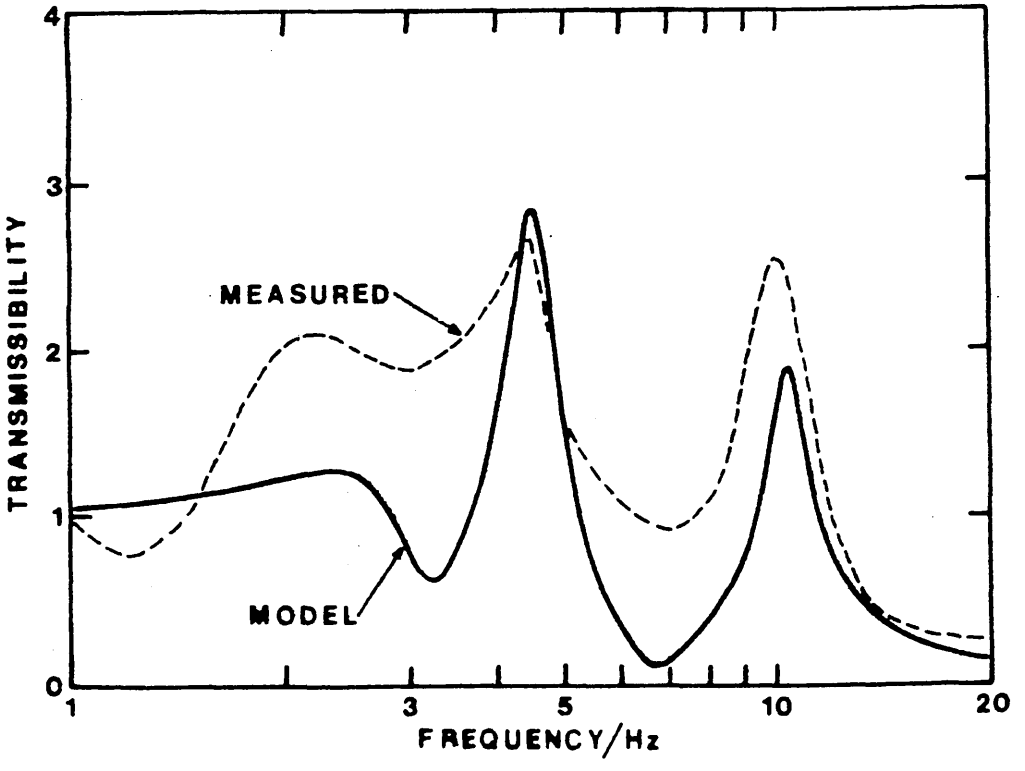

FIGURE 5.17

$T(\omega)$ Against Frequency For an Off-Road JCB Earth Moving Vehicle [102]. Broken Line; Field Measurements, Solid Line; Model Prediction.

TABLE 5.2 The Parameter Values Required to Produce Figures 5.14-5.17.

PARAMETER	FIGURE			
	5.12	5.13	5.14	5.15
M_1 /kg	6.8	6.8	6.8	6.8
S'_1 /kN m^{-1}	2.6	4.0	5.0	3.0
d_1	0.1	0.1	0.3	0.2
M_2 /kg	27.2	27.2	27.2	27.2
S'_2 /kN m^{-1}	90	90	70	45
d_2	0.2	0.2	0.1	0.2
M_3 /kg	29	29	29	29
S'_3 /kN m^{-1}	30	40	40	45
d_3	0.2	0.2	0.1	0.1

[112]. In addition, the vibration was assumed to consist of a single frequency sinusoid. In fact the frequency spectrum of the vibrations entering the base of the seat contains both random and periodic vibrations, as described above. This difference will not affect the simple model treatment outlined above, but when extensions to the basic model are considered, this difference may become important.

Despite its simplicity, the 3-DOF person-seat model outlined above has proved capable of recreating the salient features of a measured vehicle seat response

curve. It is hoped that the model may be used to predict the response of a particular person-seat combination in order to predict the optimum material properties for the seat cusion. Another group of workers have recently developed a vibration control (VC) additive for cushion foams during manufacture. This additive is claimed to change the fluid flow properties of the material, as explained in Chapter 3. The inclusion of the VC additive allows control over the fluid flow damping process discussed in section 4.2. The inclusion of fluid flow damping processes in the cushion material allows predictions to be made on the possible effect of such additives. In the present work the treatment is restricted to compressible or incompressible Newtonian fluids

5.1.4 The Inclusion of Fluid Flow Damping Processes in the Cushion Material

The theory of Newtonian fluid flow damping has been discussed in section 4.2 and reviewed elsewhere [49]. Extensions to the 3-DOF person-seat model described above have been developed for both compressible and incompressible fluids. In each case, the flow of the enclosed fluid through the cellular matrix of the cushion material causes the stiffness and damping of the material to become frequency dependent. For incompressible fluids, if the cushion has height H and width W then

$$S'_3(\omega) = \frac{S'_3\{1 + \beta(1 + \beta)\gamma^2\}}{1 + \beta^2\gamma^2}$$

$$d_3(\omega) = \frac{d_3\{1 + \beta^2\gamma^2\} + \gamma}{1 + \beta(1 + \beta)\gamma^2} \qquad 5.13$$

where

$$\beta = 3(S'_3/S_t)(H/W)^2$$

$$\gamma = (\omega\eta W^2)/(12S'_3K(\omega))$$

S_t is the stiffness of the material in the transverse direction and $K(\bar{\omega})$ is defined by equation 4.14. If ω_{max} is the frequency at which the maximum damping occurs, and γ_{max} is the equivalent value of γ at this frequency, then

$$\gamma = \omega(\omega_{max}/\gamma_{max})$$

In their origional treatment, Gent and Rusch [39,74] found that γ_{max} was related to the parameter β by the approximate expression

$$\gamma_{max} \cong 1/(\beta + \beta^2)^{\frac{1}{2}} - d_3/(1 + \beta) \qquad 5.14$$

Thus the incompressible fluid flow damping effect can be selected by specifying the values of the two parameters β and ω_{max}.

In the case of compressible fluids it can be shown that the stiffness and damping of the cushion are given by relations of the form

$$S'_3(\omega) = S'_3(1 + 1/\alpha - \delta\psi_1/\alpha) \qquad 5.15$$

$$d_3(\omega) = (\alpha d_3 + \delta\psi_2)/(\alpha + 1 - \delta\psi_1) \qquad 5.16$$

ψ_1 and ψ_2 are given by equations 4.21-4.22 and $\beta = S'_3/S_g$,

where S_g is the stiffness of the fluid. γ can be found using the relation [39].

$$\gamma = \frac{12\omega}{\omega_{max}} \left\{0.83/(1 + 1.2\alpha) - d_3/(1 + 1.2\alpha)\right\} \quad 5.17$$

In this case $S_3'(\omega)$ and $d_3(\omega)$ can be specified by the values of the parameters α and ω_{max}. The coefficients ψ_1 and ψ_2 are the sums of infinite series. However, the series converge rapidly and it was only necessary to consider the first 10 terms.

The above equations for the inclusion of fluid flow damping effects in the seat cushion do not account for the differential deformation of the cushion material, due to the shape of the buttocks. No published work has appeared on the effect of a deformation system such as this on the fluid flow process. It is thought that the behavior of the material will be similar. As different areas of the cushion are subject to different levels of pre-strain, the fluid flow damping maximum will occur at different frequencies in each local area. The effect of this averaged over the whole of the cushion is not known. For the present work it has been assumed that the mechanical properties of the cushion will be modified in a similar manner to that found for cellular materials under uniform compressive deformation.

For investigations into the effect of fluid flow damping processes on $T(\omega)$, the amount of fluid flow damping, and the frequencies at which it occurs have been specified by

choosing values of α or β and ω_{max} directly. No attempt has been made to relate these values to the structure of the cushion material.

Figure 5.18 shows the variation of the cushion stiffness and damping with frequency for differing levels of incompressible fluid flow damping. For figure 5.18 the maximum damping frequency, ω_{max}, was set to 5 Hz. The shape of the curves for compressible fluids were similar. The only difference was at frequencies above the maximum, where the damping with compressive fluids was slightly lower than that found for an incompressible liquid [49].

Fluid flow damping in the cushion material could have a considerable effect on the vibration transmissibility exhibited by the cushion. This has been investigated by incorporating equations 5.12 and 5.13 into the 3-DOF person-seat model. Figure 5.19 shows the effect of incompressible fluid flow damping on a typical cushion transmissibility curve, predicted by the model. The solid line shows $T(\omega)$ for a cushion with no fluid flow effects. The stiffness and damping of the cushion material varied with frequency as shown in figure 5.18.

To date, no attempt has been made to improve the predictions of figures 5.14-5.17 by incorporating fluid flow processes in the cushion material. The seat cushions taken from a JCB earth moving vehicle were found to have a value of α of about 0.2 (assuming the volume fraction of open cells was about 0.9). An approximate

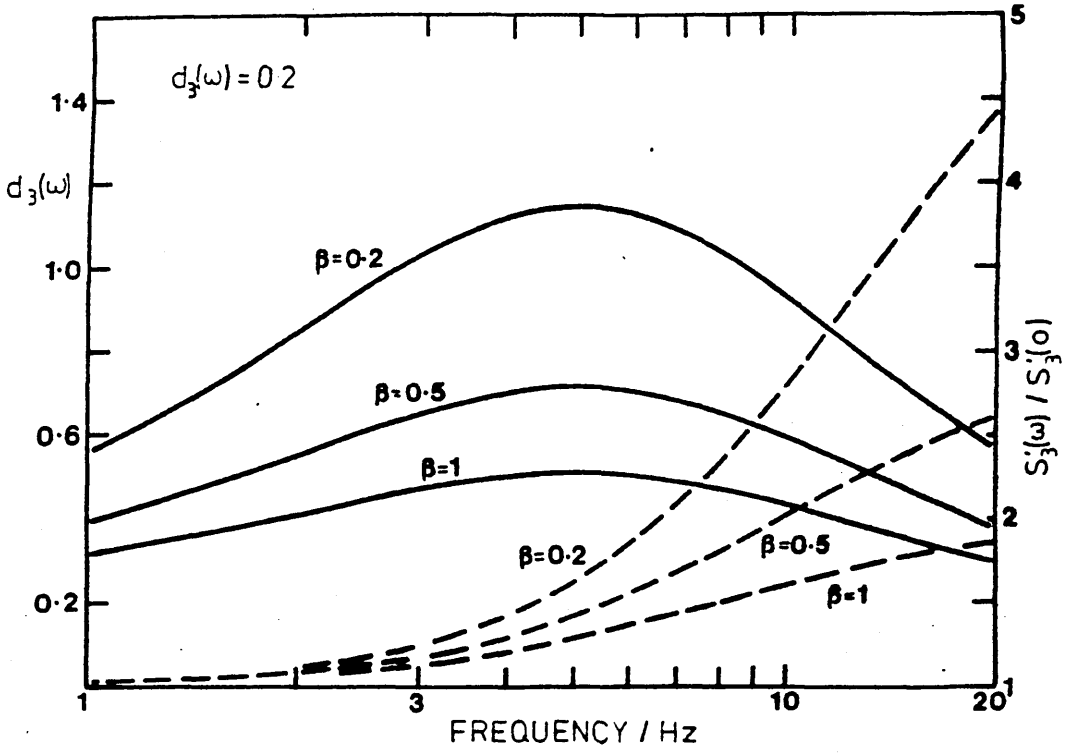

FIGURE 5.18

Effect of the Parameter $\beta = 3(S'_3/S_t)(H/W)^2$ on the Dynamic Mechanical Properties of an Open Cell Cushion Foam.

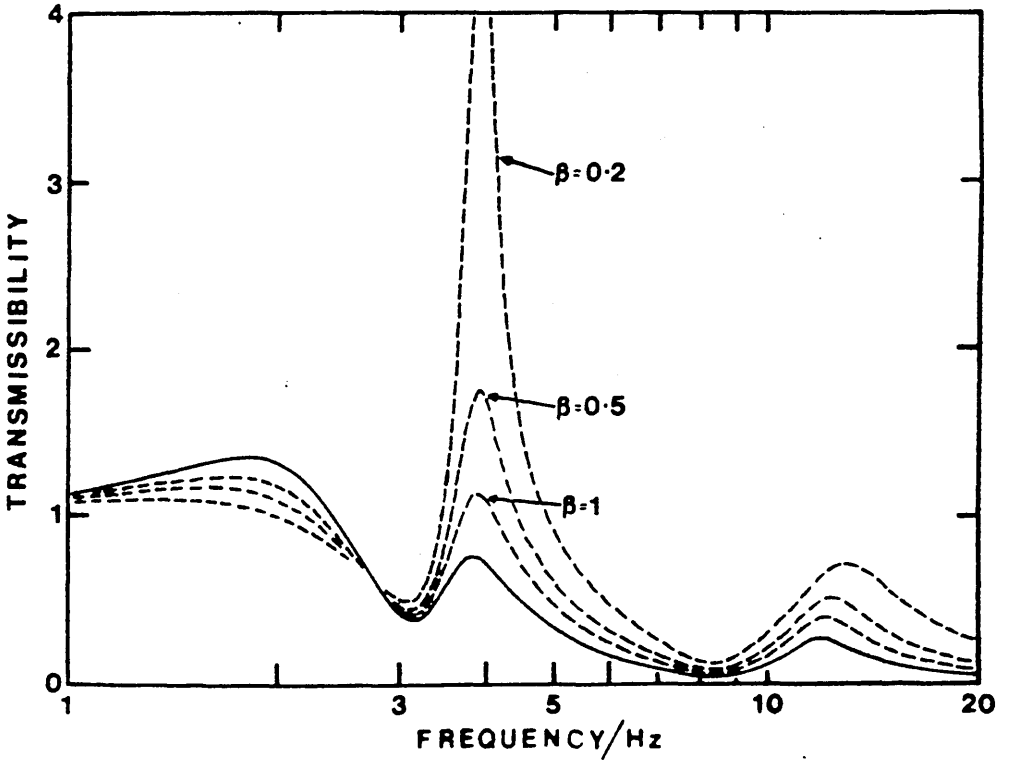

FIGURE 5.19

Effect of the Parameter β on the Cushion Transmissibility Predicted by the 3-DOF Model Incorporating Fluid Flow Effects. Solid Line; No Fluid Flow Effect.

calculation with the material properties of the cushion shows that, with the material filled with air, the damping maximum occurs at about 100 Hz. However, the presence of the 70kg person on the top of the seat will produce a significant deformation in the centre of the cushion and reduce the maximum damping frequency in this area, along the lines described in section 4.2. Before the fluid flow process is used to improve the predictions of the person-seat model, however, more information is needed on the fluid flow effects in non-uniformly deformed materials and the effects of cushion covering. The potential implications of the work done so far are discussed in chapter 6.

5.2 The Response of a Non-Linear Vibration Isolating System to Large Amplitude Oscillatory Motion

5.2.1 Introduction

At very small vibration amplitudes the dynamic mechanical properties of viscoelastic materials may be assumed to be essentially independent of the amplitude of the mechanical deformation, although they will vary as the level of static pre-compression is increased. This behaviour has been considered in section 4.1. Under these conditions the vibration isolation characteristics of a simple isolator system, such as that shown in figure 5.20, will be a function of the mechanical properties of the isolator and the frequency of mechanical excitation.

At higher vibration amplitudes the mechanical properties

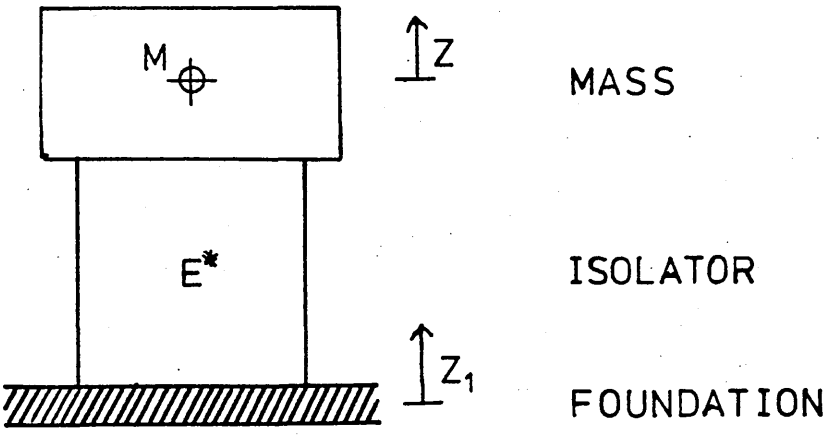

FIGURE 5.20

A Simple Mass Isolator System Consisting of a Rigid Mass Supported on a Distributed Viscoelastic Isolator.

become functions of the vibration amplitude, and the response of the isolator system in figure 5.20 becomes non-linear [117,118]. The response curves for systems with linear, strain hardening and strain softening resilient members are shown in figure 5.21.

The behaviour of such systems to mechanical excitations have been reviewed elsewhere [120,121,122]. Thompson [123] includes a discussion of the catastrophic instabilites which arise with responses such as those shown in figures 5.21b and 5.21c. The area of the response curve between the two points marked A and B on figure 5.21 is known as the region of instability. The non-linear behaviour exhibited by strain hardening and strain softening systems results in the resonant frequency of the system becoming dependent on the amplitude of the mechanical excitation.

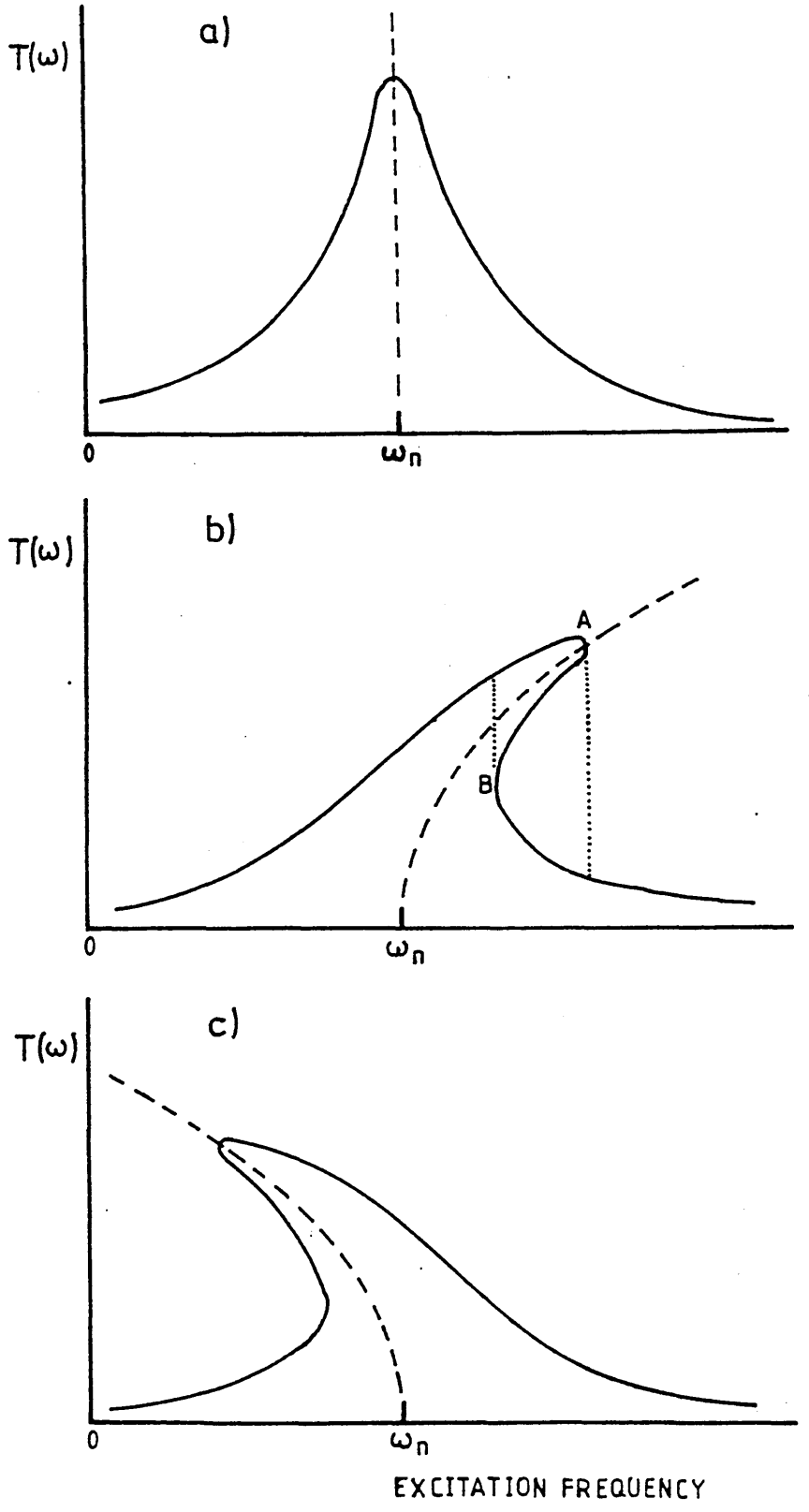

FIGURE 5.21

Typical Transmissibility Response Curves for Simple Isolator Systems Exhibiting a) Linear, b) Strain Hardening and c) Strain Softening Behaviour.

In the case of flexible cellular materials the system has been found to be strain amplitude softening, with the damping only a weakly dependant on strain amplitude.

The situation is more complex with real isolators, as oscillation of the mass is not restricted to vertical motion. Vibration in other directions will occur, even at very low amplitudes, with purely vertical excitations. In fact, for a 3-dimensional (3-D) isolator, a total of 6 modes of vibration are possible. With reference to figure 5.22 two shear modes (in the longitudinal, x, and transverse, y,directions),two rocking modes (in the α and β directions) and one torsional mode (inthe γ direction) may by excited, besides vertical motion in the z direction. Each of these modes will occur when the vertical excitation frequency approaches the natural frequency of the system in that direction.

Crede and Ruzicke [119] developed equations for 3-D isolators based on a model composed of linear springs. They found that coupled oscillation will occur in the x and β directions, and in the y and α directions. This will appear as a combined shear and rocking motion. The torsional and vertical modes were found to be uncoupled. The equations they generated related the frequencies at which these coupled modes occur to the isolator properties and geometry, and the resonance frequency of the system in the vertical direction. Crede and Ruzicke did not consider distributed systems, or incorporate non-

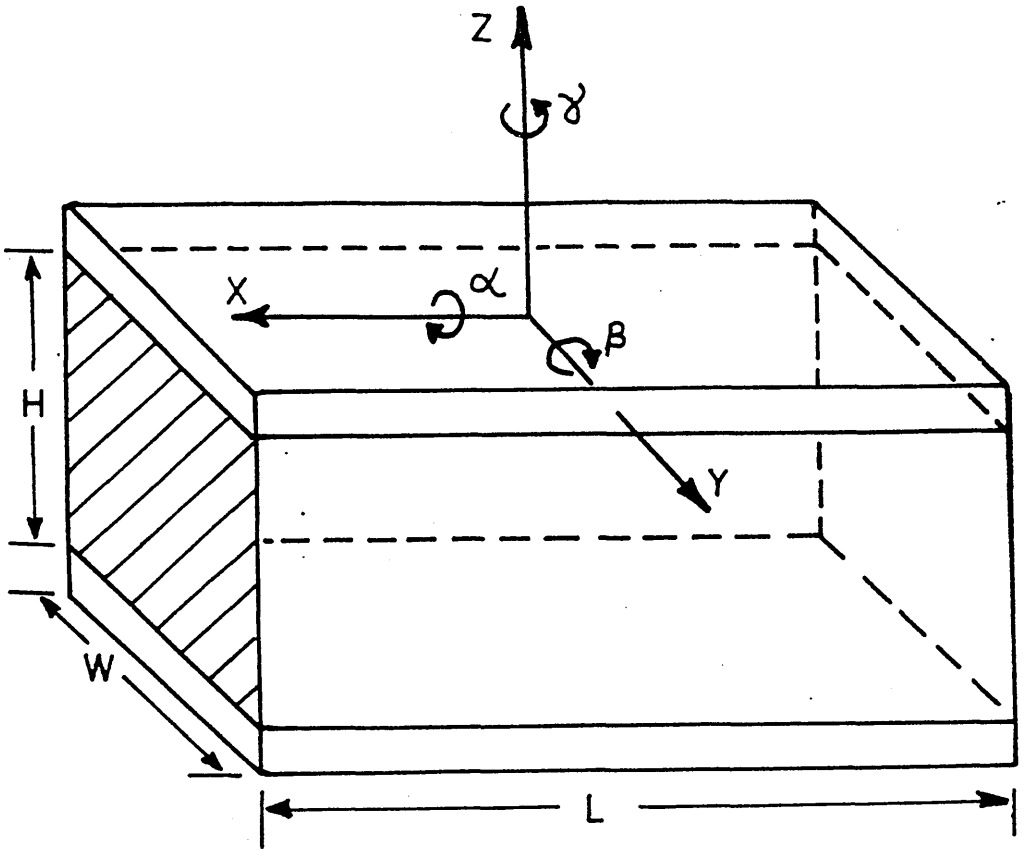

FIGURE 5.22
Experimental Arrangement Showing the Six Directions in Which Motion of the Isolated Mass Can Occur in a Real Mass-Isolator System.

linearities into the analysis.

At very large vibration amplitudes the properties of the isolator in figure 5.18 become highly non-linear. No previous work has been published on the response of 3-D distributed isolators to large amplitude excitations.

The response of a freely vibrating system, composed of a flexible foam isolator and a mass, to large amplitude, vertical, sinusoidal vibrations has been measured. The coupled modes predicted by Crede and Ruzicke have been identified and the frequencies at which they occur,

related to the predictions of their model. Above a certain level of excitation the classical approach to vibration isolation outlined above is found to break down. This break down appears as a cascade of subharmonic frequencies in the vertical oscillation of the mass. The resulting motion is highly complex and might be considered to be chaotic, although whether the system fulfills the mathematical requirements for chaos is uncertain. Preliminary results of the work in our laboratories has been published [124].

5.2.2 Review of Chaotic Motion

The notion, that given the initial conditions we know what a deterministic system will do far into the future, has been known to be false for some time. For many systems, given infinitesimally different starting conditions, the outcome can be completely different. It has been found that almost any non-linear system will exhibit chaotic behaviour [125]. A familiar example is turbulence.

More recenly chaos has been observed in many widely different situations, such as thermal convection [126,127], chemical reactions [128], opto-electronic processes [129], electronic circuit responses [130] and population dynamics [131]. Mees and Sparrow [132] have described chaotic solutions to state equations as those with persisting modes of dynamic behaviour that have no simple recurrence properties, even though they are not

stochastic. Chaotic solutions have been found to equations which are themselves relatively simple.

The phenomenon of chaos has been reviewed extensively in the literature [125,133,134] and only the broad outlines will be discussed here. The transition to chaos has been found to occur via bifurcation and period doubling [135,136]. A major discovery was made by Feigenbaum [137,138] who found that the transitions to chaos via the bifurcation cascade display a universal behaviour which is independent of the system under consideration. This discovery, for one-dimensional mapping [139], has also been observed in simulation experiments with higher dimensionality. The transition from order to chaos can be illustated by consideration of the one-dimensional map

$$x_{i+1} = Rx_i(1 - x_i) \qquad 5.18$$

Equation 5.18 has been used to predict the behaviour of a population [131]. R is known as the growth parameter. The behaviour of equation 5.18 for different values of R is shown in figure 5.23. Also shown in figure 5.23 is the power spectrum, $P(\omega)$, defined by the relation

$$P(\omega) = \frac{1}{N} \left| \sum_{i=1}^{N} x_i \exp[2\pi j \omega_i] \right|^2 \qquad 5.19$$

For values of R less than unity, regardless of the starting value of x, the population decays to zero (figure 5.23a). Above R=1 the population will settle down to a steady value, x_s which is independent of the starting value. x_s is related to the growth parameter by

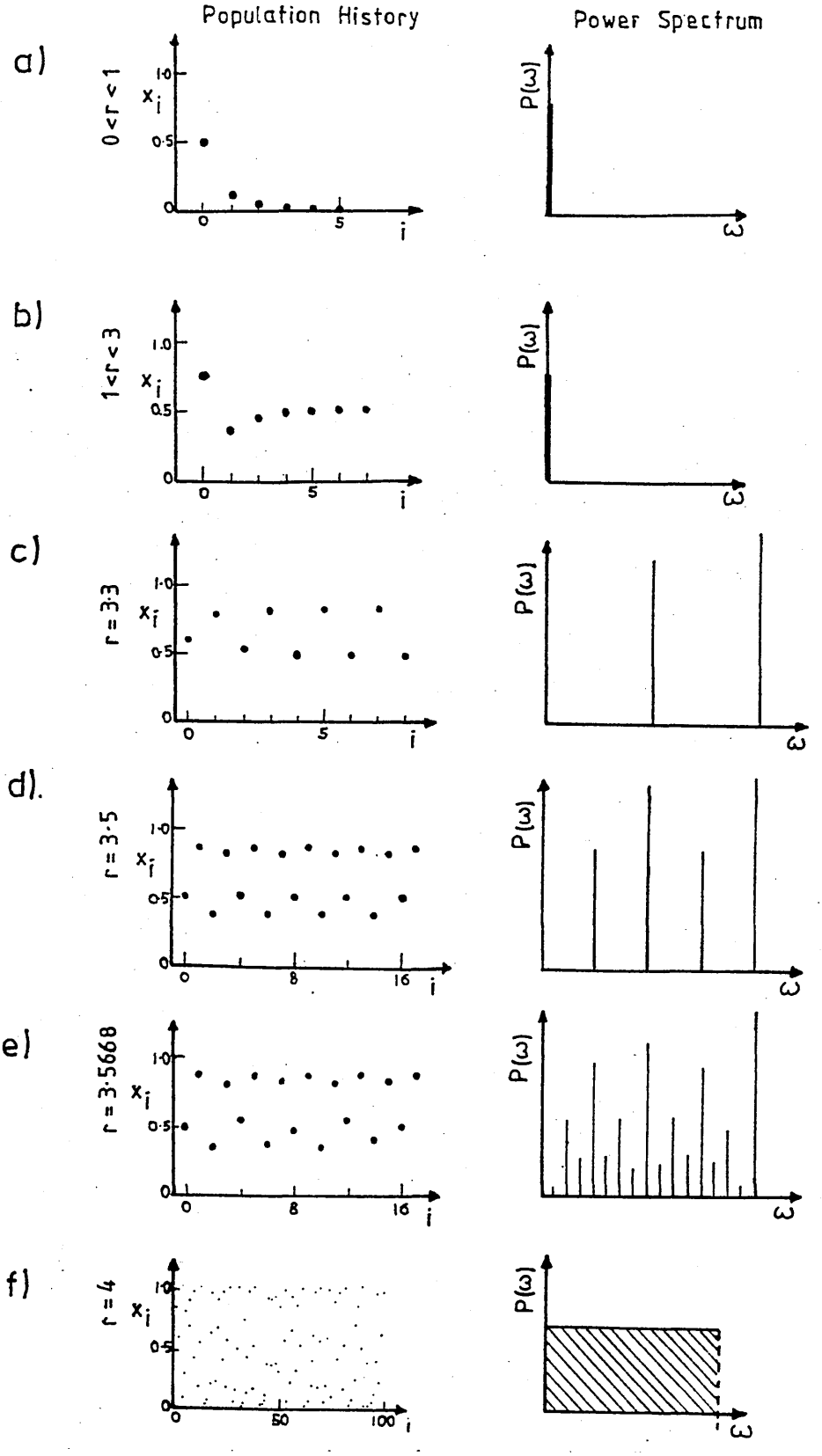

FIGURE 5.23

Behaviour of a Population that Obeys a Non-Linear Reproduction Equation (5.19), for Various Values of the Growth Parameter R. Taken from Kandoff [131].

$$x_s = 1 - 1/R \qquad 5.20$$

This behaviour is shown in figure 5.23b, and will persist as R increases, until a critical value of R=3.3 is reached. At this point the population becomes unstable and oscilates between two levels (figure 5.23c). This transition is associated with the generation of a subharmonic in the power spectrum. A further increase in R, to 3.5, produces a second transition, shown in figure 5.23d. This is associated with a further subdivision of the power spectrum, producing a four cycle plot. Further subdivisions occur as R is increased. The example of a 16 cycle plot (4th transition) is given in figure 5.23e. The cascade of bifurcations culminates at R=4 with a chaotic solution. Here the power spectrum is flat and the value of x is apparently unrelated to what has occured previously (figure 2.23f).

The period doubling bifurcation cascade for a system can also be illustrated in phase space. Figure 5.24 shows the first three period doubling bifurcations for a thermal convection system, in this form [125]. The Poincare surface, marked on figure 5.24, can be used to illustrate the onset of chaos by reducing the dimensionality of the phase space. The Poincare map for the data of figure 5.24 is shown in figure 5.25. The non-linearity parameter is the quantity whose value is changed to bring about the transition to the chaotic state.

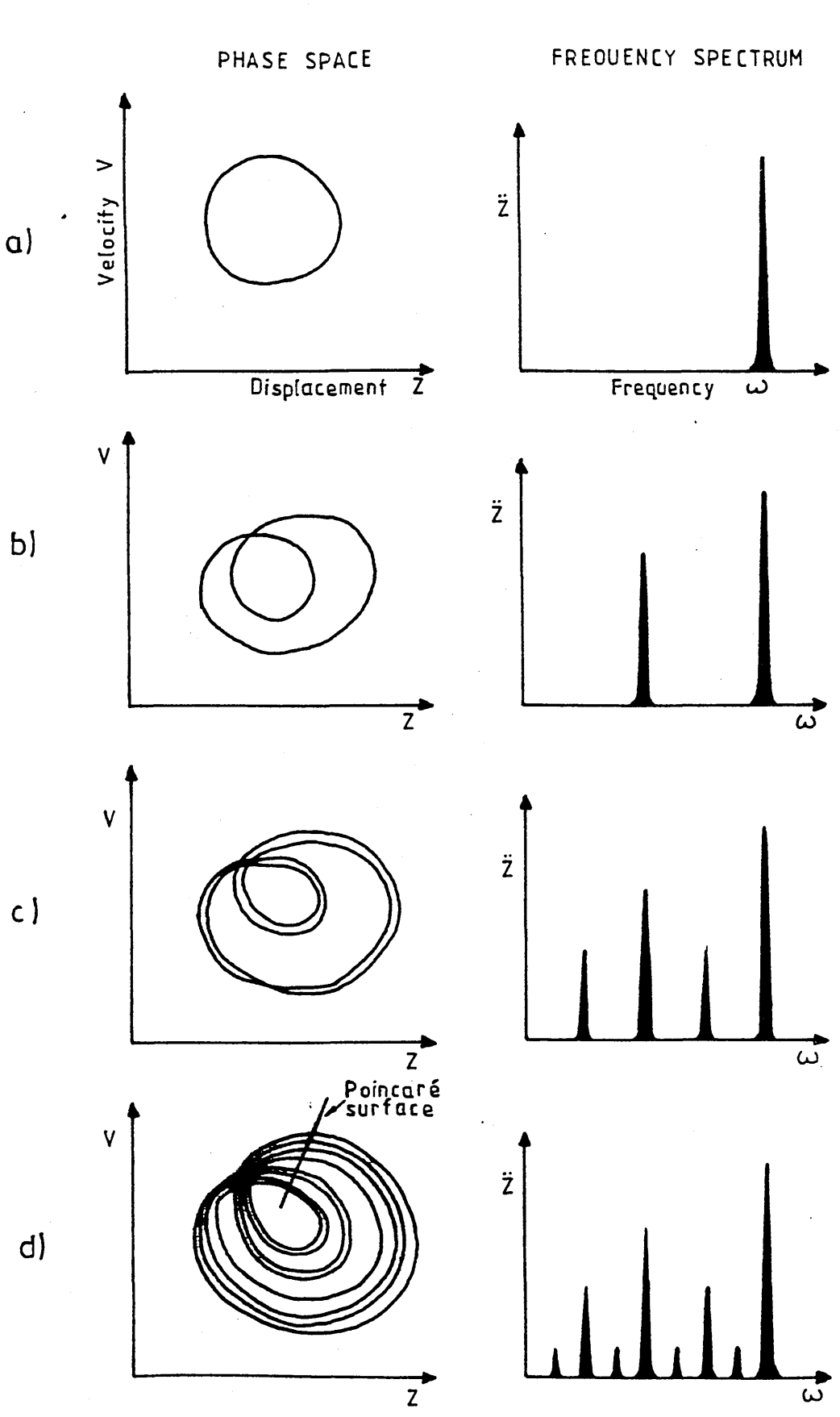

FIGURE 5.24

Behaviour of a Thermal Convection System as the Temperature Differential Increases, taken from Cvitanovic [125]. Data Plotted in Phase Space (Velocity-Distance) and as a Frequency Spectrum.

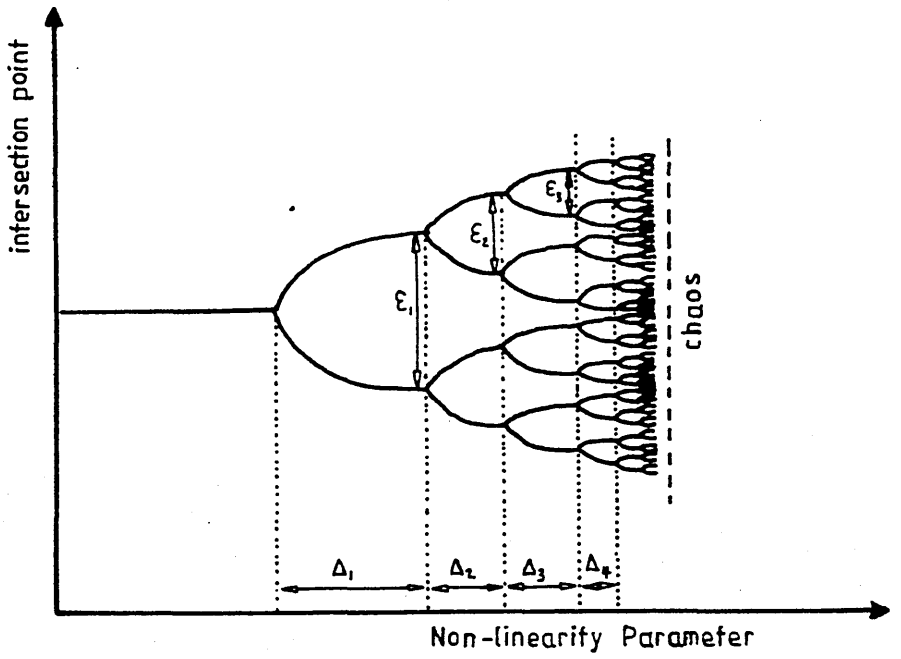

FIGURE 5.25
Poincare Map for the Data of Figure 5.24, Additionally Showing the Culmination of the Period Doubling Bifurcation Cascade in the Chaotic State.

The discovery of universality in the transition to chaos, made by Feigenbaum [137], was that the quantities Δ_i and ε_i, shown in figure 5.25, behave in a similar manner for all one dimensional systems. For large values of i, Feigenbaum found

$$\frac{\Delta_i}{\Delta_{i+1}} \rightarrow \delta = 4.6692 \qquad 5.21$$

$$\frac{\varepsilon_i}{\varepsilon_{i+1}} \rightarrow \alpha = 2.5029 \qquad 5.22$$

Equations 5.21 and 5.22 allow predictions on the route to chaos, providing this route involves an infinite series of period doubling bifurcations. Feigenbaum also found that the ratio of sucessive subharmionic amplitudes in the power spectrum, μ, also follows a universal

behaviour.

$$\mu = 2(1/\alpha^2 + 1/\alpha^4)^{-\frac{1}{2}} = 4.648 \ldots . \qquad 5.23$$

The above definitions of δ, α and μ assume that the number of period doubling bifurcations is large. In addition, in real systems the subharmonic amplitudes are often strongly modulated. The theory does not account for this behaviour. Many experiments have been performed to calculate the values of δ, α and μ. Cvitanovic [125] summarises the state of these experimental determinations. In most cases the number of period doubling bifurcations observed was less than 5. No references are given to determinations of these constants for chaotic motion in dynamic mechanical experiments.

5.2.3 Experimental Determinations

The experimental arrangement, shown in figure 5.22, consisted of a rectangular block of conventional polyurethane cushion foam of dimensions L=24 cm, W=7.6 cm and H=7.6 cm with aluminium plates of thickness 1.3 cm bonded to the top and bottom faces. The upper plate (isolated mass) had a mass of 640 g. The lower plate was rigidly connected to the electromagnetic shaker in use with the dynamic mechanical spectrometer (Chapter 2). The upper plate was unconstrained. The measuring system and sample mounting system of the spectrometer were not used in this application.

The motion of the shake table, $Z_1 = Z_{1o}\sin\omega t$, provided the

excitation to the system and was, to normal engineering tolerances, through the centre of mass of the lower plate and isolated mass. The acceleration of the isolated mass could be measured in any of the three directions, x, y, z, by means of a triaxial accelerometer. The signal from the triaxial accelerometer was displayed either as a phase space trajectory (velocity vs displacement) on an oscilloscope, or a power spectrum via a Real-Time Analyser. Frequencies in the range 10-100 Hz were used with deformation amplitudes in the range 0.01-8mm.

The vertical accleration, $\ddot{Z}$, of the isolated mass at a constant, moderate excitation amplitude of 0.5mm is shown in figure 5.26, as a function of the excitation frequency. The peak marked V was found to be the vertical resonance frequency of the mass-isolator system. The peaks marked L_1 and L_2 were associated with coupled shear and rocking motion in the x and β directions, while T_2 was found to be a coupled oscillation in the y-α directions.

The coupled frequencies of oscillation have been predicted for the system in use using the equations developed by Crede and Ruzicke [122]. Hilyard [140] gives a method by which the distributed isolator of figure 5.22 can be approximated by a system of springs. Using the treatment of Hilyard the model of figure 5.27 can be drawn. If I_x, I_y and I_z are the moments of ineria of the system then the coupled oscillation in the x-β

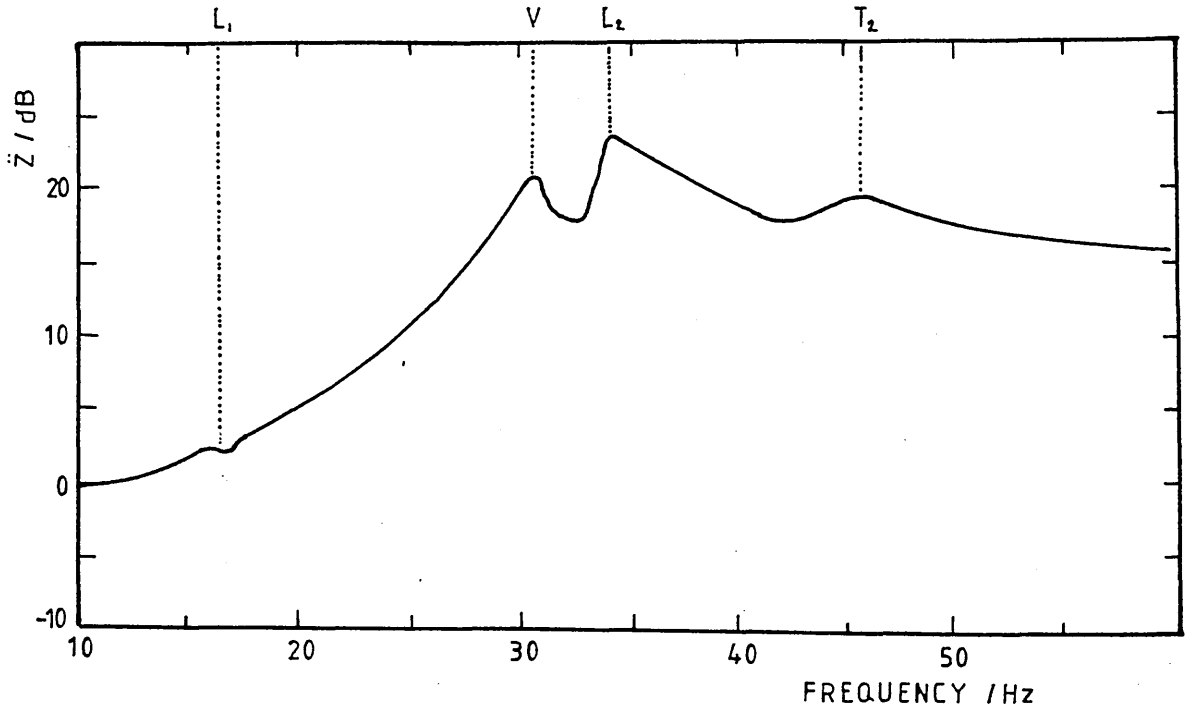

FIGURE 5.26

Acceleration, $\ddot{Z}$, of the Isolated Mass in the Direction of Excitation as a Function of Frequency at a Constant Excitation Amplitude of 0.5mm.

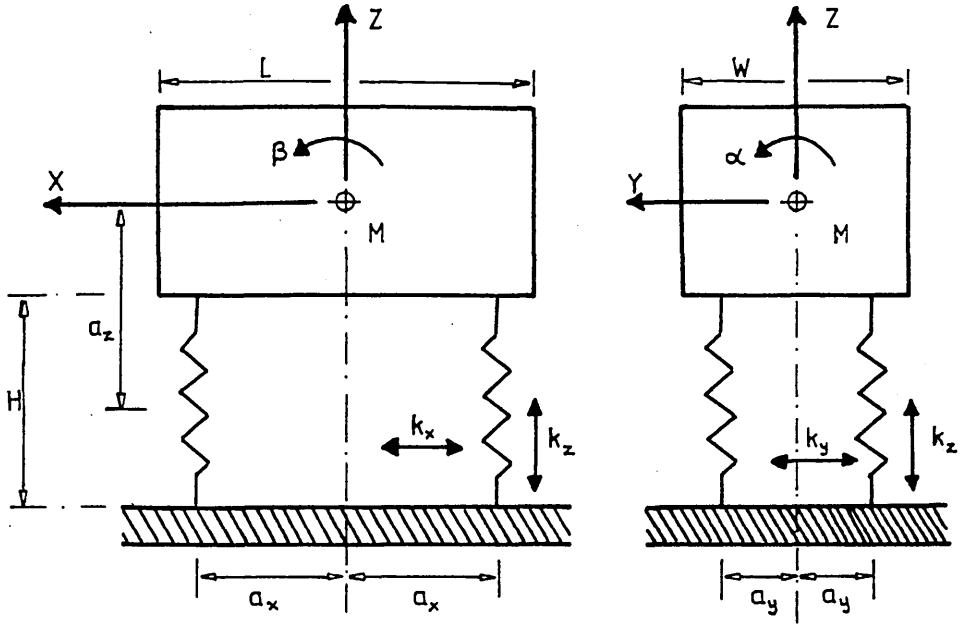

FIGURE 5.27

Equivalent Model of a Distributed Viscoelastic Isolator Using the Procedure of Hilyard [140], With Lumped Parameter Isolators Having Transverse and Vertical Stiffness.

direction has natural frequencies, $\omega_{x\beta}$, given by the relationship [122]

$$\frac{\omega_{\alpha\beta}}{\omega_z} = \frac{a_x}{\sqrt{2}\,\nu_y}\sqrt{\kappa\left(\frac{\nu_y}{a_x}\right)^2\left[1+\frac{a^2 z}{\nu_y^2}\right] + 1 \pm \sqrt{\left\{\kappa\left(\frac{\nu_y}{a_x}\right)^2\left[1+\frac{a^2 z}{\nu_y^2}\right]+1\right\}^2 - 4\kappa\left(\frac{\nu_y}{a_x}\right)^2}}$$

5.24

where

$$\nu_x = \sqrt{I_x/M}$$

$$\nu_y = \sqrt{I_y/M}$$

$$\kappa = k_x/k_z$$

where ω_z is the natural frequency of the system in the vertical, z, direction. A similar relationship to equation 5.24 holds for coupled oscillation in the y-α directions. Equation 5.24 predicts two frequencies at which coupled motion in these directions, will occur. Using values for the stiffness of the foam, measured as described in section 4.1, these frequencies have been calculated for the isolating system under consideration. The results are given in table 5.3, together with the values measured from figure 5.26.

It can be seen from table 5.3, that the agreement between the measured frequencies of coupled motion, and the predictions of equation 5.24 is good. In this case the lower transverse coupled mode, T_1, was below the lowest frequency used in the experiment, ie $T_1 < 10$ Hz.

Due to the non-linear nature of the mechanical properties exhibited by flexible cellular foams, the

TABLE 5.3 Comparison Between the Natural Frequencies of Coupled Modes of Vibration, Measured for a Foam Isolator and Predicted by Equation 5.25

MODE	MEASURED /Hz	PREDICTED /Hz	OBSERVED DIRECTION OF MOTION
V_1	30.6	30.7	VERTICAL
L_1	16.5	16.6	LONGITUDINAL
L_2	34.5	33.2	TRANSVERSE
T_1	-	9.2	-
T_2	45.1	46.2	TRANSVERSE

transmissibility of the system changed as the level of excitation increased. Figure 5.28 shows the transmissibility for four different levels of input acceleration. As the measurements for each curve were made at constant acceleration, the amplitude of the dynamic deformation decreases as the frequency is increased. It can be seen that the frequencies at which the resonances occur decreases as the level of the excitation increases. In addition the level of the transmissibility at the resonances decreased with increasing excitation amplitude. These observations indicate that the foam isolator is a strain softening system with increasing damping. This is in qualitative agreement with the results of work done in other areas of the present investigation (section 4.1) and that reported by other workers [120].

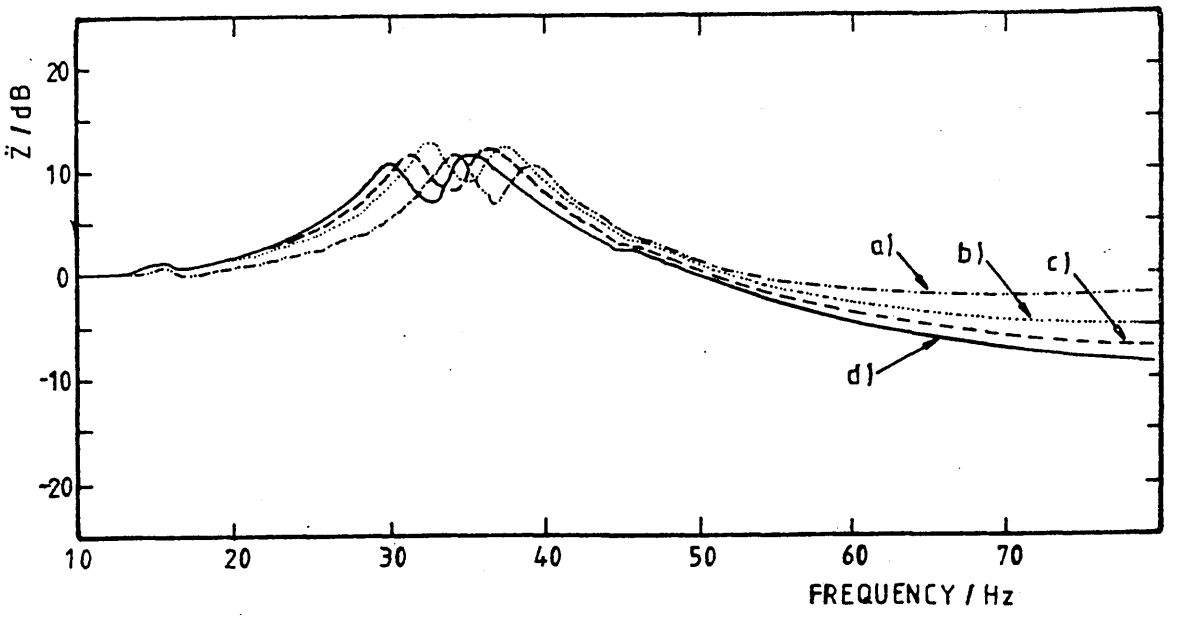

FIGURE 5.28

Transmissibility of the Isolator System As a Function of Frequency for Four Different Constant Acceleration Amplitudes of 0.25g, 0.5g, 0.75g and 1.0g.

The behaviour of the system of figure 5.22 at high excitations did not follow that described above. This is illustrated, for a particular excitation frequency of 50 Hz, in figures 5.29-5.31. Figure 5.29 shows the power spectra of the acceleration of the isolated mass, $\ddot{Z}$, and the phase plane trajectories ($\dot{Z}$-Z) at three different levels of excitation. The origional photographs of the phase plane plots at different levels of excitation are included in figure 5.30. The relative levels of the the peaks in the power spectra are shown in figure 5.31 as a function of the excitation amplitude. The development of the complex motion observed is noted below.

At low excitation amplitudes (<0.5mm) the phase plane trajectory followed a simple limit cycle and the power spectrum contained a single peak. As the excitation was

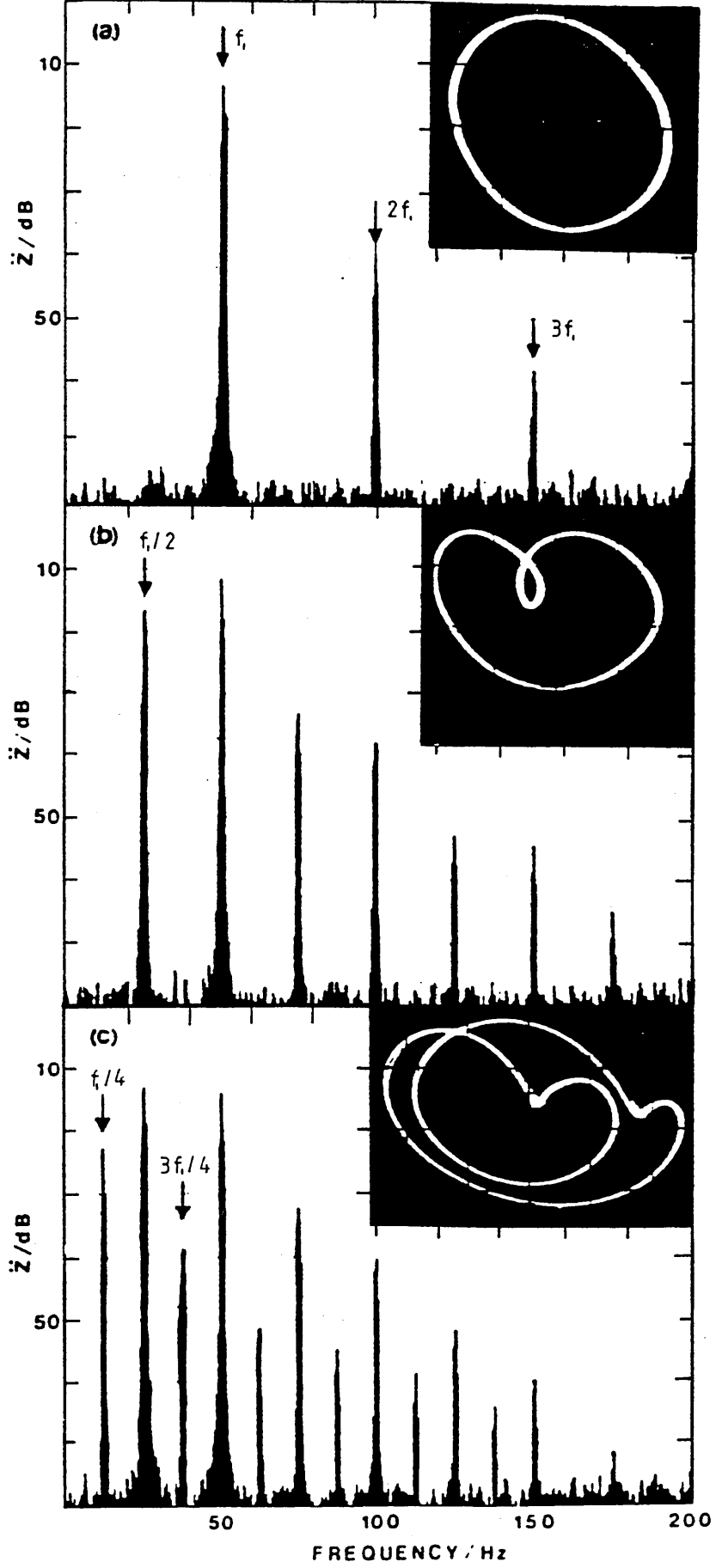

FIGURE 5.29

Power Spectra and Phase Plane Plots Measured for a Cellular Foam Isolator at an Excitation Frequency of 50 Hz and Amplitudes of a) 1.5mm, b) 2.5mm and c) 3.26mm.

FIGURE 5-30

The Origional Phase Plane Trajectory Photographs for Figure 5*29 At Excitation Amplitudes of a) 1.5mm, b) 2.5mm c) 3»26mm and d) 5»4mm.

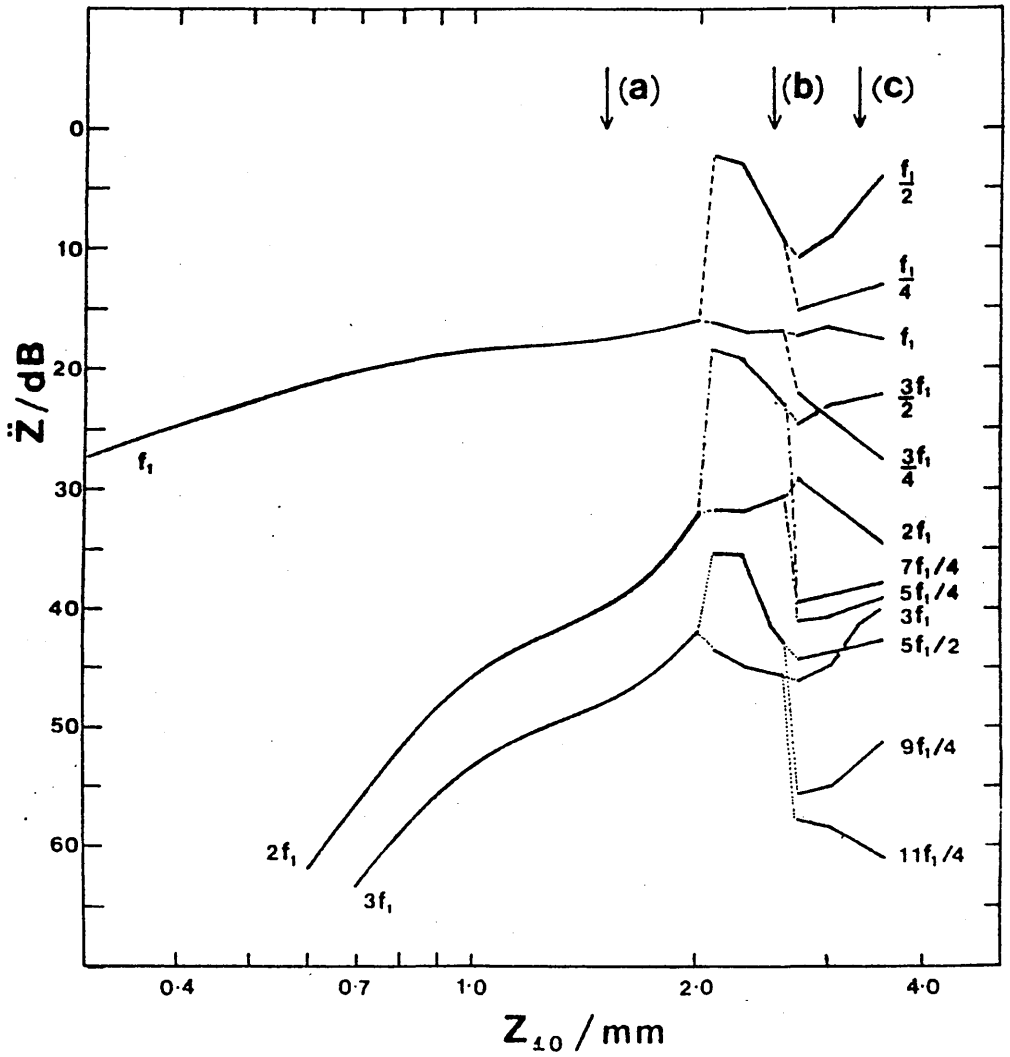

FIGURE 5.31

Relative Levels of the Peaks in the Power Spectra at an Excitation Frequency of 50 Hz as a Function of the Excitation Amplitude.

increased superharmonics appeared in the spectrun (figure 5.29a). At a critical excitation amplitude of about 2.0mm a period doubling bifurcation occured with the appearence of subharmonics of the excitation frequency and the superharmonics. These bifurcations occured at the same time for all frequencies and over a very small range of excitation amplitudes. At this point the phase plane trajectory became a "pretzel" (figure 5.29b), as

described by Cvitanovic [125]. A second period doubling bifurcation was noted when the level of excitation exceeded an amplitude of 2.8mm, leading to fine splitting of the phase plane trajectory (figure 5.29c). At higher excitation amplitudes a cascade of bifurcations occured leading to multiple fine splitting of the phase plane trajectory and a multitude of subharmonics. The shape of the phase plane trajectory in this case is shown in figure 5.30d.

Figure 5.32 shows a similar experiment for the same mass-isolator system at a frequency of 29 Hz. This frequency is close to the resonance frequency of the system in the vertical direction. In this case the bifurcation cascade did not follow the simple period doubling observed previously. Instead the bifurcation produced splits into odd multiples of the excitation frequency, eg 3,6,9,12 and 17. Figure 5.32b shows the example of a 6 cycle spectrum. This behaviour has been observed in other experimental systems [141]. For the measurements made previously the base noise level remained essentially constant. However at very high excitation amplitudes (> 4.0mm) a cascade of bifurcations was noted, culminating in a broad band spectrum (figure 5.32c). It was found that the chaotic state as indicated by the broad band spectrum, appeared to be made up of a multitude of separate frequency peaks and could only be generated around the primary resonance of the isolator in the vertical direction. This is probably due to the

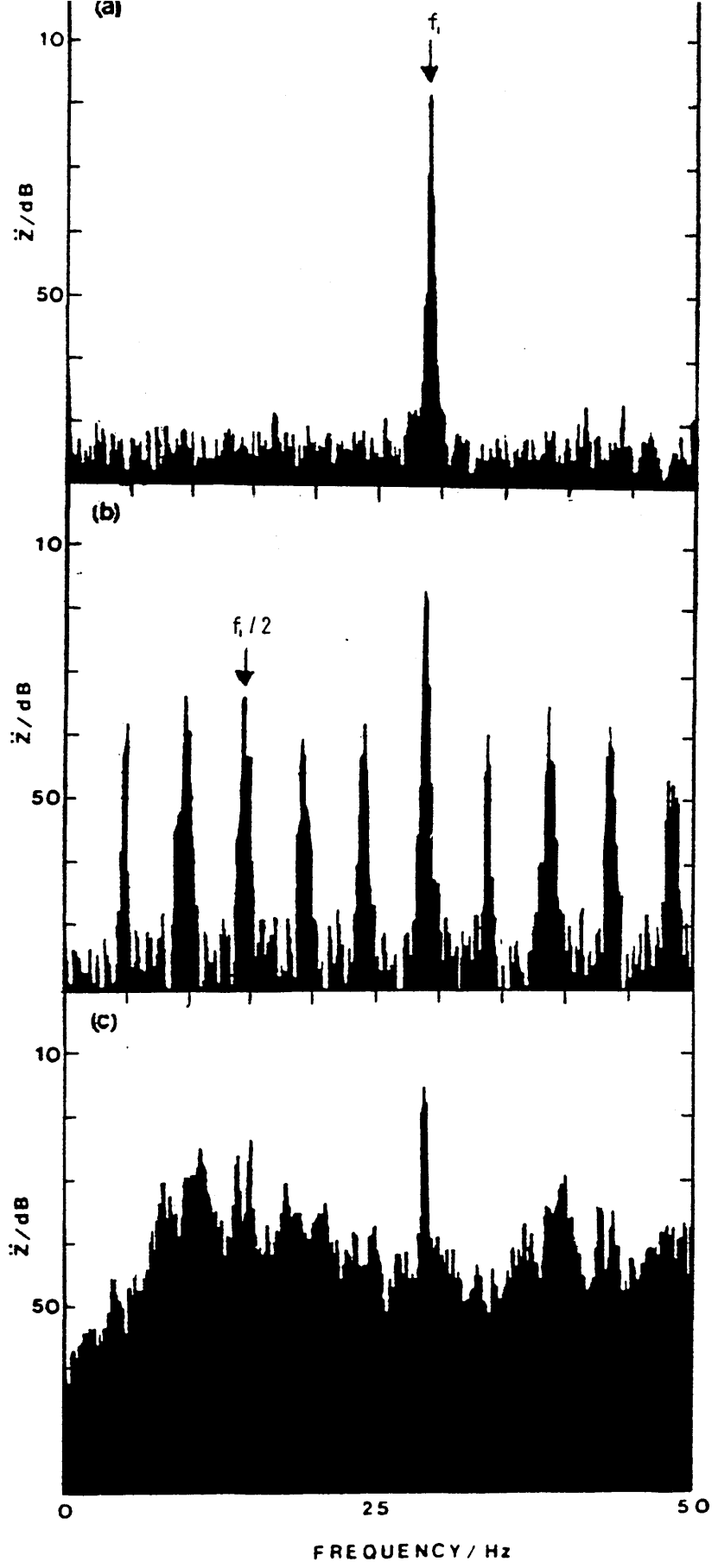

FIGURE 5.32

Power Spectra for the Same System as Used in Figures 5.29-5.31 at an Excitation Frequency of 29 Hz and Amplitudes of a) 0.25mm, b) 3.0mm and c) 5.0mm.

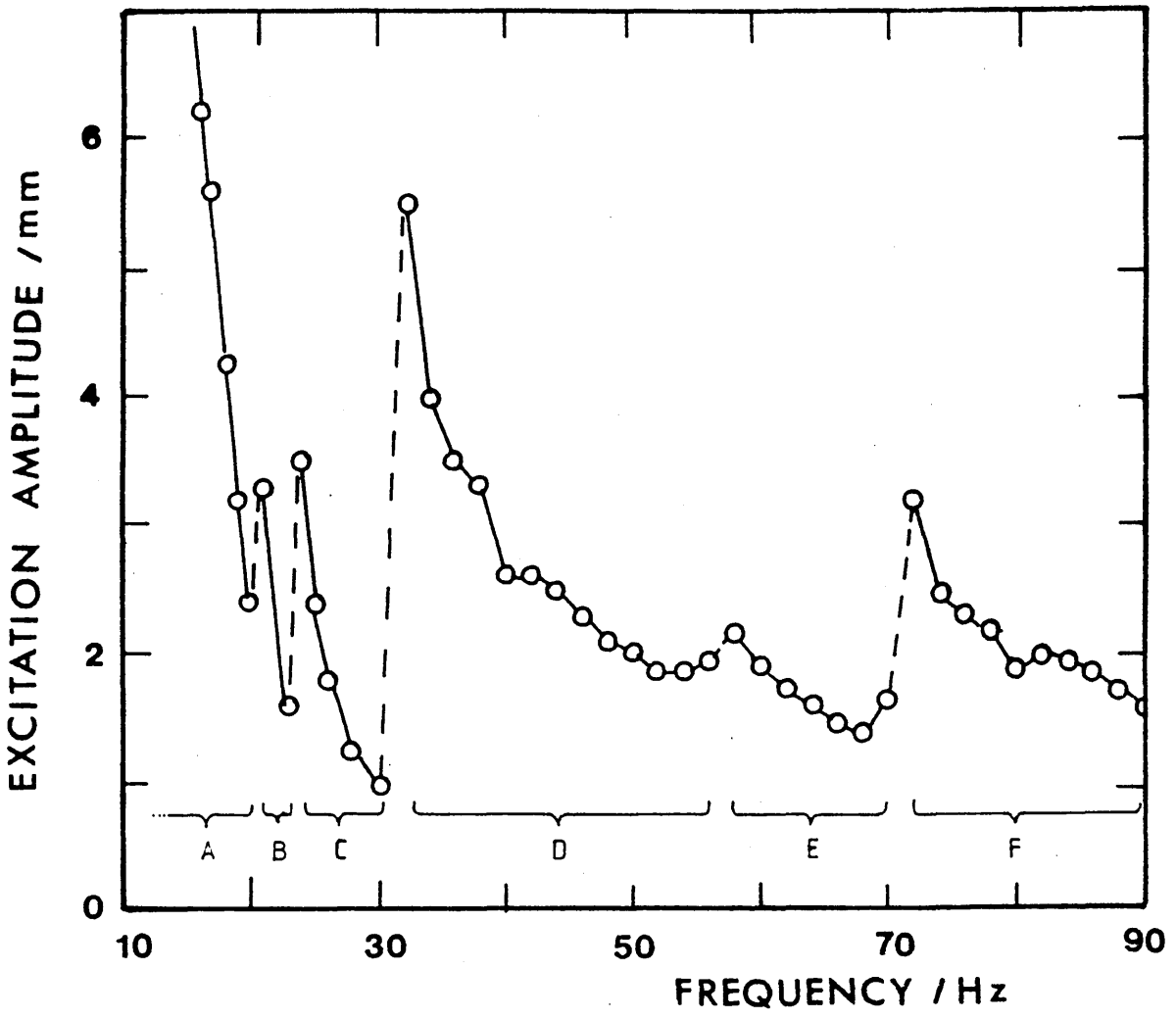

FIGURE 5.33
Minimum Excitation Amplitude Required to Produce the First Stable Period Doubling Bifurcation as a Function of Frequency.

vibration amplification of the system in this area. At resonance the relative deformation of the isolator is larger than other sectors in the frequency range.

The excitation level required to generate the first period doubling bifurcation was also found to depend on the frequency of excitation. The minimum excitation amplitude required to produce the first stable bifurcation is shown in figure 5.33 as a function of the

excitation frequency. The foam isolator in this case had a different stiffness to that of the data in figures 5.29-5.31, but had similar dimensions and the value of the mass was the same. The vertical resonant frequency at low excitations was at 38 Hz, but decreased as the level of the excitation increased.

The onset of the first period doubling bifurcation was associated with motion in different directions at different frequencies throughout the range. These are summarised in table 5.4. The behaviour in the region marked B on figure 5.33 is notable. In this region two modes of oscillation were generated, transverse shear (y direction) and longitudinal rocking (β direction). These two modes of vibration did not co-exist. Rather the system repeatedly moved from one mode to the other with a time period which was long (several seconds) compared to the frequency of excitation. The position and level of the peaks in the frequency spectrum for this motion appeared to be independent of the mode of oscillation. In the region marked D on figure 5.33 the motion took the form of a rocking motion about one end of the test piece. As the frequency was increased the axis of the vibration moved towards the centre of the isolator. This behaviour could be caused by the combination of oscillations in the z and β directions. However if this were the case the relative amplitudes and phases of the two modes of vibration would have to be matched very accurately in order to generate the observed behaviour.

TABLE 5.4 Summary of the Motion of the Isolated Mass Associated with the First Bifurcation in Different Areas of the Frequency Range

LABEL (FIGURE 5.30)	FREQUENCY RANGE /Hz	MOTION OF ISOLATED MASS
A	14 - 20	TRANSVERSE SHEAR
B	21 - 23	TRANSVERSE SHEAR AND LONGITUDINAL ROCKING
C	24 - 30	TORSION
D	32 - 56	LONGITUDUINAL ROCKING AND VERTICAL
E	58 - 70	LONGITUDINAL ROCKING
F	72 - 94	TRANSVERSE ROCKING

It is thought that if the excitation frequency is close to a resonance frequency in one of the six modes of vibration, then the system will undergo the first period doubling bifurcation at a lower excitation amplitude and oscillate in this direction. The mechanism which produces this behaviour is not known.

Attempts have been made to analyse the onset of chaotic motion by a calculation of the Feigenbaum constants μ and δ [142]. However this has met with little success. The main difficulty was that only the first two period doubling bifurcations have been observed regularly, although the third bifurcation (to an 8 cycle plot) was detected at particular frequencies. Feigenbaum states that the universal values of μ and δ only apply when a

large number of bifurcations have taken place. The previous experimental determinations which have met this constraint [125] have produced values of μ and δ which are close to those predicted by Fiegenbaum [142]. In addition it was found that the subharmonics were heavily modulated by some mechanism as yet unknown and that this modulation was different for different excitation frequencies.

As an attempt to simulate the behaviour exhibited by the isolating foam system of figure 5.22, computer simulation experiments were set up. Several models given in the literature have been considered, including the Duffing equation [143] and the forced Van der Pol equation [144]. The forced Van der Pol equation takes the form

$$\ddot{Z} + c\,\dot{Z}(Z^2 - 1) + Z = F k \cos(\omega t) \qquad 5.25$$

For $0 < F < 2/3$ the solution of equation 5.25 has a countable set of complicated unstable periodic solutions and an uncountable set of unstable, aperiodic but quasi-recurrent solutions. The Duffing equation takes the form

$$\ddot{Z} - Z + Z^3 = k(F\cos(\omega t) - c\dot{Z}) \qquad 5.26$$

where k is a small scaling (pertubation) parameter and c represents the damping. However the characteristics of the foam isolator and the observed behaviour did not conform to the behaviour of these equations. Instead a modification has been made to the bilinear stiffness

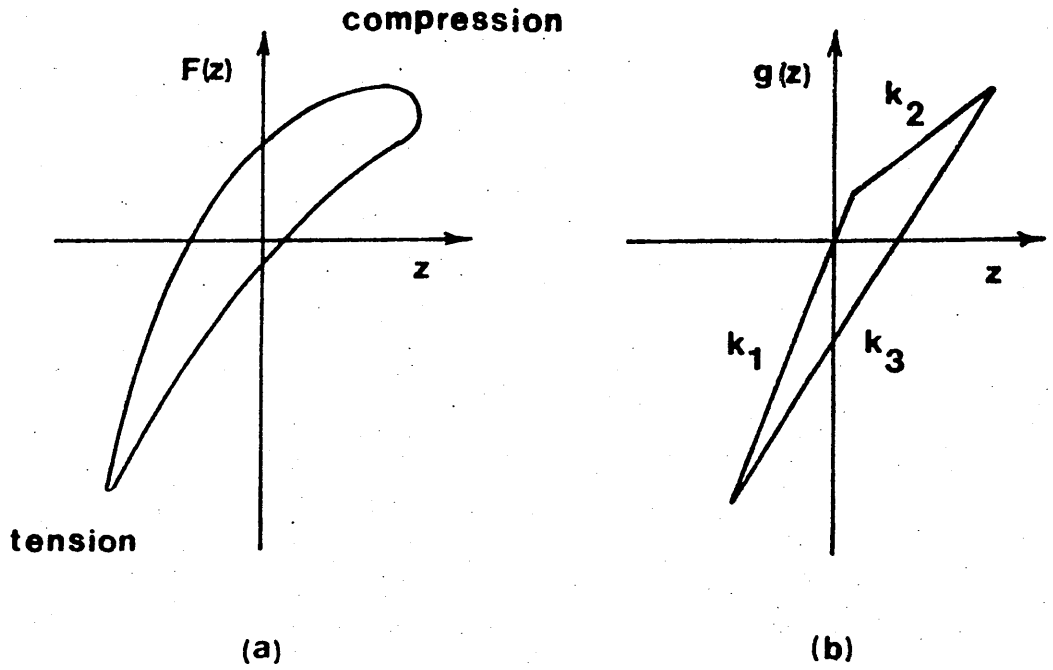

FIGURE 5.34
a) Measured Dynamic Force-Deformation Curve for A Cellular Material at Large Excitations. b) Piecewise Linear Stiffness Model Used in the Computer Simulation Model.

equation of Thompson and Elvey [145]. The basic equation is

$$M\ddot{Z} + c\dot{Z} + g(Z) = F\sin(\omega t) \qquad 5.27$$

where ω is the excitation frequency and the restoring function $g(Z)$ is piecewise linear. A schematic representation of a measured force deformation diagram for a flexible cellular foam is shown in figure 5.34a. This has been modelled using the arrangement in figure 5.34b. As a first approximation the stiffnesses k_1, k_2, k_3 used in the model have been assumed to be constant. In practice the force deformation curve of figure 5.34a will change as the amplitude of the excitation increases.

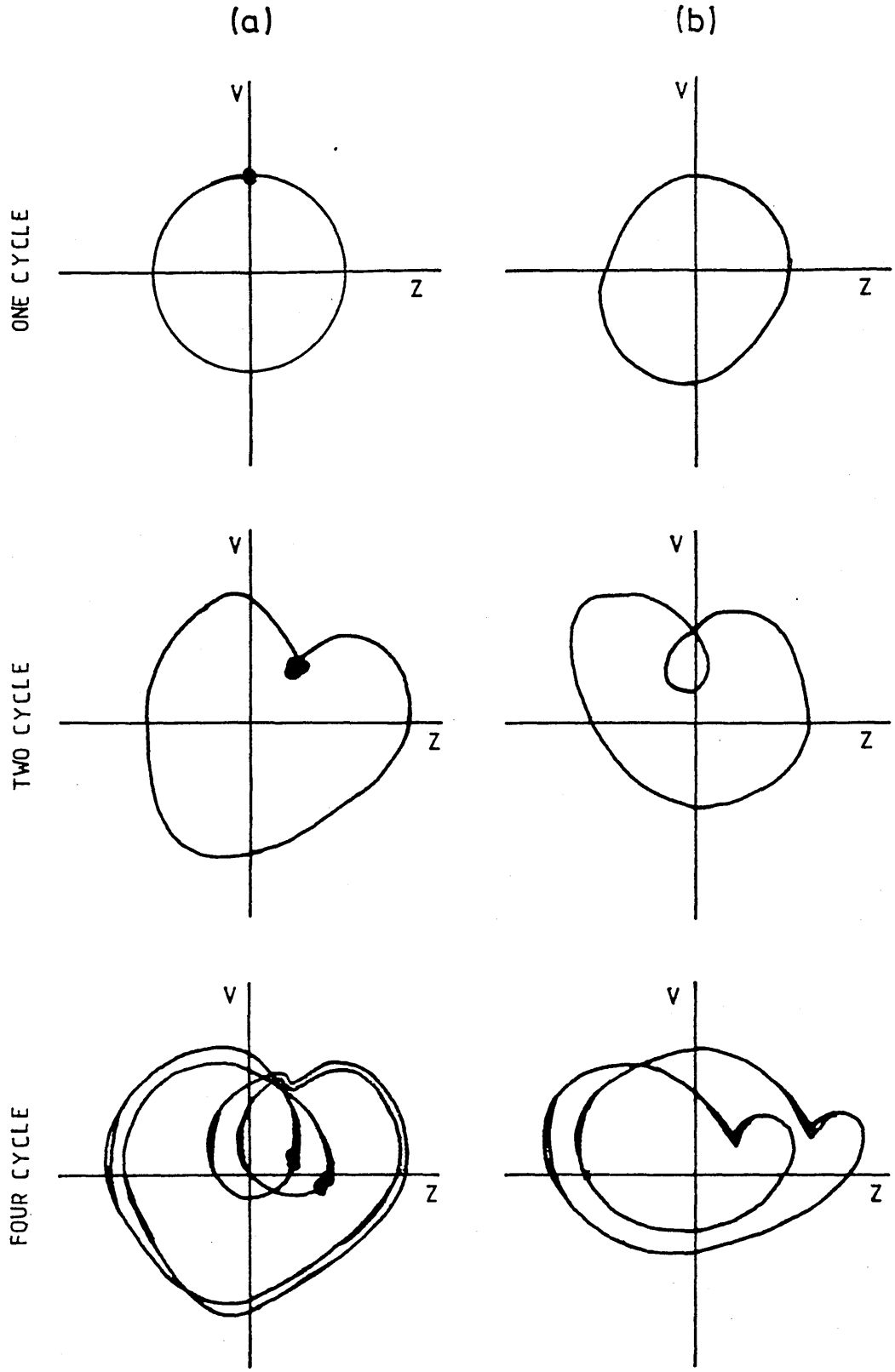

FIGURE 5.35
Phase Plane Trajectories for the First two Period Doubling Bifurcations a) Predicted by the Model of Equation 5.27 and b) Measured for a Flexible Cellular Foam Isolator at 50 Hz. The Model Parameters do not Correspond to the Mechanical Properties of the Isolator.

The model represented in figure 5.34b has been used together with equation 5.27 to reproduce the first three bifurcations observed with the foam isolator. The predicted phase plane plots are qualitatively similar to those shown in figure 5.30. In figure 3.35 the phase plane trajectories generated using the above model are compared to some real trajectories measured for the isolator system. However the values of the parameters in equation 5.27 required to produce these trajectories bear little relation to the material properties of the foams in use. The small circles on the phase plane plots generated by the model in figure 5.35 are the Poincare points [145]. The computer draws one of these points at the end of a time equal to the period of the excitation frequency. The number of circles on the phase plane plot enabled the periodicity of the resulting motion to be found. Even though there is only qualitative agreement between the model predictions and the measured phase plane trajectories, it is encouraging that these bifurcations have been generated by increasing the amplitude of the forcing function, F. This is equivalent to raising the amplitude of the dynamic excitation in the real isolator-mass system.

6. CONCLUSIONS

The vibration isolating behaviour of cushion foams depends on a number of interacting factors, eg dynamic stiffness, viscoelastic damping, hysteresis, fluidic (or pneumatic) damping and so on. The processes are governed by certain physical parameters characteristic of the material and the conditions of use, eg permeability, elastic modulus and critical buckling strain which themselves are related to the composition of the matrix polymer, the cellular structure and the static pre-compression. In this investigation a systematic study has been made of the some of the most important factors relevant to the performance of these materials in transportation situations. The conclusions arrived at are summarised below.

6.1 Air-Flow Properties of Cellular Plastics

The pressure gradient required to maintain fluid flow in a wide range of conventional and high-resiliency polyurethane (PU) foam test pieces has been found to follow the two term flow equation of Gent and Rusch [28].

$$\frac{dP}{dx} = \frac{\eta u}{K} + \frac{\rho}{B} u^2 \qquad 6.1$$

where η and ρ are the viscosity and density of the fluid in use and u is the velocity of flow. This equation has been found to hold when the sample is subject to a compressive deformation normal to the direction of flow. It has been found that the model presented by Gent and

Rusch, based on flow through arrays of pipes, did not produce the correct strain dependence of the parameters K and B. It was therefore necessary to develop a new model to relate K and B to cellular structure. This model, based on Newtonian fluid flow through a packed bed, is outlined in chapter 3 and predicts that the coefficients K and B are given by

$$K = \xi(1- \phi_o)d^2/180 \qquad 6.2$$

$$B = \xi(1- \phi_o)^2 d/(3C_f\tau^3) \qquad 6.3$$

where d is the average diameter of the cells forming the matrix and ϕ_o is the volume fraction of polymer. Values of K measured according to BS 4443 have been found to fit the relationship of equation 6.2 well. It has been shown that the dominant influence on K is the gross dimensions of the cells forming the matrix. Foams with different cellular structures have been found to fit the relationship of equation 6.2 equally well.

The flow resistance coefficient, B, in the second term of equation 6.1 has been found to be much more dependent upon the detailed structure of the cellular matrix. This dependence is contained in the friction coefficient, C_f. Unfortunately it has not been possible in the present project to relate the friction coefficient directly to the specific cell structure in the foam.

The model developed to describe the air flow properties of cellular materials has been used to predict the

variation of the K and B values with an imposed pre-compression normal to the direction of flow. The model predicts the variations with pre-strain to be of the form

$$\frac{K(e)}{K(o)} = \left\{\frac{(1 - e) - \phi_0}{(1 - e)(1 - \phi_0)}\right\}^3 (1 - e)^2 \qquad 6.4$$

$$\frac{B(e)}{B(o)} = \left\{\frac{(1 - e) - \phi_0}{(1 - e)(1 - \phi_0)}\right\}^3 (1 - e) \qquad 6.5$$

where e is the fractional compressive pre-strain. K(o) and B(o) are the values of K and B at zero pre-strain. The measured data for a wide range of PU foams in the strain range 0-60% have been found to give good agreement with the predictions of equations 6.4 and 6.5, unlike the models of earlier investigators, based on flow through arrays of pipes, which failed to correctly predict the strain dependence of K and B.

A series of high-resiliency PU foams containing different amounts of a vibration control (VC) additive have been tested. The manufacturers claimed that this additive could control the vibration isolation characteristics of cushion foams by influencing the energy absorption process due to fluid flow, outlined in section 4.2. The additive was claimed to influence the fluid flow properties of the material by changing the cell size. This claim has been found to be false for the series of foams tested. In fact the reduction in the K and B values as the amount of VC additive is increased appears to be caused by the introduction of thin membranes between adjacent cells. These membranes are easily

ruptured by imposing a large compressive static deformation to the test piece. This makes the VC additive unsuitable for cushioning applications where the material is subject to large static or dynamic compressive strains, as the membranes would quickly rupture and cause degradation of the functional performance of the cushion.

Future work in this field should include a closer examination of the factors influencing the value of B. It is thought that the pores between adjacent cells will be the dominant influence rather than the average cell diameter. The work in this area will include the development of a relationship between the friction coefficient defined here and the specific geometry of the cells forming the material.

It has been suggested elsewhere [49] that the performance of a cellular plastic vibration isolator might be improved by incorporating a non-Newtonian fluid, specifically a shear-thinning liquid, within the matrix. As no analysis of non-Newtonian flow in these materials had been reported previously it was necessary to undertake such an investigation and this is recorded in section 3.1.4 for a power-law fluid. It was found that only the first term of the flow equation need be modified for fluids of this type. For this case the two term flow equation takes the form

$$\frac{dP}{dx} = \frac{\mu}{K(n)} u^n + \frac{\rho}{B} u^2 \qquad 6.6$$

where μ is the zero strain viscosity and n is the fluid index. The permeability of the matrix in this case becomes a function of the fluid in use. This non-Newtonian permeability, K(n), is given by

$$\frac{K(n)}{K} = \left[\frac{(1 + 3n)}{n}\right]\left\{\frac{\xi(1 - \phi_0)d}{6\tau}\right\}^{n-1} \qquad 6.7$$

where K is the Newtonian permeability of equation 6.2. This expression has not been tested directly but is incorporated into a model for fluid flow damping which is discussed below. When n becomes unity the fluid becomes Newtonian and equation 6.6 reduces to equation 6.1

6.2 The Effects of Compressive Pre-Strain on Dynamic Properties

When used in vehicle seat cushions the cellular material is subject to static (or quiescent) pre-compressions so that the variation of the small strain dynamic modulus and loss tangent with pre-strain is of interest. This has been measured for a number of conventional and high-resilieny foam test-pieces. The dynamic properties have been found to be very different to those inferred from quasi-static stress-strain curves.

A strain dependent shape function has been defined to characterise the dynamic modulus. This shape function was defined in a similar manner to the Rusch shape function

[54] for quasi-static behaviour and took the form

$$\Xi(e) = r\, e^{-v} + s\, e^{w} \qquad 6.8$$

where r, s, v and w are empirical curve fitting constants and e is the static pre-strain. The relationship between the coefficients of equation 6.8 and those of the Rusch shape function has been investigated. Little correspondence has been found between the two. It has been found that when under a static deformation the dynamic modulus is related to the gradient of the unloading part of the F-D curve at the point where the strain cycle changes from loading to unloading. Correspondence between the dynamic modulus and the unloading gradient is good. That is, in structural terms, the dynamic modulus is governed by the recovery of the buckled cell struts. This observation is worthy of further study.

At low pre-strains the viscoelastic damping exhibited by conventional foam test-pieces is higher than for high-resiliency foams. As the level of pre-compression is incresed the damping of the high-resiliency samples increases dramatically to be comparable in size to the conventional samples. No explanation has been found for this behaviour. At high pre-strains the damping for both types of foam increases. This has been attributed to the interaction between adjacent buckled cell walls, the strain at which this occurs being approximately the same as the strain at which inter-cellular interactions become

apparent in the static F-D curve.

As the level of pre-strain changes the frequency dependence of the loss tangent also changes. This has not been reported previously and the cause of the behaviour is not known. The dependence is small and it is thought that this phenomenon would not seriously influence the vibration transmissibility of a cushion.

In cushion foams several mechanisms give rise to energy disipation under dynamic compression. These mechanisms are mentioned in Chapter 1. One of these, fluid flow damping has been the subject of interest recently as a means of improving the vibration isolation characteristics of vehicle cushion materials. this process operates at all levels of pre-strain and over a relatively small frequency range. By designing the foam-fluid combination in such a way that the damping maximum of the material occurs close to the resonance frequency of the isolator system it has been hoped that the transmissibility of the system would be reduced at resonance. The theory of fluid flow damping was developed some time ago by Gent and Rusch [28,74], but was restricted to Newtonian fluids in foams subject to small static and dynamic deformations. In order to obtain a better understanding of how this process operates in real applications, an investigation has been undertaken to study the effects of pre-compression on the fluid flow process. The theoretical treatment has been

extended further to allow for the incorporation of incompressible non-Newtonian fluids. The resulting equations for the storage modulus and loss tangent of the material have been found to take the form

$$E'(\omega) = \frac{E'_m \{1 + \beta(1 + \beta)\gamma^2\}}{1 + \beta^2\gamma^2} \qquad 6.9$$

$$d(\omega) = \frac{d_m\{1 + \beta^2\gamma^2\} + \gamma}{1 + \beta(1 + \beta)\gamma^2} \qquad 6.10$$

where

$$\beta = 3(E'_m/E_t)(H/W)^2$$

$$\gamma = \frac{\mu\varepsilon_0{}^{n-1}\omega^n}{(n+2)K(n,\omega)E'_m}\left(\frac{W}{2}\right)^{n+1}$$

These are the same as the Gent-Rusch equations except for the parameter γ, which includes the non-Newtonian permeability of equation 6.7 (through $K(n,\omega)$) and a strain amplitude term. The frequency dependence of γ also becomes a function of the fluid index, n.

The effect of fluid flow on the dynamic mechanical properties of cellular plastics has been measured for a number of foam test pieces incorporating both Newtonian and non-Newtonian fluids. The variation of the storage modulus and damping with frequency for the two fluid types has been found to have a similar shape, while the specific frequency dependence is different.

The measured values of $E'(\omega)$ and $d(\omega)$ have been fitted to equations 6.9 and 6.10, using a fitting technique which is superior to those used by previous workers. The

fitting technique based on a non-linear least squares search method made no a priori assumptions about the frequency dependence of the parameter γ and used measured data from the whole of the frequency range of interest. The previous treatment used by Gent and Rusch [39] relied on a few data points at very low frequencies, and around the damping maximum.

The frequency dependence of γ, measured for several foam-fluid combinations, has been found to give reasonable quantitative agreement to the theoretical predictions. For two foam types filled with a 0.5% solution of CMC the exponent n was found to be in the range 0.53-0.69. This compares with the fluid index of the solution which was found to be 0.55. The best correspondence between experiment and theory was found at relatively low levels of pre-strain (<10%). Here the range of measured frequency exponents was 0.53-0.58. At higher pre-compressions the measured values were higher. This has been attributed to the effective neglect of inertial flow in the treatment. For foam test pieces filled with water the parameter γ was found to be directly proportional to the frequency. As expected the use of a shear-thinning fluid broadens the observed damping peak. However the difference between the damping peaks for Newtonian and shear-thinning fluids, as shown in figure 6.1, is small and it is thought that the incorporation of shear-thinning fluids will have a relatively minor effect on the vibration isolation characteristics of cellular

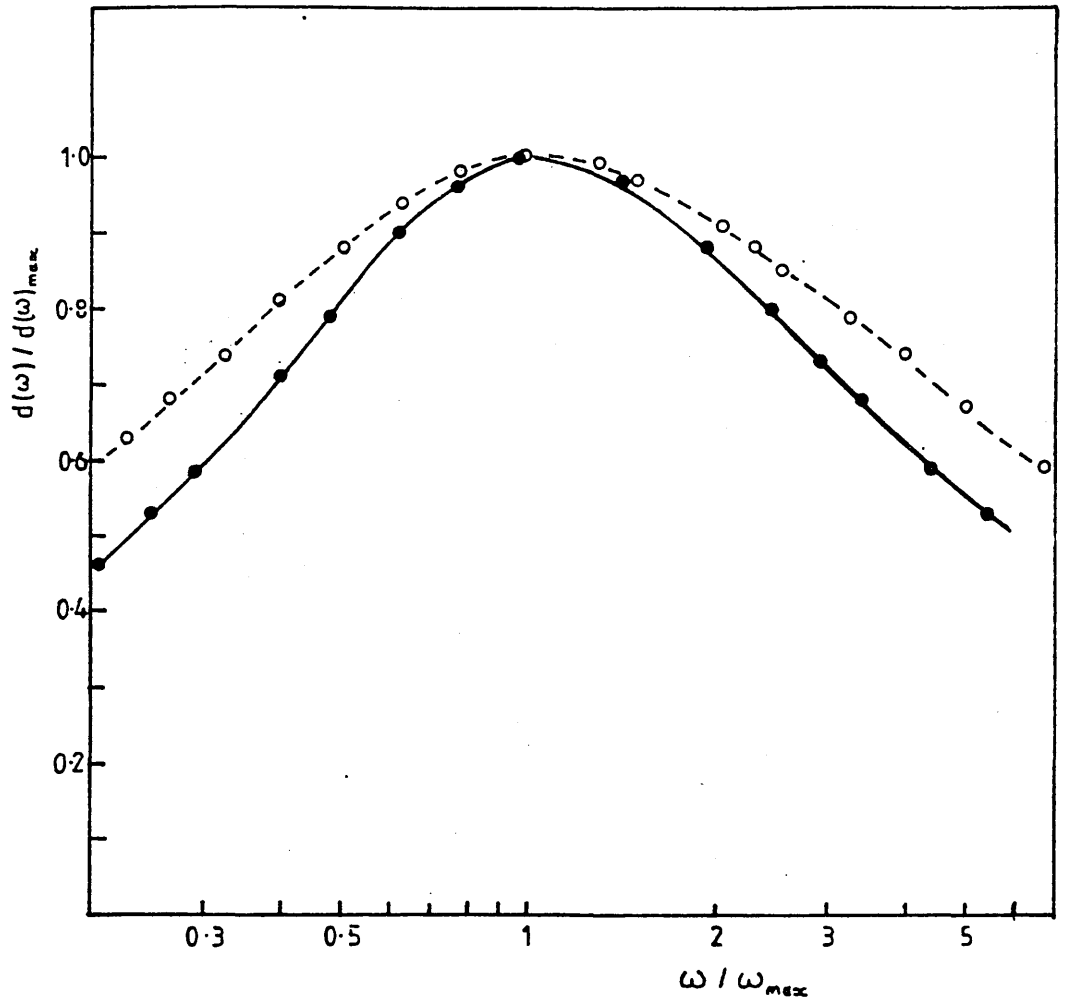

FIGURE 6.1
The Variation of $d(\omega)$ with Frequency Around the Damping Maximum. Closed Circles; Newtonian Fluid Filled System. Open Circles; Foam Filled with a Shear-Thinning Fluid.

cushion materials exhibiting fluid flow damping.

It has been established in this work that the frequency dependence of the damping resulting from fluid flow is different for Newtonian and shear-thinning fluids. However it will be necessary to test the model predictions with a wider range of non-Newtonian fluids before the conclusions of the theoretical treatment can be accepted. From the work already done it is obvious

that while the model developed provides a good first approximation to the behaviour, more involved theoretical treatments will be necessary to completely explain the observed fluid flow damping process. It is expected that this work will include the inertial flow loss term of the flow equation, characterised by the coefficient B, and the frequency dependence of the matrix modulus and damping.

One failing of the non-Newtonian analysis is that the matrix damping, d_m, obtained by fitting measured data to the model was lower than expected. The modulus of the foam, however, found using the same technique has been found to follow a similar dependence on the level of pre-strain as has been measured in the absence of fluid flow effects.

The effective permeability of the foam has been calculated from the observed data of the fluid flow process. The resulting values compare well with those inferred from the air flow properties of the test pieces.

The strain dependence of the parameters β and (through θ) γ have been investigated. γ has been found to be approximately proportional to $e^{1.2}$. This is a much simpler dependence than would have been expected from an examination of the strain dependence of the parameters in the equation governing the value of γ. The strain dependence of β is more complex than expected. This is

thought to be due to changes in the ratio of the transverse modulus to the compressive modulus as the level of compressive pre-strain increases.

Future work in this area should include measurements on foam samples having different cell structure and geometry with a wider range of non-Newtonian fluids. Extensions to the treatment may be required, especially at high levels of pre-strain, to reduce the discrepancies noted between experiment and theory. An analysis of the strain dependence of the tensile modulus normal to the direction of compression is desirable in order to explain the observed changes in the parameter β as the level of pre-strain increases.

6.3 The Behaviour of Non-Linear Vibration Isolators

The vibration isolation characteristics of non-linear flexible cushion foams have been studied under small and large dynamic strain amplitude conditions. Under small strain amplitude conditions, the properties of the material behave in the way described in section 4.1. For high excitation amplitudes the properties become highly non-linear and the resulting response is complex.

In the case of small amplitude excitations the application of vehicle seating has been studied, with a view to investigating the effect of cushion properties, ie stiffness and damping, on the response of the vehicle cushion to dynamic excitation. In order to do this it

has been necessary to develop a multi-degree of freedom model of the person-seat system. Previous workers have used single-degree of freedom (1-DOF) models but these have proved to be inadequate for a realistic description of the dynamic interaction between the person and the cushion.

The multi-DOF model is presented in section 5.1.2 and behaviour predicted by the model is compared with responses of vehicle seats measured in the field by other workers. The correlation between predicted and measured transmissibility curves is good. In one case, however, the agreement was not so good. This was for the response of the seat cushion in a JCB earth moving vehicle. In this case the acceleration levels experienced by the operator were high and it is postulated that under the conditions found in off-road vehicles, such as this, the assumption of small strain amplitude conditions would not hold. Under these conditions the cushion would exhibit non-linear mechanical properties.

As mentioned above, there is interest in using the fluid flow damping process as a means of improving the vibration isolation characteristics of cushion foams. The model studies carried out in this work have been extended to include the effects of fluid flow damping in the seat cushion and the resulting model used to predict the influence on dynamic ride comfort. The results predicted by the model are di sappointing in the sense

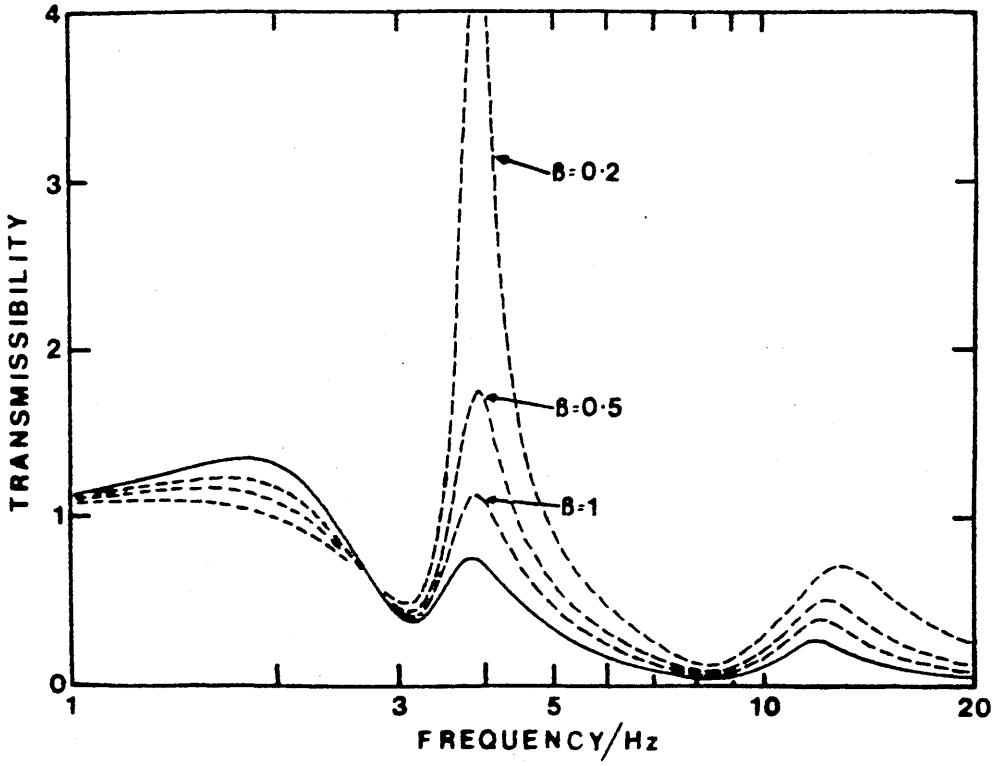

FIGURE 6.2
The Effect of Fluid Flow Damping on Cushion Transmissibility Predicted by the 3-DOF Model. Solid Line; No Fluid Flow Effect. Decreasing Values of β Equivalent to Increasing the Fluid Flow Damping.

that, while the vibration magnification is reduced in one area of the frequency range, it increases in others. This behaviour is illustrated in figure 6.2 which is a reproduction of the data presented in section 5.1.4. The parameter β controls the amount of fluid flow damping, as β decreases the maximum damping value increases. It can be seen that as the amount of fluid flow damping is increased, the transmissibility at low frequencies is decreased. However at frequencies above 3 Hz the vibration magnification of the cushion is increased dramatically. The data of figure 6.2 was predicted for a maximum damping frequency of 5 Hz. The effect of varying the frequency at which the maximum damping occurs has not

been investigated due to lack of time. It is obvious from the data of figure 6.2 that the model predicts that the dynamic ride comfort provided by the seat cushion would not be improved by the incorporation of fluid flow effects and in most cases would be seriously degraded. Since these observations are central to the use of pneumatic processes to enhance ride comfort these model studies should be carried further.

For a simple isolator system the vibration isolation characteristics are predicted to be improved by the inclusion of fluid flow effects. Another group of workers have used the VC additive described above and measured the transmissibility of the whole cushion. The experimental results of these investigators are presented in figure 6.3 together with the predicted response for an 'ideal' 1-DOF foam isolator system with fluid flow damping. It can be seen that the addition of the VC additive reduced the vibration magnification of the material from 4 (for no additive, open circles) to about 2 (for 2 pbw additive, closed circles). The solid lines show the predicted response of a 1-DOF isolator incorporating fluid flow effects. The line corresponding to $\beta = 100$ is equivalent to no fluid flow effects while the second line at $\beta = 1$ was selected to match the maximum vibration magnification of the real system with the VC additive. In each case the shape of the measured response curves are very different to those predicted by the model based on an 'ideal' isolator system. The reason for this is not known.

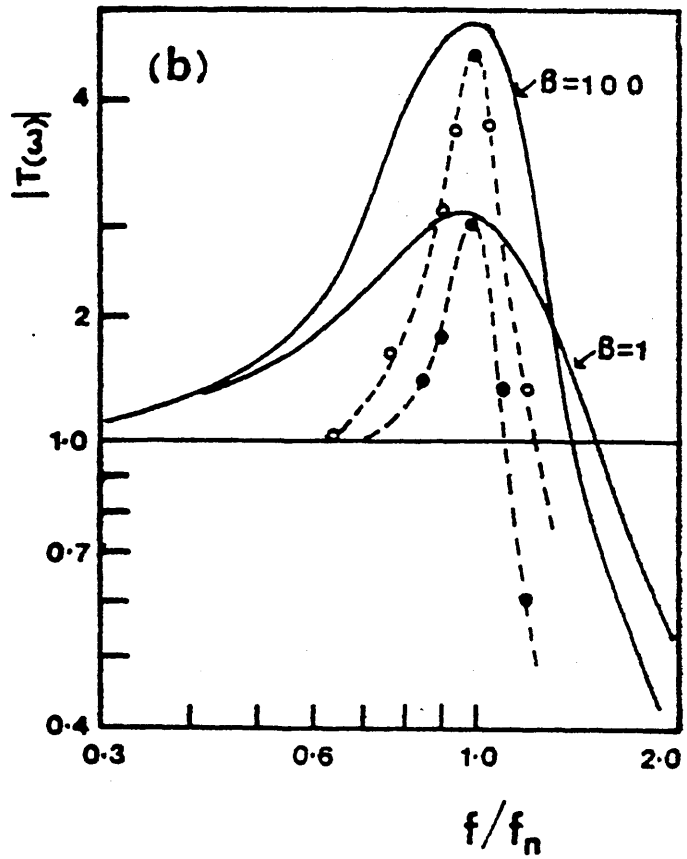

FIGURE 6.3

Broken Lines; Vibration Transmissibility of a Whole Cushion with No VC Additive (Open Circles) and 2pbw VC Additive (Closed Circles) [38]. Solid Lines; Predicted Transmissibility for an 'Ideal' 1-DOF Isolator System Incorporating Fluid Flow Processes.

It appears that while fluid flow damping is capable of improving the vibration isolation characteristics of simple 1-DOF isolator systems, with more complex situations such as the person-seat system, the dynamic interaction between the person and the cushion produces a response which may not be improved by the inclusion of fluid flow effects.

In section 5.2 the response of a distributed non-linear viscoelastic isolator to large amplitude dynamic

excitations is considered. At moderate excitations the response of the isolator, in the vertical direction,is found to be non-linear and indicative of a strain softening system with the damping a weak function of the excitation amplitude, as expected. As the level of excitation is increased motion of the isolated mass has been found to occur in any of 6 directions as shown in figure 5.22. Motion in the x and β directions and the y and α directions appeared as a coupled shear and rocking vibration while the vertical and torsional modes were uncoupled. The experimentally determined values of the frequencies at which the coupled oscillations occur are in good agreement with those predicted by the equations of Crede and Ruzicke [122] using material values taken from the work in Chapter 4 of this report.

At high levels of excitation the classical theories of vibration isolation are found to break down. This manifests itself with the appearence of subharmonics of the excitation frequency and its superharmonics. The occurence of superharmonics in the power spectrum of the response was expected but the appearence of subharmonics was not. This behaviour is qualitatively similar to the period doubling bifurcation cascade described by Cvitanovic [125] and others, and has been proposed as a possible route to chaos. However in our case only the first few period doubling bifurcations were observed. Above this point the experimental determinations on foam isolators depart from the predicted route with the

generation of odd subharmonics of the excitation frequency.

At frequencies close to the primary resonance of the system the period doubling bifurcation cascade culminates in a broad band spectrum which appeared to be made up of a multitude of discrete frequency peaks. This behaviour is characteristic of a system in the chaotic state and apparently only occurs near the primary resonance because of the vibration amplification of the system in this frequency region.

The distributed non-linear isolator system studied in this project exhibits behaviour which is in some ways similar to the transition to chaos described by mathematicians. However it has not yet been established that the observed behaviour is truly chaotic in the mathematical sense.

In the chaotic state the motion of the isolated mass is extremely complex and its mathematical description is beyond the scope of the present work. However an attempt has been made to simulate the observed behaviour using a modified bilinear stiffness model. The equation of motion of the isolated mass in the vertical direction has been described using the equation

$$M\ddot{Z} + cZ + g(Z) = F\sin(\omega t) \qquad 6.11$$

where g(Z) is piecewise linear and is shown in figure

5.34. Attempts have been made to reproduce the first few period doubling bifurcations observed with the real isolator system. This has been moderately sucessful. By increasing the excitation amplitude, F, in the model it has been possible to produce period doubling bifurcations with phase plane plots which are qualitatively similar to those observed with the real system. The parameter values required in equation 6.11 to produce this behavior bear little resemblence to the material properties of the foams in use. It is thought that renormalisation of the model may be required.

The complex motion of the isolator system at large excitations is interesting and has not been reported in the literature previously. Although the mechanical system used for this work is simple the behaviour is complex; involving a highly non-linear material, with rate dependent properties and several degrees of freedom. This situation could occur in many practical vibration isolation applications.

6.4 Future Improvements to the Spectrometer System

The dynamic mechanical spectrometer designed for use in the present work has proved to be a versatile measurement system capable of accurate measurements of the mechanical properties of flexible cellular materials under various conditions. However several improvements could be made to the spectrometer system as a whole. Many of these may be introduced with the minimum of interference to the

present system. These areas of improvement have been expanded in the user manual written for the system [2]. It is likely that areas of improvement will include:

a) The provision of a compressed air cooling system for the electromagnetic shaker. The shaker table suffers from relatively high levels of residual motion at 50 and 100 Hz caused by the cooling fan within the shakers casing. This measure will improve the accuracy of the spectrometer.

b) Replacement of the present Digital Sine Wave Interface by an intellegent digital signal generation system, enabling a single signal generation system to be used and releasing large areas of the computers memory.

c) Provision of an automatic zero-offset system. The dc component of the incom ing signal can be measured using the algorithm outlined in section 2.4. By inserting a negative voltage of this size into the zero-offset circuits via a digital to analog converter, it would be possible to dispense with the manual setting of the signal zero.

d) Improvement of the autoranging system to allow ranging down as well as ranging up the gain of the ADC input boards. Using a data scan immediately after acquisition a full scale reading of $FFF (4095), or a zero reading would indicate that the gain of the board should be reduced.

REFERENCES

1. Collier P, Care C M & Hilyard N C, J Phys E:Scientific Instruments, Accepted for publication (1985).

2. Collier P, The Microprocessor Controlled Dynamic Mechanical Spectrometer-A user Guide, Sheffield City Polytechnic (1985), Unpublished.

3. Bruel and Kjaer (UK) Ltd, Instruction Manual, Electromagnetic Exciter, type 4801.

4. Bruel and Kjaer (UK) Ltd, Instruction Manual, Power Amplifier, type 2707.

5. Bruel and Kjaer (UK) Ltd, Instruction Manual, Exciter Controller , type 1047.

6. Lucas Logic Ltd, Nascom III Mcrocomputer, User Manual.

7. Lucas Logic Ltd, Nas-Dos 1.4, Operating Manual.

8. ZilogZ80, Technical Manual: Central Processing unit.

9. Hottinger Baldwin Messtechnic GMBH, Operating Manual, Type U2 200kg Force Transducer.

10. Hottinger Baldwin Messtechnic GMBH, Operating Manual, Type MG 20 DC Amplifier.

11. Dornier GMBH, Technical Manual: I-W-A Displacement Measuring System.

12. Dornier GmBH, Private Communication.

13. Radio Spares Ltd., Product Catalogue, pp 269-273.

14. Radio Spares Ltd., Product Data Sheet, No. 4692.

15. Radio Spares Ltd., Product Data Sheet, No. 4642.

16. Digital Design and Development Ltd, User Manual, type II04 input board.

17. Markus J., Modern Electronic Circuits Reference Manual, Mc Graw Hill, p319, (1980).

18. PASCLDOS, Programming and user Manual, Business and Leisure Microcomputers Ltd.

19. Lucas Logic Ltd, Nascom Pascal: Operating Manual.

20. Lucas Logic Ltd, Nascom Pascal: Programming Manual.

21. Lucas Logic Ltd, Nascom, Program Manual, ZEAP editor/assembler.

22. McGregor J J and Watt A H, Pascal for Science and Engineering, Pitman , (1983).

23. Findley W and Watt D A, Pascal-An Introduction to Methodical Programming, Pitman International, (1978).

24. Leventhal L.A., Z80 Asembly Language Programming, Osborne/Mc Graw Hill, (1979).

25. Forchheimer P, Zeitschr Vereins Deutsch Ing, 45, 1781-8, (1901).

26. Green L Jr & Duwez P, J Appl Mech, 18, 39-45, (1951).

27. Tek M R, J Petrol Technol, 9, No. 6, 45-7, (1957).

28. Gent A N & Rusch K C, Rubber Chem Technol, 39, 389, (1966).

27. Tek M R, J Petrol Technol, 9, No 6, 45-7, (1959).

30. Kozeny J, Akad Wiss Wien Ber, 136, 2a, 271-306, (1927).

31. Chiltern T H & Colburn A P, Indust Engng Chem, 23, 913-9, (1931).

32. Kay J M, Fluid Mechanics and Heat Transfer, ch 21, 253, 2nd Edition, Cambridge University Press, (1963).

33. Ashby M F, Metulurgical Transactions, 14A, 1755-69, (1983).

34. British Standards Institute, BS 4443, part 6, method 16, (1980).

35. Addison H, Hydraulic Measurements, 2nd Edition, J Wiley & Sons, N.Y., (1946).

36. Kaufmann W, Fluid Mechanics, McGraw Hill, N.Y., (1963).

37. B.P. Chemicals, proc Sitev '80, Geneva, (1980).

38. Kleiner G A, Pham T & Tenhagen R J, J Cell Plast, 20, 49, (1984).

39. Rusch K C, Phd Thesis, University of Akron, USA, (1966).

40. Wilkinson W L, Non-Newtonian Fluids, Pergamon Press, (1970).

41. Ostwald W, Kollaidzchr, 38, 261, (1926).

42. Reiner M, Deformation and Flow, Lewis, London, (1949).

43. Christopher R H & Middlema S, I & E C Fundamentals, 4, 422, (1965).

44. Jarebski A B & Thullie J, Chem Engng Journal, 22, 243-5, (1981).

45. Bird R B, Ann Rev Fluid Mech, 8, 13-34, (1976).

46. Bird R B, Stewart W E & Lightfoot E N, Transport Phenomenon, ch1, J Wiley & Sons, N.Y., (1960).

47. Bear J, Flow Through Porous Media, ch4, Ed DeWeist R J M, Academic Press, (1969).

48. Snowdon J C, Vibration and Shock in Damped Mechanical Systems, ch1, J Wiley & Sons, (1968).

49. Hilyard N C, Mechanics of Cellular Plastics, ch4, Ed Hilyard N C, Appl Sci Publ, (1982).

50. Ferry J D, Viscoelastic Properties of Polymers, ch1, 3rd Edition, J Wiley & Sons, (1980).

51. Wolfe H W, Mechanics of Cellular Plastics, ch3, Ed Hilyard N C, Appl Sci Publ, (1982).

52. Hartings J W & Hagen J H, J Cell Plast, 14, 81, (1978).

53. Ashe W A, Proc Soc Auto Eng, Michigan USA, (1976).

54. Rusch K C, J App Polym Sci, 13, 2297, (1969).

55. Skochpole R E & Rubens, J Cell Plast, 1, 91-6, (1965).

56. Kanakkanatt S V, J Cell Plast, 9, 50, (1973).

57. Metha B S & Columbo E A, J Cell Plast, 12, 59, (1976).

58. Gent A N and Thomas A G, J Appl Polym Sci, 1, 107, (1959).

59. Rusch K C, J Appl Polym Sci, 14, 1433, (1970).

60. Hilyard N C & Djiauw L K, J Cell Plast, 7, 33, (1971).

61. Bigg D M, SPE proc 38th Ann Tech Conf, N.Y., 514-7, (1980).

62. Dement'ev A G & Tarakanov O G, Polym Mech, 6, 594-602, (1970).

63. Dement'ev A G & Tarakanov O G, Polym Mech, 6, 744-9, (1970).

64. Dement'ev A G & Tarakanov O G, Polym Mech, 6, 395-400, (1973).

65. British Standards Institute, BS 4443, Part 1, Method 6a, (1979).

66. ESH Ltd, Electo Servo Hydraulic Testing Machine, User Manual.

67. Crockett J H A, Plas & Rubb Processing & Applications, 5, 267-275, (1985).

68. Ferry J D et al, Ind Eng Chem, 44, 703, (1952).

69. Williams M L, Landel R F & Ferry J D, J Am Chem Soc, 77, 3701, (1975).

70. Jones R E & Fesman G, J Cell Plast, 1, 200, (1965).

71. Saunders J H & Frisch K C, Polyurethanes Chemistry and Technology, Part 1, Inerscience Publishers, N.Y., 255-8, (1962).

72. Jones R E, Hersch P, Stier G G & Dombrow B A, Plast Technol, 5, 55-9, (1959).

73. Kosten C W & Zwikker C, Rubb Chem Technol, 12, 105-11, (1939).

74. Gent A N & Rusch K C, J Cell Plast, 2, 59, (1966).

75. Hilyard N C & Kanakkanatt S V, J Phys D:Appl Phys, 3, 906, (1970).

76. Kanakkanatt S V, Phd Thesis, University of Akron, Ohio, (1969)

77. Haake Inc, Draht Haakebrueder Werk, New Jersey, Haake Viscometer, Model Rotovisco RV3 MK 5000, Instruction Manual.

78. Abadie J, Non-Linear Programming, North Holland Publishing Co, Amsterdam, (1967).

79. Kuhn H W & Tucker A W, proc 2nd Berkley Symp on Math, Stat & Prob, Univ Calafornia Press, 481-92, (1951).

80. Keifer J, J Soc Indust Appl Math, 5, 105-136, (1957).

81. Curry H B, Q Appl Math, 2, 258-60, (1944).

82. Stein M L, National Bureau Standards Rept, 52-7, (1951).

83. Rosen J B, J Soc Indust Appl Math, 9, 514-532, (1961).

84. Zoutendijk G, Methods of Feasable Directions, Elsevier Publishing Co, Amsterdam, (1960).

85. Hooke R & Jeeves T A, J Assoc for Computing Machinery, 8, 212-220, (1961).

86. Hilyard N C, Mechanics of Cellular Plastics, ch2, Ed Hilyard N C, Appl Sci Publ, (1982).

87. Draganski R S, J Cell Plast, 14, 282, (1978).

88. Hartings J W & Hagen J H, J Cell Plast, 14, 81, (1978).

89. Patten W & Seerfried C J, J Cell Plast, 12, 41, (1976).

90. Westfall P M, J Cell Plast, 19, 375-380, (1983).

91. Fabris H J, Advances in Urethane Science and Technology, Vol 2, 203, (1973).

92. Ick J, Rothermell H M & Hauptman H G, J Cell Plast, 12, 41, (1976).

93. Bayer A G, 'Bayfit & Hot-Moulded Foam for the Automobile Industry', Product Catalog No PU 54059, ed 3.79.E.26-759/847744.

94. International Standards, ISO 2631-1978(E), (1978).

95. Hilyard N C, Collier P & Care C M, proc, Dynamics in Auto Engineering, Cranfield I.T., Bedford, April 5-6, A.1, (1984).

96. Hilyard N C & Collier P, proc, Plastics on the Road, London, December 5-6, (1984).

97. British Standards Institute, BS 4443, Part 1, Method 5A.

98. Witham E M & Griffin M J, Soc Auto Engineers, Paper 770253, (1977).

99. S.A.E Recommended Practice, SAE J1013, SAE Handbook, Part II, (1974).

100. Griffin M J, Applied Ergonomics, 9, 15, (1978).

101. McNulty G J & Douglas D, proc, 4th Conf on Teaching Noise and Vibration, Sheffield City Poly, 283, (1982).

102. McNulty G J, Douglas D, Hilyard N C & Collier P, proc, Internoise '83, Edinburgh, July 13-15, 913-916, (1983).

103. Bruns H J & Ronitz R, Automobile Engineer, pp26-28 and 45-47, (1971).

104. Dahlberg T, J Sound & Vib, 58, 179, (1978).

105. Ryba D, Vehicle System Dynamics, 2, 1-32, (1973).

106. Ryba D, Vehicle System Dynamics, 3, pp17-46 and 55-98, (1974).

107. Fairley T E & Griffin M J, proc, Internoise '83, Edinburgh, July 13-15, 533-536, (1983).

108. Fairley T E, Proc, UK Informal Group on Human Response to Vibration, Heriot-Watt, Edinburgh, (1984).

109. Hilyard N C, Collier P, McNulty G J & Douglas D, proc, Internoise '83, Edinburgh, July 13-15, 527-532, (1983).

110. Hilyard N C, Collier P & Care C M, proc, UK Informal Group on Human Response to Vibration, N.I.A.E., Silsoe, Bedfordshire, (1983).

111. Snowdon J C, Vibration and Shock in Damped Mechanical Systems, ch2, J Wiley & Sons, (1968).

112. Payne P R & Band E G U, Wright-Patterson AFB, Ohio, AMRL-TR-70-35, (1970).

113. International Standards, ISO 5982-1981(E), (1981)..

114. Payne P R, Wright-Patterson AFB, Ohio, AMRL-TR-71-29, (1971).

115. Guignard J C, Private Communication.

116. Griffin M J, Aviation Space & Envir Med, 265, (1975).

117. Frolov K V, Dynamic Response of Biomechanical Systems, Ed Perrone N, 146, (1970).

118. Lange K O & Edwards R G, Aerospace Med, 41, 532, (1970).

119. Collier P, Norcliffe A & Hilyard N C, Proc, Fifth British Conf on Teaching Noise & Vibration, Sheffield City Polytechnic, July 3-5, 23-32, (1985).

120. Mustin G S, Theory & Practice of Cushion Design, Washington; The Shock & Vibration Information Centre, United States Department of Defense, 220-247, (1968).

121. Abramson H N, Shock & Vibration Handbook, Ed Harris C M & Crede C M, 2nd Edition, McGraw Hill, 4.1-4.36, (1976).

122. Crede C M & Ruzicke J E, Shock & Vibration Handbook, Ed Harris C M & Crede C M, 2nd Edition, McGraw Hill, 30.1-30.25, (1976).

123. Thompson J M T, Instabilities and Catastrophes in Science and Engineering, J Wiley & Sons, (1982).

124. Hilyard N C & Collier P, J Sound & Vib, Letters, Accepted for Publication, (1985).

125. Cvitanovic P, Universality in Chaos, Ed Cvitanovic P, Adam Hilger Ltd, Bristol, 1-34, (1984).

126. Moore D R, Toome J, Knobloch E & Weiss N O, Nature, 23, 663-7, (1983).

127. Huppert H E & Turner J S, J fluid Mech, 78, 821-854, (1976).

128. Hudson J L & Mankin J C, J Chem Phys, 74, 6171, (1981).

129. Weiss C O & King H, Optics Communications, 44, 59-61, (1982).

130. Testa J, Perez J & Jeffries C, Phys Rev Lett, 48, 714, (1982).

131. Kandoff L P, Physics Today, 46-53, (December 1983).

132. Mees A I & Sparrow C T, IEEE Proc, 128, 201, (1981).

133. Hao B-L, Chaos, World Scientific Publishing Co, (1984).

134. May R M, Nature, 261, 459, (1976).

135. Lorenz E N, J Atmos Sci, 20, 130, (1963).

136. Hao B-L & Zhang S-Y, J Stat Phys, 28, 769, (1982).

137. Feigenbaum M J, J Stat Phys, 19, 25, (1978).

138. Feigenbaum M J, J Stat Phys, 21, 669, (1979).

139. Wolfe A, Nature, 305, 182, (1983).

140. Hilyard N C, J Sound & Vib, Accepted for Publication, (1985).

141. Lichaber A & Maurer J, Non-Linear Phenomenon at Phase Transitions & Instabilities, Ed Riste T, Plenum Publishing Co, 259-286, (1982).

142. Feigenbaum M J, Los Alamos Sci, 1, 4-27, (1980).

143. Holmes P J & Marsden J E, Archive for Rational Mechanics & Analysis, 76, 135-166, (1981).

144. Cartwright M L & Littlewood J E, J London Math Soc, 20, 180-189, (1945).

145. Thompson J M & Elvey J S N, Int J Mech Sci, 26, 419-426, (1984).

APPENDIX I

DYNAMIC MECHANICAL SPECTROMETER

SYSTEM SPECIFICATIONS

GENERAL

EXCITATION	DIGITAL OR ANALOG
FREQUENCY RANGE	
DIGITAL	0.0608 - 18 Hz
ANALOG	5 - 100 Hz
CONTROL	Via a System of Menus
NUMBER OF COMMANDS	58

FACILITIES : Automatic Frequency Sweeps, Data Acquisition, On-Line Analysis, Autoranging, Compression on Displacement, Averaging of Results, Storage, Mass Compensation and Display.

SAMPLE ENVIROMENT		Air or Liquid Filled
MAX SAMPLE SIZE :		
AIR FILLED SAMPLES	: HEIGHT	11 cm
	WIDTH	20 cm
	LENGTH	40 cm
LIQUID FILLED SAMPLES	: HEIGHT	7 cm
	WIDTH	40 cm
	LENGTH	24 cm
MAX STATIC SAMPLE PRE-STRAIN		80 %
MAX DISPLACEMENT AMPLITUDE:		
0.0608 - 0.8 Hz		8 mm
0.8 - 1.5 Hz		1 mm
1.5 - 20 Hz		5 mm
20 - 100 Hz		8 mm

ELECTROMAGNETIC EXCITER

MANUFACTURER	BRUEL & KJAER
TYPE	4801 ; 4812 HEAD
POWER REQUIREMENT	1200 VA
COOLING	Blower Cooled by Ambient air
MAX FORCE	45 kgf
MOVING ELEMENT WEIGHT	0.45 kg
DISPLACEMENT LIMIT	13 mm
SIDE LOAD LIMIT	5.5 kg at 75 mm
RESONANT FREQUENCY	7.2 kHz

POWER AMPLIFIER

MANUFACTURER	BRUEL & KJAER
TYPE	2707
OUPUT VOLTAGE	10 V RMS
MAX OUPUT CURRENT:	
DC - 5 Hz	10 A
40 Hz - 100 Hz	22 A
INPUT IMPEDENCE	10 kOhm
OUTPUT IMPEDENCE	0.02 Ohm
HARMONIC DISTORTION (FULL CAPACITY)	0.1%
NOISE & HUM	85 dB

EXCITER CONTROL

MANUFACTURER	BRUEL & KJAER
TYPE	1047
FREQUENCY RANGE	5 Hz - 10 kHz
SWEEP RATES:	
LOGARITHMIC	0.1 - 100 octaves/min
LINEAR	0.1 - 100 Hz/second
COMPRESSOR DYNAMIC RANGE	80 dB
COMPRESSION RANGES:	
ACCELERATION	1,10,100,1000 g
VELOCITY	0.1, 1, 10, 100 ins/sec
DISPLACEMENT	0.01,0.1,1,10 ins

DIGITAL SIGNAL GENERATION INTERFACE

NUMBER OF BITS:	
SINE WAVE DATA	12
AMPLITUDE DATA	8
HANDSHAKE LINES	2
OUTPUT	MAX 20V PK-PK
LINEARITY vs AMPLITUDE	0.5%
LOW PASS FILTER:	
CUT OFF (-3 dB)	30 Hz
ULTIMATE SLOPE	6 dB/octave

INPUT ADC BOARDS

MANUFACTURER	Digital Design & Development
TYPE	II04
INTERFACING	Memory Mapped
NUMBER OF BOARDS	2
ACCURACY	12 BIT
NUMBER OF CHANNELS/BOARD	8
TYPE OF SIGNAL INPUT	Fully Differential
CONVERSION TIME	25 microseconds
PROGRAMMABLE GAIN RANGES	1,2,4,8,16,32,64 & 128
SIGNAL RANGES	Unipolar or Bipolar 5 or 10 V

LOW PASS FILTERS

CUT OFF FREQUENCY (-3dB)	500 Hz
ULTIMATE SLOPE	36 dB/octave
LINEARITY (0 - 100 Hz)	1%

DISPLACEMENT TRANSDUCER & CONDITIONER

MANUFACTURER	Dornier GmbH
TYPE	I-W-S A42
MEASURING RANGE (STEEL)	20 mm
SENSITIVITY	0.5 V/mm
NON-LINEAR DISTORTION	0.2 %
LONG TERM DRIFT	0.1 %/month
OUTPUT SIGNAL RANGE	0 ... +10 V

FORCE TRANSDUCER & CONDITIONER

MANUFACTURER	HBM GmbH
TYPE:	
TRANSDUCER	U2
AMPLIFIER	MG20

NOMINAL LOAD	200 kg
MODE	Tension or Compression
NATURAL FREQUENCY	8.7 kHz
WEIGHT	0.6 kg
NOMINAL OUTPUT VOLTAGE	-10 .... +10 V
FREQUENCY RANGE (-1 dB)	0 .... 10 000 Hz

MICROPROCESSOR CONTROLLER

MANUFACTURER	Lucas Logic
TYPE	Nascom III
NUMBER OF BIT	8
MEMORY	64 kbytes
SYSTEM CLOCK	4 mHz
CENTRAL PROCESSING UNIT	Zilog Z80A
OPERATING SYSTEMS	
NAS-SYS	$0000 - $0FFF
NAS-DOS	$D000 - $DFFF
PASCLDOS	$C000 - $CFFF
BASIC	$E000 - $FFFF
ZEAP (ASSEMBLER)	$1000
PASCAL	$1000
INTERNAL PERIPHERAL CIRCUITS	
PARALLEL INPUT OUTPUT DEVICES	4
COUNTER TIMER CITCUITS	1
SERIAL INPUT OUTPUT DEVICES	2
FLOPPY DISC UNITS	80 track single sided twin drives
CASTLE (TAPE) INTERFACE	1
EXTERNAL PERIPHERAL DEVICES	
KEYBOARD	ASCII Repeating
MONITOR	Monochrome
PRINTER	80 Column Dot Matrix
PLOTTER	A3 10 Pen Watanabe

APPENDIX II

PASCAL SOURCE TEXT FOR THE DYNAMIC MECHANICAL SPECTROMETER'S CONTROL SYSTEM

PROGRAMS

CONTROL , CALIBRAT & ANALYSIS

```
RAM CONTROL(INPUT,OUTPUT);
L
 1,10,20,21,62,80,503,DIGIT,ANALOG,DIGREC,ANAREC,MANIP,FINI;
T
EBIT =256.0;  B4GAN =$96D4; CONTWORD =$96E5; TDELAY=$96D8;
CLOCK=4.0E-6; TIMCON=$96E2; REMAIN   =$96EC; TOPLIN=$0BC9;
POS  =$A00C;  NCOUNT=$96EA; SINCON   =$96E4; STEP  =35;
B0GAN=$96D2;  SINTIM=$96E0; AMPLITUDE=$96D0; g     =9.81029;

V,FACTOR,H,I,J,CTC,NO,Q,Z,FAG1,FAG2,BRODY,READY,FACDIS,FACFOR,PAT:INTEGER;
L,W,H,UF,DIGFREQ,B,COMPRESSION,ERR,INTERMED,STAT,DEFH,TEMP,HUMID:REAL;
DIGITAL,SWAP,BAD:BOOLEAN;
DI:ARRAY[1..40,1..8]OF REAL;
AN:ARRAY[1..50,1..8]OF REAL;
DIGTABLE:ARRAY[1..30] OF REAL;
HEADING:STRING[48];ST,MENU:STRING[1];
NAME:STRING[8];DATE:STRING[255];

TION Discname:STRING[8];                                    EXTERNAL $C03C;
EDURE initdisc;                                             EXTERNAL $C036;
EDURE Drive(I:INTEGER);                                     EXTERNAL $C048;
EDURE Chain(FILE:STRING[8]);                                EXTERNAL $C039;
EDURE Topline(S:STRING[48]);                                EXTERNAL $C05D;
EDURE Delete(VAR BAD:BOOLEAN;FILE:STRING[8]);               EXTERNAL $C033;
EDURE Prepwrite(VAR BAD:BOOLEAN;SIZE:INTEGER;FILENAME:STRING[8]);
                                                            EXTERNAL $C01B;
EDURE Openwrite(VAR BAD:BOOLEAN;FILE:STRING[8]);            EXTERNAL $C01E;
EDURE Writereal(R:REAL);                                    EXTERNAL $C027;
EDURE Writeinteger(I:INTEGER);                              EXTERNAL $C024;
EDURE Writestring(S:STRING[255]);                           EXTERNAL $C021;
EDURE Clseqwr;                                              EXTERNAL $C02A;
```

```
DURE Openread(VAR BAD:BOOLEAN;NAME:STRING[8]);      EXTERNAL $C006;
DURE Readreal(VAR BAD:BOOLEAN;VAR R:REAL);          EXTERNAL $C00F;
DURE Readinteger(VAR BAD:BOOLEAN;VAR I:INTEGER);    EXTERNAL $C00C;
DURE Readstring(VAR BAD:BOOLEAN;VAR S:STRING[255]);EXTERNAL $C009;
DURE Clseqread;                                     EXTERNAL $C012;
DURE Savemc(VAR BAD:BOOLEAN;ST,FIN,EXCT:INTEGER;NAM:STRING[8]);
                                                    EXTERNAL $C04E;
DURE Loadmc(VAR BAD:BOOLEAN;FILE:STRING[8]);        EXTERNAL $C04B;
DURE initialise; CODE $CD,$00,$B4;
DURE singen;     CODE $CD,$04,$B4;
DURE drop;       CODE $CD,$08,$B4;
DURE upsweep;    CODE $CD,$0C,$B4;
DURE downsweep;  CODE $CD,$10,$B4;
DURE stopsin;    CODE $CD,$14,$B4;
DURE newfreq;    CODE $CD,$18,$B4;
DURE newamp;     CODE $CD,$1C,$B4;
DURE drop2;      CODE $CD,$20,$B4;
DURE freqer;     CODE $CD,$24,$B4;
DURE backspace;  CODE $3E,$08,$F7;

DURE screenclear;
VAR I:INTEGER;
BEGIN
    FOR I:=1 TO 15 DO WRITELN;
END;  (* of clearscreen  *)

DURE Zeroatend;
BEGIN stopsin;out(20,0);out(21,152);out(21,16);END;


DURE screenwrite(DISAMP,FORAMP,FREQUENCY,LOSTAN,STDIS,STFOR,STLOS,STFREQ:
                 REAL;N,FAC1,FAC2:INTEGER;BOD:BOOLEAN);
LABEL 301;
BEGIN
    screenclear;
    WRITELN('At a frequency of ',FREQUENCY:5:3,' +/- ',STFREQ:1:3,' Hz');
    IF BOD THEN GOTO 301;
    WRITELN('the number of samples was ',N:5);
    WRITELN;
    WRITELN('B000 GAIN ><',FAC1:3,'     B004 GAIN ><',FAC2:3);

    WRITELN;
    WRITELN('B000 Amplitude= ',DISAMP:9,' +/- ',STDIS:9,'  metres');
    WRITELN('B004 Amplitude= ',FORAMP:9,' +/- ',STFOR:9,'  Newtons');
    WRITELN;
    WRITELN('Phase difference = ',LOSTAN:3:3,' +/- ',STLOS:1:3,' DEG.');
    WRITELN;
END; (* of screenwrite  *)

DURE select(PRES:INTEGER;VAR FACT:INTEGER);
BEGIN
    CASE PRES OF
        0:FACT:=1;
        8:FACT:=2;
       16:FACT:=4;
       24:FACT:=8;
       32:FACT:=16;
       40:FACT:=32;
```

```
        48:FACT:=64;
        56:FACT:=128;
    END;
END; (* of select *)

DURE timconst(TT:REAL;VAR FACTR:INTEGER);
VAR RAT:REAL;
BEGIN
    RAT:=TT/2.0E-3;FACTR:=1;
    IF RAT<40 THEN RAT:=40;
    mem[TIMCONJ]:=round(RAT+0.5);
    mem[CONTWORDJ]:=149;
END; (* of timconst *)

DURE compressor(VAR COMPRESS:REAL);
BEGIN
    screenclear;
    WRITELN('  The old compression level was ',COMPRESS:4:2,' mm');
    WRITE('Enter the new level,in mm ');READLN(COMPRESS);
END;

DURE iigains(VAR FAG1,FAG2:INTEGER);
BEGIN
    screenclear;
    WRITE('B000 board gain,0-56 in 8''ts.? ');READLN(FAG1);
    WRITE('B004 board gain,0-56 in 8''ts.? ');READLN(FAG2);
    mem[B4GANJ]:=FAG2;mem[B0GANJ]:=FAG1;
END; (* of iigains *)

DURE newfrequency(VAR FACTR:INTEGER;SWEEP:BOOLEAN;FREQ:REAL);
LABEL 82;
VAR RAT:REAL;
    CTC:INTEGER;
BEGIN
    IF SWEEP THEN GOTO 82;screenclear;
    WRITELN('   The digital frequency may be set anywhere');
    WRITELN('between 0.07 Hz and 18 Hz ');
    WRITE('Enter required frequency in Hz ? ');READLN(FREQ);

    RAT:=1/(1000*FREQ*CLOCK);
    IF RAT > 255 THEN
    BEGIN
        RAT:=RAT/16;FACTR:=16;
    END ELSE FACTR:=1;
    CTC:=trunc(RAT);
    CASE FACTR OF
        1:BEGIN mem[SINCONJ]:=149;mem[CONTWORDJ]:=149;END;
       16:BEGIN mem[SINCONJ]:=181;mem[CONTWORDJ]:=181;END;
    END;
    mem[SINTIMJ]:=CTC;mem[TIMCONJ]:=CTC;
END;  (* of newfrequency *)

DURE sweeprate;
VAR RAT:INTEGER;
BEGIN
    screenclear;
    WRITE('Enter the sweep time in unit seconds  ');READLN(RAT);
    mem[TDELAYJ]:=RAT;
```

```
END;

DURE newamplitude;
VAR AMP:INTEGER;
BEGIN
     screenclear;
     AMP:=mem[AMPLITUDE];WRITE('Old amp=',AMP:3,' New amp=? ');READLN(AMP);
     mem[AMPLITUDE]:=AMP;
END;

DURE adder(BOT,TOP:INTEGER;SAMP:REAL;VAR SUMS1,SUMS2:REAL);
VAR  P,I,DSUML,DSUMU,FSUML,FSUMU:INTEGER;
BEGIN
     DSUML:=0;DSUMU:=0;FSUML:=0;FSUMU:=0;
     FOR I:=(BOT) TO (TOP) DO
     BEGIN
          P:=4*I;
          DSUML:=DSUML+mem[POS+P];
          DSUMU:=DSUMU+mem[POS+1+P] AND $0F;
          FSUML:=FSUML+mem[POS+2+P];
          FSUMU:=FSUMU+mem[POS+3+P] AND $0F;
     END;
     SUMS1:=SAMP*(EBIT*DSUMU+DSUML);
     SUMS2:=SAMP*(EBIT*FSUMU+FSUML);
END; (* of adder *)

DURE correction(Z:INTEGER;VAR DEL1,DEL2:REAL);
BEGIN
     DEL1:=mem[POS+Z]+mem[POS+Z+4]+EBIT*((mem[POS+1+Z] AND $0F)
                +(mem[POS+Z+5] AND $0F));
     DEL2:=mem[POS+Z+2]+mem[POS+Z+6]+EBIT*((mem[POS+Z+3] AND $0F)
                +(mem[POS+Z+7] AND $0F));
END;(* of correction *)

DURE amplitudes(DIGOT:BOOLEAN;VAR T,BOOO,BOO4,OMEG:REAL;VAR N:INTEGER);
VAR  V,M,K,L:INTEGER;
      REMC,TSAM,DELTD,DELTF,ADELD,ADELF,ALBER,BERAL:REAL;
      A1D,A2D,A1F,A2F,THETA,PSI:REAL;
      IND,INF,SD,SF:ARRAY[0..4] OF REAL;
BEGIN
     N:=0;M:=0;K:=0;L:=0;T:=0;BOOO:=0;BOO4:=0;REMC:=0;
     FOR V:=0 TO 4 DO
     BEGIN
          IND[V]:=0;INF[V]:=0;SD[V]:=0;SF[V]:=0;
     END;
     IF NOT DIGOT THEN drop ELSE drop2;
     N:=trunc(EBIT*mem[NCOUNT+1]+mem[NCOUNT]);
     TSAM:=mem[TIMCON];
     REMC:=mem[REMAIN];
     IF DIGOT THEN TSAM:=2*TSAM;
     T:=(N*TSAM)+(TSAM-REMC);
     K:=trunc(((T/4)+(TSAM/2))/TSAM);
     M:=trunc(((T/2)+(TSAM/2))/TSAM);
     L:=trunc(((3*T/4)+(TSAM/2))/TSAM);

     adder(1,K,TSAM,SD[1],SF[1]);
     adder(K+1,M,TSAM,SD[2],SF[2]);
     adder(M+1,L,TSAM,SD[3],SF[3]);
```

```
    adder(L+1,N,TSAM,SD[4],SF[4]);

    correction(4*N,DELTD,DELTF);
    ALBER:=(1/2)*(TSAM-REMC);
    IND[0]:=SD[1]+SD[2]+SD[3]+SD[4]+(DELTD*ALBER);
    INF[0]:=SF[1]+SF[2]+SF[3]+SF[4]+(DELTF*ALBER);

    correction(4*M,DELTD,DELTF);
    ALBER:=((T/2)-TSAM*M)/2;
    IND[1]:=SD[1]+SD[2]+(DELTD*ALBER);
    INF[1]:=SF[1]+SF[2]+(DELTF*ALBER);

    IND[2]:=IND[0]-IND[1];
    INF[2]:=INF[0]-INF[1];

    correction(4*K,DELTD,DELTF);
    correction(4*L,ADELD,ADELF);
    ALBER:=((TSAM*K)-(T/4))/2;
    BERAL:=((3*T/4)-(TSAM*L))/2;
    IND[3]:=SD[2]+SD[3]+(DELTD*ALBER)+(ADELD*BERAL);
    INF[3]:=SF[2]+SF[3]+(DELTF*ALBER)+(ADELF*BERAL);

    IND[4]:=IND[0]-IND[3];
    INF[4]:=INF[0]-INF[3];

    A1D:=(IND[1]-IND[2]);
    A2D:=(IND[3]-IND[4]);
    A1F:=(INF[1]-INF[2]);
    A2F:=(INF[3]-INF[4]);

    B000:=(SQRT(A1D*A1D+A2D*A2D))*(PI/(T*409));
    B004:=(SQRT(A1F*A1F+A2F*A2F))*(PI/(T*409));
    THETA:=arctan(A2D/A1D);
    PSI:=arctan(A2F/A1F);
    IF A1F=0 THEN PSI:=PI/2;IF A1D=0 THEN THETA:=PI/2;
    IF A1D < 0 THEN THETA:=THETA-PI;
    IF A1F < 0 THEN PSI:=PSI-PI;
    OMEG:=THETA-PSI;
END;  (*  of amplitudes  *)

EDURE autorange(B0SIZ,B4SIZ:REAL;VAR REDO:BOOLEAN;VAR DGAIN,FGAIN:INTEGER);
 VAR DADJUS,FADJUS,AGAIN,AGAIN2:BOOLEAN;L:INTEGER;
 BEGIN
    IF REDO=TRUE THEN FOR L:=1 TO 38 DO WRITE(chr(8));
    WRITE('B000 GAIN No.=',DGAIN:4,'  B004 GAIN No.=',FGAIN:4);
    IF B0SIZ < 4.0 THEN DADJUS:=TRUE ELSE DADJUS:=FALSE;
    IF B4SIZ < 4.0 THEN FADJUS:=TRUE ELSE FADJUS:=FALSE;
    IF DADJUS THEN
    BEGIN
        DGAIN:=mem[B0GAN];
        IF DGAIN <53 THEN
        BEGIN
            DGAIN:=DGAIN+8;
            mem[B0GAN]:=DGAIN;
            AGAIN:=TRUE;
        END ELSE AGAIN:=FALSE;
    END ELSE AGAIN:=FALSE;
    IF FADJUS THEN
```

```
    BEGIN
        FGAIN:=mem[B4GAN];
        IF FGAIN <53 THEN
        BEGIN
            FGAIN:=FGAIN+8;
            mem[B4GAN]:=FGAIN;
            AGAIN2:=TRUE;
        END ELSE AGAIN2:=FALSE;
    END ELSE AGAIN2:=FALSE;
    IF (AGAIN) OR (AGAIN2) THEN REDO:=TRUE ELSE REDO:= FALSE;
END; (* of autorange *)

EDURE analysis(FAG1,FAG2,CONFACTOR:INTEGER;COMPR:REAL;VAR DISAMP,FORAMP,
      FREQUENCY,LOSTANGENT,STDIS,STFOR,STLOS,STFREQ:REAL;VAR N,FAC1,FAC2:
      INTEGER;DIGITA:BOOLEAN);
LABEL 15,74,501;
VAR
    DUD,BUB,P,I,DGAIN,FGAIN,ERR,PAX:INTEGER;REDO:BOOLEAN;
    T:REAL;
    B0HIZ,B4HIZ,LOSTAN,FRE:ARRAY[0..10] OF REAL;

BEGIN
    mem[B0GAN]:=FAG1;mem[B4GAN]:=FAG2;DGAIN:=FAG1;FGAIN:=FAG2;

    I:=0;DISAMP:=0;FORAMP:=0;FREQUENCY:=0;LOSTANGENT:=0;
    amplitudes(DIGITA,T,B0HIZ[0],B4HIZ[0],LOSTAN[0],N);
    autorange(B0HIZ[0],B4HIZ[0],REDO,DGAIN,FGAIN);
    IF REDO THEN GOTO 15;
    select(DGAIN,FAC1);
    select(FGAIN,FAC2);WRITELN;
    DISAMP:=(2.0E-3*B0HIZ[0])/FAC1;
    WRITELN(' Displacement = ',DISAMP*1000:4:2,' mm      ',mem[AMPLITUDE]);
    FRE[0]:=(1/(T*CLOCK*CONFACTOR));
    FREQUENCY:=FRE[0];
    IF DIGITA THEN
    BEGIN
        ERR:=round((COMPR-(DISAMP*1000))*STEP);
        IF (ERR>=1) OR (ERR<=-1) THEN
        BEGIN
            IF FRE[0] <= 0.2 THEN BEGIN
                IF abs((COMPR-(DISAMP*1000))/COMPR)<0.05 THEN GOTO 74;
            END;
            IF ERR>0 THEN PAX:=ERR ELSE PAX:=-ERR;
            FOR I:=1 TO PAX DO
            BEGIN
                mem[AMPLITUDE]:=mem[AMPLITUDE]+ERR DIV PAX;
                OUT(24,mem[AMPLITUDE]);FOR P:=1 TO 10000 DO;
            END;
            FOR P:=1 TO 500 DO BEGIN;I:=keyboard;IF I=27 THEN GOTO 501;END
            DGAIN:=FAG1;FGAIN:=FAG2;
            mem[B0GAN]:=FAG1;mem[B4GAN]:=FAG2;GOTO 15;
        END;

        WRITE('Compression completed.');
    END;
    WRITE('Starting averaging..... ');backspace;WRITE('1');
    FORAMP:=(20*g*B4HIZ[0])/FAC2;
    LOSTANGENT:=LOSTAN[0];
```

```
    FOR I:=1 TO 9 DO
    BEGIN
        backspace;WRITE(I+1:1);
        amplitudes(DIGITA,T,B0HIZ[I],B4HIZ[I],LOSTAN[I],N);
        FRE[I]:=(1/(T*CLOCK*CONFACTOR));
        DISAMP:=DISAMP+(2.0E-3*B0HIZ[I])/FAC1;
        FORAMP:=FORAMP+(20*g*B4HIZ[I])/FAC2;
        FREQUENCY:=FREQUENCY+FRE[I];
        LOSTANGENT:=LOSTANGENT+LOSTAN[I];
    END;
    DISAMP:=DISAMP/10;FORAMP:=FORAMP/10;FREQUENCY:=FREQUENCY/10;
    LOSTANGENT:=LOSTANGENT/10;STDIS:=0;STFOR:=0;STLOS:=0;STFREQ:=0;WRITELN
    FOR I:=0 TO 9 DO
    BEGIN
        B0HIZ[I]:=(2.0E-3*B0HIZ[I])/FAC1;B4HIZ[I]:=(20*g*B4HIZ[I])/FAC2;
        STDIS:=STDIS+sqr(B0HIZ[I]-DISAMP);
        STFOR:=STFOR+sqr(B4HIZ[I]-FORAMP);
        STLOS:=STLOS+sqr(LOSTAN[I]-LOSTANGENT);
        STFREQ:=STFREQ+sqr(FRE[I]-FREQUENCY);
    END;
    STDIS:=sqrt(STDIS/10);STFOR:=sqrt(STFOR/10);STLOS:=sqrt(STLOS/10);
    STFREQ:=sqrt(STFREQ/10);
    IF LOSTANGENT<0 THEN LOSTANGENT:=LOSTANGENT+2*PI;

END; (* of analysis procedure *)

N

Loadmc(BAD,'routine1');Loadmc(BAD,'routine2');mem[TDELAY]:=1;
initdisc;initialise;mem[AMPLITUDE]:=16;newamp;Q:=1;Z:=1;
INIT DIGTABLE TO 0.07,0.08,0.091,0.105,0.13,0.16,0.205,0.25,0.31,0.41,0.51,
0.8,0.9,1.01,1.3,1.6,2.01,3.01,4.01,5.01,6.01,7.01,8.01,9.01,10.01,11,12,13
T:
out(20,0);out(21,152);out(21,16);
HEADING:='   DIGITAL SIGNAL GENERATION';Topline(HEADING);DIGITAL:=TRUE;

screenclear;
WRITELN('******************** MENU ************************');
WRITELN('**      <C>   To set compression level          **');
WRITELN('**      <M>   For a measurement                 **');
WRITELN('**      <S>   Record digital sweep results      **');
WRITELN('**      <F>   To set/start digital sine wave    **');
WRITELN('**      <E>   To stop sine wave                 **');
WRITELN('**      <A>   To set new signal amplitude       **');
WRITELN('**      <G>   For a new input board gain        **');
WRITELN('**      <X>   To move current array point       **');
WRITELN('**      <L>   Analogue signal menu              **');
WRITELN('**      <R>   Results manipulation menu         **');
WRITELN('**      <Z>   Zero / calibration menu           **');
WRITELN('**      <H>   To abort  (data may be saved)     **');
WRITELN('************************************************');
WRITE(' ? ');READ(MENU);backspace;WRITE(MENU);
CASE MENU OF
  'Z':BEGIN Drive(2);
        Delete(BAD,'VARTABLE');Savemc(BAD,$6800,$9600,$1000,'VARTABLE');
        Drive(0);Chain('calibrat');END;
  'H':GOTO FINI;
  'M':BEGIN screenclear;
```

```
      analysis(FAG1,FAG2,FACTOR,COMPRESSION,DIGQ,1],DIGQ,2],DIGQ,3],DIGQ,4],
                  DIGQ,5],DIGQ,6],DIGQ,7],DIGQ,8],NO,FACDIS,FACFOR,DIGITAL);
     screenwrite(DIGQ,1],DIGQ,2],DIGQ,3],DIGQ,4]*360/(2*PI),DIGQ,5],DIGQ,6],
                  DIGQ,7]*360/(2*PI),DIGQ,8],NO,FACDIS,FACFOR,FALSE);
          WRITELN('Digital Run No. ',Q:3,' completed.');
          WRITE('Do you want to save these  results ? Y/N ');READ(ST);
          WRITELN(ST);IF ST='Y' THEN BEGIN
               WRITELN('Digital run ',Q:3,' saved ',40-Q:3,' left ');Q:=Q+1;
          END ELSE WRITELN('Run deleted ');
          IF Q>40 THEN Topline('********** DIGITAL ARRAY FULL *********');
          WRITE('Enter to continue..... ');READLN(BRODY);
       END;
   'R':BEGIN Zeroatend;DIGITAL:=FALSE;GOTO MANIP;END;
   'L':BEGIN Zeroatend;DIGITAL:=FALSE;GOTO ANALOG;END;
   'G':iigains(FAG1,FAG2);
   'A':BEGIN newamplitude;newamp;END;
   'C':compressor(COMPRESSION);
   'E':Zeroatend;
   'F':BEGIN newfrequency(FACTOR,FALSE,0);singen;END;
   'X':BEGIN WRITELN;WRITE('New array index? ');READ(Q);END;
   'S':BEGIN screenclear;V:=1;WHILE V < 29 DO BEGIN
       DIGFREQ:=DIGTABLE[V];newfrequency(FACTOR,TRUE,DIGFREQ);singen;
       FOR I:=1 TO 10000 DO;
       analysis(FAG1,FAG2,FACTOR,COMPRESSION,DIGQ,1],DIGQ,2],DIGQ,3],DIGQ,4],
                  DIGQ,5],DIGQ,6],DIGQ,7],DIGQ,8],NO,FACDIS,FACFOR,DIGITAL),
       screenwrite(DIGQ,1],DIGQ,2],DIGQ,3],DIGQ,4]*360/(2*PI),DIGQ,5],
                 DIGQ,6],DIGQ,7]*360/(2*PI),DIGQ,8],NO,FACDIS,FACFOR,FALSE),
       WRITELN('Digital sweep point ',V:3,' completed.');
       WRITE('<ESC> to abort sweep.....');
       FOR I:=1 TO 200 DO BEGIN
          J:=keyboard;IF J=27 THEN GOTO 10;END;
       WRITELN('....Too late! ');Q:=Q+1;V:=V+1;
       IF Q>40 THEN GOTO 10;END;
       Zeroatend;
       END;
END;
GOTO 10;

 G:
 EADING:='  ANALOGUE SIGNAL GENERATION SECTION';Topline(HEADING);

creenclear;
 RITELN('******************** MENU ***********************');
WRITELN('**      <M>   For a single measurement         **');
 RITELN('**      <S>   Record analog sweep results      **');
'RITELN('**      <P>   To set sweep period              **');
WRITELN('**      <U>   To sweep frequency up            **');
WRITELN('**      <D>   To sweep frequency down          **');
WRITELN('**      <G>   For a new input board gain       **');
WRITELN('**      <X>   To move current array index      **');
WRITELN('**      <L>   Move to digital signal menu      **');
WRITELN('**      <R>   For results manipulation menu    **');
WRITELN('**      <Z>   Zero / calibration menu          **');
WRITELN('**      <H>   Abort    (data may be saved)     **');
WRITELN('************************************************');
WRITE(' ? ');READ(MENU);backspace;WRITELN(MENU);
CASE MENU OF
   'Z':BEGIN Drive(2);
```

```
        Delete(BAD,'VARTABLE');Savemc(BAD,$6900,$9600,$1000,'VARTABLE');
        Drive(0);Chain('calibrat');END;
  'H':GOTO FINI;
  'R':GOTO MANIP;
  'L':GOTO DIGIT;
  'G':iigains(FAG1,FAG2);
  'D':downsweep;
  'U':upsweep;
  'P':sweeprate;
  'X':BEGIN WRITELN;WRITE('New array index? ');READ(Z);GOTO 20;END;
  'M':BEGIN screenclear;
        freqer;B:=((EBIT*mem[NCOUNT+1]+mem[NCOUNT])*mem[TIMCON]);
        B:=(B+(mem[TIMCON]-mem[REMAIN]))*CLOCK;timconst(B,FACTOR);
        analysis(FAG1,FAG2,FACTOR,COMPRESSION,AN[Z,1],AN[Z,2],AN[Z,3],
        AN[Z,4],AN[Z,5],AN[Z,6],AN[Z,7],AN[Z,8],NO,FACDIS,FACFOR,DIGITAL)
        screenwrite(AN[Z,1],AN[Z,2],AN[Z,3],AN[Z,4]*360/(2*PI),AN[Z,5],
        AN[Z,6],AN[Z,7]*360/(2*PI),AN[Z,8],NO,FACDIS,FACFOR,FALSE);
        WRITELN('Analog run No. ',Z:3,' completed.');
        WRITE('Do you want these results ? Y/N ');READ(ST);WRITELN(ST);
        IF ST='Y' THEN BEGIN
            WRITELN('Analog run ',Z:3,' saved ',50-Z:3,' left ');Z:=Z+1
        END ELSE WRITELN('Run deleted  ');
        IF Z>50 THEN Topline('********** ANALOG ARRAY FULL **********');
        WRITE(' <ENTER> to continue.....');READLN(BRODY);
     END;
  'S':BEGIN screenclear;V:=1;WRITE('upper frequency ? ');READLN(UF);
          freqer;B:=((EBIT*mem[NCOUNT+1]+mem[NCOUNT])*mem[TIMCON]);
          B:=(B+(mem[TIMCON]-mem[REMAIN]))*CLOCK;timconst(B,FACTOR);

          freqer;B:=((EBIT*mem[NCOUNT+1]+mem[NCOUNT])*mem[TIMCON]);
          B:=(B+(mem[TIMCON]-mem[REMAIN]))*CLOCK;timconst(B,FACTOR);
        analysis(FAG1,FAG2,FACTOR,COMPRESSION,AN[Z,1],AN[Z,2],AN[Z,3],
        AN[Z,4],AN[Z,5],AN[Z,6],AN[Z,7],AN[Z,8],NO,FACDIS,FACFOR,DIGITAL)
        screenwrite(AN[Z,1],AN[Z,2],AN[Z,3],AN[Z,4]*360/(2*PI),AN[Z,5],
        AN[Z,6],AN[Z,7]*360/(2*PI),AN[Z,8],NO,FACDIS,FACFOR,FALSE);
          WRITELN('Analog sweep point ',V:3,' completed.');
          IF AN[Z,3] >= UF THEN BEGIN
              mem[TDELAY]:=V;downsweep;mem[TDELAY]:=1;GOTO 20;END;
          WRITE('<ESC> to abort sweep.....');
          FOR I:=1 TO 200 DO BEGIN;J:=keyboard;IF J=27 THEN GOTO 20;END;
          WRITELN('..Too late! ');Z:=Z+1;V:=V+1;IF Z>50 THEN GOTO 20;
          upsweep;GOTO 503;END;
END;
GOTO 20;

P:
HEADING:=' RESULTS MANIPULATION SECTION ';Topline(HEADING);

screenclear;
WRITELN('******************** MENU **********************');
WRITELN('**     <R>   Reload variables after an abort  **');
WRITELN('**     <T>   Reload a data file               **');
WRITELN('**     <D>   Resequence digital array         **');
WRITELN('**     <E>   Resequence analogue array        **');
WRITELN('**     <P>   Display results of any digital run*');
WRITELN('**     <Q>   Display results of any analog run**');
WRITELN('**     <S>   Save arrays on disc              **');
WRITELN('**     <A>   Move to ANALYSIS program         **');
```

```
WRITELN('**     <C>   Chain to another program          **');
WRITELN('**     <1>   Return to digital generation menu**');
WRITELN('**     <2>   Return to analog generation menu **');
WRITELN('**     <H>   Abort  (data can be saved)        **');
WRITELN('*********************************************');
WRITE(' ? ');READ(MENU);backspace;WRITELN(MENU);
CASE MENU OF
     'R':BEGIN
           screenclear;Drive(2);Loadmc(BAD,'VARTABLE');
         END;
     'T':BEGIN Drive(2);
           WRITELN(' Disc in drive2 is ',Discname,' which file ?');
           READLN(NAME);Openread(BAD,NAME);IF BAD THEN GOTO 80;
           Readinteger(BAD,Q);Readinteger(BAD,Z);
         FOR I:=1 TO Q DO BEGIN FOR J:=1 TO 8 DO Readreal(BAD,DI[I,J]);END
         FOR I:=1 TO Z DO BEGIN FOR J:=1 TO 8 DO Readreal(BAD,AN[I,J]);END
           Readreal(BAD,STAT);Readreal(BAD,L);Readreal(BAD,W);
           Readreal(BAD,H);Readinteger(BAD,PAT);Readstring(BAD,DATE);
           Readreal(BAD,DEFH);Readreal(BAD,TEMP);Readreal(BAD,HUMID);
           Closeqread;
         END;
     'D':BEGIN
EC:
            SWAP:=FALSE;
            FOR I:=1 TO (Q-2) DO BEGIN
                IF (DI[I,3])>DI[I+1,3] THEN BEGIN
                    FOR J:=1 TO 8 DO BEGIN
                        INTERMED:=DI[I+1,J];DI[I+1,J]:=DI[I,J];
                        DI[I,J]:=INTERMED;
                        SWAP:=TRUE;
                    END;
                END;
             END;
             IF SWAP THEN GOTO DIGREC;
         END;
     'E':BEGIN
EC:
            SWAP:=FALSE;
            FOR I:=1 TO (Z-2) DO BEGIN
                IF (AN[I,3])>(AN[I+1,3]) THEN BEGIN
                    FOR J:=1 TO 8 DO BEGIN
                        INTERMED:=AN[I+1,J];AN[I+1,J]:=AN[I,J];
                        AN[I,J]:=INTERMED;
                        SWAP:=TRUE;
                    END;
                 END;
            END;
            IF SWAP THEN GOTO ANAREC;
         END;
     'P':BEGIN WRITE('Which run ?  ');READLN(I);
           screenwrite(DI[I,1],DI[I,2],DI[I,3],DI[I,4]*360/(2*PI),
                DI[I,5],DI[I,6],DI[I,7]*360/(2*PI),DI[I,8],0,0,0,TRUE);
           WRITE('Digital run ',I:3,' enter to continue. ');
           READLN(BRODY);GOTO 80;END;
     'Q':BEGIN WRITE('Which run ? ');READLN(I);
           screenwrite(AN[I,1],AN[I,2],AN[I,3],AN[I,4]*360/(2*PI),
                AN[I,5],AN[I,6],AN[I,7]*360/(2*PI),AN[I,8],0,0,0,TRUE);
           WRITE('Analog run ',I:3,' enter to continue. ');
```

```
            READLN(BRODY);GOTO 80;END;
    'S':BEGIN screenclear;Drive(2);
            WRITELN('Disc in drive2 is ',Discname,' enter file name');
            READLN(NAME);

            Prepwrite(BAD,25,NAME);
            IF BAD THEN BEGIN
                WRITELN('File already exists.Do you wish to: ');
                WRITELN('  Delete file on disc <X> ');
                WRITE('  Enter new file name <N>  ? ');READLN(ST);
                CASE ST OF
                  'X':BEGIN Delete(BAD,NAME);GOTO 62;END;
                  'N':BEGIN WRITE('Enter new file name ');READLN(NAME);
                      GOTO 62;END;
                END;
            END;
            WRITELN('File  ',NAME,'  opened.');
            Writeinteger(Q-1);Writeinteger(Z-1);
            FOR J:=1 TO (Q-1) DO BEGIN
                FOR I:=1 TO 8 DO Writereal(DIEJ,I]);END;
            FOR J:=1 TO (Z-1) DO BEGIN
                FOR I:=1 TO 8 DO Writereal(ANEJ,I]);END;
            WRITE(' Static force /N ');READLN(STAT);Writereal(STAT);
            WRITE('Sample length /m ');READLN(L);Writereal(L);
            WRITE('         width /m ');READLN(W);Writereal(W);
            WRITE('        height /m ');READLN(H);Writereal(H);
            WRITE('Plate  number used  ');READLN(PAT);Writeinteger(PAT);
            WRITE('File  date  ');READLN(DATE);Writestring(DATE);
            WRITE('Deformed height /m ');READLN(DEFH);Writereal(DEFH);
            WRITE('Temperature /deg C ');READLN(TEMP);Writereal(TEMP);
            WRITE('Humidity / %       ');READLN(HUMID);Writereal(HUMID);
            Clseqwr;WRITELN;WRITELN('Transfer to disc complete');
            FOR I:=1 TO 10000 DO;
        END;
    'A':BEGIN Drive(0);Chain('analysis');END;
    'C':BEGIN WRITE('Enter program name, drive 0  ');READLN(NAME);
            Drive(0);Chain(NAME);Drive(2);END;
    '1':GOTO DIGIT;
    '2':GOTO ANALOG;
    'H':GOTO FINI;
END;
GOTO 80;

:
Zeroatend;
WRITE(' Do you wish to save the variables Y/N ');READLN(ST);Drive(2);
IF ST='Y' THEN BEGIN Delete(BAD,'VARTABLE');
    Savemc(BAD,$6800,$9600,$1000,'VARTABLE');END;
```

```
RAM CALIBRATE(INPUT,OUTPUT);
L 1,21,99,FINI;
T
EBIT =256.0;
TOPLIN=$0BC9;
g=9.81029;
I,GAINS1,GAINS2,CHAN:INTEGER;WHITCH:BOOLEAN;
HEADING:STRING[48];
ST,MENU:STRING[1];

TION RtoS(R:REAL;L,P:INTEGER):STRING[60];          EXTERNAL $C057;
EDURE initdisc;                                    EXTERNAL $C036;
EDURE Drive(I:INTEGER);                            EXTERNAL $C048;
EDURE Chain(FILE:STRING[8]);                       EXTERNAL $C039;
EDURE Topline(S:STRING[48]);                       EXTERNAL $C05D;

EDURE screenclear;
 VAR I:INTEGER;
 BEGIN
     FOR I:=1 TO 15 DO WRITELN;
 END;  (* of clearscreen  *)

EDURE select(PRES:INTEGER;VAR FACT:INTEGER);
 BEGIN
     CASE PRES OF
          0:FACT:=1;
          8:FACT:=2;
         16:FACT:=4;
         24:FACT:=8;
         32:FACT:=16;
         40:FACT:=32;
         48:FACT:=64;
         56:FACT:=128;
     END;
 END; (* of select *)

EDURE iigains(VAR FAG1,FAG2:INTEGER);
 BEGIN
     screenclear;
     WRITE('B000 board gain,0-56 in 8''ts.? ');READLN(FAG1);
     WRITE('B004 board gain,0-56 in 8''ts.? ');READLN(FAG2);
 END; (* of iigains *)

EDURE diginputs(UNORDIG:BOOLEAN;VAR GAN1,GAN2:INTEGER;CHAN:INTEGER);
 LABEL REP,CIRC;
 CONST LINER=$098C;LINER2=$0A0C;
 VAR I,J,FAC1,FAC2,BB1,BB2:INTEGER;DISIG,FORSIG,FORINS:REAL;
     DIS,FIS,WORDS1,WORDS2:STRING[12];A:STRING[1];
 BEGIN
     screenclear;
     WORDS1:='Displacement';WORDS2:='Force';

     BB1:=GAN1+CHAN;BB2:=GAN2+CHAN;
     DISIG:=0;FORSIG:=0;
     FOR I:=1 TO 100 DO
     BEGIN
          mem[$B000]:=BB1;mem[$B004]:=BB2;FOR J:=1 TO 10 DO;
```

```
        DISIG:=DISIG+mem[$B000]+EBIT*(mem[$B001] AND $0F);
        FORSIG:=FORSIG+mem[$B004]+EBIT*(mem[$B005] AND $0F);
    END;
    DISIG:=DISIG/100;FORSIG:=FORSIG/100;
    IF UNORDIG THEN
    BEGIN
        select(GAN1,FAC1);DISIG:=(2*(DISIG-2045))/(409*FAC1);
        select(GAN2,FAC2);FORINS:=(20*g*(FORSIG-2045))/(409*FAC2);
        DIS:=RtoS(DISIG,7,3);FIS:=RtoS(FORINS,6,2);
    END ELSE BEGIN DIS:=RtoS(DISIG,6,0);FIS:=RtoS(FORSIG,6,0);END;
    I:=16;
    FOR J:=1 TO 35 DO BEGIN mem[J+LINER1]:=32;mem[J+LINER2]:=32;END;
    FOR J:=1 TO length(DIS) DO mem[J+LINER1]:=ord(mid(DIS,J,1));
    FOR J:=1 TO length(WORDS1) DO mem[J+I+LINER1]:=ord(mid(WORDS1,J,1));
    FOR J:=1 TO length(FIS) DO mem[J+LINER2]:=ord(mid(FIS,J,1));
    FOR J:=1 TO length(WORDS2) DO mem[J+I+LINER2]:=ord(mid(WORDS2,J,1));
    I:=keyboard;IF I<>27 THEN GOTO REP;
    WRITE(' New gains ? Y/N ');READLN(A);
    IF A='Y' THEN BEGIN iigains(GAN1,GAN2);screenclear;GOTO REP;END;
END;   (*  of diginputs   *)

N
HEADING:=' SET-ZERO  AND  CALIBRATION  MODE';topline(HEADING);

screenclear;
WRITELN('*************** CALIBRATION MENU **************');
WRITELN('**    <G>    To set the input board gains    **');
WRITELN('**                                           **');
WRITELN('**    <D>    To read inputs: 12-bit digital  **');
WRITELN('**    <U>    To read inputs:measurement units**');
WRITELN('**                                           **');
WRITELN('**    <F>    To read ch 2 inputs:digital     **');
WRITELN('**    <A>    To read ch 2 inputs:meas units  **');
WRITELN('**                                           **');
WRITELN('**    <R>    To return to measurement mode   **');
WRITELN('**    <H>    To abort program                **');
WRITELN('***********************************************');
WRITE(' ? ');

READLN(MENU);
CASE MENU OF
   'H':GOTO FINI;
   'G':BEGIN iigains(GAINS1,GAINS2);GOTO 1;END;
   'D':BEGIN WHITCH:=FALSE;CHAN:=0;diginputs(WHITCH,GAINS1,GAINS2,CHAN);
       GOTO 1;END;
   'U':BEGIN WHITCH:=TRUE;CHAN:=0;diginputs(WHITCH,GAINS1,GAINS2,CHAN);
       GOTO 1;END;
   'F':BEGIN WHITCH:=FALSE;CHAN:=1;diginputs(WHITCH,GAINS1,GAINS2,CHAN);
       GOTO 1;END;
   'A':BEGIN WHITCH:=TRUE;CHAN:=1;diginputs(WHITCH,GAINS1,GAINS2,CHAN);
       GOTO 1;END;
   'R':GOTO 99;
  OTHERS:GOTO 1;
END;
GOTO 1;

screenclear;
WRITELN('In order to recover the data in the control');
```

```
WRITELN(' program you must type <R>,<R>,<Y>, once the');
WRITELN(' control program is rejoined. If you immedi-');
WRITELN(' ately use the "Z" command all the data will');
WRITE(' be lost. OK Y');READLN(ST);
Drive(0);Chain('control');

:
```

```
RAM ANALYSIS(INPUT,OUTPUT);
L 10,20,62,101,READER,MASSCOM,COMASS,MAIN,MASSPLOT,FINI;
T  RAD=0.0174533;

LO,UP,PAT,IND,P,R,S,A,D,I,J,Q,Z:INTEGER;
S,STAT,MIN,LLF,L,W,H,DEL,DEL2,MAXSTIF,B,Y,X,FDASH,FDOUBDASH,M,HITAN:REAL;
CMOD,DCMOD,LOMOD,STMOD,DELST,DELOS,DEFH,TEMP,HUMID:REAL;
STORE,LOSS,COMP,BAD,REDEM:BOOLEAN;
A,MM:ARRAY[1..8] OF REAL;
PLD,DI:ARRAY[1..40,1..8] OF REAL;
PLA,AN:ARRAY[1..50,1..8] OF REAL;
DP,SD,MD:ARRAY[1..40,1..4] OF REAL;
AP,SA,MA:ARRAY[1..50,1..4] OF REAL;
NAME:STRING[6];HEAD:STRING[30];DATE:STRING[255];
HEADER:STRING[48];PRI1,PRI2:STRING[80];
TM,TP,ST,MENU:STRING[1];

TION ItoS(I:INTEGER):STRING[6];          EXTERNAL $C051;
TION Power(M:INTEGER;N:INTEGER):REAL;
N
IF N=0 THEN Power:=1
ELSE IF N=1 THEN Power:=M ELSE Power:=M*Power(M,N-1);

TION  Discname:STRING[8];                                    EXTERNAL $C03C;

EDURE Initdisc;                                              EXTERNAL $C036;
EDURE Chain(FILE:STRING[8]);                                 EXTERNAL $C039;
EDURE Delete(VAR BAD:BOOLEAN;FILE:STRING[8]);                EXTERNAL $C033;
EDURE Openread(VAR BAD:BOOLEAN;NAME:STRING[8]);              EXTERNAL $C006;
EDURE Readreal(VAR BAD:BOOLEAN;VAR R:REAL);                  EXTERNAL $C00F;
EDURE Readinteger(VAR BAD:BOOLEAN;VAR I:INTEGER);            EXTERNAL $C00C;
EDURE Readstring(VAR BAD:BOOLEAN;VAR S:STRING[255]);         EXTERNAL $C009;
EDURE Prepwrite(VAR BAD:BOOLEAN;S:INTEGER;FILE:STRING[8]);EXTERNAL $C01B;
EDURE Openwrite(VAR BAD:BOOLEAN;FILE:STRING[8]);             EXTERNAL $C01E;
EDURE Writereal(R:REAL);                                     EXTERNAL $C027;
EDURE Writeinteger(I:INTEGER);                               EXTERNAL $C024;
EDURE Writestring(S:STRING[255]);                            EXTERNAL $C021;
EDURE Clseqread;                                             EXTERNAL $C012;
EDURE Clseqwr;                                               EXTERNAL $C02A;
EDURE Drive(I:INTEGER);                                      EXTERNAL $C048;
EDURE Topline(S:STRING[48]);                                 EXTERNAL $C05D;
EDURE Serprint;   CODE $21,$90,$C0,$22,$78,$0C;
EDURE Printeron;  CODE $DF,$55;
EDURE Printeroff; CODE $DF,$4E;
EDURE Backspace;  CODE $3E,$08,$F7;

EDURE Screenclear;
K:INTEGER;
N FOR K:=1 TO 15 DO WRITELN;END;

EDURE Comparator(VAR PFREQ,MODFREQ,MIN:REAL;VAR K,IND:INTEGER);
N
IF abs(MODFREQ-PFREQ)<MIN THEN BEGIN
     MIN:=abs(MODFREQ-PFREQ);IND:=K;END;


EDURE Stiff(DIS,FOR,PHAS,DDIS,DFOR,DPHAS:REAL;VAR S1,S2,S3,S4:REAL;
                                                    W,H,L:REAL);
```

```
N
S1:=(FOR/DIS)*H/(W*L);S2:=PHAS;S4:=DPHAS;
S3:=S1*sqrt(sqr(DFOR/FOR)+sqr(DDIS/DIS));


EDURE Simass(FREQ,MOD,THETA,DELMOD,DELTHE,DELFREQ,M:REAL;
                                                    VAR M1,M2,M3,M4:REAL);
FDASH,FDUBDASH,DEL,DEL2:REAL;
N
DEL:=0;
FDASH:=(MOD*cos(THETA))+(sqr(2*PI*FREQ)*M);
FDUBDASH:=MOD*sin(THETA);
M2:=(FDUBDASH/FDASH);
M1:=sqrt(sqr(FDASH)+sqr(FDUBDASH));
DEL:=2*(sqr(DELMOD/MOD)+sqr(DELFREQ/FREQ));
DEL:=DEL+sqr(sin(THETA)/cos(THETA)*sqr(DELTHE));
M4:=sqrt(DEL)*M2;M3:=sqrt(2*DEL)*M1;


EDURE Compmass(P1,P2,P3,P4,S1,S2,S3,S4:REAL;VAR M1,M2,M3,M4:REAL);
PLVER,SDVER,PLHOR,SDHOR,DEL1:REAL;
N
PLVER:=P1*sin(P2);PLHOR:=P1*cos(P2);
SDVER:=S1*sin(S2);SDHOR:=S1*cos(S2);
DEL1:=sqr(P4/P2)+sqr(S4/S2)+sqr(P3/P1)+sqr(S3/S1);
M1:=sqrt(sqr(SDVER-PLVER)+sqr(SDHOR-PLHOR));
M3:=(sqrt(4*DEL1))*M1;
M2:=(SDVER-PLVER)/(SDHOR-PLHOR);
M4:=(sqrt(2*DEL1))*M2;


EDURE Box(TITLE:STRING[48]);
L 50,51;
I:INTEGER;S,D,X,P:REAL;AGAIN:BOOLEAN;
N
'RITELN('M400,300,D400,2300,3400,2300,3400,300,400,300!!');AGAIN:=TRUE;
 :=300;D:=100;AGAIN:=TRUE;

 HILE D > 0.05 DO BEGIN
    FOR I:=2 TO 10 DO BEGIN
        X:=1554.9+(434.29*LN(I/D));
        IF (X >= 400) AND (X <= 3400) THEN
             WRITELN('M',X:5:2,',',S:5:2,',D',X:5:2,',',S+30:5:2,'!!,');
    END;
    D:=D/10;
 ND;
 F AGAIN THEN BEGIN AGAIN:=FALSE;S:=2270;D:=100;GOTO 50;END;
 :=230;WRITELN('S30,030,M520,250,P0.1!!,');
'RITELN('M1554.9,250,P1!!,M2535,250,P10!!,M3370,250,P70!!,M1500,120,S40');
'RITELN('Q40,PFREQUENCY / Hz!!,S55,Q55,M700,2400,P',TITLE,'!!,S30,Q30,');
 RITELN('Z3600,2300,');
 (* of box  *)

 DURE stiffax(C,G:INTEGER);
 ,X,Y:REAL;D,I:INTEGER;
N
 :=400;
 OR D:=0 TO C DO BEGIN
```

```
   X:=Power(10,D);
   Y:=285+(2000/C)*D;
   WRITELN('M270,',Y:5:2,',P10!!,00,15,P',D+G:1,'!!,');
   FOR I:=2 TO 10 DO BEGIN
        Y:=300+(2000/C)*0.434294*LN(I*X);
        IF Y <= 2300 THEN
            WRITELN('M',S:5:2,',',Y:5:2,'D',S+20:5:2,',',Y:5:2,'!!');
   END;
ND;
  (*  of stiffax  *)

DURE prinit(FREQ,DISP,DIST,VARB,VAST,PHAS,PHST:REAL);

RITE(FREQ:6:3,'   ',DISP:10,' +-',DIST:9,'   ',VARB:10,' +-',VAST:9);
RITELN('   ',PHAS:9:4,' +-',PHST:9);


DURE Pointplot(FREQ,VARB,VAST,FACTOR:REAL;A:INTEGER);
 87;
,Y,B:REAL;

:=1554.9+(434.29*LN(FREQ));
:=300+(FACTOR*VARB);
F (VARB-VAST < 0.01*VARB) OR (VARB-VAST > 0.5*VARB) THEN GOTO 87;
:=FACTOR*VAST;
RITELN('M',X:5:2,',',Y-B:5:2,'D',X:5:2,',',Y+B:5:2,'!!,');

RITELN('M',X:5:2,',',Y:5:2,',N',A:2);



DURE Pointplot2(FREQ,VARB,VAST,FACTOR:REAL;A,G:INTEGER);
 88;
,Y,Y1,Y2:REAL;

:=1554.99+(434.29*LN(FREQ));
:=300+FACTOR*0.434294*LN(VARB/Power(10,G));
F (VARB-VAST < 0.01*VARB) OR (VARB-VAST > 0.5*VARB) THEN GOTO 88;
1:=VARB+VAST;Y2:=VARB-VAST;
1:=300+FACTOR*0.434294*LN(Y1/Power(10,G));
2:=300+FACTOR*0.434294*LN(Y2/Power(10,G));
RITELN('M',X:5:2,',',Y2:5:2,'D',X:5:2,',',Y1:5:2,'!!,');

RITELN('M',X:5:2,',',Y:5:3,',N',A:2);


URE Epsomon(P1,P2:STRING[80];TIT:STRING[30];D,N:STRING[8]);
:INTEGER;

 rprint;Printeron;
RITELN(chr(14),'File ',N,TIT);
RITELN;WRITELN(chr(14),' file dated ',D,'.');
RITELN;WRITELN;WRITELN(P1);WRITELN(P2);WRITELN;
RITELN('  DIGITAL RESULTS------');WRITELN;
 (* of epsomon  *)

URE Epsomoff(H,W,L,STAT,DEFH,TEMP,HUMID:REAL;FAT:INTEGER;NAME:STRING[8]);
```

```
WRITELN;WRITELN('Static force    = ',STAT:5:1,' N');
RITELN;WRITELN('Deformed height= ',DEFH:6:4,' m');
RITELN;WRITE('Sample temp.    = ',TEMP:3:1,' ',chr(27),'S',chr(0),'0');
RITELN(chr(27),'T','C');
'RITELN;WRITELN('Humidity        = ',HUMID:3:0,' %');WRITELN;
'RITELN;WRITELN(chr(14),'Plate used   ',PAT:2);WRITELN;
'RITELN;WRITELN(chr(14),'Static strain  = ',(H-DEFH)*100/H:5:2,' % ');
RITELN;WRITELN(chr(14),'Sample dimensions ');WRITELN;
'RITELN(chr(14),'     ',L:5:3,' X ',W:5:3,' X ',H:5:3,'  metre'); WRITELN;
RITELN;WRITELN;WRITELN(chr(14),'File ',NAME ,' end.',chr(12));
'rinteroff;


DURE Watanabeon(STORE,LOSS,COMP:BOOLEAN;VAR UP,LO:INTEGER;VAR HITAN:REAL);
 35;
,X,SCAL:REAL;I,E,NUMB,NUMB2:INTEGER;
ITLE:STRING[48];ST:STRING[1];
]
'RITE(' Is plotter connected Y? ');READLN(ST);
RITELN(' Enter the plot title , <48 characters ');READLN(TITLE);
F COMP THEN BEGIN
     WRITE('Upper MODULUS limit in powers of 10? ');READLN(UP);
     WRITE('Lower MODULUS limit in powers of 10? ');READLN(LO);
     WRITE('Highest loss tangent ? ');READLN(HITAN);
     NUMB:=round(HITAN*2);SCAL:=0.5;
ND ELSE BEGIN NUMB:=9;SCAL:=20;END;
erprint;Printeron;WRITE(':,');FOR I:=1 TO 2000 DO;
RITELN('=!!,S30,Q30,');Printeroff;
'RITE('Do you want 1/4 page printout? Y/N ');READLN(ST);
F ST='Y' THEN BEGIN
     WRITE('Which quadrant 1-4 ? ');READLN(E);
     Printeron;WRITE('&,1,1,2,');
     CASE E OF
          1:WRITELN('^-90,1270,');
          2:WRITELN('^-90,0,');
          3:WRITELN('^1910,1270,');
          4:WRITELN('^1910,0,');
     END;Printeroff;
ND ELSE BEGIN WRITE('How about A4 size Y/N ? ');READLN(ST);
     IF ST='Y' THEN BEGIN
          Printeron;WRITELN('&,7,7,10,^300,300');Printeroff;
     END;
ND;
'RITE(' Do you need the scales drawing Y/N? ');READLN(ST);
F ST<>'Y' THEN BEGIN Printeron;GOTO 35;END;
'rinteron;Box(TITLE);
F COMP THEN stiffax(UP-LO,LO) ELSE stiffax(3,3);
'RITELN('R900,S40,Q40,M240,1050,');
F COMP THEN BEGIN
    IF STORE THEN WRITELN('PStorage Modulus N/m!!');
    IF LOSS THEN WRITELN('PLoss Modulus N/m!!');
    IF NOT STORE AND NOT LOSS THEN WRITELN('PComplex Modulus N/m!!');
ND ELSE WRITELN('PComplex Modulus N/m!!');
'RITE('O-30,15,S20,P2!!,S30,Q30,R0,M3400,300,X2,2000,');
F COMP THEN WRITELN(trunc(HITAN*10),',') ELSE WRITELN('18,');
:=3430;
OR I:=1 TO NUMB DO BEGIN
  X:=290+(2000/NUMB)*I;
```

```
   WRITELN('M',S:5:2,',',X:5:2,',P',(SCAL*I):3:1,'!!');
END;
WRITELN('R900,S40,Q40,M3650,1320,');
IF COMP THEN WRITELN('PLoss tangent!!') ELSE WRITELN('PLoss angle / deg!!'),

WRITELN('R0,S35,Q35,');
  (* of Watanabeon *)


N
:
HEADER:='  ANALYIS AND DISPLAY SECTION  ';Topline(HEADER);

Screenclear;
WRITELN('******************** MENU ************************');
WRITELN('**     <R>   To read or re-read raw data       **');
WRITELN('**                                             **');
WRITELN('**     <S>   To calculate dynamic modulus      **');
WRITELN('**     <V>   For hard copy of dynamic modulus  **');
WRITELN('**     <P>   To plot dynamic modulus           **');
WRITELN('**                                             **');
WRITELN('**     <M>   Move to mass compensation menu    **');
WRITELN('**                                             **');
WRITELN('**     <A>   Return to CONTROL program         **');
WRITELN('**     <C>   To chain to another program       **');
WRITELN('**     <H>   To abort program                  **');
WRITELN('*************************************************');
WRITE(' ? ');READ(MENU);Backspace;WRITELN(MENU);
CASE MENU OF
    'R':BEGIN
          Screenclear;Drive(2);
          WRITE('Disc in drive 2 is ',Discname,' is this OK?Y');READLN(ST)

          WRITELN;WRITE('Which file is to be accessed ? ');READLN(NAME);
          WRITELN;Openread(BAD,NAME);
          IF BAD THEN BEGIN WRITELN('File not present on disc,try again');
                      GOTO 20;END;
          WRITELN('File  ',NAME,'  opened ');WRITELN;
          Readinteger(BAD,Q);Readinteger(BAD,Z);
          FOR I:=1 TO Q DO FOR J:=1 TO 8 DO Readreal(BAD,DI[I,J);
          FOR I:=1 TO Z DO FOR J:=1 TO 8 DO Readreal(BAD,AN[I,J);
          Readreal(BAD,STAT);Readreal(BAD,L);Readreal(BAD,W);
          Readreal(BAD,H);Readinteger(BAD,PAT);Readstring(BAD,DATE);
          Readreal(BAD,DEFH);Readreal(BAD,TEMP);Readreal(BAD,HUMID);
          WRITELN;Clseqread;WRITELN('File ',NAME,' closed.');
          FOR I:=1 TO 20000 DO;REDEM:=TRUE;
        END;
    'A':BEGIN Drive(0);Chain('control');END;
    'C':BEGIN Drive(0);WRITE('Enter prog file name,drive 0 ');READLN(NAME);
          Chain(NAME);Drive(2);END;
    'H':GOTO FINI;
    'S':BEGIN
          FOR I:=1 TO Q DO Stiff(DI[I,1],DI[I,2],DI[I,4],DI[I,5],DI[I,6],
                                 DI[I,7],SD[I,1],SD[I,2],SD[I,3],SD[I,4],W,H,L);
          FOR I:=1 TO Z DO Stiff(AN[I,1],AN[I,2],AN[I,4],AN[I,5],AN[I,6],
                                 AN[I,7],SA[I,1],SA[I,2],SA[I,3],SA[I,4],W,H,L);
        END;
    'V':BEGIN WRITE('Is Rx-80 on line ?Y ');READLN(ST);
```

```
:='FREQ.          DISPLACEMENT                MODULUS              PHASDIFERENCE';
:='(Hz)               (m)                      (N/m)                  (deg.)    ';
            HEAD:=' modulus results';
            Epsomon(PRI1,PRI2,HEAD,DATE,NAME);
            FOR I:=1 TO Q DO
                prinit(DI[I,3],DI[I,1],DI[I,5],SD[I,1],SD[I,3],
                       SD[I,2]/RAD,SD[I,4]/RAD);
            WRITELN;WRITELN('  ANALOG RESULTS------');WRITELN;
            FOR I:=1 TO Z DO
                prinit(AN[I,3],AN[I,1],AN[I,5],SA[I,1],SA[I,3],
                       SA[I,2]/RAD,SA[I,4]/RAD);
            Epsomoff(H,W,L,STAT,DEFH,TEMP,HUMID,PAT,NAME);
        END;
    'M':GOTO MASSCOM;
    'P':BEGIN
            Watanabeon(FALSE,FALSE,FALSE,UP,LO,HITAN);
            FOR I:=1 TO Q DO Pointplot2(DI[I,3],SD[I,1],SD[I,3],2000/3,2,3);
            FOR I:=1 TO Z DO Pointplot2(AN[I,3],SA[I,1],SA[I,3],2000/3,4,3);
            WRITELN('J2,');
            FOR I:=1 TO Q DO Pointplot(DI[I,3],SD[I,2]/RAD,SD[I,4]/RAD,
                                                              100/9,14);
            FOR I:=1 TO Z DO Pointplot(AN[I,3],SA[I,2]/RAD,SA[I,4]/RAD,
                                                              100/9,15);
            WRITELN('H,');Printeroff;
        END;
ND;GOTO 10;


OM:
EADER:='  MASS COMPENSATION SECTION ';Topline(HEADER);

creenclear;
'RITELN('******************** MENU ************************');
 RITELN('**                                              **');
'RITELN('**  <S>   For simple mass compensation          **');
'RITELN('**  <C>   For "dry run" mass compensation       **');
'RITELN('**                                              **');
!RITELN('**  <W>   For hard copy of complex modulus      **');
!RITELN('**  <V>   Hard copy of loss & storage moduli    **');
!RITELN('**  <P>   To plot compensated results           **');
'RITELN('**                                              **');
'RITELN('**  <F>   To record mass compensated results    **');
'RITELN('**  <L>   Move to main menu                     **');
!RITELN('**  <H>   To abort program                      **');
.RITELN('**                                              **');
!RITELN('**************************************************');
!RITE(' ? ');READ(MENU);Backspace;WRITELN(MENU);
ASE MENU OF
    'H':GOTO FINI;
    'L':GOTO MAIN;
    'S':BEGIN
            Screenclear;Drive(0);Openread(BAD,'massfile');
            FOR I:=1 TO PAT DO BEGIN
                Readreal(BAD,MM[1]);Readreal(BAD,MM[2]);Readreal(BAD,MM[3]);
            END;
            WRITE('Fluid identification letter? ');READ(ST);WRITELN(ST);
            CASE ST OF 'A':M:=MM[1];'W':M:=MM[2];'O':M:=MM[3];END;
            Closeqread;Drive(2);M:=(M*H)/(W*L);
```

```
        FOR I:=1 TO Q DO
            Simass(DI[I,3],SD[I,1],SD[I,2],SD[I,3],SD[I,4],DI[I,8],M,
                   MD[I,1],MD[I,2],MD[I,3],MD[I,4]);
        FOR I:=1 TO Z DO
            Simass(AN[I,3],SA[I,1],SA[I,2],SA[I,3],SA[I,4],AN[I,8],M,
                   MA[I,1],MA[I,2],MA[I,3],MA[I,4]);
        COMP:=TRUE;
    END;
'C':BEGIN
        LLF:=4.0;
        WRITE('Enter fluid identification letter ');READ(ST);
        WRITELN(ST);
        Openread(BAD,concat('PLATE',ItoS(PAT),ST));
        IF BAD THEN GOTO 101;
        Readinteger(BAD,R);Readinteger(BAD,P);
        FOR I:=1 TO R DO BEGIN
            FOR J:=1 TO 8 DO Readreal(BAD,PLD[I,J]);
            Stiff(PLD[I,1],PLD[I,2],PLD[I,4],PLD[I,5],PLD[I,6],
                  PLD[I,7],DP[I,1],DP[I,2],DP[I,3],DP[I,4],W,H,L);
        END;
        FOR I:= 1 TO Q DO BEGIN
            IF DI[I,3]<LLF THEN BEGIN
                MD[I,1]:=SD[I,1];MD[I,3]:=SD[I,3];
                MD[I,2]:=sin(SD[I,2])/cos(SD[I,2]);
                MD[I,4]:=sin(SD[I,4])/cos(SD[I,4]);
            END ELSE BEGIN
                MIN:=10;
                FOR J:=1 TO R DO Comparator(PLD[J,3],DI[I,3],MIN,J,IND);
                IF MIN=10 THEN BEGIN
                    WRITE('No match for this run aborting compensation');
                    Clseqread;GOTO 101;
                END ELSE BEGIN
                    compmass(DP[IND,1],DP[IND,2],DP[IND,3],DP[IND,4],
                          SD[I,1],SD[I,2],SD[I,3],SD[I,4],MD[I,1],MD[I,2],
                          MD[I,3],MD[I,4]);
                END;
            END;
        END;
        FOR I:=1 TO P DO BEGIN
            FOR J:=1 TO 8 DO Readreal(BAD,PLA[I,J]);
            Stiff(PLA[I,1],PLA[I,2],PLA[I,4],PLA[I,5],PLA[I,6],
                  PLA[I,7],AP[I,1],AP[I,2],AP[I,3],AP[I,4],W,H,L);
        END;
        FOR I:=1 TO Z DO BEGIN
            IF AN[I,3]<LLF THEN BEGIN
                MA[I,1]:=SA[I,1];MA[I,3]:=SA[I,3];
                MA[I,2]:=sin(SA[I,2])/cos(SA[I,2]);
                MA[I,4]:=sin(SA[I,4])/cos(SA[I,4]);
            END ELSE BEGIN
                MIN:=10;
                FOR J:=1 TO P DO Comparator(PLA[J,3],AN[I,3],MIN,J,IND);
                IF MIN=10 THEN BEGIN
                    WRITE('No match for this run aborting compensation').
                    Clseqread;GOTO 101;
                END ELSE BEGIN
                    compmass(AP[IND,1],AP[IND,2],AP[IND,3],AP[IND,4],
                          SA[I,1],SA[I,2],SA[I,3],SA[I,4],MA[I,1],MA[I,2],
                          MA[I,3],MA[I,4]);
```

```
                END;
            END;
        END;
        Clseqread;
        COMP:=TRUE;
    END;
'P':BEGIN
        STORE:=FALSE;LOSS:=FALSE;
        WRITE('S torage or L oss or C omplex Modulus plot ?');READLN(TP);
        CASE TP OF
            'S':STORE:=TRUE;
            'L':LOSS:=TRUE;
        END;
        Watanabeon(STORE,LOSS,COMP,UP,LO,HITAN);
        FOR I:=1 TO Q DO BEGIN
            IF STORE THEN CMOD:=MD[I,1]*cos(arctan(MD[I,2]));
            IF LOSS THEN CMOD:=MD[I,1]*sin(arctan(MD[I,2]));
            IF NOT LOSS AND NOT STORE THEN CMOD:=MD[I,1];
            DCMOD:=(MD[I,3]/MD[I,1])*CMOD;
            Pointplot2(DI[I,3],CMOD,DCMOD,2000/(UP-LO),2,LO);
        END;
        FOR I:=1 TO Z DO BEGIN
            IF STORE THEN CMOD:=MA[I,1]*cos(arctan(MA[I,2]));
            IF LOSS THEN CMOD:=MA[I,1]*sin(arctan(MA[I,2]));
            IF NOT LOSS AND NOT STORE THEN CMOD:=MA[I,1];
            DCMOD:=(MA[I,3]/MA[I,1])*CMOD;
            Pointplot2(AN[I,3],CMOD,DCMOD,2000/(UP-LO),4,LO);
        END;
        WRITELN('J2,');
        FOR I:=1 TO Q DO
            Pointplot(DI[I,3],MD[I,2],MD[I,4],2000/HITAN,14);
        FOR I:=1 TO Z DO
            Pointplot(AN[I,3],MA[I,2],MA[I,4],2000/HITAN,15);
        WRITELN('H,');Printeroff;GOTO 101;
    END;
'W':BEGIN WRITE('Is Rx-80 on line ?Y ');READLN(ST);
:='FREQ.          DISPLACEMENT                MODULUS              LOSS TANGENT '
:='(Hz)               (m)                     (N/m*m)                           '
        HEAD:=' complex modulus';
        Epsomon(PRI1,PRI2,HEAD,DATE,NAME);
        FOR I:=1 TO Q DO
            prinit(DI[I,3],DI[I,1],DI[I,5],MD[I,1],MD[I,3],MD[I,2],
                MD[I,4]);
        WRITELN;WRITELN('  ANALOG RESULTS------');WRITELN;
        FOR I:=1 TO Z DO
            prinit(AN[I,3],AN[I,1],AN[I,5],MA[I,1],MA[I,3],MA[I,2],
                MA[I,4]);
        Epsomoff(H,W,L,STAT,DEFH,TEMP,HUMID,PAT,NAME);
    END;
'V':BEGIN WRITE('Is Rx-80 on line ?Y ');READLN(ST);
        WRITELN('Do you want true modulus (including change in');
        WRITE('height due to strain imposed ? Y/N '); READLN(TM);
:='FREQ.        LOSS MODULUS              STORAGE MODULUS          LOSS TANGENT'
:='(Hz)             (N/m*m)                   (N/m*m)                         '
        IF TM='Y' THEN HEAD:='true storage & loss mod.'
            ELSE HEAD:=' storage & loss moduli';
        Epsomon(PRI1,PRI2,HEAD,DATE,NAME);
        FOR I:=1 TO Q DO BEGIN
```

```
            STMOD:=MD[I,1]*cos(arctan(MD[I,2]));
            LOMOD:=MD[I,1]*sin(arctan(MD[I,2]));
            DELST:=(MD[I,3]/MD[I,1])*STMOD;
            DELOS:=(MD[I,3]/MD[I,1])*LOMOD;
            IF TM='Y' THEN
                 prinit(DI[I,3],LOMOD*DEFH/H,DELOS,STMOD*DEFH/H,DELST,
                        MD[I,2],MD[I,4])
            ELSE prinit(DI[I,3],LOMOD,DELOS,STMOD,DELST,MD[I,2],
                        MD[I,4]);
        END;
        WRITELN;WRITELN('  ANALOG RESULTS------');WRITELN;
        FOR I:=1 TO Z DO BEGIN
            STMOD:=MA[I,1]*cos(arctan(MA[I,2]));
            LOMOD:=MA[I,1]*sin(arctan(MA[I,2]));
            DELST:=(MA[I,3]/MA[I,1])*STMOD;
            DELOS:=(MA[I,3]/MA[I,1])*LOMOD;
            IF TM='Y' THEN
                 prinit(AN[I,3],LOMOD*DEFH/H,DELOS,STMOD*DEFH/H,DELST,
                        MA[I,2],MA[I,4])
            ELSE prinit(AN[I,3],LOMOD,DELOS,STMOD,DELST,MA[I,2],MA[I,4])
        END;
        Epsomoff(H,W,L,STAT,DEFH,TEMP,HUMID,PAT,NAME);
    END;
'F':BEGIN Screenclear;Drive(2);WRITE('Disc in 2 is, ',Discname);
        WRITELN(' name of file ? ');READLN(NAME);

        Prepwrite(BAD,20,NAME);
        IF BAD THEN BEGIN
            WRITELN('File already exists...');
            WRITELN(' X : to delete disc file');
            WRITE(' N : for new file name  ');READLN(ST);
            CASE ST OF
              'X':BEGIN Delete(BAD,NAME);GOTO 62;END;
              'N':BEGIN WRITE('Enter new name');READLN(NAME);GOTO 62;END
            END;
        END;
        WRITELN(' File ',NAME,' opened');
        Writeinteger(Q);Writeinteger(Z);
        FOR I:=1 TO Q DO BEGIN
            Writereal(DI[I,3]);
            FOR J:=1 TO 4 DO Writereal(MD[I,J]);
        END;
        FOR I:=1 TO Z DO BEGIN
            Writereal(AN[I,3]);
            FOR J:=1 TO 4 DO Writereal(MA[I,J]);
        END;
        Writereal(H);Writereal(W);Writereal(L);Writereal(STAT);
        Writereal(DEFH);Writereal(TEMP);Writereal(HUMID);
        Writestring(DATE);Clseqwr;WRITELN('Transfer complete ');
        FOR I:=1 TO 2000 DO;
    END;
END;GOTO 101;
```

APPENDIX III

FLOW CHARTS FOR THE MACHINE CODE ROUTINES OF THE DYNAMIC MECHANICAL SPECTROMETER'S CONTROL SYSTEM

The Machine Code Routine INIT

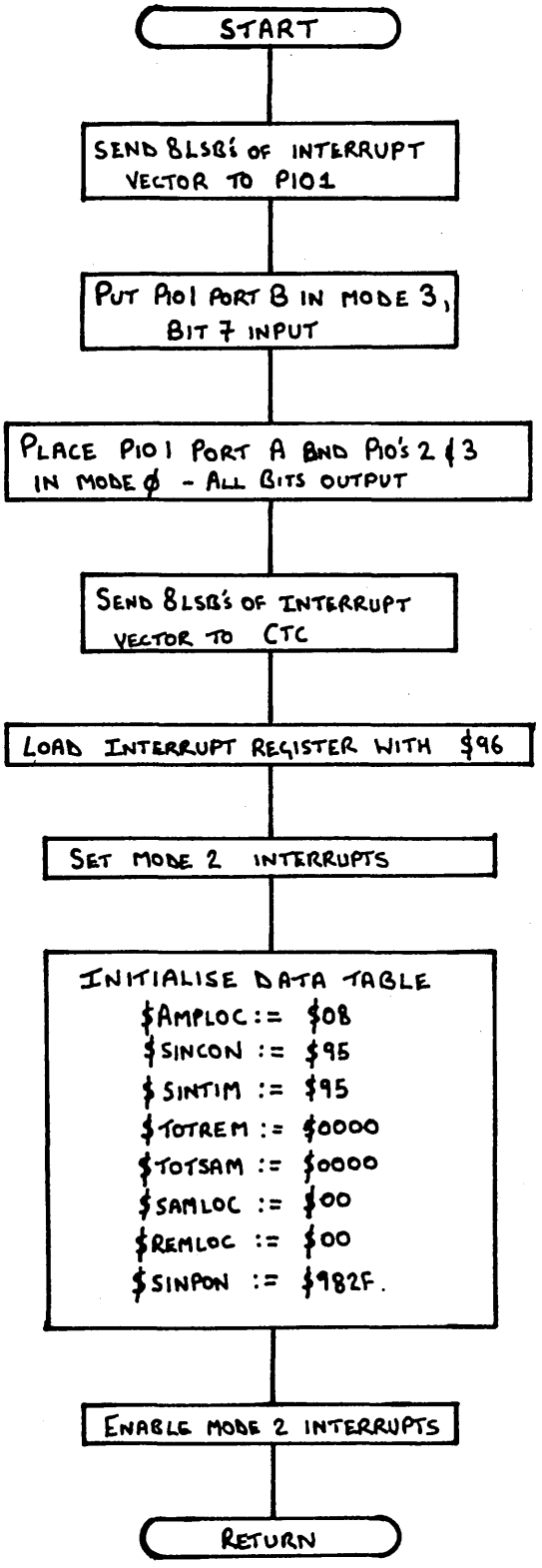

The Machine Code Routine FREQER

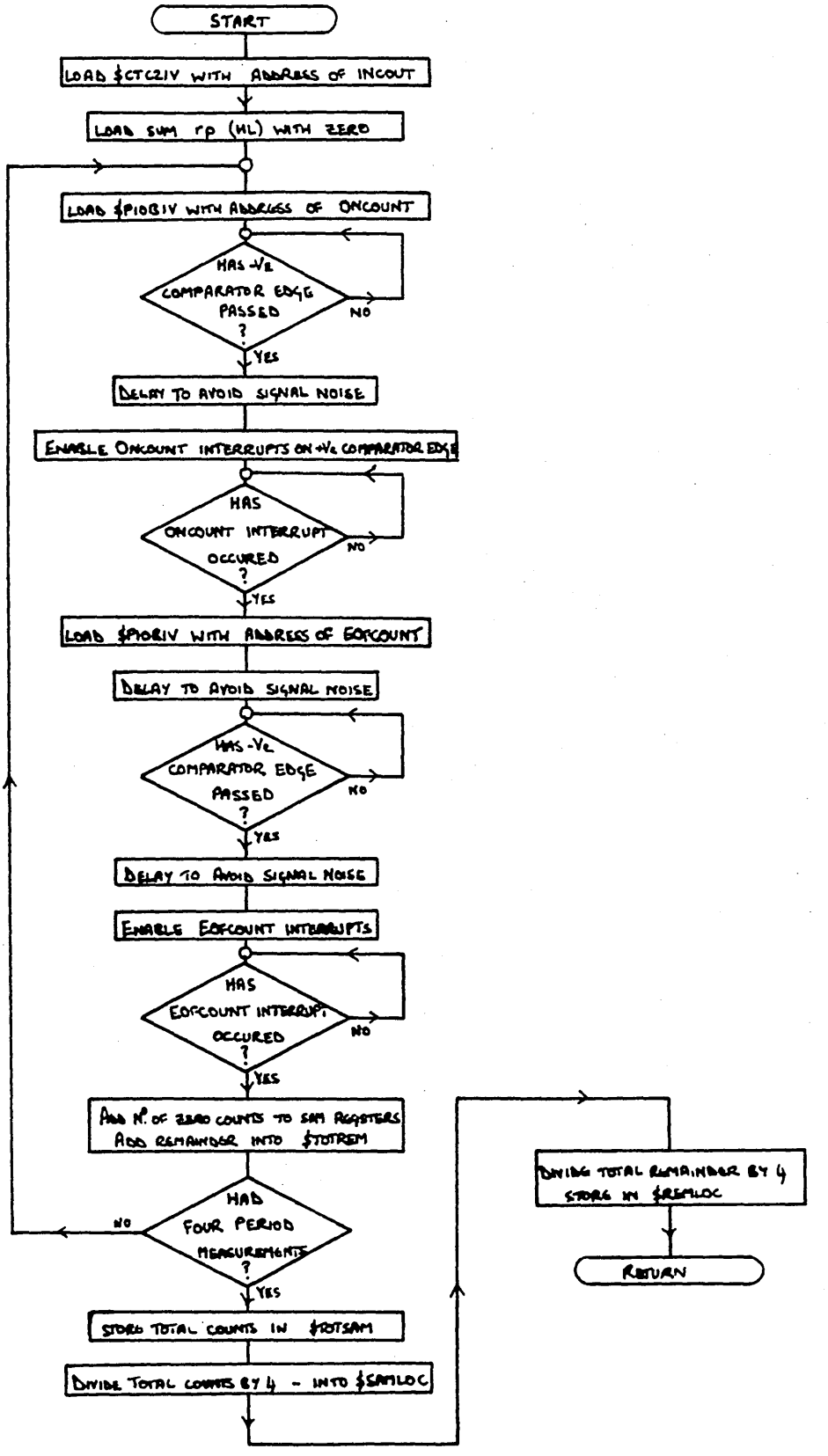

The Machine Code Routine DROP

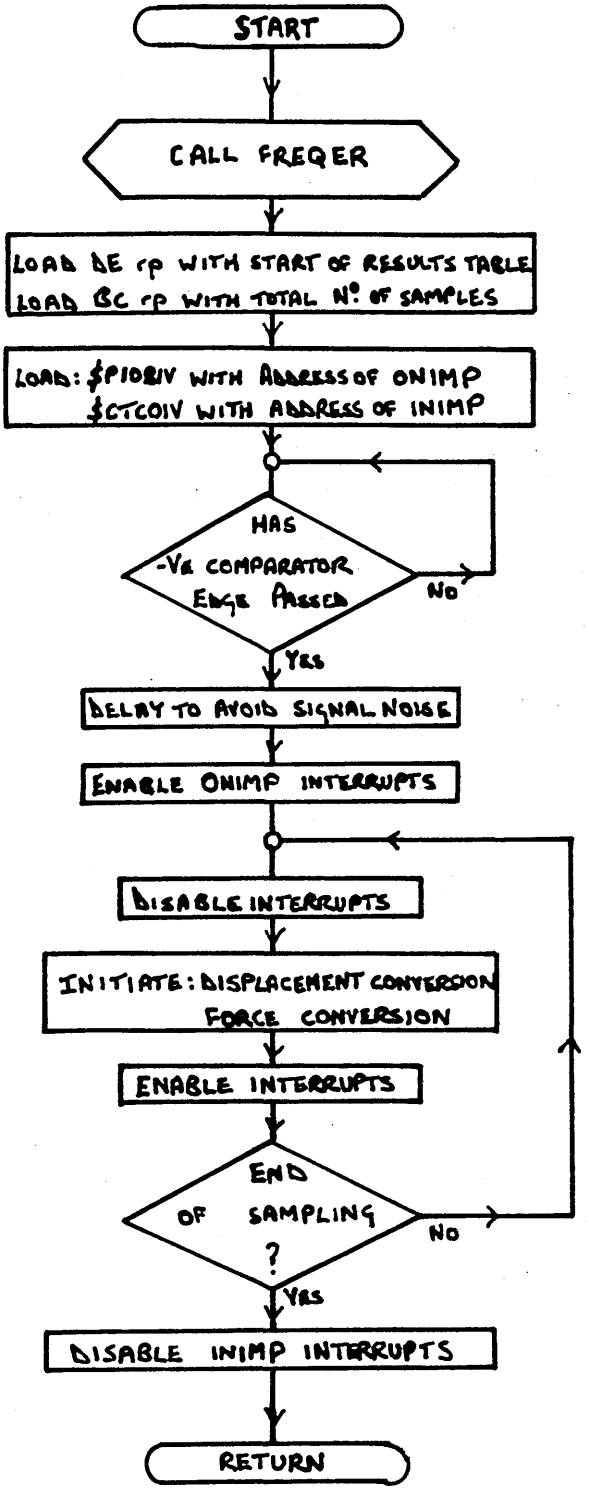

The Machine Code Routine DROP2

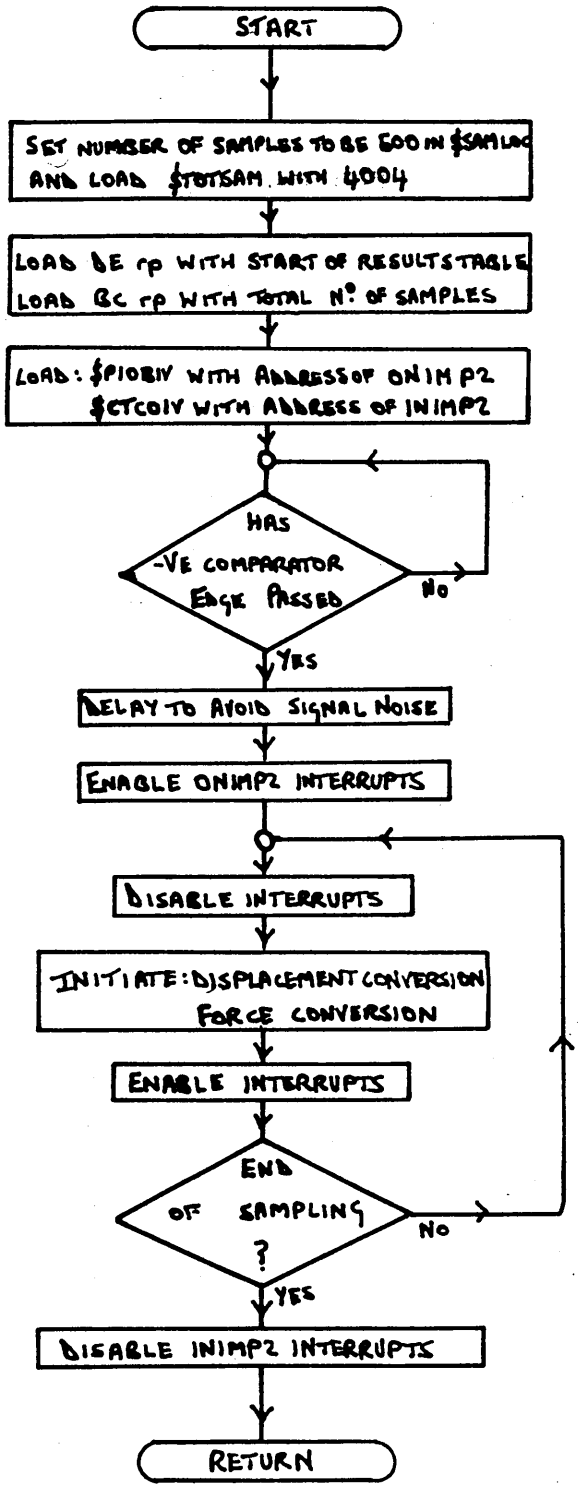

The Machine Code Routine SINGEN

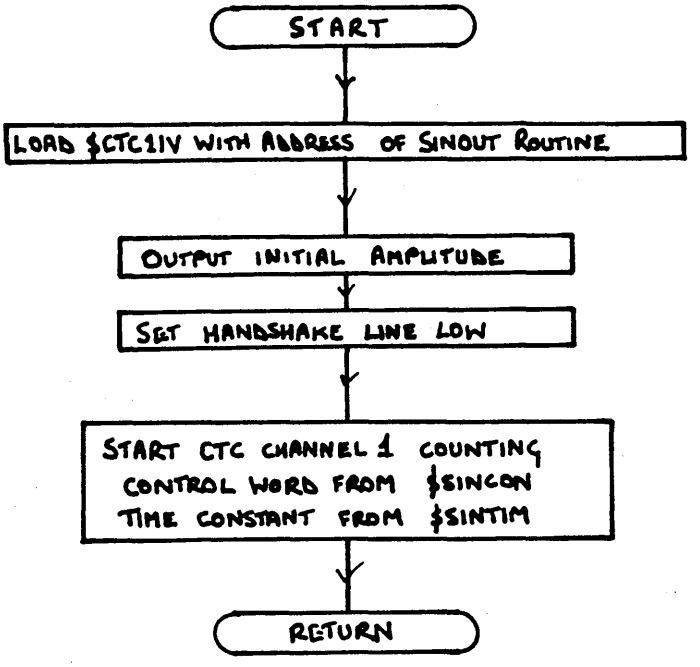

The Interrupt Service Routine SINOUT

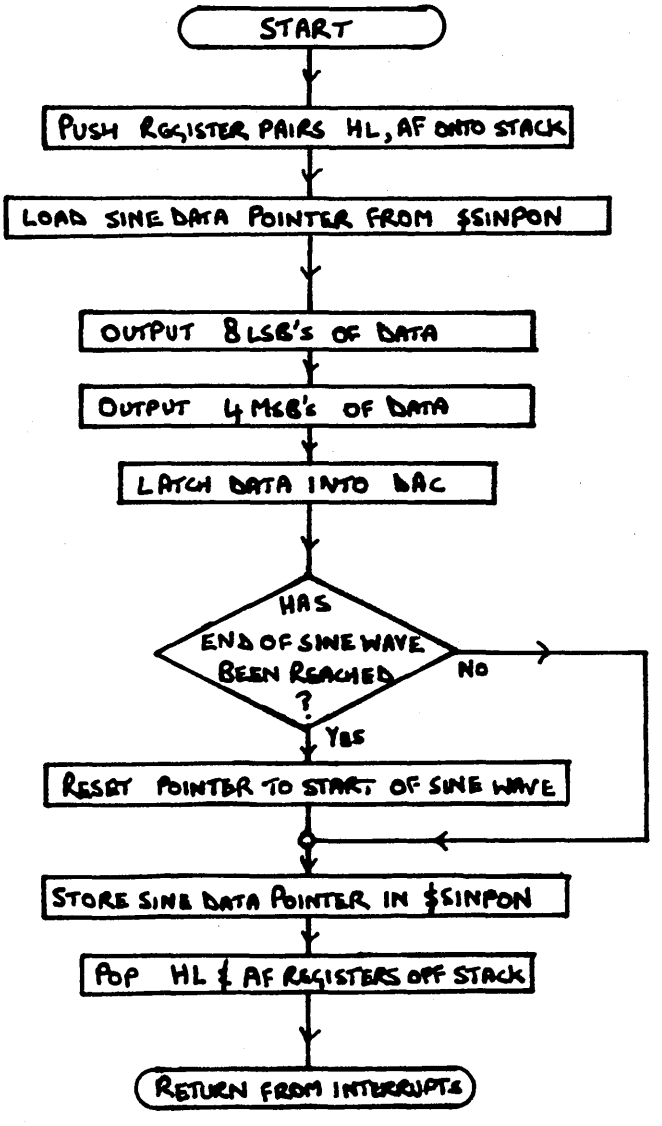

The Machine Code Routine **NEWAMP**

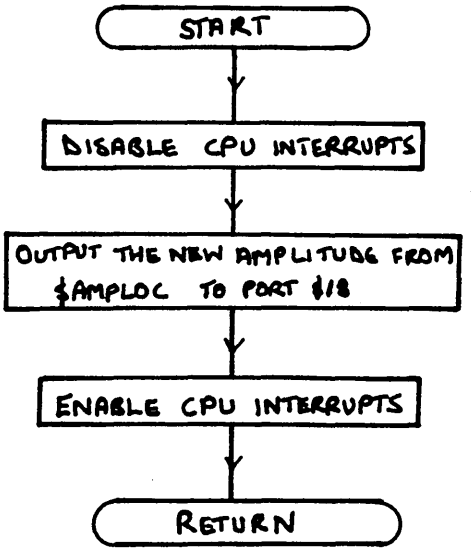

The Machine Code Routine **STOSIN**

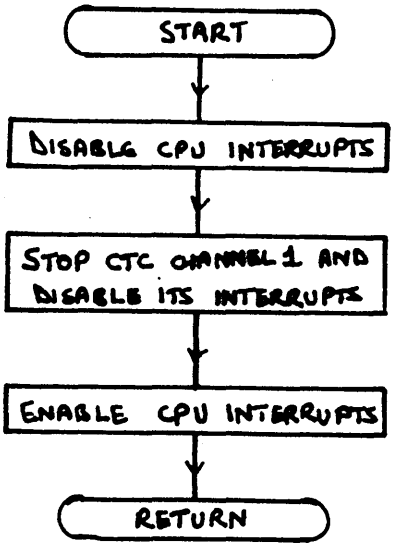

The Machine Code Routine UPSWP

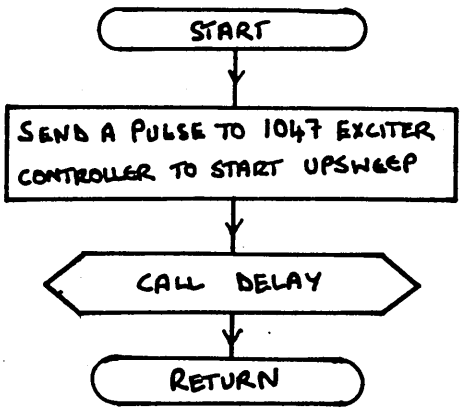

The Machine Code Routine DNSWP

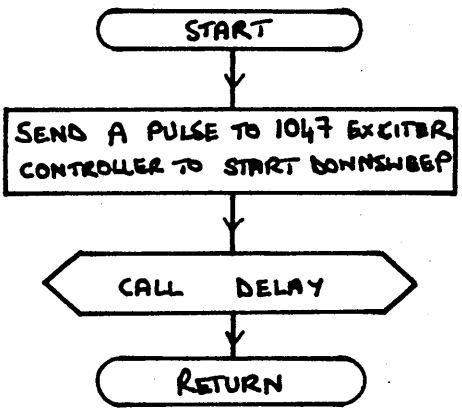

The Machine Code Subroutine DELAY

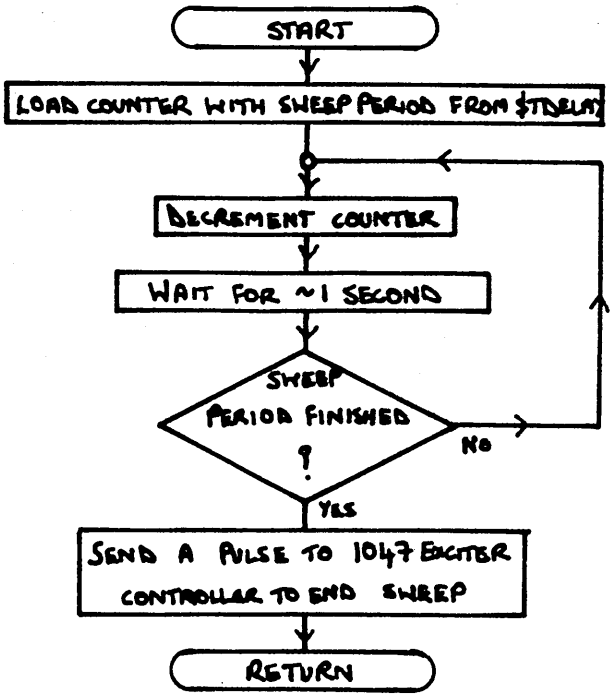

The Interrupt Service Routine **ONCOUNT**

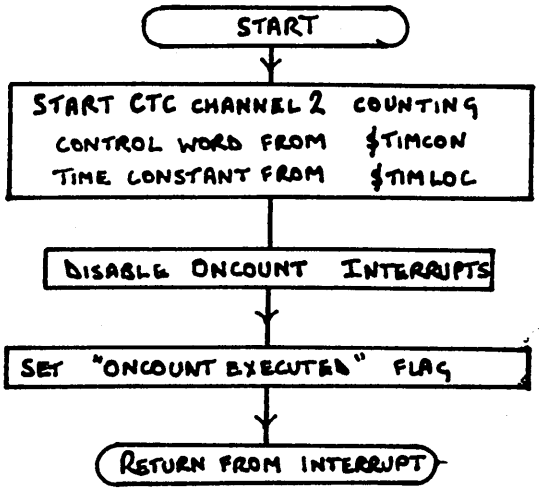

The Interrupt Service Routine **INCOUNT**

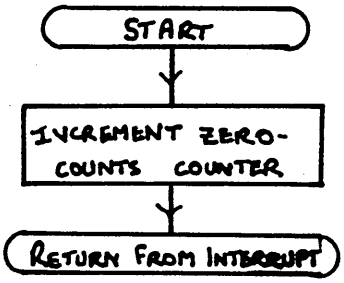

The Interrupt Service Routine **EOFCOUNT**

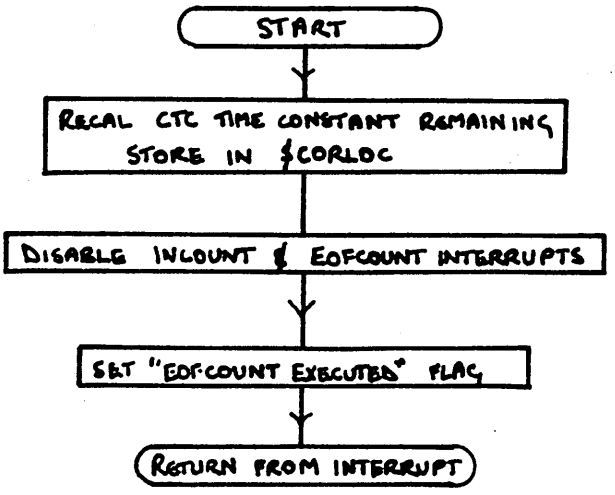

The Interrupt Service Routine **ONIMP**

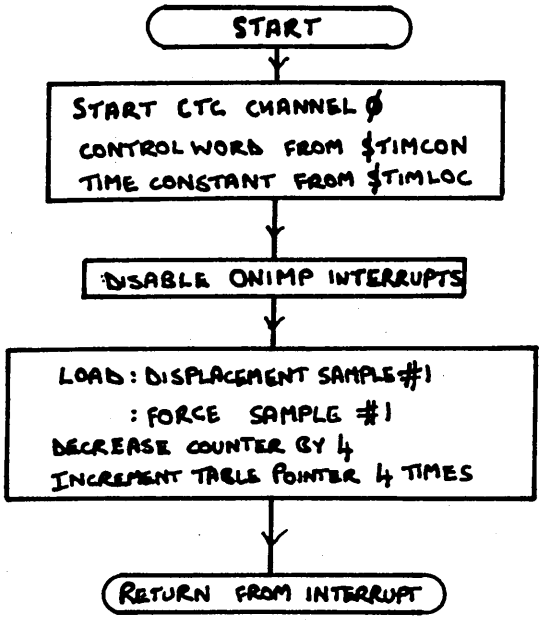

The Interrupt Service Routine **INIMP**

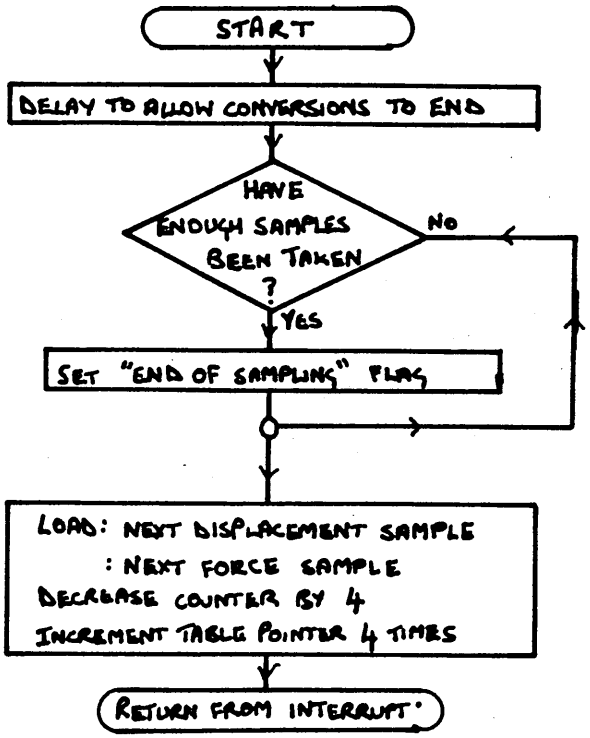

The Interrupt Service Routine ONIMP2

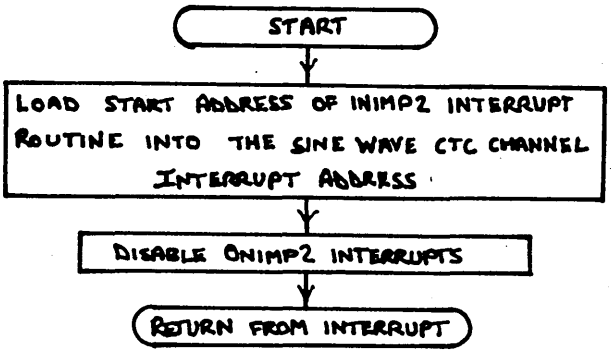

The Interrupt Service Routine INIMP2

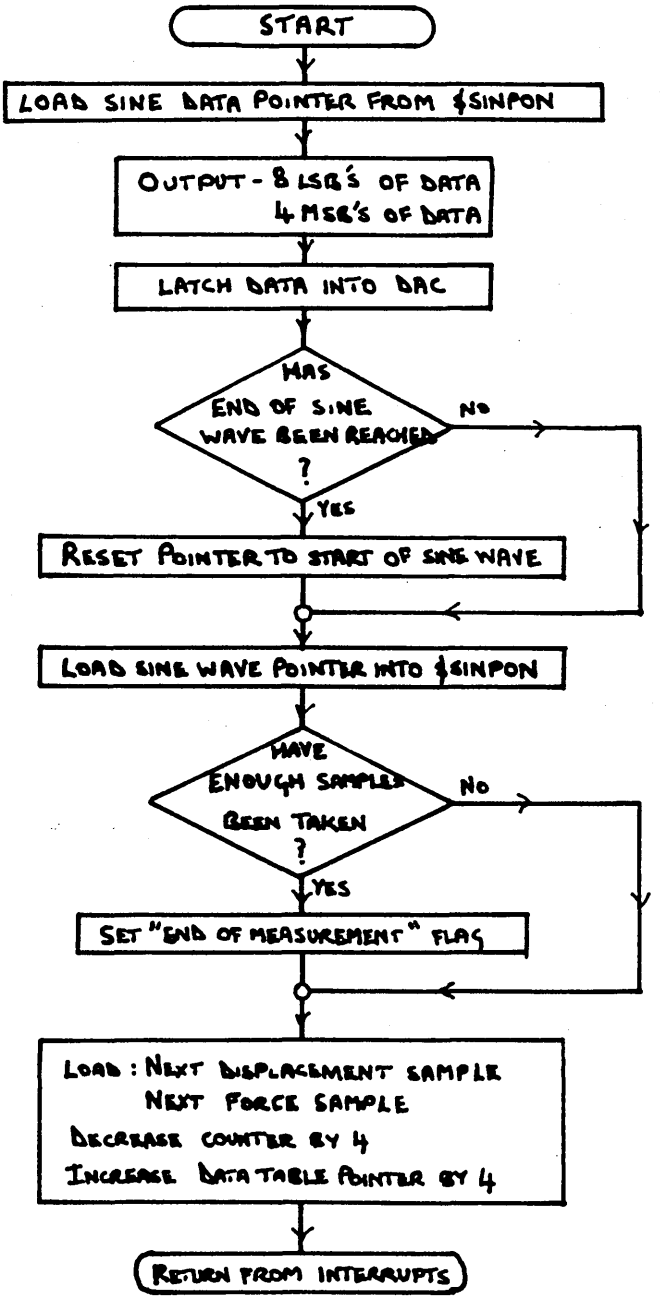

APPENDIX IV

Z80 ASSEMBLER SOURCE CODE LISTINGS OF THE MACHINE CODE ROUTINES IN THE SPECTROMETER'S CONTROL SYSTEM

```
                    0010 ;%%%
```

```
B400            0530        ORG  0B400H
                0540 ;
B400 CD50B4     0550        CALL INIT
B403 C9         0560        RET
B404 CDE3B5     0570        CALL SINGEN
B407 C9         0580        RET
B408 CD37B5     0590        CALL DROP
B40B C9         0600        RET
B40C CDFEB5     0610        CALL UPSWP
B40F C9         0620        RET
B410 CD0AB6     0630        CALL DNSWP
B413 C9         0640        RET
B414 CD16B6     0650        CALL STOSIN
B417 C9         0660        RET
B418 CD1DB6     0690        CALL NEWAMP
B41B C9         0700        RET
B41C CD82B5     0710        CALL DROP2
B41F C9         0720        RET
B420 CD9EB4     0730        CALL FREQER
B423 C9         0740        RET
                0750 ;
                0760 ; The next table holds jump addresses for
                0770 ;the interrupt service routines used....
                0780 ;
B430            0790        ORG  0B430H
                0800 ;
B430 CD20B7     0810        CALL SINOUT
B433 C9         0820        RET
B434 CD00B7     0830        CALL ONCNT
B437 C9         0840        RET
B438 CD48B7     0850        CALL EOFCNT
B43B C9         0860        RET
B43C CD70B7     0870        CALL INCNT
B43F C9         0880        RET
B440 CD80B7     0890        CALL ONIMP
B443 C9         0900        RET
B444 CD00B8     0910        CALL INCIMP
B447 C9         0920        RET
B448 CDB0B7     0930        CALL ONIMP2
B44B C9         0940        RET
B44C CD80B8     0950        CALL INIMP2
                0960 ;
                0970 ;
                0980 ;*********************************************
                0990 ;**                                         **
                1000 ;**      INITIALISATION  ROUTINE            **
                1010 ;**                                         **
                1020 ;**              "INIT"                     **
                1030 ;*********************************************
                1040 ;
                1050 ;
B450            1060        ORG  0B450H
                1070 ;
                1080 ; Send the PIO1 B Interrupt vector
                1090 ;
B450 3EF0       1100 INIT   LD   A,0F0H
B452 D307       1110        OUT  (07H),A
                1120 ;
```

```
                1130 ; Put PIO1 A in mode 3 ....
                1140 ;
B454 3ECF       1150        LD   A,0CFH
B456 D307       1160        OUT  (07H),A
                1170 ;
                1180 ;...Bit 7 input,the rest output
                1190 ;
B458 3E80       1200        LD   A,80H
B45A D307       1210        OUT  (07H),A
                1220 ;
                1230 ; Put PIO's 2 & 3 in mode 0
                1240 ;
B45C 3E0F       1250        LD   A,0FH
B45E D306       1260        OUT  (06H),A
B460 D316       1270        OUT  (16H),A
B462 D317       1280        OUT  (17H),A
B464 D31A       1290        OUT  (1AH),A
                1300 ;
                1310 ; Send the CTC Interrupt vector
                1320 ;
B466 3EF8       1330        LD   A,0F8H
B468 D308       1340        OUT  (08H),A
                1350 ;
B46A 3E96       1360        LD   A,96H
B46C ED47       1370        LD   I,A
B46E ED5E       1380        IM   2
                1390 ;
B470 3E08       1400        LD   A,08H
B472 32D096     1410        LD   (AMPLOC),A
                1420 ;
B475 3E95       1430        LD   A,95H
B477 32E496     1440        LD   (SINCON),A
B47A 32E596     1450        LD   (TIMCON),A
                1460 ;
B47D 210000     1470        LD   HL,0000H
B480 22E696     1480        LD   (TOTREM),HL
B483 22E896     1490        LD   (TOTSAM),HL
B486 22EA96     1500        LD   (SAMLOC),HL
B489 22EC96     1510        LD   (REMLOC),HL
                1520 ;
B48C 212F98     1530        LD   HL,982FH
B48F 22D696     1540        LD   (SINPON),HL
                1550 ;
B492 3EFF       1560        LD   A,0FFH
B494 D314       1570        OUT  (14H),A
B496 D315       1580        OUT  (15H),A
B498 3E15       1590        LD   A,15H
B49A D315       1600        OUT  (15H),A
                1610 ;
B49C FB         1620        EI
B49D C9         1630        RET
                1640 ;
                1650 ;
                1660 ;*****************************************
                1670 ;**                                     **
                1680 ;**   FREQUENCY MEASUREMENT ROUTINE     **
                1690 ;**                                     **
                1700 ;**            "FREQER"                 **
```

```
                    1710 ;*****************************************
                    1720 ;
                    1730 ;
                    1740 ; This routine makes the measurement of
                    1750 ;the frequency.
                    1760 ;
B49E 2170B7         1770 FREQER LD   HL,0B770H
B4A1 22FC96         1780        LD   (CTC2IV),HL
                    1790 ;
B4A4 210000         1800        LD   HL,0000H
B4A7 0E00           1810        LD   C,00H
                    1820 ;
B4A9 FD2100B7       1830 NEXT   LD   IY,0B700H
B4AD FD22F096       1840        LD   (PIOBIV),IY
B4B1 110000         1850        LD   DE,0000H
                    1860 ;
                    1870 ; Wait for start of cycle.
                    1880 ;
B4B4 DB05           1890 INCH   IN   A,(05H)
B4B6 CB7F           1900        BIT  7,A
B4B8 C2B4B4         1910        JP   NZ INCH
                    1920 ;
B4BB 3AE296         1930        LD   A,(TIMLOC)
B4BE 3D             1940 B00B   DEC  A
B4BF F600           1950        OR   00H
B4C1 C2BEB4         1960        JP   NZ B00B
                    1970 ;
                    1980 ;Enable 'ONCOUNT' interrupt.
                    1990 ;
B4C4 3EB7           2000        LD   A,0B7H
B4C6 D307           2010        OUT  (07H),A
B4C8 3E7F           2020        LD   A,7FH
B4CA D307           2030        OUT  (07H),A
                    2040 ;
                    2050 ;Wait until the count is started.
                    2060 ;
B4CC CB78           2070 LOOP   BIT  7,B
B4CE CACCB4         2080        JP   Z LOOP
                    2090 ;
B4D1 CBB8           2100        RES  7,B
                    2110 ;
B4D3 FD2148B7       2120        LD   IY,0B748H
B4D7 FD22F096       2130        LD   (PIOBIV),IY
                    2140 ;
                    2150 ;Hang on till the negative part of the
                    2160 ; sin wave.
                    2170 ;
B4DB 3AE296         2180        LD   A,(TIMLOC)
B4DE 3D             2190 GAF    DEC  A
B4DF F600           2200        OR   00H
B4E1 C2DEB4         2210        JP   NZ GAF
                    2220 ;
B4E4 DB05           2230 WALLY  IN   A,(05H)
B4E6 CB7F           2240        BIT  7,A
B4E8 C2E4B4         2250        JP   NZ WALLY
                    2260 ;
B4EB 3AE296         2270        LD   A,(TIMLOC)
B4EE 3D             2280 GUFF   DEC  A
```

```
B4EF F600      2290         OR    00H
B4F1 C2EEB4    2300         JP    NZ GUFF
               2310 ;
               2320 ;Enable EOFCOUNT interrupts.
               2330 ;
B4F4 3EB7      2340         LD    A,0B7H
B4F6 D307      2350         OUT   (07H),A
B4F8 3E7F      2360         LD    A,7FH
B4FA D307      2370         OUT   (07H),A
               2380 ;
B4FC CB78      2390 CENT    BIT   7,B
B4FE CAFCB4    2400         JP    Z CENT
               2410 ;
B501 CBB8      2420         RES   7,B
               2430 ;
               2440 ; Sum the count over 4 cycles
               2450 ;
B503 19        2460         ADD   HL,DE
               2470 ;
               2480 ;
B504 C5        2490 NYET    PUSH  BC
B505 DD2AE696  2500         LD    IX,(TOTREM)
B509 ED4BED96  2510         LD    BC,(CORLOC)
B50D DD09      2520         ADD   IX,BC
B50F DD22E696  2530         LD    (TOTREM),IX
B513 C1        2540         POP   BC
               2550 ;
               2560 ;
B514 04        2570         INC   B
B515 CB50      2580         BIT   2,B
B517 CAA9B4    2590         JP    Z NEXT
B51A 22E896    2600         LD    (TOTSAM),HL
               2610 ;
               2620 ;Divide by 4 to get average no. per cycle
               2630 ;
B51D CB3C      2640         SRL   H
B51F CB1D      2650         RR    L
B521 CB3C      2660         SRL   H
B523 CB1D      2670         RR    L
               2680 ;
               2690 ;Store the total in SAMLOC :$96EA
               2700 ;
B525 22EA96    2710         LD    (SAMLOC),HL
               2720 ;
               2730 ;Divide the remainder by 4 ....
               2740 ;
B528 2AE696    2750         LD    HL,(TOTREM)
B52B CB3C      2760         SRL   H
B52D CB1D      2770         RR    L
B52F CB3C      2780         SRL   H
B531 CB1D      2790         RR    L
               2800 ;
               2810 ;Store the result in REMLOC :$96EC
               2820 ;
B533 22EC96    2830         LD    (REMLOC),HL
               2840 ;
B536 C9        2850         RET
               2860 ;
```

```
                2870 ;
                2880 ;*****************************************
                2890 ;**                                     **
                2900 ;**       DATA AQUISITION ROUTINE       **
                2910 ;**                                     **
                2920 ;**              "DROP"                 **
                2930 ;*****************************************
                2940 ;
                2950 ;
B537 CD9EB4     2960 DROP   CALL FREQER
                2970 ;
B53A 1110A0     2980        LD   DE,0A010H
B53D 2AE896     2990        LD   HL,(TOTSAM)
B540 0E08       3000        LD   C,08H
B542 ED4A       3010        ADC  HL,BC
B544 44         3020        LD   B,H
B545 4D         3030        LD   C,L
                3040 ;
                3050 ;Load interrupt addres's for ONIMP &INCIMP
                3060 ;
B546 2180B7     3070        LD   HL,0B780H
B549 22F096     3080        LD   (PIOBIV),HL
                3090 ;
B54C 2100B8     3100        LD   HL,0B800H
B54F 22F896     3110        LD   (CTCOIV),HL
                3120 ;
                3130 ;Wait for start of cycle.
                3140 ;
B552 DB05       3150 BOBY   IN   A,(05H)
B554 CB7F       3160        BIT  7,A
B556 C252B5     3170        JP   NZ BOBY
                3180 ;
B559 3AE296     3190        LD   A,(TIMLOC)
B55C 3D         3200 TPOT   DEC  A
B55D F600       3210        OR   00H
B55F C25CB5     3220        JP   NZ TPOT
                3230 ;
                3240 ;
                3250 ;Enable ONIMP interrupt.
                3260 ;
B562 3EB7       3270        LD   A,0B7H
B564 D307       3280        OUT  (07H),A
B566 3E7F       3290        LD   A,7FH
B568 D307       3300        OUT  (07H),A
                3310 ;
                3320 ;Take samples.........
                3330 ;
B56A F3         3340 ALBE   DI
                3350 ;
B56B 3AD296     3360        LD   A,(BOGAN)
B56E 3200B0     3370        LD   (0B000H),A
B571 3AD496     3380        LD   A,(B4GAN)
B574 3204B0     3390        LD   (0B004H),A
                3400 ;
B577 FB         3410        EI
B578 CB78       3420        BIT  7,B
B57A CA6AB5     3430        JP   Z ALBE
                3440 ;
```

```
                    3450 ;.....disable sampling.
                    3460 ;
B57D 3E03           3470         LD   A,03H
B57F D308           3480         OUT  (08H),A
                    3490 ;
                    3500 ;Return to PASCAL for analysis.........
                    3510 ;
B581 C9             3520         RET
                    3530 ;
                    3540 ;
                    3550 ;
                    3560 ;*********************************************
                    3570 ;**                                         **
                    3580 ;**   FREQUENCY MEASUREMENT AND DATA        **
                    3590 ;**   ACQUISUTION ROUTINE FOR DIGITAL       **
                    3600 ;**          SIGNAL SECTION                 **
                    3610 ;**                                         **
                    3620 ;**              "DROP2"                    **
                    3630 ;*********************************************
                    3640 ;
                    3650 ;
B582 21F401         3660 DROP2   LD   HL,01F4H
B585 22EA96         3670         LD   (SAMLOC),HL
B588 21A80F         3680         LD   HL,0FA8H
B58B 22E896         3690         LD   (TOTSAM),HL
B58E 3E00           3700         LD   A,00H
B590 32EC96         3710         LD   (REMLOC),A
                    3720 ;
                    3730 ; Next sample both signals over 1 cycle
                    3740 ;while outputting the sine wave.
                    3750 ;
B593 1110A0         3760         LD   DE,0A010H
B596 ED4BE896       3770         LD   BC,(TOTSAM)
                    3780 ;
                    3790 ; Load interrupt address for ONIMP2
                    3800 ;
B59A FD21B0B7       3810         LD   IY,0B7B0H
B59E FD22F096       3820         LD   (PIOBIV),IY
                    3830 ;
B5A2 DB05           3840 BOBY2   IN   A,(05H)
B5A4 CB7F           3850         BIT  7,A
B5A6 C2A2B5         3860         JP   NZ BOBY2
                    3870 ;
B5A9 3AE296         3880         LD   A,(TIMLOC)
B5AC 3D             3890 TPOT2   DEC  A
B5AD F600           3900         OR   00H
B5AF C2ACB5         3910         JP   NZ TPOT2
                    3920 ;
B5B2 3AE596         3930         LD   A,(TIMCON)
B5B5 CB6F           3940         BIT  5,A
B5B7 CABDB5         3950         JP   Z LEM03
B5BA CD3BB6         3960         CALL MISNOS
                    3970 ;
                    3980 ; Enable ONIMP2 interrupts.
                    3990 ;
B5BD 3EB7           4000 LEM03   LD   A,0B7H
B5BF D307           4010         OUT  (07H),A
B5C1 3E7F           4020         LD   A,7FH
```

```
B5C3 D307      4030          OUT   (07H),A
               4040 ;
               4050 ; Take samples.......
               4060 ;
B5C5 F3        4070 ALBE2    DI
B5C6 3AD296    4080          LD    A,(BOGAN)
B5C9 3200B0    4090          LD    (0B000H),A
B5CC 3AD496    4100          LD    A,(B4GAN)
B5CF 3204B0    4110          LD    (0B004H),A
               4120 ;
B5D2 FB        4130          EI
B5D3 CB78      4140          BIT   7,B
B5D5 CAC5B5    4150          JP    Z ALBE2
               4160 ;
B5D8 F3        4170          DI
B5D9 FD2120B7  4180          LD    IY,0B720H
B5DD FD22FA96  4190          LD    (CTC1IV),IY
B5E1 FB        4200          EI
               4210 ;
               4220 ;
B5E2 C9        4230          RET
               4240 ;
               4250 ;
               4260 ;*********************************************
               4270 ;**                                          **
               4280 ;**        12-BIT SINE WAVE OUTPUT           **
               4290 ;**                PROGRAM                   **
               4300 ;**                                          **
               4310 ;**              "SINGEN"                    **
               4320 ;*********************************************
               4330 ;
               4340 ;
B5E3 1120B7    4350 SINGEN LD    DE,0B720H
B5E6 ED53FA96  4360          LD    (CTC1IV),DE
               4370 ;
               4380 ; Set the amplitude of the output sine
               4390 ;wave to the initial value in $AMPLOC
               4400 ;
B5EA 3AD096    4410          LD    A,(AMPLOC)
B5ED D318      4420          OUT   (18H),A
               4430 ;
               4440 ; Set the WR/RL line to logic LOW
               4450 ;
B5EF 3E4F      4460          LD    A,4FH
B5F1 D315      4470          OUT   (15H),A
               4480 ;
               4490 ; Start CTC ch1 with control from $SINCON
               4500 ;and time constant from $TIMLOC
               4510 ;
B5F3 3AE496    4520          LD    A,(SINCON)
B5F6 D309      4530          OUT   (09H),A
B5F8 3AE096    4540          LD    A,(SINTIM)
B5FB D309      4550          OUT   (09H),A
               4560 ;
B5FD C9        4570          RET
               4580 ;
               4590 ;
               4600 ;*********************************************
```

```
                4610 ;**                                              **
                4620 ;**       1047 FREQUENCY SWEEP-UP                **
                4630 ;**              ROUTINE                         **
                4640 ;**                                              **
                4650 ;**              "UPSWP"                         **
                4660 ;**********************************************
                4670 ;
                4680 ;
                4690 ; Will sweep up the frequency set by the
                4700 ;1047 controller for a time determined by
                4710 ;the value in $TDEL ( 1sec for each unit).
                4720 ; The sweep rate is set on the panel of
                4730 ;the 1047.
                4740 ;
B5FE 3E00       4750 UPSWP  LD   A,00H
B600 D304       4760        OUT  (04H),A
B602 CBCF       4770        SET  1,A
B604 D304       4780        OUT  (04H),A
                4790 ;
B606 CD25B6     4800        CALL DELAY
                4810 ;
B609 C9         4820        RET
                4830 ;
                4840 ;
                4850 ;**********************************************
                4860 ;**                                            **
                4870 ;**      1047 FREQUENCY SWEEP-DOWN             **
                4880 ;**             ROUTINE                        **
                4890 ;**                                            **
                4900 ;**             "DNSWP"                        **
                4910 ;**********************************************
                4920 ;
                4930 ;
                4940 ; As UPSWP but sweep direction is down.
                4950 ;
B60A 3E04       4960 DNSWP  LD   A,04H
B60C D304       4970        OUT  (04H),A
B60E CB97       4980        RES  2,A
B610 D304       4990        OUT  (04H),A
                5000 ;
B612 CD25B6     5010        CALL DELAY
                5020 ;
B615 C9         5030        RET
                5040 ;
                5050 ;
                5060 ;**********************************************
                5070 ;**                                            **
                5080 ;**   CEASE SENDING DRIVING SINE WAVE          **
                5090 ;**             ROUTINE                        **
                5100 ;**                                            **
                5110 ;**            "STOSIN"                        **
                5120 ;**********************************************
                5130 ;
                5140 ;
B616 F3         5150 STOSIN DI
B617 3E03       5160        LD   A,03H
B619 D309       5170        OUT  (09H),A
B61B FB         5180        EI
```

```
                    5190 ;
B61C C9             5200        RET
                    5210 ;
                    5220 ;
                    5230 ;*******************************************
                    5240 ;**                                       **
                    5250 ;**       NEW DIGITAL AMPLITUDE           **
                    5260 ;**            ROUTINE                    **
                    5270 ;**                                       **
                    5280 ;**            "NEWAMP"                   **
                    5290 ;*******************************************
                    5300 ;
B61D F3             5310 NEWAMP DI
B61E 3AD096         5320        LD    A,(AMPLOC)
B621 D318           5330        OUT   (18H),A
B623 FB             5340        EI
                    5350 ;
B624 C9             5360        RET
                    5370 ;
                    5380 ;
                    5390 ;%%%%%%%%%%%%%%%%%%%%%%%%%%%%%%%%%%%%%%%%%%%
                    5400 ;%%                                       %%
                    5410 ;%%            SUBROUTINES                %%
                    5420 ;%%                                       %%
                    5430 ;%%%%%%%%%%%%%%%%%%%%%%%%%%%%%%%%%%%%%%%%%%%
                    5440 ;
                    5450 ;
                    5460 ;*******************************************
                    5470 ;**                DELAY                  **
                    5480 ;*******************************************
                    5490 ;
                    5500 ;
B625 3AD896         5510 DELAY  LD    A,(TDELAY)
                    5520 ;
B628 3D             5530 TDEL   DEC   A
                    5540 ;
B629 08             5550        EX    AF,AF'
B62A DF5D           5560        SCAL  5DH
B62C 08             5570        EX    AF,AF'
                    5580 ;
B62D F600           5590        OR    00H
B62F C228B6         5600        JP    NZ TDEL
                    5610 ;
B632 3E01           5620        LD    A,01H
B634 D304           5630        OUT   (04H),A
B636 CB87           5640        RES   0,A
B638 D304           5650        OUT   (04H),A
                    5660 ;
B63A C9             5670        RET
                    5680 ;
                    5690 ;
                    5700 ;*******************************************
                    5710 ;**               MISNOS                  **
                    5720 ;*******************************************
                    5730 ;
                    5740 ;
B63B 3AE296         5750 MISNOS LD    A,(TIMLOC)
B63E 3D             5760 LOP01  DEC   A
```

```
B63F F600      5770          OR    00H
B641 C23EB6    5780          JP    NZ LOP01
               5790 ;
B644 3AE296    5800          LD    A,(TIMLOC)
B647 3D        5810 LOP02    DEC   A
B648 F600      5820          OR    00H
B64A C247B6    5830          JP    NZ,LOP02
               5840 ;
B64D 3AE296    5850          LD    A,(TIMLOC)
B650 3D        5860 LOP03    DEC   A
B651 F600      5870          OR    00H
B653 C250B6    5880          JP    NZ ,LOP03
               5890 ;
B656 C9        5900          RET
               5910 ;
               5920 ;
               5930 ;%%%%%%%%%%%%%%%%%%%%%%%%%%%%%%%%%%%%%%%%%%%%%%%%%%%%%%%%%%%%%%%%
               5940 ;%%                                                              %%
               5950 ;%%            INTERRUPT SERVICE                                 %%
               5960 ;%%                ROUTINES                                      %%
               5970 ;%%                                                              %%
               5980 ;%%%%%%%%%%%%%%%%%%%%%%%%%%%%%%%%%%%%%%%%%%%%%%%%%%%%%%%%%%%%%%%%
               5990 ;
               6000 ;
               6010 ;*****************************************************
               6020 ;**          'SINOUT' SERVICE ROUTINE                 **
               6030 ;*****************************************************
               6040 ;
               6050 ;
B720           6060          ORG   0B720H
               6070 ;
B720 E5        6080 SINOUT   PUSH  HL
B721 F5        6090          PUSH  AF
B722 2AD696    6100          LD    HL,(SINPON)
               6110 ;
               6120 ; Output the 8 LSB's and increment port
               6130 ;
B725 7E        6140          LD    A,(HL)
B726 D314      6150          OUT   (14H),A
B728 23        6160          INC   HL
               6170 ;
               6180 ; output 4 MSB's and set WR/RL HIGH
               6190 ;
B729 7E        6200          LD    A,(HL)
B72A D315      6210          OUT   (15H),A
B72C 23        6220          INC   HL
               6230 ;
               6240 ; Reset WR/RL to latch data
               6250 ;
B72D 3E15      6260          LD    A,15H
B72F D315      6270          OUT   (15H),A
               6280 ;
               6290 ; Test for end of cycle.YES? reset pointer
               6300 ;
B731 CB6C      6310          BIT   5,H
B733 CA39B7    6320          JP    Z,MISS
B736 212F98    6330          LD    HL,982FH
               6340 ;
```

```
B739 22D696    6350 MISS   LD    (SINPON),HL
B73C F1        6360        POP   AF
B73D E1        6370        POP   HL
B73E FB        6380        EI
B73F ED4D      6390        RETI
               6400 ;
               6410 ;
               6420 ;*******************************************
               6430 ;**       'ONCOUNT' SERVICE ROUTINE       **
               6440 ;*******************************************
               6450 ;
B700           6460        ORG   0B700H
               6470 ;
B700 3AE596    6480 ONCNT  LD    A,(TIMCON)
B703 D30A      6490        OUT   (0AH),A
B705 3AE296    6500        LD    A,(TIMLOC)
B708 D30A      6510        OUT   (0AH),A
               6520 ;
B70A 3E03      6530        LD    A,03H
B70C D307      6540        OUT   (07H),A
               6550 ;
B70E CBF8      6560        SET   7,B
               6570 ;
B710 FB        6580        EI
B711 ED4D      6590        RETI
               6600 ;
               6610 ;
               6620 ;*******************************************
               6630 ;**    'EOFCOUNT' SERVICE ROUTINE         **
               6640 ;*******************************************
               6650 ;
B748           6660        ORG   0B748H
               6670 ;
B748 DB0A      6680 EOFCNT IN    A,(0AH)
B74A 32ED96    6690        LD    (CORLOC),A
               6700 ;
B74D 3E03      6710        LD    A,03H
B74F D307      6720        OUT   (07H),A
B751 D30A      6730        OUT   (0AH),A
               6740 ;
B753 CBF8      6750        SET   7,B
               6760 ;
B755 FB        6770        EI
B756 ED4D      6780        RETI
               6790 ;
               6800 ;
               6810 ;*******************************************
               6820 ;**       'INCOUNT' SERVICE ROUTINE       **
               6830 ;*******************************************
               6840 ;
B770           6850        ORG   0B770H
               6860 ;
B770 13        6870 INCNT  INC   DE
               6880 ;
B771 FB        6890        EI
B772 ED4D      6900        RETI
               6910 ;
               6920 ;
```

```
                    6930 ;*****************************************
                    6940 ;**       'ONIMP' SERVICE ROUTINE         **
                    6950 ;*****************************************
                    6960 ;
B780                6970         ORG   0B780H
                    6980 ;
B780 08             6990 ONIMP   EX    AF,AF'
B781 3AE596         7000         LD    A,(TIMCON)
B784 D308           7010         OUT   (08H),A
B786 3AE296         7020         LD    A,(TIMLOC)
B789 D308           7030         OUT   (08H),A
                    7040 ;
B78B 3E03           7050         LD    A,03H
B78D D307           7060         OUT   (07H),A
                    7070 ;
B78F 2100B0         7080         LD    HL,0B000H
B792 03             7090         INC   BC
B793 03             7100         INC   BC
B794 03             7110         INC   BC
B795 03             7120         INC   BC
                    7130 ;
B796 EDA0           7140         LDI
B798 EDA0           7150         LDI
                    7160 ;
B79A 23             7170         INC   HL
B79B 23             7180         INC   HL
                    7190 ;
B79C EDA0           7200         LDI
B79E EDA0           7210         LDI
                    7220 ;
B7A0 08             7230         EX    AF,AF'
                    7240 ;
B7A1 FB             7250         EI
B7A2 ED4D           7260         RETI
                    7270 ;
                    7280 ;
                    7290 ;
                    7300 ;*****************************************
                    7310 ;**       'INCIMP' SERVICE ROUTINE        **
                    7320 ;*****************************************
                    7330 ;
B800                7340         ORG   0B800H
                    7350 ;
B800 08             7360 INCIMP  EX    AF,AF'
B801 2100B0         7370         LD    HL,0B000H
                    7380 ;
B804 3E02           7390         LD    A,02H
B806 3D             7400 LILT    DEC   A
B807 F600           7410         OR    00H
B809 00             7420         NOP
B80A C206B8         7430         JP    NZ LILT
                    7440 ;
B80D 78             7450         LD    A,B
B80E B1             7460         OR    C
B80F C216B8         7470         JP    NZ NOOP
B812 08             7480         EX    AF,AF'
B813 CBFF           7490         SET   7,A
B815 08             7500         EX    AF,AF'
```

```
                    7510 ;
B816 EDA0           7520 NOOP   LDI
B818 EDA0           7530        LDI
                    7540 ;
B81A 23             7550        INC  HL
B81B 23             7560        INC  HL
                    7570 ;
B81C EDA0           7580        LDI
B81E EDA0           7590        LDI
                    7600 ;
B820 08             7610        EX   AF,AF'
B821 FB             7620        EI
B822 ED4D           7630        RETI
                    7640 ;
                    7650 ;
                    7660 ;*******************************************
                    7670 ;**      'ONIMP2' INTERRUPT ROUTINE       **
                    7680 ;*******************************************
                    7690 ;
B7B0                7700        ORG  0B7B0H
                    7710 ;
B7B0 08             7720 ONIMP2 EX   AF,AF'
B7B1 2180B8         7730        LD   HL,0B880H
B7B4 22FA96         7740        LD   (CTC1IV),HL
                    7750 ;
B7B7 3E03           7760        LD   A,03H
B7B9 D307           7770        OUT  (07H),A
                    7780 ;
B7BB 08             7790        EX   AF,AF'
                    7800 ;
                    7810 ;
B7BC FB             7820        EI
B7BD ED4D           7830        RETI
                    7840 ;
                    7850 ;
                    7860 ;*******************************************
                    7870 ;**      'INIMP2' INTERRUPT ROUTINE       **
                    7880 ;*******************************************
                    7890 ;
B880                7900        ORG  0B880H
                    7910 ;
B880 08             7920 INIMP2 EX   AF,AF'
B881 2AD696         7930        LD   HL,(SINPON)
                    7940 ;
                    7950 ; Load sine point out.
                    7960 ;
B884 7E             7970        LD   A,(HL)
B885 D314           7980        OUT  (14H),A
B887 23             7990        INC  HL
B888 7E             8000        LD   A,(HL)
B889 D315           8010        OUT  (15H),A
B88B 23             8020        INC  HL
                    8030 ;
B88C 3E15           8040        LD   A,15H
B88E D315           8050        OUT  (15H),A
                    8060 ;
                    8070 ; Test for end of sine wave.
                    8080 ;
```

```
B890 CB6C      8090          BIT   5,H
B892 CA98B8    8100          JP    Z MISS2
B895 212F98    8110          LD    HL,982FH
               8120 ;
B898 22D696    8130 MISS2    LD    (SINPON),HL
B89B CB51      8140          BIT   2,C
B89D C2A7B8    8150          JP    NZ PONT
B8A0 0B        8160          DEC   BC
B8A1 0B        8170          DEC   BC
B8A2 0B        8180          DEC   BC
B8A3 0B        8190          DEC   BC
B8A4 C3B4B8    8200          JP    NPONT
B8A7 2100B0    8210 PONT     LD    HL,0B000H
               8220 ;
B8AA EDA0      8230          LDI
B8AC EDA0      8240          LDI
               8250 ;
B8AE 23        8260          INC   HL
B8AF 23        8270          INC   HL
               8280 ;
B8B0 EDA0      8290          LDI
B8B2 EDA0      8300          LDI
               8310 ;
B8B4 08        8320 NPONT    EX    AF,AF'
B8B5 FB        8330          EI
B8B6 ED4D      8340          RETI
               8350 ;
               8360 ;
               8370 ;%%%%%%%%%%%%%%%%%%%%%%%%%%%%%%%%%%%%%%%%%%%%%%%%%%%%%%%%
               8380 ;%%                                                      %%
               8390 ;%%                        END                           %%
               8400 ;%%                                                      %%
               8410 ;%%%%%%%%%%%%%%%%%%%%%%%%%%%%%%%%%%%%%%%%%%%%%%%%%%%%%%%%
```

APPENDIX V

THE HOOKE-JEEVES NON-LINEAR SEARCH OPTIMISATION TECHNIQUE [85]

This algorithm is one of the most widely used direct search methods. Using functional evaluations only, the method attempts to align the search direction with the principle axis of the objective function using two strategies; exploratory moves and pattern moves. Consider a function of the form

$$Y(\underline{p}) = Y(p_1, p_2, p_3 \cdots\cdots p_N)$$

where the p_i are the independent variables of the function, Y. Then the mean square variation, $G(\underline{p})$, of the measured data points, y, about the fitting function, $Y(\underline{p})$ is given by

$$G(\underline{p}) = \frac{1}{N} \sum_{k=1}^{N} \{y_k - Y_k(\underline{p})\}^2$$

It is necessary to minimise the value of $G(\underline{p})$ by altering the values of the independent variables. The method requires an initial base point, $\underline{p}=\underline{b}_1$, and a set of step lengths, h_i, one for each independent variable. For optimum accuracy the step lengths are chosen so as to equalise the quantities

$$G(\underline{b}_1 + h_i \underline{e}_i) - G(\underline{b}_1)$$

where $\underline{e}_j$ are the unit vectors. The two types of move are described below.

Exploratory Moves

The purpose of an exploratory move is to find information about $G(\underline{p})$ in the neibourhood of the current base point. The steps in an exploratory move are as follows:

Step 1 : Evaluate $G(\underline{b}_1 + h_1\underline{e}_1)$. If this move yields $G(\underline{b}_1 + h_1\underline{e}_1) < G(\underline{b}_1)$ then the move is termed a sucess and $\underline{b}_1$ is replaced with $\underline{b}_1+h_1\underline{e}_1$. If it is a failure then $G(\underline{b}_1 - h_1\underline{e}_1)$ is evaluated in a similar manner. If this is sucessful then $\underline{b}_1$ is replaced with $\underline{b}_1-h_1\underline{e}_1$.

If both attempts end in failure the value of $\underline{b}_1$ is retained.

Step 2 : Step 1 is repeated for each of the variables p_i arriving at a new base point $\underline{b}_2$.

Step 3 : If $\underline{b}_2 = \underline{b}_1$ then no progress has been made. In this case the lengths of the steps should be reduced. The method ends when the step lengths have been reduced to some proscribed level. Otherwise a return should be made to step 1.

If $\underline{b}_2 \neq \underline{b}_1$ then a patten move should be made from $\underline{b}_2$.

Pattern Moves

In a pattern move an attempt is made to speed the algorithm by moving in the direction $\underline{b}_2 - \underline{b}_1$. This is sensible as an exploratory move in this direction has already yielded a reduction in the mean square variation. The steps in a pattern move are as follows:

Step 1 : Move from $\underline{b}_2$ to $\underline{b}_3 = \underline{b}_2 + (\underline{b}_2 - \underline{b}_1)$ and perform a sequence of exploratory moves about $\underline{b}_3$.

Step 2 : If the lovest value of $G(\underline{p})$ in step 1 is less than $G(\underline{b}_2)$ then a new base point $\underline{b}_4$ has been reached. In this case a return should be made to step one with all of the suffuxes double

incremented. Otherwise the pattern move from $\underline{b}_2$ must be abandoned and an exploratory move attempted at the point $\underline{b}_2$.

According to Hooke and Jeeves, their method has been used sucessfully to solve curve fitting problems for which other methods have failed. The algorithm is quite simple, unlike some of the more sophisticated gradient methods. The large number of evaluations required is sometimes a disadvantage, but overall the method is considered to be an effective numerical search algorithm.